AN INTEGRATED ANALYSIS OF CARBONATE MUDROCKS AND MIXED CARBONATE – SILICICLASTIC RESERVOIRS TO DEFINE THE EFFECTS OF MICRO- TO NANO-METER SCALE PORE ARCHITECTURE ON THE ABILITY TO PREDICT POROSITY OR PERMEABILITY

By

BETH ANN VANDEN BERG

Bachelor of Science in Geology
Calvin College
Grand Rapids, Michigan
2001

Master of Science in Hydrogeology
Clemson University
Clemson, South Carolina
2003

Submitted to the Faculty of the
Graduate College of the
Oklahoma State University
in partial fulfillment of
the requirements for
the Degree of
DOCTOR OF PHILOSOPHY
July, 2016

AN INTEGRATED ANALYSIS OF CARBONATE MUDROCKS AND MIXED CARBONATE – SILICICLASTIC RESERVOIRS TO DEFINE THE EFFECTS OF MICRO- TO NANO-METER SCALE PORE ARCHITECTURE ON THE ABILITY TO PREDICT POROSITY OR PERMEABILITY

Dissertation Approved:

Dr. G.Michael Grammer

Dissertation Adviser

Dr. Gregor Eberli

Dr. James Puckette

Dr. Jay Gregg

Dr. Adam Molnar

.

ACKNOWLEDGEMENTS

The completion of this degree would not have been possible if not for the help, support, and encouragement of many friends and family members. I would like to thank my advisor Dr. G. Michael Grammer, for his support, guidance, and encouragement throughout this research. I would also like to thank each of my committee members, Dr. Jim Puckette, Dr. Gregor Eberli, Dr. Jay Gregg, and Dr. Adam Molnar, for their guidance, support, and encouragement throughout this research project. Although there are too many people to name I would like to say "thank you!" to my fellow graduate students and colleagues from Oklahoma State University, Western Michigan University, and the University of Miami –RSMAS who have become friends through mutual support, and encouragement, throughout our continued research endeavors. A special "thank you" goes to my husband Clay Alsip for his love, support and encouragement through all of the ups and downs in pursuit of this degree.

It is also only possible through generous financial contributions from the OSU Reservoir Distribution and Characterization of Mid-Continent Mississippian Carbonates—A Major Unconventional Resource Play Consortium, AAPG Grants-in-Aid (2014, 2015), the Oklahoma Geological Survey Susan Takken Fellowship (2015), and the Boone Pickens School of Geology. Additionally, Redfork Energy, Devon Energy, and Maverick Brothers generously provided access to cores and associated contract laboratory data. Scanning electron microscope (SEM) was performed at the Oklahoma State University Microscopy laboratory. Laboratory measured sonic velocity response was performed at the University of Miami –Rosenstiel School of Marine and Atmospheric Sciences (RSMAS).

Name: BETH ANN VANDEN BERG

Date of Degree: JULY, 2016

Title of Study: AN INTEGRATED ANALYSIS OF CARBONATE MUDROCKS AND MIXED CARBONATE – SILICICLASTIC RESERVOIRS TO DEFINE THE EFFECTS OF MICRO- TO NANO-METER SCALE PORE ARCHITECTURE ON THE ABILITY TO PREDICT POROSITY OR PERMEABILITY

Major Field: GEOLOGY

Abstract:

The primary focus of this research is to increase the understanding of carbonate mudrock reservoirs through a first-order analysis of the micro- to nanopore architecture. Facies interpretation and development of a high resolution sequence stratigraphic-based depositional architecture in Mississippian-age carbonates from three regions of the Mid-Continent are integrated with key petrophysical data, analysis of the pore architecture, and acoustic response data to provide insight into primary reservoir controls and trends that can be applied to other areas of these Mississippian age strata and to carbonate mudrocks on a global scale.

Facies transition from very fine grain carbonaceous mudstone, wackestones, and grainstones, to near-shore wackestone, packstones, and peritidal deposits. All cores show a shallowing upward facies succession, similar sequence stratigraphic framework, and highest porosity and permeability within the large-scale sequence regressive phase. Horizontal porosity ranges from 0.1 - 12% (avg.2.5%) and 13 - 45% (avg. 31%) with correlative permeability of 0.0001mD-3.4mD (avg. 0.05mD) and 5.92mD - 163mD (avg. 43mD) in fine and coarse grained facies respectively.

Qualitative analysis identified samples with significant clay mineral precipitation, which sub-divides the pore space, correlates with relatively low porosity and permeability. Samples with lesser amounts of clay mineral precipitation correlate with relatively high porosity and permeability. Quantitative analysis shows the relationships between measured geometric parameters of carbonate mudrocks with micro- to nano-meter scale porosity (<62µm diam.) may differ significantly when compared to conventional carbonate reservoirs with primarily macro-porosity (256-4mm diam.). The complex pore architecture equates to the inapplicability of standard methods to predict key reservoir properties.

Acoustic response data are inversely related to porosity, with a data shift as related to the empirical Wyllie time average equation. The observed shift is a result of complexity within the micro- to nanoscale pore architecture, coupling of grains at the micro- to nanoscale, and mixed mineralogy, whose combined effects create significantly different elastic properties. A comparison of data from different basins and geological ages shows a consistent inverse relationship in carbonate samples; however reservoir specific data should be analyzed to identify the specific relationship between velocity and porosity prior to application of established proxies used to predict permeability.

TABLE OF CONTENTS

LIST OF TABLES

Table Page

LIST OF FIGURES

Figure Page

CHAPTER I

INTRODUCTION

Over the last decade unconventional resources, defined by low porosity and low permeability, have taken a prominent place in oil and gas exploration. This change in focus for exploration and reservoir development has created a need to better understand shale and mudrock depositional environments and their reservoir characteristics. Much of the research on shale and mudrock reservoirs has been focused on siliciclastic shale and mudrocks such as the Barnett Shale (Mississippian) in the Fort Worth Basin, and the Utica Shale (Ordovician) in the Appalachian Basin (e.g. Dorsch, 1995; Loucks et al., 2009; Davies et al., 1991; Dewhurst et al., 1999; Reed and Loucks, 2007; Ruppel and Loucks, 2008; Nelson, 2009; Slatt and O'Neal, 2011). There are also limited studies published on the pore architecture in carbonate and calcareous mudstones or chalk deposits, primarily related to the Cretaceous Eagle Ford and Niobrara Formations (e.g. Abouelresh, 2015; Loucks and Rowe, 2014; Loucks, et. al., 2014; Michaels and Budd, 2014). This research increases our understanding of carbonate mudrocks from a depositional and sequence stratigraphic perspective, while also providing some of the first insight into the nature of micro- to nano-pore systems in carbonate mudrocks, the pore system types and three dimensional architecture, and how the pore systems relate to permeability in the reservoirs

and how that permeability may be predicted based upon acoustical properties of the rock.

Previous research on carbonate muds has focused on describing the constituents to differentiate depositional environments (e.g. Ginsburg, 1956; Gischler et al., 2013), correlation with flow rate and carbonate mud deposition (Schieber et al., 2013), understanding diagenetic processes (e.g. Andrews, 1991; Rude and Aller, 1991), the role of diagenesis as it relates to the acoustic response of deep sea carbonate (e.g. Dae-Choul et al., 1985; Grützner and Mienert, 1999), and early diagenesis related to lithification of carbonate muds (e.g. Bathurst, 1970; Dix and Nelson, 2006).

The Mississippian age Limestone reservoir ("Mississippi Lime" play) is located in the North American Mid-Continent throughout North-Central Oklahoma and Southern Kansas. Energy companies have been producing oil and gas from this reservoir from vertical wells for over 50 years. In the recent decade, this reservoir system has undergone a revival in production through advances in horizontal drilling technology that have enhanced the ability to efficiently extract hydrocarbons in the reservoir. Accompanying this renewed interest, is a critical need to understand the details and complexities that exist within the reservoir architecture to target the highest producing intervals and extract the hydrocarbons in the most environmentally sensitive and economically expedient manner. A fundamental control on reservoir systems and production capabilities is often linked facies types and their corresponding geometrical attributes derived from interpretation of the primary depositional environments, as well as petrophysical characteristics that are identified through facies analysis of cored intervals at the micro- and nanoscale to the meter-scale. The Mississippian age stratigraphy deposited in what is present day North American Mid-continent (Kansas and Oklahoma), with the abundance of outcrop and subsurface data, provides a unique study area to provide insight to the depositional environments and pore architecture that control reservoir-scale porosity and permeability in this carbonate mudrock-dominated system.

Although this research was conducted using an integrated methodology that incorporates several different data sets, there are specific, focus areas of the research that have been defined with clearly stated objectives. Each of these topics and the specific goals are outlined below for each

component of this research project. As necessary, additional introductory or background information is provided to highlight the academic and/or energy industry application and potential implementation of observations and conclusions.

Research Topic #1: Characterization of the 2-D Pore Architecture of a Carbonate Mudrock Reservoir: Insights from the Mid-Continent "Mississippi Lime"

One application of understanding the pore architecture in a reservoir system is to enhance the predictability of reservoir properties that influence the feasibility of development and use of that reservoir. This is true for the extraction of hydrocarbons, use of the reservoir as a potable water system, or for the purposes of carbon dioxide (CO_2) sequestration. The dominant pore types in conventional carbonate reservoircontain significant macroporosity (256mm to 4mm diameter) and mesoporosity (62µm to 4mm), as defined by Loucks et al. (2012), and are well understood and can be easily described with relation to facies, depositional environments, diagenesis, and reservoir properties (Archie, 1952; Folk, 1959; Dunham, 1962; Embry and Klovan, 1971; Choquette and Pray, 1970; Lucia 1983; Lucia, 1995).

With the exception of a few recent papers (e.g. Milliken, 2014; Loucks et al., 2012), the current literature is markedly absent of successful and applicable descriptive methodologies and observations for carbonate mudrock reservoirs that contain significant microporosity (62.5 -1µm) and nanoporosity (1µm-1nm). While the use of established terminology for macropore systems is logical, this does not always accurately describe the pore architecture (pore size, shape, and distribution) or the relationship to both depositional environments and predictable diagenetic processes. Therefore, at this point of mudrock research it is prudent to continue to add observations regarding the applicability of using conventional terminology to describe siliciclastic mudrocks, or conventional carbonate systems as well as denote cases where the conventional terminology is unable to accurately portray observations from carbonate mudrocks. The research presented in this paper has utilized an integrated methodology where the pore architecture is quantitatively and qualitatively described from photomicrographs that identify general and unique characteristics (pore size distribution, pore shape)

to better understand how the variability at the micro- to nanometer pore scale is related to key petrophysical properties such as porosity, permeability, and the sonic velocity response.

A fundamental relationship between pore type and permeability in carbonates has been documented (Lucia 1999) and can be applied through a variety of methods (density-neutron log analysis, sonic velocity – porosity relationship) to predict the porosity and permeability along a borehole. When facies analysis and sequence stratigraphy can be related to the pore architecture, it becomes possible to predict porosity and permeability on the reservoir scale in 3 dimensions (Grammer et al., 2004). Although it is logical to assume the same relationships that exist in conventional macropore systems also exist in unconventional carbonate mudrocks on a fractal scale, the fundamental pore architecture remains poorly described because until recently, documentation of the basic carbonate mudrock pore types has not been a primary focus of mudrock research, nor have the necessary technological tools been available to image pores at the nanometer scale. For this reason, relationships between pore type, porosity, permeability, and pore architecture are also undefined.

Understanding the fundamental carbonate mudrock pore architecture and how this relates to other reservoir properties can have a significant impact on reservoir development within the "Mississippi Lime" play and also provide an analog for other carbonate mudrock reservoirs worldwide. One component of this characterization is the distribution of the pore sizes and pore network to understand how micro- to nanopores impact permeability.

The focus of this component of the dissertation research is to document the pore architecture of carbonate mud-dominated facies within a core that has proven reservoir quality. The pore architecture is described both qualitatively and quantitatively in such a way that it can be integrated into subsequent detailed analysis to further increase the predictability of petrophysical properties in similar carbonate mudrock systems through a better understanding of the fundamental relationship between pore architecture, porosity, permeability, facies and sequence stratigraphic framework. The

primary goal is to provide a first-order descriptive classification of carbonate mudrock pore architecture using the "Mississippian Lime" play as a case study through the following objectives:

1. Quantitatively describe the pore architecture from key measurements obtained from digital image analysis of photomicrographs obtained using light microscopy (LM) and an environmental scanning electron microscope (ESEM);
2. Qualitatively describe the pore types as observed in thin section and at higher magnifications using a scanning electron microscope;
3. Identify facies associated with unique depositional environments to define a sequence stratigraphic framework for the data set;
4. Characterize fundamental relationships between quantitative pore architecture data, porosity, permeability, and the facies and sequence stratigraphic framework;
5. Identify the overall relationship between compressional velocity and porosity in carbonate mudrocks to determine potential use as a predictive tool in carbonate mudrock systems.

Research Topic #2: A quantitative evaluation of the pore system architecture and acoustic response of micro- to nanometer-scale pores in carbonate mudrocks

The second major topic of this dissertation expands the 2-D image data set to include observations from five cores from three locations within the Mississippian age North American Mid-Continent basin while also tying the pore systems to sonic velocity data to develop a proxy for predicting permeability in carbonate mudrocks. This research integrates qualitative and quantitative observations from representative photographs collected using thin sections with a magnification of 5x-40x, and ion milled samples viewed with an ESEM with a magnification of 100x-1,000,000x. The primary goals of this component of the research are as follows:

1. To apply quantitative and qualitative observations and measurements of the pore architecture to understand the porosity and permeability trends within the study area and to tie these pore systems to laboratory measured sonic velocity data.

2. To perform a statistical analysis of the image and sonic velocity data to identify key geometric features within the pore system architecture that can be used to increase the predictability of porosity and permeability within a micro- to nanopore dominated carbonate mudrock reservoir.
3. To identify trends and relationships that can be applied in other areas of the basin, as well as in other carbonate mudrocks to increase the predictability of key petrophysical properties in these types of reservoirs on a global scale.

Research topic #3: Testing the applicability of identified relationships between velocity response and permeability in Cenozoic and Mesozoic carbonates to Paleozoic carbonates from multiple depositional basins

In Cenozoic-age carbonates with conventional reservoir characteristics, the relationship between porosity and acoustic response (sonic velocity) has a clearly identified inverse relationship that can be approximated by the Wyllie time average equation (Anselmetti and Eberli 1993). Scatter present within the data set, and deviations from the fundamental relationship between velocity and porosity have been explained through the relationship to the dominant pore type (Anselmetti and Eberli 1993; Anselmetti et al. 1997). Understanding how this fundamental relationship between velocity and porosity can vary when applied to data sets from Mesozoic or Paleozoic age carbonates from different depositional basins and depositional textures (conventional versus unconventional reservoir types) was done to evaluate the potential relationship to the dominant pore type and relationship to permeability in ma wider spectrum of carbonate reservoir types and of significantly different ages.

As an example of the application of this approach, considering two samples with the same total porosity within a carbonate system, one with intergranular porosity (higher permeability) and one with moldic porosity (lower permeability), the sample with the intergranular porosity will typically have a slower velocity than a sample with moldic porosity because of the difference in connectivity of the pores and the effect this has on the elastic properties of the sample. Because there

is typically greater connectivity of the pores in intergranular samples, which indicates a higher permeability, it can be generally stated that in carbonates where the velocity response is lower than expected, the permeability is relatively higher than in rocks where the actual velocity is close to or higher than the value predicted by the Wyllie time average equation. However, these relationships and trends were previously based primarily on a data set of "young" carbonate rocks that are late Mesozoic to Cenozoic in age, collected from the Neogene of Great Bahama Bank, the Mailla Platform, an exhumed Cretaceous-aged carbonate platform in Italy, and modern compacted mud samples from Florida Bay. From a petrophysical standpoint, however, there are significant questions how these relationships and trends may apply to:(1) "older" carbonates that have undergone compaction and increased diagenetic modification, (2) carbonates from different depositional basins, and (3) carbonates that have a mixed mineral composition either from original depositional characteristics or from diagenetic alteration. With these questions in mind, the goal of this paper is to:

1. Identify how the relationship between velocity response and porosity compares from different basins and from different geologic time periods (Ordovician and Silurian of the Michigan Basin, Pennsylvanian of the Paradox Basin, and Mississippian of the North American Mid-Continent).
2. Identify how the relationship between velocity response, porosity, and permeability changes with different fundamental pore system architectures, specifically between a macro- to mesopore dominated system and a micro- to nanopore dominated system.

These goals were addressed through a series of observations and analyses of laboratory measured velocity response data, and the associated laboratory measured porosity values. Where available, this data was also compared to laboratory measured permeability data to identify relationships, or lack thereof, to the velocity-porosity trend and infer the potential for this to be related to the pore type, facies, or to be applied to accurately predict permeability.

Research topic #4: Integrated reservoir characterization to provide insight into porosity and permeability in a mixed carbonate-siliciclastic reservoir

A fourth research focus is to use an integrated analysis to provide insight into possible depositional environments found within the study area, and to identify methods and tools that increase knowledge of the reservoir properties, including the hydrocarbon production potential. As part of a larger research consortium, conclusions from this analysis provide one component of a very complicated depositional and diagenetic history of the Mississippian age carbonate – siliciclastic reservoir in North-central Oklahoma and South-Central Kansas, U.S.A.

The primary goals of this component of the research were met through the following four objectives:

1. To define the high-resolution sequence stratigraphic framework to enhance the predictability of strata in the subsurface through detailed facies analysis from core and thin section data, and the application of idealized vertical stacking patterns for five cores from three regions in the basin;
2. Compare the sequence stratigraphic hierarchy to wire line log signatures and conventional, petrophysical laboratory data (porosity, air permeability, and Klinkenberg permeability) to identify trends that can potentially be applicable to other parts of the basin, and other unconventional carbonate – siliciclastic reservoir systems.
3. To understand how the acoustic response relates to porosity and pore type in the very fine grained, low porosity and low permeability, unconventional, facies in the study area, and if a relationship exists that correlates facies and/or sequence stratigraphy to porosity and permeability.

Identifying relationships between common well log data, traditional laboratory measured petrophysical data and a detailed sequence stratigraphic framework increases the predictability of reservoir-quality units in the subsurface, allows for an enhanced understanding of reservoir and seal

geometries and distributions, and ultimately leads to enhanced hydrocarbon production. The results from this study should be applicable to other areas within the "Mississippian Limes" play outside of the study areas included in this research, and also be applicable as an analog for other carbonate – siliciclastic systems deposited in similar environmental conditions on an attached carbonate ramp or attached, distally steepened carbonate ramp, adjacent to an actively subsiding foreland basin. This phase of the study has led to a better understanding of how the acoustic response relates to porosity and pore type within the basin as tied to facies and the sequence stratigraphic architecture, and how the response can be used to enhance the ability to predict permeability in these types of depositional systems.

CHAPTER II

2-D PORE ARCHITECTURE CHARACTERIZATION OF A CARBONATE MUDROCK RESERVOIR: INSIGHTS FROM THE MID-CONTINENT "MISSISSIPPI LIME"

ABSTRACT

This study shows examples of how fundamental relationships between pore shape, porosity, permeability, and acoustic response differ in carbonate mudrocks with micro- to picoporosity (<62 μm diameter) compared to conventional carbonates with primarily macroporosity (256–4 mm diameter). Quantitative data show that some positive correlations exist between porosity and permeability, similar to those observed in conventional carbonates. However, several expected relationships between properties, such as pore shape and laboratory-measured porosity and permeability, are not readily apparent and appear to be complicated by the internal pore architecture coupled with diagenetic alterations and a multiscale fracture network. Additionally, there is a significant shift in measured sonic velocity relative to values calculated from empirically derived equations that are applicable to conventional carbonates. Deviations

from expected quantitative data trends can be partially explained through qualitative observations of the pore types and internal pore geometries. Visual observations show how diagenesis can increase the complexity of the internal pore network by non-systematically subdividing the pores. When correlated to facies, the internal pore geometry partially clarifies deviations to expected relationships between quantitative pore architecture measurements, porosity, and permeability. Although there is an added level of complexity in the pore architecture of carbonate mudrocks, this study shows there are fundamental relationships that exist between the pore architecture, pore shape, porosity, permeability, acoustic response, facies, and sequence stratigraphic framework with variable levels of predictability that, when used as an integrated data set, can be used to enhance the predictability of key petrophysical properties within these types of reservoir systems.

INTRODUCTION

Over the last decade, unconventional low porosity and low permeability resources have taken a prominent place in oil and gas exploration. This change in focus for exploration and reservoir development has created a need to better understand shale and mudrock depositional environments and their reservoir characteristics. Much of the research on shale and mudrock reservoirs has been focused on siliciclastic shale and mudrocks such as the Barnett Shale in the Fort Worth Basin and the Utica Shale in the Appalachian Basin (e.g., Davies et al., 1991; Dorsch, 1995; Dewhurst et al., 1999; Reed and Loucks, 2007; Ruppel and Loucks, 2008; Loucks et al., 2009; Nelson, 2009; Slatt and O'Neal, 2011). There are also limited studies published on the pore architecture in carbonate and calcareous mudstones or chalk deposits, primarily related to the Eagle Ford and Niobrara Formations (e.g., Loucks and Rowe, 2014; Loucks, et. al., 2014; Michaels and Budd, 2014; Abouelresh, 2015). This research will add to the knowledge bank and

provide insight into how the pore architecture found in carbonate and calcareous mudstone systems relates to key petrophysical properties.

Previous research on carbonate muds has focused on describing the constituents to differentiate depositional environments (e.g., Ginsburg, 1956; Gischler et al., 2013), correlation with flow rate and carbonate mud deposition (Schieber et al., 2013), understanding diagenetic processes (e.g., Andrews, 1991; Rude and Aller, 1991), the role of diagenesis as it relates to the acoustic response of deep sea carbonate (e.g., Dae-Choul et al., 1985; Grützner and Mienert, 1999), and early diagenesis related to lithification of carbonate muds (e.g., Bathurst, 1970; Dix and Nelson, 2006).

The midcontinent "Mississippi Lime" play is a suitable candidate to add as a case study for better understanding the deposition and petrophysical properties of an unconventional carbonate mudrock reservoir. The Mississippi Lime play, which extends throughout north-central Oklahoma and southern Kansas, has seen oil and gas production from vertical wells for more than 50 years. However, the Mississippi Lime has recently seen a revival in production through advances in horizontal drilling technology. With this renewed interest, it is increasingly important to understand the complexity of this reservoir system to target the most hydrocarbon productive intervals. To accomplish this, it is necessary to understand the fundamental depositional and petrophysical characteristics beginning with the fundamental properties of the pore system scale (nanometer to millimeter), prior to upscaling to the larger reservoir scale (meter to decameter).

One application of understanding the pore architecture in a reservoir system is to enhance the predictability of reservoir properties that influence the feasibility of development and use of that reservoir. This is true for the extraction of hydrocarbons, use as a potable water system, or use as carbon dioxide (CO_2) storage. The dominant pore types in conventional

carbonates that contain significant macroporosity (256–4 mm diameter) and mesoporosity (62 µm–4 mm) are well understood and can be easily described with relation to facies, depositional environments, diagenesis, and reservoir properties (Archie, 1952; Folk, 1959; Dunham, 1962; Choquette and Pray, 1970; Embry and Klovan, 1971; Lucia, 1983, 1995).

With the exception of a couple of authors (e.g., Loucks et al., 2012; Milliken, 2014), the current literature is markedly absent of successful and applicable descriptive methodologies and observations for carbonate mudrock reservoirs that contain significant microporosity (62.5–1 µm) and nanoporosity (1 µm–1 nm). Although the use of established terminology for macropore systems is logical, this does not always accurately describe the pore architecture (pore size, shape, and distribution) or the relationship to either depositional environments or predictable diagenetic processes. Therefore, at this point of mudrock research it is prudent to continue to add observations regarding the applicability of using conventional terminology to describe siliciclastic mudrocks or conventional carbonate systems as well as denote cases where the conventional terminology is unable to accurately portray observations from carbonate mudrocks. The research presented in this chapter has utilized an integrated methodology where the pore architecture is quantitatively and qualitatively described from photomicrographs that identify general and unique characteristics (pore size distribution and pore shape) to better understand how the variability at the micro- to nanometer pore scale is related to key petrophysical properties such as porosity, permeability, and the sonic velocity response.

A fundamental relationship between pore type and permeability in carbonates has been documented (Lucia, 1999) and can be applied through a variety of methods (density–neutron log analysis and sonic velocity–porosity relationship(Eberli et al., 2003)) to predict the porosity and permeability along a borehole. When facies analysis and sequence stratigraphy can be related to the pore architecture, it becomes possible to predict porosity and permeability on the

reservoir scale in three dimensions (Grammer et al., 2004). Although it is logical to assume that the same relationships that exist in conventional macropore systems also exist in unconventional carbonate mudrocks, the fundamental pore architecture remains poorly described because, until recently, documentation of the basic carbonate mudrock pore types has not been a primary focus of mudrock research. For this reason, relationships between pore type, porosity, permeability, and pore architecture are also undefined.

Understanding the fundamental carbonate mudrock pore architecture and how this relates to other reservoir properties can have a significant impact on reservoir development within the Mississippi Lime play and also provide an analog for other carbonate mudrock reservoirs. One component of this characterization is the distribution of the pore sizes and pore network to understand how micro- to nanopores impact permeability.

The focus of the research presented in this chapter is to document the pore architecture of mud-dominated facies within a core that has proven reservoir quality. The pore architecture has been described both qualitatively and quantitatively in such a way that it can be integrated into subsequent detailed analysis that further increase the predictability of petrophysical properties in similar carbonate mudrock systems through a better understanding of the fundamental relationship between pore architecture, porosity, permeability, and facies and sequence stratigraphic framework. The primary goal is to provide a first-order descriptive classification of carbonate mudrock pore architecture using the Mississippian Lime play as a case study through the following objectives:

(1) Quantitatively describe the pore architecture from the key measurements obtained from digital image analysis of photomicrographs obtained using light microscopy (LM) and a scanning electron microscope (SEM).

(2) Qualitatively describe the pore types as observed in thin-section and higher magnifications using a scanning electron microscope.

(3) Identify facies associated with unique depositional environments to define a sequence stratigraphic framework for the data set.

(4) Characterize fundamental relationships between quantitative pore architecture data, porosity, permeability, and the facies and sequence stratigraphic framework.

(5) Identify the overall relationship between compressional velocity and porosity in carbonate mudrocks to determine potential use as a predictive tool in carbonate mudrock systems.

GEOLOGIC BACKGROUND

During the Mississippian Period, present-day southern North America was covered by a shallow, tropical, epeiric sea that established a broad carbonate depositional system (Gutschick and Sandberg, 1983). Paleogeographic reconstruction indicates the present-day midcontinent United States straddled the paleoequator during this time, which placed most of North American within 5–30^{o} north or south of the equator (Lane and De Keyser, 1980; Gutschick and Sandberg, 1983; Scotese et al., 1999). The Mississippian was a transitional time period with global climate shifting from greenhouse to icehouse conditions (Gutschick and Sandberg, 1983; Buggisch et al., 2008; Haq and Schutter, 2008;). Paleozoic sea level curves show the Mississippian Period experienced an overall regression throughout this transition period (Vail et al., 1977; Haq and Schutter, 2008; Snedden and Liu, 2010). It is agreed that at least two major marine transgressions occurred in the midcontinent area during the Mississippian Period, one during the Late Visean (Meramecian) stage and one during the Serpukhovian (Chesterian) stage (Curtis and Champlin, 1959; Kump and Arthur, 1999; Saltzman, 2002; Saltzman et al., 2004; Buggisch et al., 2008; Kammer and Matchen, 2008). Additionally, oxygen and carbon isotope

data indicate the Tournasian (Kinderhookian) and Serpukhovian (Chesterian) experienced either two major cooling periods (Buggisch et al., 2008) or extensive exposure and weathering of the carbonate platform that can be regionally correlated (Kump and Arthur, 1999; Saltzman, 2002).

Depositional Environments

Deposition at the beginning of the Mississippian Period in the midcontinent occurred primarily in quiet environments with several areas protected by scattered, low-relief islands close to sea level or extending slightly above sea level that were likely planed remnants of the Devonian Woodford shale (Curtis and Champlin, 1959). This relatively quiet environment encouraged carbonate muds and carbonate oozes to accumulate below wave base, while above wave base ooids and skeletal carbonate sands formed and marine biota thrived. The major depositional environments that existed in the midcontinent area varied from high-energy nearshore beaches, sand shoals, and tidal complexes to aerially extensive, lower energy and sheltered mid-ramp and outer-ramp mud and ooze deposition with localized bioherms, reefs, and muddy lagoons (Curtis and Chapman, 1959).

The regional tectonic regime resulted in continuous changes to both the regional and localized basin geometries throughout the Mississippian Period that continue to be studied from outcrop and subsurface data sets to better understand both regional and local basin geometries throughout the midcontinent area (Watney et al., 2001; Mazzullo et al., 2009, 2011; Mazzullo, 2011; Boardman et al., 2013a,b; Grammer et al., 2013; Morris et al., 2013; LeBlanc, 2014; Price, 2014). This regional tectonic regime created large structural features, such as the Nemaha Ridge and Ozark Uplift, that locally impacted the rates of siliciclastic deposition mixed with the carbonate deposition and also affected the subsidence rates resulting in sub-basins that had locally restricted depositional environments (Curtis and Champlin, 1959; Meckel et al., 1992; Robin et al., 2011). Therefore, although regional facies maps (e.g., Gutschick and Sandberg,

1983) provide a regional perspective of depositional environments, specific correlations require high-resolution analysis of core and/or outcrop.

Midcontinent Mississippi Lime Play

Although the Mississippian Lime play has been producing oil and gas from vertical wells for over 50 years, the internal stratigraphy and reservoir petrophysical characteristics are poorly understood (Mazzullo, 2011). In general, the Mississippi Lime play is an unconventional carbonate reservoir with low porosity (<10%) and low permeability (<1.0 mD), where oil and gas production is assumed to be through a combined micro- to macropore system coupled with an extensive fracture network (Camargo and Fons, 1965). Continued development of this play makes it critical to understand reservoir controls to better predict intervals with the best reservoir quality. This research will contribute to understanding potential governing dynamics of these systems by qualitatively and quantitatively describing the pore architecture as observed in thin sections and using an SEM, and integrating these observations with a high-resolution sequence stratigraphic architecture and laboratory-measured sonic velocity response.

Mineralogy

Although the Mississippian Lime is overall a carbonate play, deposition occurred on an attached ramp system where local topographic variations resulted in significant, albeit episodic contributions of terrestrial (siliciclastic) material. Siliciclastic material was introduced from the underlying Devonian shale during transgressive phases, and through mixed deposition from localized topographic highs. In addition to partial mixed depositional systems, some diagenetic processes have resulted in mixed mineralogy of preserved depositional environments, primarily as a result of partial to complete silicification of facies. Therefore, it is important to understand the present-day bulk composition when interpreting the results and correlation to specific facies.

Determining the bulk mineralogy and identifying occasionally occurring minerals observed in thin section and SEM are important for two primary reasons. First, the extent of the mixed deposition could affect the potential diagenetic alterations and resultant pore architecture observed today. Second, the resultant bulk composition that is observed today could have had a significant impact on the relationships observed between the pore architecture, velocity response, porosity, and permeability.

METHODS

Data Set

Data used in this study were obtained from core plugs, whole core analysis, and thin sections. Data include laboratory-measured porosity and permeability, thin-section and SEM photomicrographs, digital image analysis of the photomicrographs, laboratory-measured velocity response, and analysis of the high-resolution sequence stratigraphic framework. Data available, but not emphasized in this research, include wireline logs, oil and water saturation data, and FMI logs. As applicable, qualitative data (visual observations) are integrated with quantitative data.

The core utilized for this research has nearly 90 m (~280 ft) of Mississippian age strata preserved from Osage County, Oklahoma (Figure II-1). The present-day burial depth of the Mississippian at this location is approximately 954 m (3130 ft). During deposition this core was located in a basin east of the Nemaha Uplift and West of the Ozark Dome in north-central Oklahoma, at approximately 20–30° south of the paleoequator. The core was selected because of the preservation of predominately low-energy, carbonate mud-rich facies with micro- to nanopores and proven reservoir quality based on verbal confirmation of oil production from an offset, vertical well. As a single, mud-dominated core, it is only representative of low-energy depositional environments, likely in a distal location relative to the shoreline, in moderately

restricted marine conditions. Characterization of the pore architecture using this core should provide useful data that can be applied to the interpretation of core from more proximal environments that also have a significant amount of micro- to nanoporosity.

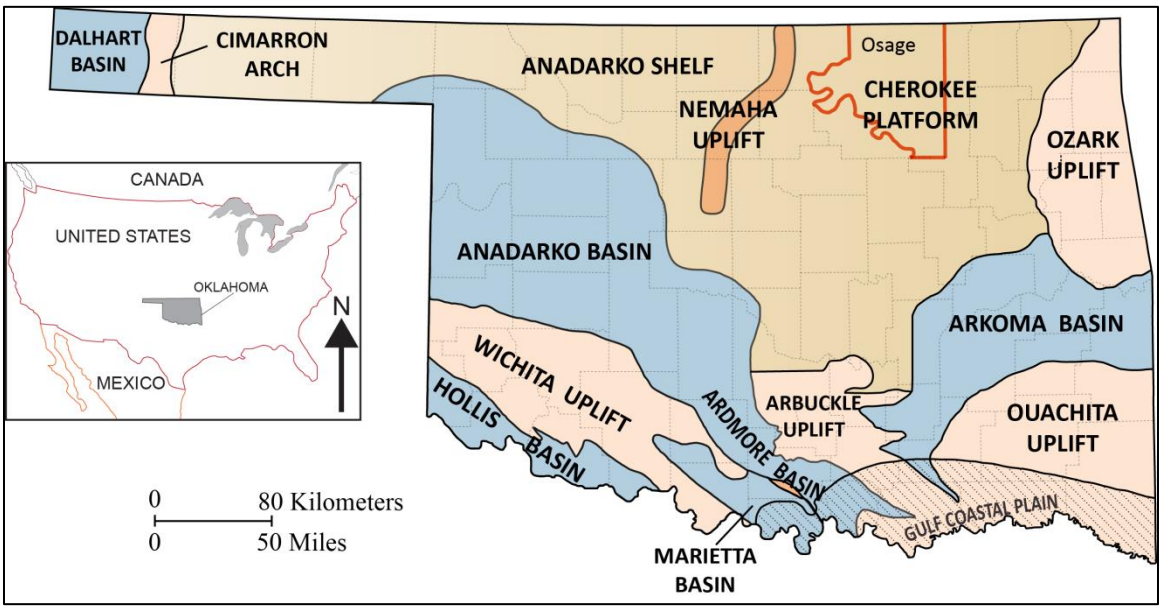

Figure II-1. *The core used in this study is from western Osage County (outlined in red) in north-central Oklahoma. The Nemaha Uplift and Ozark Uplift are two major structural features that were active during the Mississippian Period and therefore likely had an impact on deposition in north-central and north-east Oklahoma throughout the Mississippian Period. The core used in this study is located in the western side of Osage County. Figure modified from Northcut and Campbell (1996).*

Facies Analysis

Facies were identified from visual observations of a single core and associated thin sections. The cored section is nearly continuous through the Mississippian section except for the upper 2–3 m (7–10 ft) beneath the Pennsylvanian contact, approximately 20 m (70 ft) above the underlying Devonian contact, and 10 m (32 ft) near the middle of the cored interval that was unrecoverable because of drilling complications. The contact with the overlying Pennsylvanian and underlying Devonian sections were identified from the distinct gamma-ray log signatures. Facies were divided based on differences in texture, sedimentary structures, composition, and

bioturbation. Facies analysis using the Dunham classification (Dunham, 1962) and interpretation of depositional environments were utilized to create an idealized facies stacking pattern, which in turn was used as the foundation for developing the sequence stratigraphic framework (Loucks and Sarg, 1993; Read, 1995; Emery and Myers, 1996; Catuneanu, 2006).

Facies colors are labeled according to the closest match from the GSA Rock-Color Chart using standard methods of color identification (Munsell, 1995). Trace fossils were identified using the *SEPM Short Course Notes 59: Applied Ichnology* collection of papers (MacEachern et al., 2009). The level of bioturbation was based on the methodology described by Miller and Smail (1997) that uses visual observations to semiquantify bioturbation based on the density of the bioturbation as related to the level of disruption to original bedding features. Bioturbation ranges from 1 to 6 where a level 1 has no visible bioturbation, and level 6 has bedding that is nearly or completely homogenized (Miller and Smail, 1997).

Mineralogy

To better understand the present-day composition of each identified facies, bulk mineralogy was analyzed using x-ray diffraction (XRD). The analysis was performed on a select number of samples representative of each identified facies. Samples were powdered by using a SPEX ball mill. XRD analysis was performed using a Philips PW3020 powder x-ray diffractometer run at a voltage of 45 kV, current of 40 mA, and calibrated with a quartz sample. Results were analyzed and matched to the most likely element using Xpert HighScore desktop software.

A secondary method of identifying the elemental composition of samples, or areas of interest within the sample set, is to use an energy dispersive x-ray spectroscopy (EDX) coupled with SEM analysis. The EDX provides a spectrum output report similar to what is reported for XRD analysis that shows the identified elemental composition of the local spot under analysis.

Sonic Velocity (Acoustic Response)

In carbonates with predominately macro- to mesopores, the relationship between porosity and the compressional sonic velocity response (V_P) has a clear inverse relationship that can be approximated by the Wyllie time average equation (Figure II-2) (Anselmetti et al., 1997; Eberli et al., 2003). Within this relationship, the scatter in the data, specifically deviations from the fundamental relationship between sonic velocity (V_P) and porosity, are related primarily to the dominant macropore type (Figure II-2) with very minimal effects observed from slight changes in mineralogy (Anselmetti and Eberli, 1993; Anselmetti et al., 1997). Understanding how the dominant pore type affects the sonic velocity (V_P) response in carbonates provides qualitative information about the relative permeability (Anselmetti and Eberli, 1993, 1999; Anselmetti et al., 1997, 1998). For example, at the same total porosity, a sample with intergranular porosity will typically have a slower sonic velocity (V_P) than a sample with moldic porosity because of the difference in connectivity of the pores and the effect on the bulk modulus of the sample. Because there is typically greater connectivity of the pores in intergranular samples, which indicates a higher permeability, it can be stated that generally if the sonic velocity (V_P) response is lower than expected, the permeability is relatively higher than in locations where the sonic velocity (V_P) is as predicted by the Wyllie time average equation and vice versa.

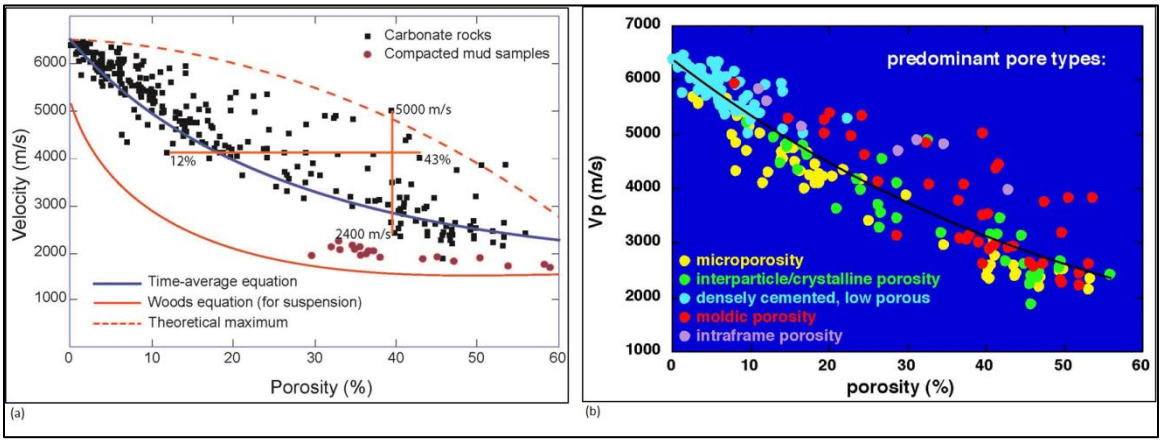

Figure II-2. *(a) The relationship between velocity and velocity in conventional carbonates with*

visible macroporosity has a predictable inverse relationship that can be approximated by the Wyllie time-average equation (blue line). The compacted mud samples, shown as red circles, have a relationship approximated by the Woods equation (red line) indicating less rigidity in the mud samples. Although there is a level of predictability in this data set, there is also a significant amount of scatter in the velocity at equal porosities and in the porosity for a given velocity (Anselmetti and Eberli, 1993; Grammer et al., 2004). (b) A plot of the same velocity and porosity data based on the predominant pore type shows the scatter in the data are a result of different elastic properties resultant from the primary pore type (Eberli, 2003; Grammer et al., 2004). (From Grammer et al., 2004, AAPG © [1999], reprinted by permission of the AAPG whose permission is required for further use).

It has been shown that the percentage of microporosity in a carbonate with predominantly macropores affects the sonic velocity (V_P) response by altering the bulk modulus and elastic properties of the rock (Baechle et al., 2008a). The result of increasing microporosity results in a slower sonic velocity (V_P) for a given porosity that are shown to be more consistent with values predicted using the Wyllie time-average equation (Baechle et al., 2008b). However, examples of how the different bulk modulus and elastic properties of a carbonate mudrock affect the sonic velocity (V_P) response for carbonate mudrocks, where the pores are predominately micro- to picopore size with little to no influence from macroporosity, is currently uncertain.

Acoustic response (compressional and shear) for this study was measured using core plugs selected to represent large variations in porosity for a given permeability and large variations in permeability for given porosities. The acoustic response was measured using an AutoLab 1000 from New England Research, Inc. that records the travel time through core plugs for one compressional wave (V_P) and two shear waves (V_S) using affixed transducers and receivers. The plugs were measured under dry, unsaturated conditions, then saturated in a 35 ppt NaCl brine solution, and re-analyzed. To measure the sonic velocity response, the plugs were placed in a rubber jacket and mounted between a transducer and receiver. The samples were placed inside a chamber filled with mineral oil that allows for adjustments of the external confining pressure to simulate burial conditions at multiple depths. The internal pore pressure

can also be adjusted to simulate various burial conditions using a liquid with the same concentration used to saturate the samples. For this study, the pore pressure was held constant at 3 MPa and the confining pressure was adjusted to simulate an effective pressure from 2 to 30 MPa, which represents variation from approximately 200 to 3000 m burial under normal hydrostatic pressure gradients of approximately 0.45 psi/ft or 10.20 KPa/m. For comparison purposes, the data reported are the sonic velocity (V_P) response at an effective pressure of 20 MPa, which correlates with a burial of approximately 2000 m, and assumes a normal formation pressure (not overpressured or underpressured) and a normal lithostatic gradient.

Microscopy

The 2-D pore architecture was captured through a series of photomicrographs using a Leica DM 2700P optical microscope or LM, and an FEI Quanta 600F field emission SEM to view pores from the macro- to nanoscale. Thin sections were impregnated with a blue epoxy, mounted onto 1 × 3-inch slides, polished to approximately 20–30 µm thickness, and viewed with the LM. Using proprietary software distributed by Leica for use with their equipment, photomicrographs were captured and analyzed to represent the dominant pore types observed in the samples. Pores observed in thin section can be accurately characterized quantitatively to approximately 0.5 µm diameter at a 40× magnification. Although the software program will output data for “pores” identified below this size, using the LM, these data are assumed to be an artifact of the software programming code and are therefore excluded from the data set. Pores with a diameter below this size are best quantified and observed using the SEM, which can view pores ranging in size from the mesopore category (3 mm) to picopores category (>1 nm) (Figure II-3).

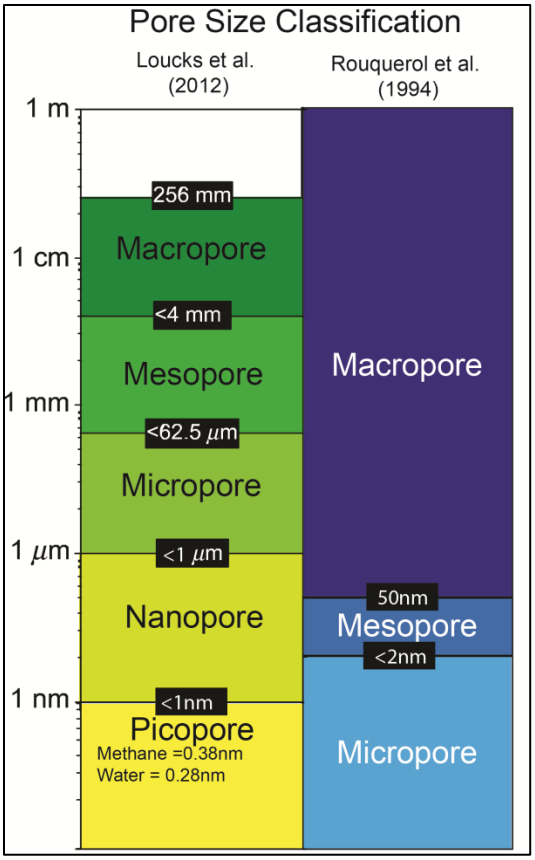

Figure II-3. *A commonly used classification of pore sizes, shown right in blue, had a wide range of values for the macropore classification, a small range of values for the mesopore classification, and defines micropores as any pores smaller than 2 nm. The classification scheme used to define pore sizes in this study is the one proposed by Loucks et al. (2012), shown in the yellow—green color scheme. This classification scheme provides a more uniform distribution of pore sizes and also introduces the category of nanopore and picopore. Use of the more evenly distributed Loucks et al. (2012) classification scheme should allow for more accurate prediction of pore size contribution to permeability. (Modified from Loucks et al., 2012 (AAPG ©[2012], reprinted by permission of the AAPG whose permission is required for further use.)*

Previous studies have shown that topographical features in fine-grained rocks that are common artifacts from standard polishing methods often produce images of artificial pores resulting from plucking of grains during the polishing (Pittman, 1992; Sondergeld et al., 2010; Loucks et al., 2012). To minimize the number of artifacts imaged, SEM photomicrographs were obtained using rock chips that were polished using a JEOL IB-19500CP cross section polisher argon ion mill. The use of an ion milling machine provides a more pristine polished surface that allows for greater confidence in quantification of the pores and more accurate observations of

the spatial distribution of the pores. One limitation of the argon mill used in this study is that the polished surface is limited to approximately a 2-mm area. However, because the sizes of the pores are primarily in the micro to nanoscale range, there is adequate coverage of each sample to observe the characteristic pore architecture. All samples polished with the ion mill were sputter-coated with gold/palladium for 20 seconds using a Balzers MED 010 sputter coater after being held under a vacuum for at least 2 hours.

Pore Classification

The primary goal in classifying the pore characteristics is to understand the fundamental features that correlate with permeability. The approach used to describe conventional carbonate pore geometry recognized the need to relate the classification to the texture (Archie, 1952; Dunham, 1962; Folk, 1962) and pore type (Choquette and Pray, 1970; Lucia, 1983, 1995) in such a way that the depositional environment and some diagenetic information could be inferred. For example, a conventional carbonate sample with moldic porosity can be assumed to have relatively large pores that typically have moderate to poor connectivity, whereas a sample with intergranular or interparticle porosity can be assumed to have moderate to excellent connectivity of the pores. Because of the obvious benefit of describing pore types in a manner that can infer pore connectivity (permeability), and even ideally be associated with specific types of depositional environments, the terminology utilized for conventional carbonates will be applied to the extent possible when describing the mudrock pore architecture. However, where the application of this terminology to carbonate mudrocks does not accurately relay the spatial distribution and connectivity of the pores, additional descriptive terminology will be included. Because a standard set of terminology for carbonate mudrock pore types is not currently in use, it is important at this stage of describing carbonate mudrock pore types to include qualitative as well as quantitative descriptions to relay a similar level of detail regarding the texture,

composition, and pore geometry of the pore architecture to help interpret potential relationships between the pore architecture and petrophysical properties such as porosity and permeability.

A key description in mudrock pore architecture is the size of the pores. Pore classification schemes for mudrocks have been proposed by Rouquerol et al. (1994) and Loucks et al. (2012). Rouquerol et al. (1994) propose the terms micropore for pores with a width less than 2 nm, mesopore for pores with widths 2–50 nm, and macropores for anything with a width larger than 50 nm. Loucks et al. (2012) have suggested a size classification scheme for mudrocks based on the measured width that further separates these terms into macro-, meso-, micro-, nano-, and picopore (Figure II-3). The classification grouping proposed by Loucks et al. (2012) has primarily been used in this study. To identify additional detail within the major classification groups, this study has used additional discretization to reveal otherwise muted trends and patterns. Data are initially grouped based on the primary classification scheme and are also plotted based on a log scale to show subtle variability of the pore size distribution within each major category. The additional discretization allows for observations to aid correlation of pore size distribution to porosity and permeability that might otherwise go unnoticed.

Digital Image Analysis (Quantitative Characterization)

The primary goal of digital image analysis is to quantify the pore architecture to identify key features that relate the pore architecture with permeability within the data set. Digital image analysis provides quantitative characteristics of the pore architecture identified via color segmentation from thin-section and SEM photomicrographs (Anselmetti et al., 1998). Color segmentation identifies pores based on differences in the hue (red, brown, and blue), chroma (saturation), and value (lightness) in the photomicrograph. The identified pores are measured for several parameters, including the pore perimeter, pore area, pore length, and pore width. By

quantifying the pore architecture, numerical attributes can be plotted in a multitude of ways and are used as input to statistical algorithms to identify the key characteristics that describe the architecture and relate the pore characteristics to other petrophysical properties. Although this initial step of quantitative characterization of the pore architecture is focused on analysis from a 2-D data set, the information provides a baseline of the average, and total distribution of the pore size and pore throat sizes. These data can be related to additional research that includes 3-D evaluations of the pore architecture to identify any bias or limitations based on conclusions from a 2-D sample set.

Using thin-section and SEM photomicrographs, quantitative measurements of the pores were documented for each identified pore in the photo using an image analysis program. As an oil and gas play, some of the pores are filled with the impregnated blue epoxy and some are filled with a trapped organic (oil) substance and therefore appear black in thin section. It is assumed that this organic (oil) substance is trapped by hydrostatic conditions and has the potential to become mobile at reservoir conditions. This assumption is based on confirmation that an adjacent well that targeted the Mississippian section is oil-productive. Compositional analysis of the organic matter was beyond the scope of this work, which focuses primarily on the characterization of the pore architecture. Future 3-D analysis, and possibly 4-D analysis showing fluid flow through selected core plugs, will be able to further elaborate on the potential for this material to move, or be moved, through the pore network. To encompass the complete pore architecture, pores quantified as part of this study include pore space that is observed as blue from the impregnated epoxy and black because of the presence of trapped organic (oil) material. Image analysis data were extracted using proprietary software available through the Leica Corporation (LAS Application Suite with Image Analysis Module). The software was created for seamless use with the Leica microscopes, but is also able to analyze imported images, such

as the SEM photomicrographs. The software also allows for user input to identify the correct color threshold of interest and allows editing of several features, including pixel size limits and the addition or exclusion of specific areas of the image. One key factor that was applied to all thin-section photomicrographs was the base diameter/length/width measurement of 0.1 μm, which was further filtered to a cut-off value of 0.5 μm based on the smallest length measurement that could be identified at a 40× magnification.

Morphology

The pore morphology is described based on visual observations from the LM and SEM photomicrographs. Visual and graphical observations attempt to show fundamental relationships that exist within carbonate mudrock pore systems in the Mississippi Lime data set to aid understanding the relationship between pore architecture and reservoir quality (i.e., permeability). As feasible, similarities identified in the pore morphology are related to the facies and sequence stratigraphic framework.

RESULTS

Facies Descriptions

Seven facies were identified using a base model hypothesis that the overall depositional environment was on an attached, gently dipping ramp with deposition shallowing from below storm wave base to below fair weather wave base. Environments of deposition were divided into distal and proximal outer ramp, middle ramp, inner ramp, and restricted lagoon. Subtle variations in environments were identified by grain size, texture, bedding features, skeletal content, degree of bioturbation, and both type and diversity of trace fossils (Table II-1). Environments identified include three below the storm wave base: outer ramp, distal middle ramp, and proximal to distal middle ramp environments; and three below the fair weather wave base: proximal to distal inner ramp, proximal inner ramp, and restricted muddy lagoon (Figure II-

4). Each of the facies shows evidence of influence from storm deposition with occasional beds of skeletal debris and occasional, isolated skeletal debris found within each facies.

Facies Number	Depositional Environment	Bedding Features	Other Comments	Munsell Color	Bioturbation Index	Primary Type of Bioturbation	Visible Skeletal Content	Primary skeletal components
1	outer ramp environment below storm wave base	laminated to planar bedded spiculitic mudstone to wackestone	skeletal debris occurs in thin (1cm) beds as well as scattered throughout the laminated matrix	N2, 5Y 6/1	1		0-10%	crinoid
2	distal middle ramp below storm weather wave base	mudstone to skeletal wackestone with 1-6cm thick nodular bedding		N2, 5Y 6/1, N5, N4	2-3	*Planolites*	0-5%	crinoid
3	proximal to distal middle ramp below storm weather wave base with intermittent storm deposition. Redeposited ooids and peloids with other skeletal debris	massive to hummocky bedded peloidal-skeletal-ooid wackestone to mud-lean packstone (storm layers)	large (>10cm) pale yellowish brown (10YR 6/12), and light olive gray (5Y 5/2) filled burrows	N2, 10YR 6/12, 5Y 5/2	3	*Thalassinoides*	0-5%	crinoid, brachiopod
4a	proximal middle ramp below storm weather wave base	skeletal-peloidal wackestones	partially mottled appearance of light olive gray (5Y 6/1), olive gray (5Y 3/2, black (N2) and medium light gray (N6) .	5Y 6/1, 5Y 3/2, N2, N6	2	*Cosmorhaphe*	0-10%	crinoid, brachiopod
4b	proximal middle ramp below storm weather wave base	skeletal-peloidal wackestones	partially mottled appearance of light olive gray (5Y 6/1), olive gray (5Y 3/2, black (N2) and medium light gray (N6) .	5Y 6/1, 5Y 3/2, N2, N6	3	*Planolites, Cosmorhaphe, Chondrites*	0-10%	crinoid, brachiopod
5	proximal middle to inner ramp in slightly more shallow water than Facies 4 or possibly in water that has better circulation	Minor relict horizontal, wavy bedding is preserved in some intervals.		N7, 5Y 6/1, 5Y 4/1	5			
6	proximal inner ramp near fair weather wave base	skeletal-peloidal wackestones	differentiated from Facies 4 and Facies 5 by the diversity of trace fossils and inferred change in environment through restriction of biota	5Y 6/1 to 5Y 4/1 matrix, 5Y 7/2	2-3	*Zoophycos*	0-10%	crinoid, brachiopod
7	restricted, muddy lagoon environment	mudstone to skeletal wackestone with wavy to lenticular bedding	occasional skeletal debris visible in thin section only.	5Y 7/2, N2	2-3		0-5%	

Table II-1. *A summary of key features that distinguish each facies identified in the core used in this study.*

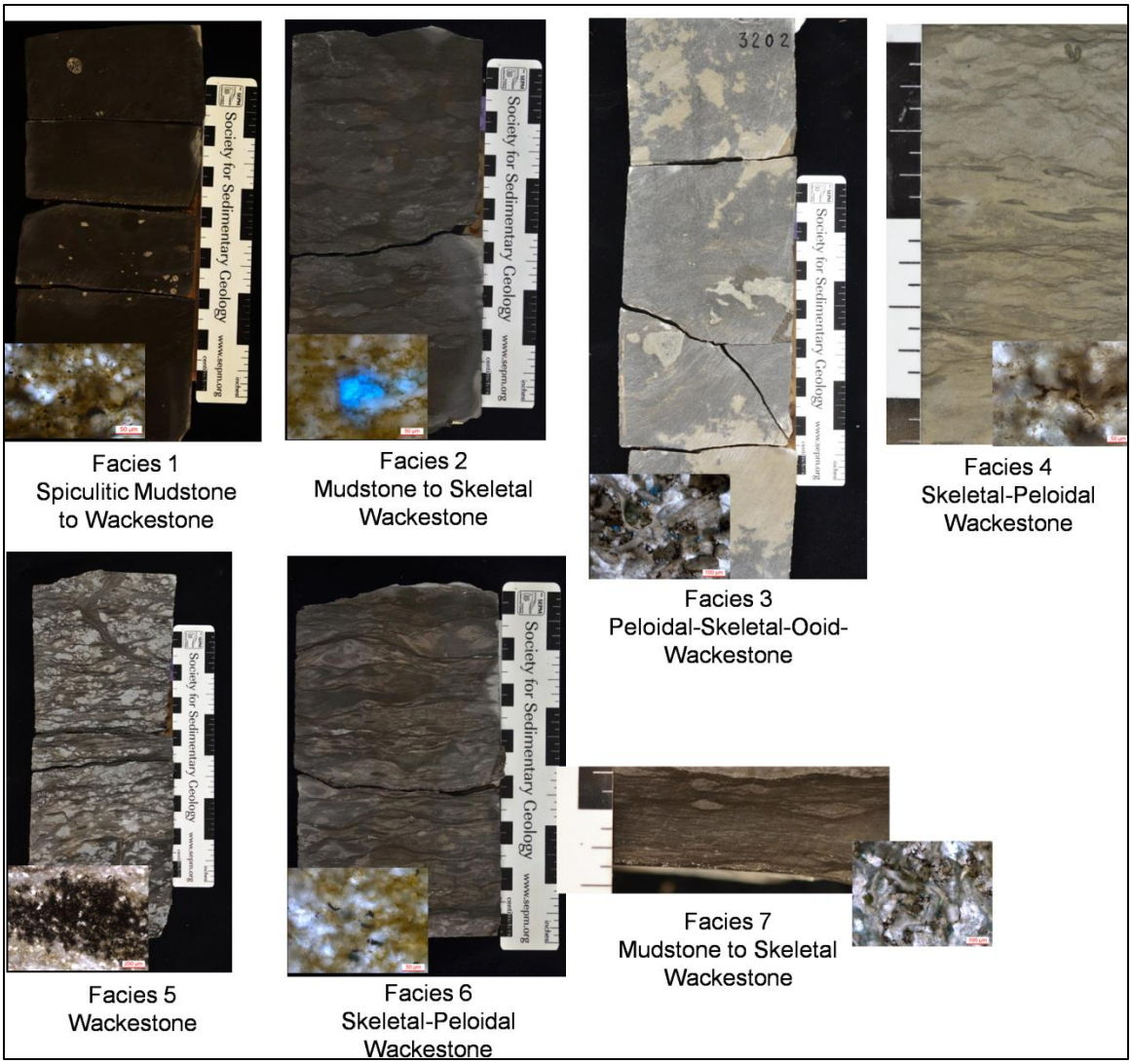

Figure II-4. *Facies were described based on visual observations from core and thin sections. Seven facies were identified based on differences in texture, color, composition, and type/intensity of bioturbation. See Table II-1 for key features used to identify the facies and depositional environment.*

A simple block diagram (Figure II-5) showing the relative spatial distribution of each depositional environment was utilized to place the facies into an idealized shallowing upward stacking pattern following principles of Walther's Law. The idealized stacking pattern was used as a foundation to identify the sequence stratigraphic framework.

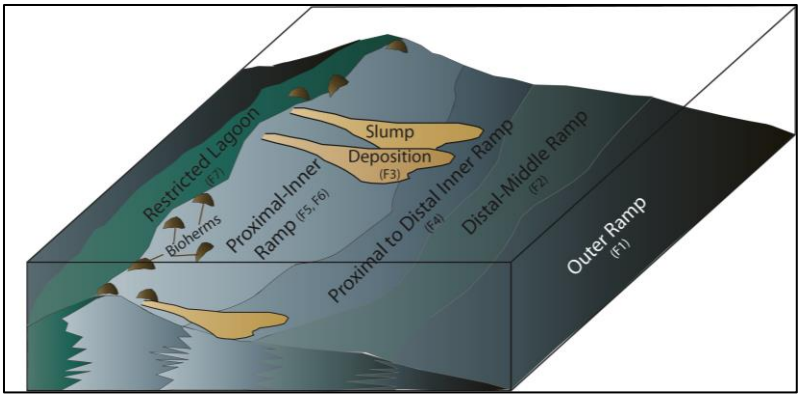

Figure II-5. *Block diagram showing generalized relationship of depositional environments and proposed lateral relationships assuming a carbonate ramp system with sub-basin topography.*

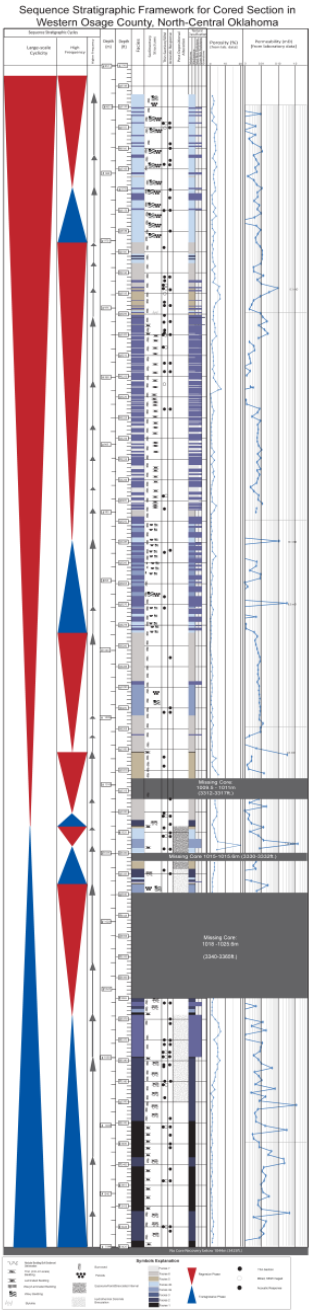

Sequence Stratigraphic Framework

Based on the identified facies, there is one large sequence with two higher order frequency sequences identified in the cored interval (Figure II-6). Because biostratigraphic analysis has not been completed on this core, the exact time intervals cannot be certain. However, at least one major unconformity exists based on evidence of exposure with karsting, solution collapse brecciation, and caliche deposits observed in core (Figure II-7).

Figure II-6. *Based on observations in core and thin section, the facies were placed into an idealized shallowing upward stacking pattern that was used as a foundation to establish the sequence stratigraphic framework. One large, probable third-order sequence is identified to exist over the entire length of the core and at least six fourth-order cycles are identified within the cored interval. Higher frequency fifth-order sequences are identified with gray arrows.*

Figure II-7. *Examples of exposure that indicate the area experienced a significant period of aerial exposure. Features observed include infiltrated sediment and karst breccias (a) as well as a 1-cm-thick caliche horizon (b).*

The cored interval used for this study represents a thickness of approximately 90 m (278 ft), which, based on facies relationships corresponds to a third-order sequence, with six higher frequency fourth-order high-frequency sequences (HFS) identified. The third-order sequence shows slight asymmetry with a longer transgressive phase than regressive phase. Assuming the missing basal section of the core is a continuation of the transgressive phase, the section is still overall regressive although more symmetrical than depicted in Figure II-6. The higher frequency fourth-order HFS's vary in thickness from approximately 5 to 30 m (14–94 ft) and show diverse asymmetry in the transgressive and regressive phase throughout the core (Figure II-6). In general, the system gradually becomes more regressive toward the top of the section. Some of the asymmetry observed in the fourth-order HFS's is likely because of variations in the local sub-

basin specific geometry, sediment supply, water circulation, and subsidence rates throughout the Mississippian Period. The fifth-order HFS's show patterns of facies thickening upward within each fourth-order HFS. The most notable exception to this pattern is observed in the fourth-order HFS package that terminates at the top of the exposure interval.

Mineralogy

The mineralogy of select samples indicates the primary constituents are calcite (11–44%), silicates (49–100%), and minerals that are diagenetically related to carbonate and dolomite (e.g., ankerite–dolomite group: $Ca(Fe, Mg, Mn)(CO_3)_2$). Thin-section and SEM analyses also indicate the presence of framboidal pyrite, partial pore-filling kaolinite cement with organized and randomly oriented platy, book-like growth, and smectite, montmorillonite, or a mixed layer illite/smectite with a ribbonlike texture and draped, grain-coated appearance.

Syn-depositional marine cementation of both silt and sand-sized grain-rich carbonates creates a rigid framework and the potential for early porosity occlusion or preservation (Bathurst, 1970; Grammer et al., 1999). Early to syn-depositional cementation in carbonates typically prevents any obvious correlation between petrophysical properties with burial depth or age. This is applicable to conventional carbonates as well as carbonate mudrocks where porosity and pore throat size do not correlate well with depth or burial age (Bathurst, 1970; Schlager et al., 1985, 1988; Dix and Nelson, 2006). Because there is mixed mineralogy within the data set with 49–100% silicate composition, it is useful to determine if there are correlations between porosity, permeability, or pore shape with depth.

Basic depth plots show that porosity, permeability, and pore shape do not show predictable correlations with depth (Figure II-8). The highest porosity values are at approximately 975.4 m (3200 ft) near the top of the cored interval, as well as approximately 1028.7 m (3375 ft) near the base of the cored interval. The highest permeability corresponds to

one of the high porosity peaks at 1028.7 m (3200 ft) with all other values showing no obvious trend with depth.

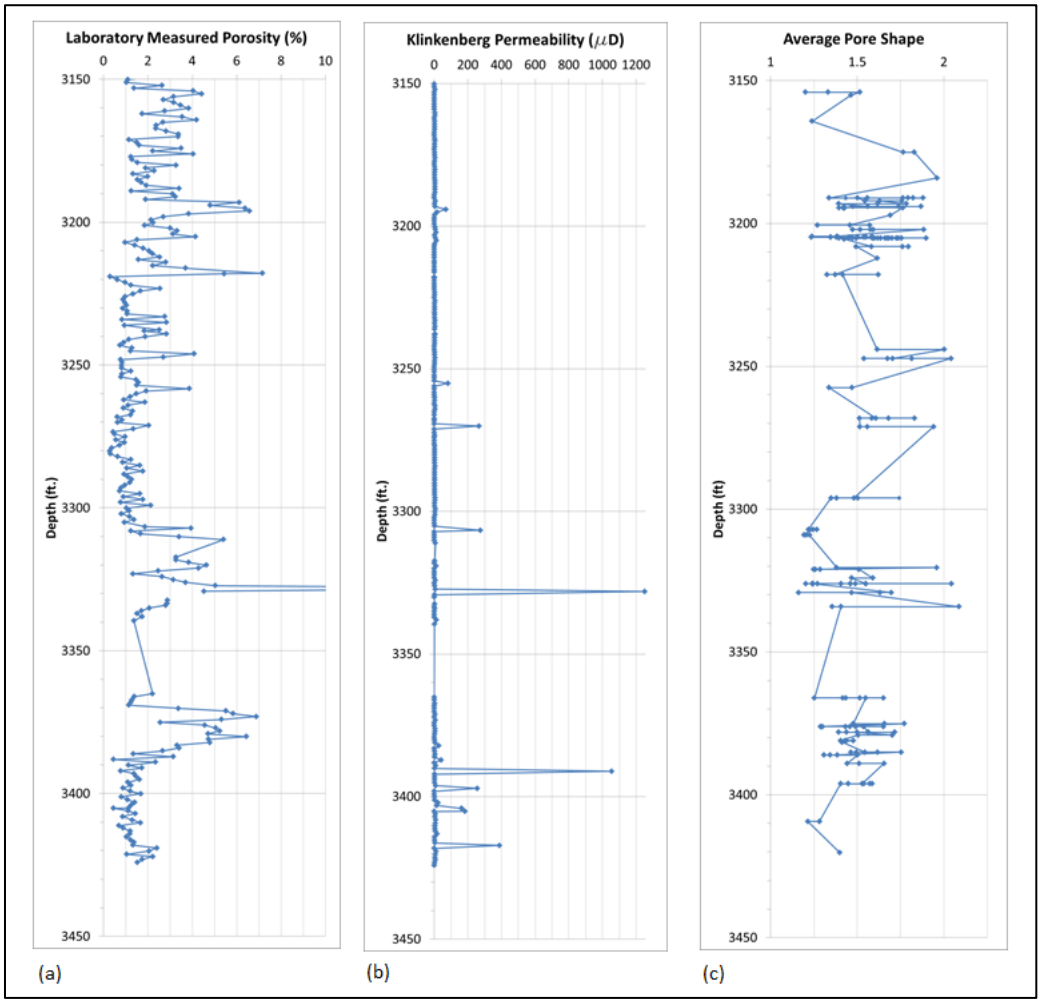

Figure II-8. *Even though bulk mineralogy shows the data set has mixed mineralogy, the fundamental depositional characteristics and postdepositional diagentic features of the data set are in agreement with other conventional carbonate systems. The lack of obvious predictability between porosity (a), permeability (b), and pore shape (c) with depth support the application of conventional carbonate interpertation methods to understand the relationships between petrophsyical properties in carbonate mudrocks.*

A lack of correlation between depth and porosity, permeability, or pore shape (Figure II-8) provides support for the assumption the original composition was primarily carbonate (calcite or dolomite) similar to what is precipitated in modern, tropical, carbonate environments (like on the Great Bahama Bank) (e.g., Ginsburg, 1956; Gischler et al., 2013). If the original depositional

environment was primarily from terrestrial input with original silicate composition, some type of correlation with depth resulting from burial pressure would be expected. For example, in a terrestrial, silicate-dominated lithology, pressure resulting from burial would likely alter the pore shape from more spherical at deposition to gradually more elongate as the grains become compacted. However, because of rapid lithification within a carbonate system, the burial pressure has little to no influence in altering the pore shape. Primary alterations result from diagenetic precipitation or dissolution processes.

The lack of any correlation with depth supports the assumption that the depositional system is more closely aligned with a carbonate-dominated system where predictable relationships with depth are not apparent. Therefore it can be assumed that the fundamental behavior governing carbonate deposition and diagenesis is also applicable to this carbonate mudrock reservoir system, and the comparison of data trends from conventional carbonates is appropriate and should be applicable to help identify basic relationships and trends in carbonate mudrock data (Figure II-8).

The high percentage of silicate composition identified in the bulk mineralogy, along with textural evidence, implies the majority of the section has undergone diagenetic alteration with significant replacement of the carbonate minerals by silicate minerals. Identification of the specific diagenetic processes and source of the silica is outside the scope of this chapter. However, whether the diagenesis occurred during early or late burial, or from contact with meteoric water, recognizing extensive diagenesis has occurred can assist the interpretation of relationships identified or obscured between the pore architecture, porosity, and permeability. In this study, it is noted that precipitation of clay minerals in the pores is associated with the relatively larger intergranular and interparticle pores, whereas the growth of well-defined quartz and calcite crystals is associated with the relatively smaller matrix or intergranular pores.

This association partially explains differences in the porosity–permeability relationship, and the relationship between pore shape and porosity is discussed in the following sections.

Sonic Velocity

The sonic velocity response measured from a representative set of samples from each facies, and with variable-measured porosity and permeability values, indicates there is an inverse relationship between the acoustic response and porosity (Figure II-9). This relationship is similar to the inverse relationship observed in conventional carbonates with predominantly macropore architecture (Figure II-2a, II-b) where the highest porosity values correlate to the lowest acoustic response and the lowest porosity values correlate with the highest acoustic response (Anselmetti and Eberli, 1993; Anselmetti et al., 1997; Eberli et al., 2003).

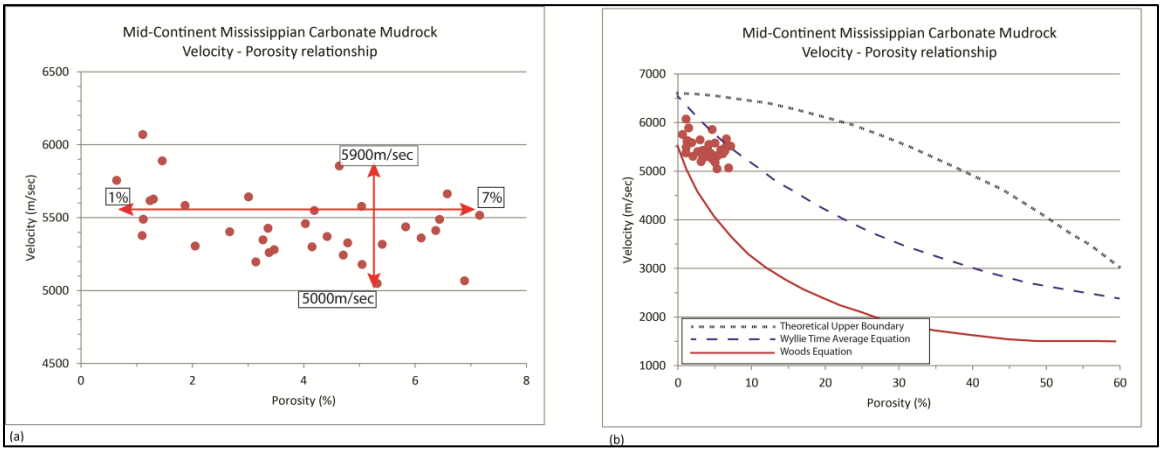

Figure II-9. *(a)The velocity–porosity relationship in the current data set shows an inverse relationship, similar to what is observed in carbonates with primarily macroporosity (see Figure* II-*2). (b) When the data are plotted on a larger porosity and velocity scale and compared to the Wyllie time-average equation, Woods equation, and maximum value applicable to macropore carbonates, a clear shift in the carbonate mudrock data is apparent. Based on this data set, the Wyllie time-average equation (center dashed line) is an upper boundary and the Woods equation (bottom solid line) is a lower boundary when using velocity to predict porosity in carbonate mudrocks.*

When the data from this study are plotted using a similar porosity and sonic (compressional) velocity scale used to plot the conventional carbonate relationship, a significant shift in the acoustic response data is identified (Figure II-9b). For low porosity values, the

predicted acoustic response based on macropore carbonates is between 5500 and 7000 m/sec (Anselmetti and Eberli, 1993, Anselmetti et al., 1997). However, the actual sonic (compressional) velocity (V_P) is between 4800 and 6500 m/sec, which is approximately 500–1000 m/sec slower than predicted. This shift in the data, where data points plot between the Woods equation and the Wyllie time-average equation, instead of plotting more closely with the Wyllie time-average equation, is likely because of the complexity in the pore architecture present in carbonate mudrocks when compared with conventional, macropore-dominated carbonates (Anselmetti et al., 1998), as well as the diagenetic alteration where some samples are partially to completely silicified.

Digital Image Analysis (Quantified Pore Characteristics)

Image analysis was completed using 305 photomicrographs where 140,330 pores were identified. The number of photomicrographs used for each sample varied based on data available and complexity of the pore types and pore sizes observed. For each identified pore, the key measured parameters reported include the pore length, width, pore shape, and perimeter/area values. A summary of the data used and generated in this study were compiled based on sample identification and facies type (Tables II-2, II-3). Contract laboratory-measured porosity, permeability, and grain density are included to compare pore architecture features measured with image analysis to standard laboratory measurements on core plugs.

DATA SUMMARY			Contract Laboratory Measured Porosity for sample sub-set			Average data values for sample set used in this study					Summary of Primary Image Analysis Measurements							Velocity Response	
Facies	Number of photos analyzed	Number of Pores Identified	Minimun (%)	Average (%)	Maximum (%)	Air Permeability (mD)	Klinkenberg Permeability (mD)	Grain Density	Sw %	So %	Image Analysis Porosity (%)	Minimum Length (µm)	Maximum Length - (µm)	Average Length (µm)	Minimum Width (µm)	Maximum Width (µm)	Average Width (µm)	Average Pore Shape (μm^2)	Vp (m/sec)	VS_{avg} (m/sec)
1	43	3983	1.10	2.34	4.71	0.0118	0.0057	2.64	39.0	1.5	32.68%	0.002	239.70	3.94	0.002	119.03	2.20	1.48	5276-5750	3109-3563
2	34	12235	1.34	2.47	4.73	0.0093	0.0043	2.64	41.0	1.0	65.28%	0.007	625.84	9.47	0.007	346.80	5.36	1.47	5314-5777	3262-3514
3	72	18102	0.62	2.98	5.23	0.0055	0.0024	2.69	37.4	4.2	41.46%	0.007	1122.97	11.40	0.003	198.17	5.53	1.53	4852-6496	2941-3700
4	40	34173	0.90	3.29	4.53	0.0075	0.0031	2.68	34.0	1.3	25.78%	0.001	375.04	4.87	0.0004	149.82	2.76	1.46	5479-5902	3224-3814
5	20	38183	1.66	3.81	4.81	0.0415	0.0283	2.67	36.5	1.8	60.54%	0.0007	617.06	4.82	0.0004	276.74	2.75	1.47	5777-6333	3361-3514
6	33	18566	3.23	4.81	6.11	0.0074	0.0029	2.69	36.0	4.0	23.51%	0.002	194.41	4.30	0.003	119.97	2.42	1.53	5179-5344	3180-3297
7	63	15088	1.28	3.18	7.16	0.0100	0.0048	2.70	40.4	2.4	35.02%	0.002	229.08	6.07	0.006	98.60	3.23	1.60	4852-5384	2768-3203
Summary:	305	140330	0.62	3.27	7.16	0.0133	0.0074	2.67	38	2	40.61%	0.007 (nanopore)	1122.97 (mesopore)	6.41 (nanopore)	0.0004 (picopore)	346.80 (micropore)	3.46 (micropores)	1.506 slightly elongate	4852-6333 Vp/Vs ratio: ~2.0 +/- 0.2	2768-3700

Table II-***2.*** *A summary of the data used in this study organized by facies.*

Basic Statistics			Contract Laboratory Analysis from whole core and 25mm diameter (1-inch) plugs					Summary of Primary Image Analysis Measurements								Velocity Response	
Facies	Number of samples	Pores Counted	Air Perm (mD)	Klinkenberg Perm (mD)	Porosity %	Grain Density (g/cc)	Photomicrograph Source	Measured Porosity	Minimum Length	Maximum Length	Average Length	Minimum Width	Maximum Width	Average Width	Average Pore Shape	Perimeter/Area	Vp	Vs
1	13	324	0.003	0.001	4.71	2.67	SEM	0.26%	0.004	2.69	0.22	0.00	1.38	0.10	1.50	0.25	5750	3355
1	1	399	0.003	0.001	4.71	2.67	LM	13.68%	1.943	239.70	10.59	0.73	106.13	6.05	1.70	0.61	5276	3297
1	2	137	0.014	0.007	1.30	2.65	LM	1.85%	1.032	35.15	5.51	0.50	19.97	3.06	1.25	0.89	5510	3109
1	10	987	0.017	0.008	1.10	2.61	SEM	0.25%	0.002	2.69	0.07	0.00	0.72	0.03	1.40	0.66		
1	13	630	0.017	0.008	1.10	2.61	SEM	0.16%	0.009	1.88	0.13	0.00	0.43	0.06	1.45	0.39	5462	3563
1	4	1506	0.017	0.008	1.10	2.61	LM	16.48%	1.275	196.20	7.12	0.55	119.03	3.92	1.58	0.56	5384	3293
2	10	652	0.004	0.002	1.34	2.60	SEM	0.09%	0.007	1.55	0.19	0.01	0.78	0.08	1.50	0.24	5777	3514
2	3	1525	0.004	0.002	1.34	2.60	LM	7.87%	1.498	167.73	7.51	0.73	60.67	4.17	1.56	0.75		
2	3	304	0.005	0.002	2.81	2.65	LM	3.64%	3.183	160.06	19.08	1.07	126.86	11.43	1.62	0.62		
2	4	903	0.010	0.004	4.73	2.61	LM	8.35%	0.637	148.51	5.36	0.50	85.85	2.98	1.44	0.45	5353	3479
2	5	998	0.010	0.005	2.67	2.61	LM	7.45%	1.044	100.40	4.33	0.50	46.39	2.32	1.57	1.23	5653	3488
2	1	521	0.014	0.007	2.56	2.61	LM	15.44%	0.729	114.39	4.64	0.50	55.49	2.23	1.40	0.92	5314	3262
2	3	1149	0.018	0.009	2.35	2.77	LM	16.37%	2.560	625.84	11.04	1.09	329.03	6.00	1.54	0.61		
2	1	223	n/a	n/a	n/a	n/a	LM	1.98%	3.400	131.14	13.46	1.46	81.60	7.76	1.41	0.49		
2	4	5960	n/a	n/a	n/a	n/a	LM	23.53%	4.533	591.44	19.60	2.43	346.80	11.29	1.43	0.32		
3	3	319	0.000	0.000	2.04	2.63	LM	3.59%	2.914	163.04	14.59	1.62	81.11	7.80	1.67	0.49		
3	6	1786	0.000	0.000	1.39	2.67	LM	3.47%	1.174	42.80	3.70	0.51	24.73	2.18	1.47	1.47	6496	3466
3	12	799	0.001	0.000	4.03	2.74	SEM	0.25%	0.007	2.63	0.35	0.00	1.56	0.17	1.52	0.18	4852	2768
3	2	22	0.001	0.000	4.03	2.74	LM	1.98%	4.787	90.63	23.21	3.46	49.15	12.91	1.27	0.23	5750	3355
3	3	4045	0.001	0.000	2.56	2.64	LM	10.83%	0.951	154.58	3.20	0.50	71.48	1.76	1.63	1.37	5819	3700
3	5	601	0.001	0.000	0.62	2.61	LM	1.41%	2.210	55.88	6.86	1.14	29.53	3.95	1.64	1.27		
3	1	215	0.002	0.001	2.53	2.75	LM	5.45%	1.700	93.74	9.43	0.97	70.67	5.47	1.62	0.64	5829	3232
3	3	435	0.006	0.002	1.89	2.70	LM	3.47%	3.440	520.56	21.63	1.86	64.68	6.73	1.64	0.67		
3	3	151	0.008	0.003	2.54	2.74	LM	2.56%	1.255	56.38	7.94	0.73	23.19	3.89	1.44	0.80	5725	3290
3	5	302	0.008	0.004	5.23	2.66	SEM	0.21%	0.016	8.90	0.19	0.01	0.67	0.08	1.50	0.37		
3	5	2738	0.008	0.004	5.23	2.66	LM	8.77%	1.749	281.42	9.47	0.73	131.24	4.93	1.54	0.50	5179	3283
3	1	255	0.008	0.004	1.99	2.72	LM	3.20%	10.686	1122.97	41.01	4.86	198.17	14.93	1.96	0.30		
3	8	2931	0.011	0.005	4.56	2.65	LM	5.75%	1.852	161.03	8.64	0.88	81.98	5.02	1.43	0.51	5613	3428
3	5	527	0.022	0.011	3.01	2.69	LM	2.70%	3.934	118.37	16.21	1.89	63.48	9.26	1.61	0.47	5251	2941
3	1	495	n/a	n/a	n/a	n/a	LM	9.56%	1.700	141.59	10.27	0.73	72.61	5.56	1.42	0.68		
3	5	1668	n/a	n/a	n/a	n/a	LM	12.45%	2.089	443.75	12.30	0.92	192.29	6.09	1.49	0.41		
3	2	670	n/a	n/a	n/a	n/a	LM	6.55%	2.125	154.09	7.79	0.91	94.05	4.21	1.40	0.68		
3	2	143	n/a	n/a	n/a	n/a	LM	3.92%	2.914	114.87	8.29	1.34	70.19	4.64	1.31	0.35		
4	8	469	0.005	0.001	4.42	2.82	SEM	0.34%	0.012	3.13	0.22	0.00	1.13	0.10	1.46	0.28		
4	2	371	0.006	0.002	2.22	2.72	LM	3.20%	2.671	139.40	8.68	1.21	54.89	4.71	1.80	0.83	5479	3224
4	8	587	0.007	0.003	3.70	2.58	SEM	0.39%	0.001	11.52	0.46	0.00	3.21	0.25	1.24	0.27		
4	10	29461	0.007	0.003	3.70	2.58	LM	6.07%	2.926	375.04	9.26	1.74	149.82	5.05	1.47	1.08		
4	1	350	0.007	0.003	4.19	2.83	LM	10.69%	0.50	153.97	0.78	0.50	84.39	0.55	1.24	0.14	5687	3383
4	4	1489	0.008	0.003	4.53	2.65	LM	6.03%	1.457	97.87	5.57	0.82	54.76	3.25	1.49	1.06	5902	3814
4	5	794	0.009	0.004	0.90	2.65	LM	3.94%	2.356	74.51	10.01	1.34	46.60	5.91	1.49	0.67	5742	3342
4	2	652	0.013	0.006	2.63	2.63	LM	6.15%	1.154	48.15	3.98	0.55	35.82	2.36	1.53	1.45		
5	4	33890	0.001	0.000	1.66	2.59	LM	4.60%	0.50	91.53	0.29	0.50	47.11	0.60	1.20	2.10		
5	4	2848	0.003	0.001	3.94	2.58	LM	2.04%	0.50	56.65	1.08	0.50	32.60	0.63	1.24	1.45		
5	1	228	0.003	0.001	3.84	2.60	LM	5.75%	2.429	106.13	9.37	1.21	69.94	5.35	1.69	0.66	6333	3361
5	8	320	0.100	0.070	4.81	2.79	SEM	0.07%	0.001	4.13	0.24	0.00	1.32	0.11	1.48	0.16		
5	3	897	0.100	0.070	4.81	2.79	LM	22.29%	2.226	617.06	12.34	1.09	276.74	6.94	1.72	0.49	5777	3514
6	7	1429	0.002	0.001	4.29	2.65	SEM	0.36%	0.002	12.55	0.99	0.00	7.06	0.45	1.51	0.24	5276	3297
6	3	13297	0.002	0.001	4.29	2.65	LM	3.40%	0.50	48.53	0.58	0.50	30.32	0.54	1.26	1.89		
6	11	881	0.010	0.004	6.11	2.72	SEM	0.11%	0.003	2.79	0.22	0.00	1.50	0.10	1.39	0.31	5179	3283
6	2	2059	0.010	0.004	6.11	2.72	LM	13.28%	2.550	794.41	9.91	1.09	119.97	5.68	1.70	0.71		
6	8	754	0.013	0.006	3.23	2.72	LM	2.82%	2.262	56.15	8.54	1.09	29.26	4.71	1.64	1.13	5344	3180
6	2	346	n/a	n/a	n/a	n/a	LM	3.55%	1.032	61.69	5.56	1.02	32.91	3.01	1.67	1.03		
7	9	3034	0.002	0.001	7.16	2.75	SEM	0.09%	0.002	5.35	0.47	0.01	2.61	0.23	1.42	0.23	5364	3203
7	6	326	0.004	0.001	1.41	2.68	SEM	0.05%	0.008	9.03	0.74	0.01	3.17	0.33	1.49	0.11	5364	3203
7	3	516	0.004	0.001	1.41	2.68	LM	4.68%	1.174	71.68	6.51	0.53	47.88	3.66	1.71	1.00		
7	5	2049	0.005	0.002	2.69	2.70	LM	4.90%	2.574	189.31	8.41	1.29	56.95	4.30	1.76	1.29		
7	2	312	0.007	0.003	1.28	2.67	LM	3.02%	0.911	52.34	4.04	0.50	25.74	2.32	1.81	1.60		
7	10	458	0.024	0.013	4.15	2.69	SEM	0.13%	0.009	2.81	0.29	0.01	1.40	0.12	1.59	0.34		
7	14	3489	0.024	0.013	4.15	2.69	LM	5.83%	2.663	196.27	10.96	1.11	64.04	6.01	1.65	0.81	4852	2768
7	7	2754	n/a	n/a	n/a	n/a	LM	9.98%	1.041	106.77	6.60	0.50	78.65	3.70	1.51	1.04		
7	7	2150	n/a	n/a	n/a	n/a	LM	6.33%	3.521	229.98	16.42	1.54	98.60	8.39	1.43	0.69		

Table II-3. *Digital image analysis results summarized by sample identification and listed by facies. The contract laboratory data were provided with access to the cored section. Primary image analysis measurements included are measurements used to portray fundamental relationships between the carbonate mudrock pore architecture and porosity and/or permeability. The parameters found to be most useful are included in the table. Additional measured features not used in this study are noted in the text.*

Pore Types and Morphology

The characteristics of the pore architecture (shape and distribution) are only partially captured through quantitative evaluation methods. Supplemental qualitative observations can be critical when interpreting the relationship between pore architecture, porosity, and permeability (see Appendix II). For example, the maximum to minimum measured lengths, widths, or averages do not appropriately describe the internal complexity in the pore morphology. This information is best relayed through a series of visual observations from thin-section and SEM photomicrographs.

The majority of the pores identified in this study are within a small, nano- to micropore, classification size, and the overall grain size is in the clay/mud (<4 μm) to silt fraction (<63 μm). The major pore type is dissolution-enhanced intercrystalline and interparticle porosity with

some samples containing intraparticle porosity, and microfracture porosity. Two other pore types have been noted, one labeled as shrinkage pore and the other labeled as matrix pore. The shrinkage pores are defined as a highly elongate void space that is associated with a well-defined crystal or grain such that the appearance is similar to a mudcrack that has had a physical separation of the matrix from the grain, or crystal that is not due to dissolution of material. Shrinkage pores as observed in the 2-D photomicrographs are rarely connected to other pores and are not part of a fracture network. Their significance to fluid flow and permeability are expected to be negligible. A matrix pore has been defined as a void space that is not associated with any obvious grain, particle, or crystal. Identified matrix pores typically have a cross-sectional area that is in the lower micro- to nanometer scale, and unlike interparticle pores are most often observed to have an open internal flow network, where it appears there are few to no obstructions within the pore space. Occasionally, matrix pores are observed with a partial pore-filling calcite crystals, but to date have not been observed to have partial pore-filling clay cementation (Figure II-10). Although there is assumed organic material observed in SEM within the data set, there have been no observed pores within the organic material. Therefore a discussion on organic porosity is unable to be included at this stage of the research. Similar to the observations in thin section, the majority of the organics appear to be trapped fluids that are most often associated with macro- to nanometer fractures or with the interparticle porosity. Where micro- to nanometer matrix pores are predominant in the sample, any organic material is observed in close proximity to the matrix pores. As shown in Figure II-11, there is a significant amount of scatter in the data when comparing statistically calculated pore shape with porosity and permeability. One reason for the scatter can be explained by integrating qualitative observations that show the majority of the micro- to nanopores are highly nongeometric. Although standard measurements (length, width, etc.) can be measured, the measurements do

not adequately portray the true pore space. By oversimplifying the geometry of the pore space, correlation to other parameters is likely to become obscured. For this reason, data that capture both major and minor variations in the pore morphology observed in thin section (Figure II-12) and with an SEM (Figures II-13, II-14) need to be incorporated into final data interpretations.

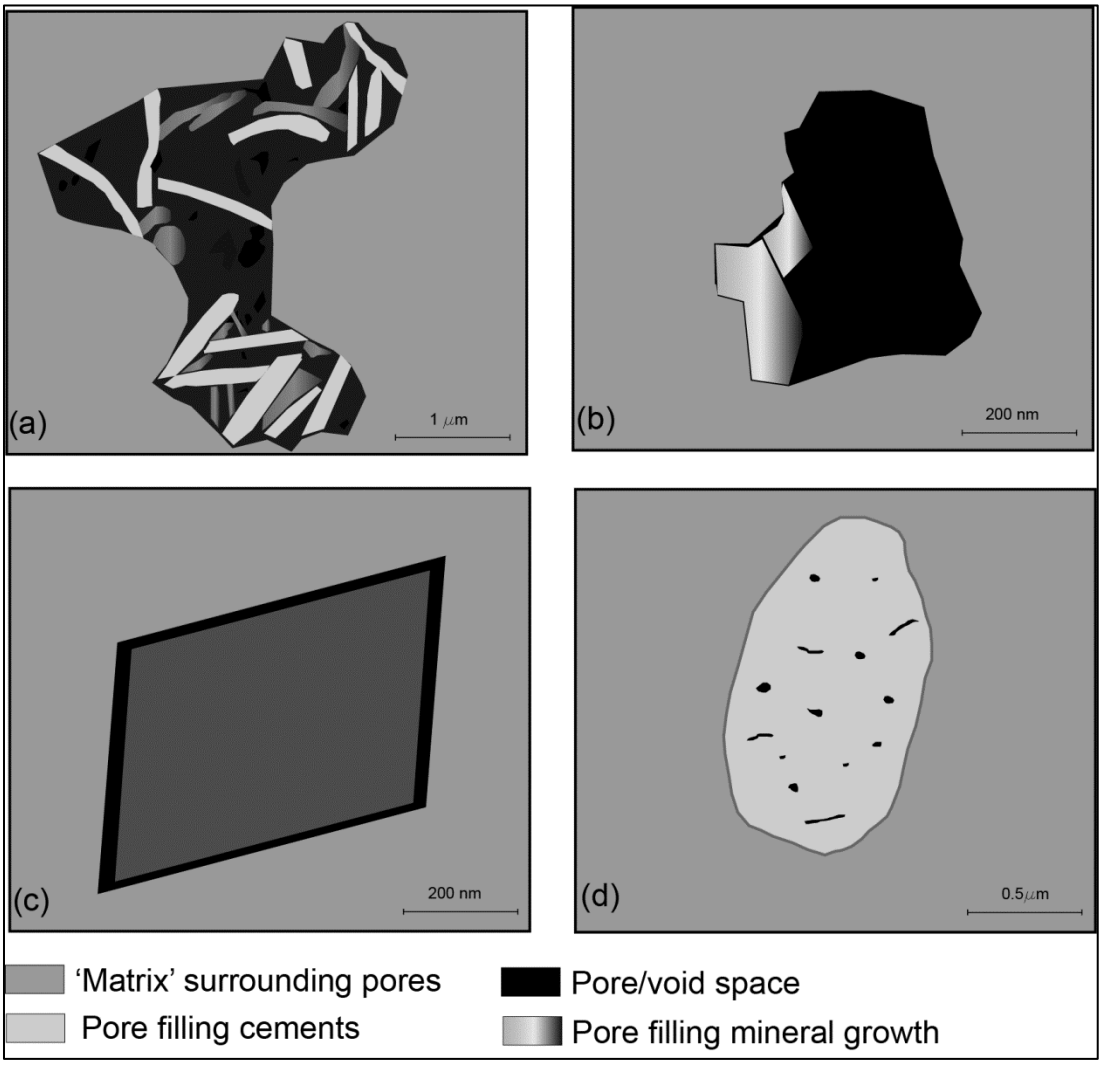

Figure II-10. *The carbonate mudrock pore types observed in this study include: intergranular/interparticle (a), matrix (b), shrinkage (c), intraparticle (d), and fracture (not pictured). Variability in the internal pore network is from precipitation of clay minerals and crystal growth within the pore space. In most of the pores observed, the internal geometry appears to have a greater control on permeability than the overall pore size. Where minerals subdivide the internal flow network, the total pore architecture becomes a system of nano- to picopore throats that connect nano- to mesopore cavities, or vugs.*

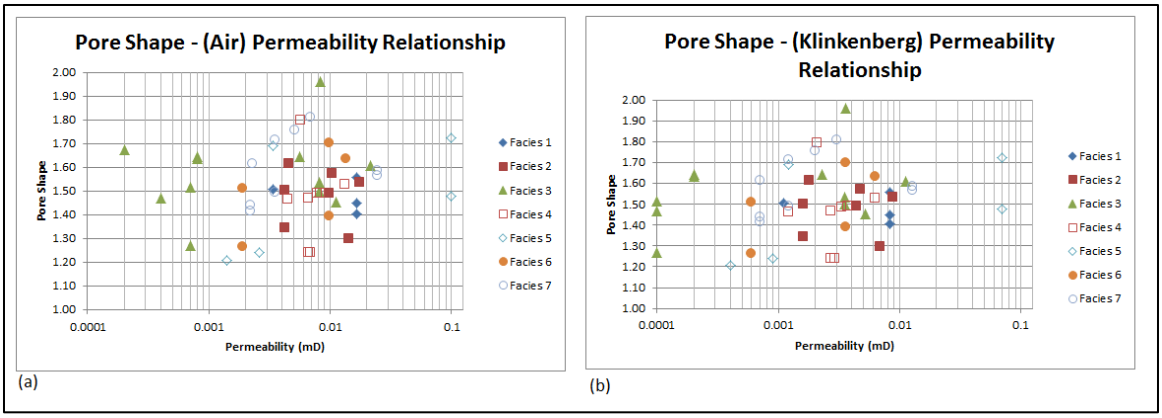

Figure II-11. *The pore shape–permeability relationship for both air permeability (a) and Klinkenberg (gas effect corrected) permeability (b) show the same overall trend. The significant difference in the two data sets is that the measured permeability value corrected for gas effects (Klinkenberg values) is approximately half the value of the air permeability value. Both graphs show an overall positive relationship with higher permeability values correlating with the more elongate pore shapes, similar to the general relationship for conventional carbonates.*

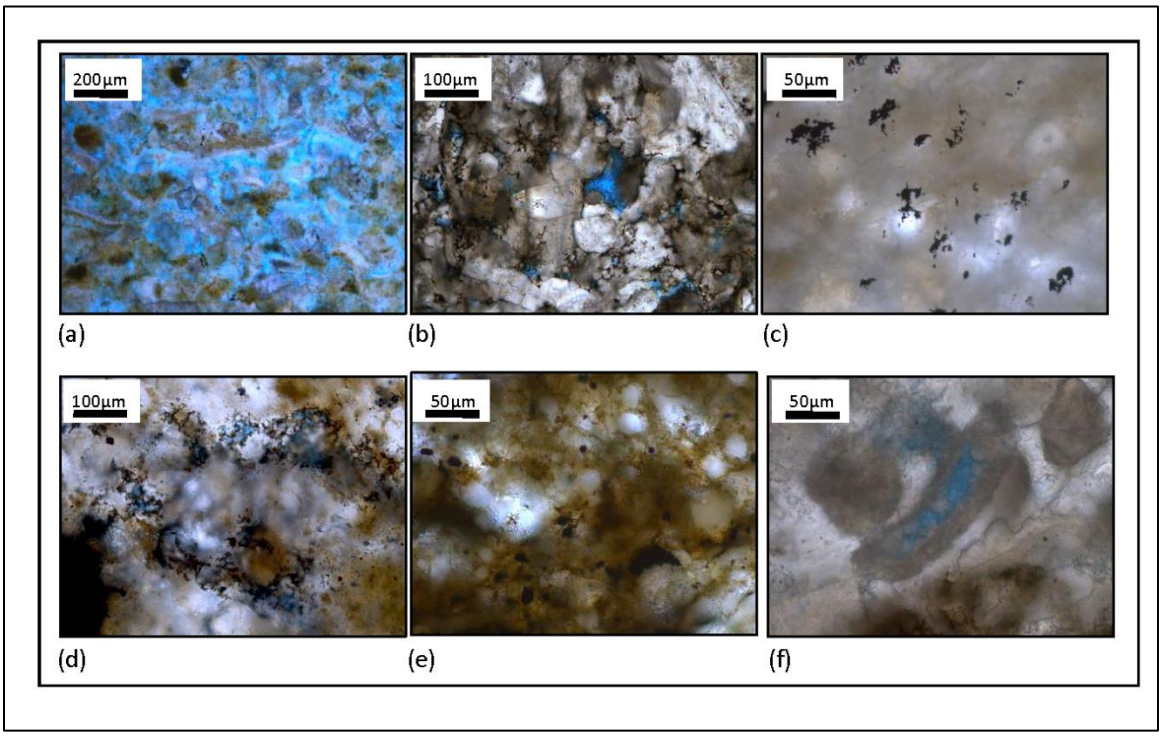

Figure II-12. *Pores observed in thin section show at least six distinct pore types and sizes. Pores in the data set are either open and well-connected as shown by the blue color (a, b, d) from an injected epoxy, or disconnected as shown by the presence of brown to black organic (oil) substance that has been trapped in the pores (b, c, d, e). The light microscope can view pores clearly to approximately 0.5 µm in size, the upper size of the nanopore group. Smaller nanopores and picoporosity are observed in thin section as brown oil-stained areas (e, f) that are typically connected to larger pores that are darker brown or black in color. Using conventional pore classification terminology, the pores are primarily intergranular/interparticle (a, b, e), intercrystalline (c), intraparticle (f), and dissolution enhanced (c, d, e).*

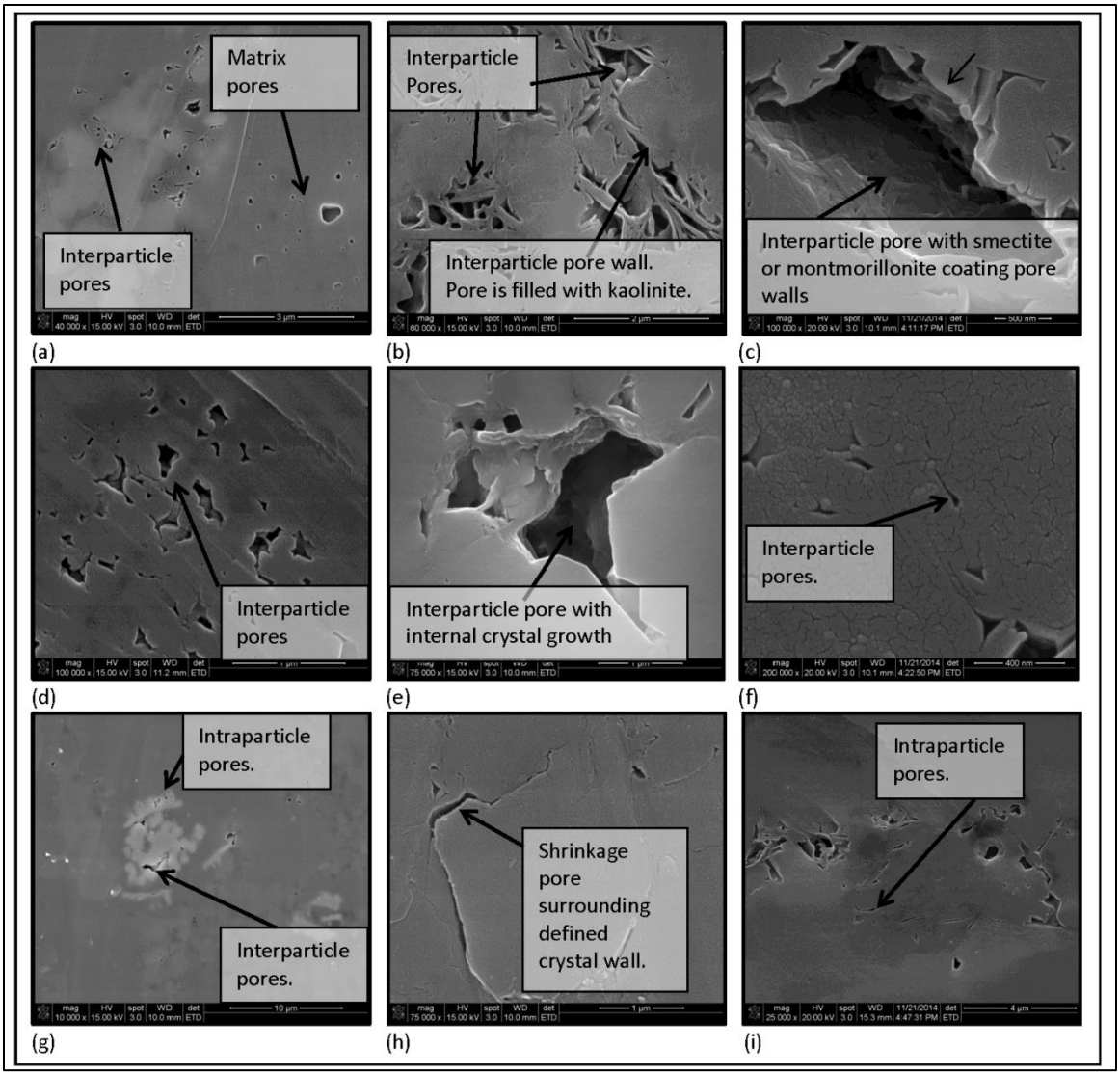

Figure II-13. *The type of pores and the connectivity is significantly different for pores located in the matrix (intercrystalline) compared with interparticle pores and pores that abut well-defined crystals. Interparticle porosity typically has a complex internal spatial network as a result of internal crystal growth and internal precipitation of clay minerals (a, b, c). Matrix, intercrystalline porosity typically has a well-defined perimeter and appears to have mostly open conduits for flow (d, e, f). Intercrystalline porosity often has internal crystal growth, or dissolution, but this is constrained to the pore walls and does not subdivide the internal pore space. Intraparticle porosity can either be morphologically similar to matrix pores with a clearly defined perimeter (g), or can have a platy, nanofracture geometry within the particle (h). Shrinkage pores have well-defined, clean pore walls with void space created between the matrix and a well-defined crystal (i).*

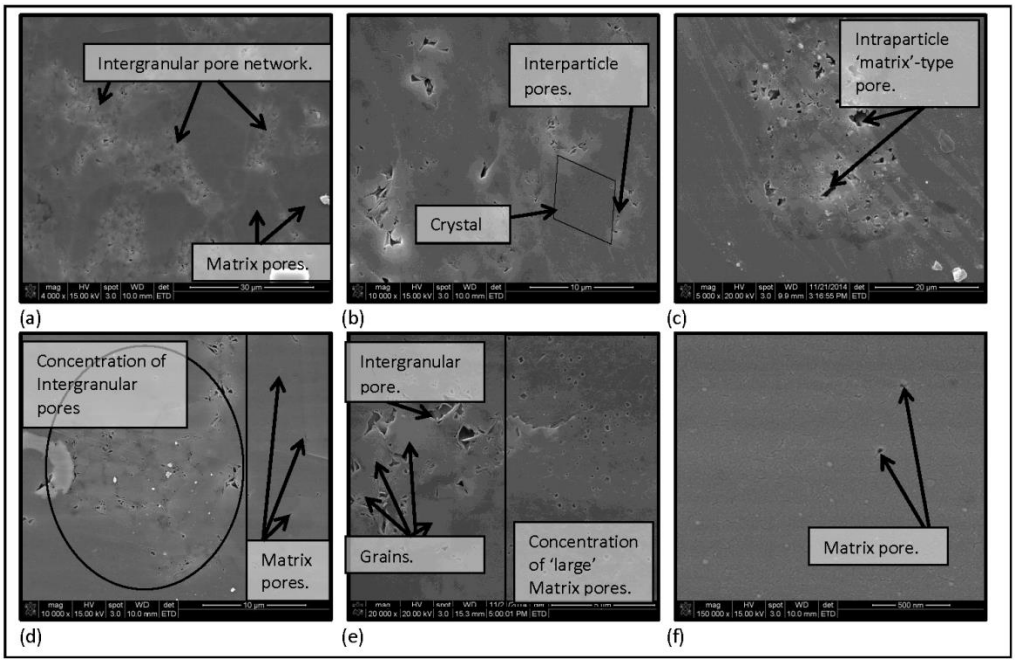

Figure II-14. *SEM photomicrographs showing the 2-D spatial distribution of the pore network. The largest pores are interparticle or intergranular with a pore network that is easily discerned at low magnifications (4,000–10,000×) as a difference in color saturation between the lighter color interparticle pore network and darker color with smaller matrix pores (a). A pore structure similar to interparticle porosity often occurs in dissolution-enhanced pores that abut clearly defined crystals within the matrix (b). Intraparticle porosity can either be closely related to interparticle porosity with significant internal clay precipitation or have matrix-type porosity with well-defined perimeters and an open internal network (c). Intergranular porosity can have a well-connected network of porosity (a, b) and can also appear to be locally concentrated (d, e). Matrix porosity has well-defined pore perimeters and is often spherical in 2-D images (e). The smallest nanopores observed are found within the matrix and have a similar distribution that can be locally concentrated (e) or widely distributed (f), but typically have simple spherical shapes and appear to have an open internal pore network.*

Pore Morphology from Thin-Section Photomicrographs

The LM used for this study is able to view large nanopores that have a length or width of at least 0.5 µm. The digital image analysis program that was utilized to analyze the photomicrographs indicated the ability to identify pores with a diameter <0.5 µm; however, confidence in accurate identification and analysis of pores with a diameter 0.5 µm seemed unreliable, and therefore a cut-off value of 0.5 µm (length or width) was applied for data used in any interpretation. The pores observed in the LM have a variety of nongeometric shapes but can

be classified generically as interparticle, intercrystalline, and intraparticle pores that have variable degrees of dissolution-enhanced pore space (Figure II-12). Most of the samples observed with the LM are filled with a trapped organic material and secondarily are open based on the in-filling with an impregnated blue epoxy. A significant amount of area has brown staining with presumed indiscernible pico- to nanopores. As observed in thin-section and SEM images, the pore types are both original and diagenetically altered, and in this location do not include significant organic porosity although the presence of trapped organics is observed.

In general, samples that are more mud-rich have poorly connected, interparticle pores that are filled with trapped organic material, and samples that are more skeletal-rich have a greater amount of open, connected pore space with odd-shaped pores related to the arrangement of the skeletal debris. The trapped organic material is primarily in the micro- to nanoscale and exists in pores that have greater tortuosity in the flow paths that ultimately lead to larger micropores with greater connectivity of the pore space or to fractures. The irregular, oval, and nongeometric pore shapes indicate there was a significant amount of dissolution enhancement prior to filing with the trapped organic material that is observed extensively in the pore space. The open interparticle pore space is primarily filled with trapped organic material, but where there is greatest connectivity, the pores are observed to have open (blue) pore space. The larger pores, and pores with trapped organic material, have more irregular shapes, likely resulting from dissolution enhancement connecting several smaller pores and creating both larger and more connected pores.

Pore Morphology from SEM Photomicrographs

The SEM used for this study is able to view pores clearly from the macroscale into the picopore scale. The pores viewed in SEM show a clear distinction in the morphology between interparticle/intergranular pores and matrix pores (Figure II-13a, Appendix II). The interparticle

pores have poorly defined perimeters with a complex internal architecture. The complexity of the internal architecture is a result of two factors. First is the growth of crystals, mostly calcite and dolomite, extending from the pore wall into the pore space. Second is the precipitation of at least two substances that have been identified primarily based on morphology because of the coarse nature of the XRD analysis and nonspecific compositional analysis performed by the SEM-coupled EDX (energy dispersive x-ray spectroscopy). The substances are identified to be clays: mixed smectite, montmorillonite, and/or illite with a ribbonlike texture and kaolinite with a platy, book-like texture (Figure II-13b, c). The ribbon texture is commonly coated on the surface of the pore walls, and the platy, book-like texture most commonly fills the pore space in randomly oriented configurations (Figure II-13b, c). Most prominent however, is the platy, book-like precipitation, where the plates are precipitated against the pore walls and in-fill the internal pore space, connecting at randomly oriented angles that effectively fills the pore network and causes a highly complex internal architecture (Figure II-13b). The kaolinite precipitation subdivides the total pore space to effectively decrease the flow network to a series of nano- and picopore size conduits connecting vuggy micropore and mesopore cavities with irregular-shaped pore walls.

In contrast to the intergranular and interparticle pores, matrix pores have well-defined perimeters with clearly defined pore walls. The matrix pores are typically smaller than the interparticle pores, but the internal pore space appears to be open with the exception of minor crystal growth that extends into the pore space (Figure II-13d, e, f). Matrix pores often show growth of well-defined calcite and quartz crystals that appear to nucleate on the pore wall and extend into the void space but do not have precipitated clays. Although the crystals extend into the internal pore space, they do not create a complicated internal network and therefore appear to have the potential for greater permeability because of less tortuosity in the flow path.

Secondary to the intergranular and matrix pore types are unique geometric relationships observed in intraparticle pores and a type of “shrinkage” porosity surrounding well-defined crystals or grains. There are two types of intraparticle pores present in the data set. One type of intraparticle pore shows dissolution of the particle revealing a well-defined internal crystallized matrix that has a similar appearance to matrix porosity (Figure II-13g). A second type of intraparticle porosity has a combination of irregular-shaped pore types and highly elongate pores that imitate micro- to nanofractures (Figure II-13h). In the 2-D data set, the pores have well-defined perimeters but appear to have poor connectivity. The shrinkage porosity is recognized as a unique form adjacent to well-defined crystals or grains within the matrix. The shrinkage pores exhibit what appears to be a physical separation between the matrix and previously abutted crystal or grain. These pores are typically highly elongate and create a void space between the matrix and crystal that mimics the outline of the crystal perimeter (Figure II-13i). These pores have well-defined, straight edge walls with variable thickness depending on how far the matrix has separated from the crystal face.

In addition to the distinct morphology of matrix and interparticle porosity, the spatial distribution of the pores can also be related to the pore type. Interparticle pores, with a complex internal architecture, are found immediately surrounding the grains, which form depositionally unique patterns and configurations through the matrix (Figure II-14). In 2-D, these pores are either well-connected throughout this patterned configuration (Figure II-14a) or are found in localized clusters that might, or might not, be well connected in three dimensions (Figure 14c, d, e). The well-defined matrix pores are only observed at higher magnifications (>50,000×) but are located throughout the matrix adjacent to intergranular pores (Figure II-14b, e), within the matrix between the intergranular pore network (Figure II-14a), and can either have a high or low density (Figure II-14e, f) with unknown connectivity in three dimensions.

These relatively lower magnification settings (4,000–10,000×), using the SEM, provide a significant amount of information regarding the dominant pore type and the 2-D spatial relationship of the pore network.

Calculated Porosity and Pore Size

The image analysis porosity measurement is the sum of all individual pore areas divided by the total image size. The porosity values are biased high because the image analysis was only performed on areas within the sample that contained porosity visible at variable magnifications used to view the samples and the resolution of the images. However, the porosity summarized through image analysis does reveal information about pore density within a sample or facies, which should provide insight into correlation, or lack of correlation between quantitative data obtained through digital image analysis and laboratory measured permeability. The lowest porosity for a single sample, based on the digital image analysis results, is 0.05% (Facies 5) and the highest is 23.5% (Facies 2). The average calculated pore space for areas within samples that have pores varies from 23.5% (Facies 6) to 65.3% (Facies 2). Given the high degree of bias in the data toward areas with void space, these data are most accurately used to say the greatest 2-D density in pore space is observed in Facies 2 and the lowest density is observed in Facies 5. The minimum measureable pore length is 0.0007 μm (0.7 nm) in Facies 2, 3, and 5, with similarly small measurements of 0.0009 μm (0.9 nm) in Facies 7 and 0.001–0.003 μm (1–3 nm) in Facies 1 and 4. This pore length is within the picopore to the smallest nanopore category. The maximum measured pore length is 1123 μm in Facies 3 with the pore length from other facies measuring a maximum length in the 200–625 μm range. The longest pore is in the mesopore range with other maximum lengths contained in the micropore to mesopore category. The minimum measured width is 0.0004 μm (0.4 nm) (from Facies 4 and 5) in the picopore category with other minimum measurements between 0.002 and 0.007 μm (2–7 nm) in the micropore category. The

maximum measured width is 347 μm from Facies 2 in the mesopore category with other maximum measurements between 98 and 350 μm, also in the mesopore category.

Pore Size Distribution

Pore size distribution can be viewed using a variety of graphical methods. A first-glance graphical depiction of the pore size distribution useful for conventional carbonate is obtained by plotting the perimeter/area on the *y*-axis against the pore area on the *x*-axis for each point (Anselmetti et al., 1998; Weger et al., 2009). In carbonate mudrocks this method also provides a simple at-a-glance method to identify the major pore size in a sample although the details of the micro- to nanopore fraction are not readily apparent (Figure II-15). For example, a comparison of two samples (Facies 7 and Facies 3) can quickly show which sample has more evenly distributed pore sizes from macro- to picopore size and which samples have more clustering of pore sizes. However, for samples where the pores are predominately within the micropore to picopores categories (<62.5 μm), the data are visually smeared along the *x*-axis. To better view this size distribution, the same data can be plotted using a semi-log scale where the pore size, or length, is plotted on a logarithmic scale. When the data are plotted in this manner, it is much easier to distinguish where the smaller pores are generally grouped between the micro- , nano-, and picopore categories (Figure II-16). Additional insight can be obtained by plotting the data obtained from the LM compared with the SEM photomicrographs. Although it is feasible the data could all plot in the same groupings, in this data set, there is a clear divergence of the pore sizes and shapes identifiable from plotting the two scales of photomicrograph sets. These plots also emphasize the importance of using imaging methods at multiple scales and magnifications to completely characterize the heterogeneity within the pore size distribution.

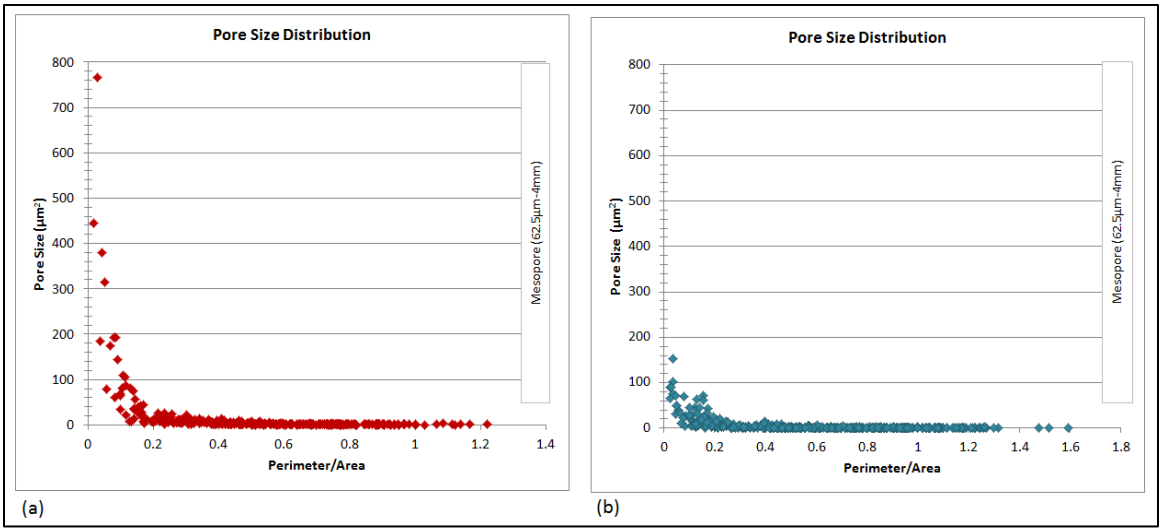

Figure II-15. *The pore area and pore perimeter/area (P/A) can be used to provide a graphical interpretation of the pore size distribution. When the P/A is plotted on the X-axis and pore area is plotted on the Y-axis, the largest pores (meso- to macroscale) align vertically along the Y-axis, and the smaller pores (micro- to picoscale) align horizontally along the X-axis. As shown in graphs, this provides an at-a-glance method to compare the pore size distribution of different samples (a, Facies 7; b, Facies 3), or of the entire sample set. The limitation of this method is the difficulty in fine-scale interpretation and inability to distinguish between the smallest micro- to picoscale pores that all align horizontally adjacent to the X-axis.*

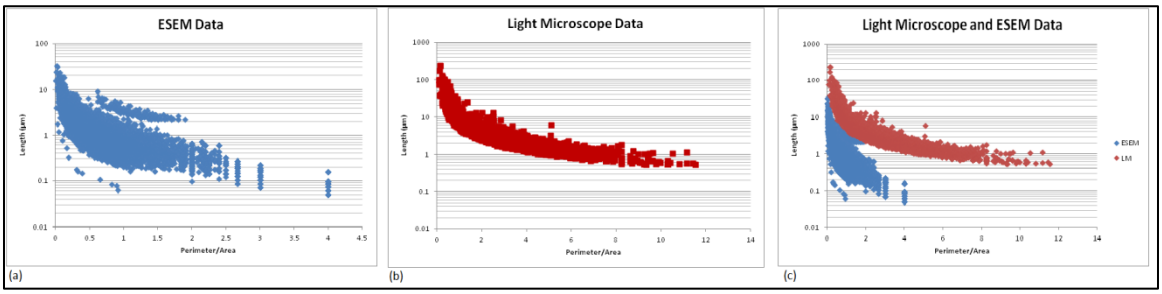

Figure II-16. *When the pore length data are plotted instead of the pore area and plotted on a semilog scale, the pore size distribution within the curve and along the X-axis are more easily distinguished and provide a better estimate of the major pore size. The same general conclusions can be stated regarding larger pores aligned vertically and smaller pores aligned horizontally. With the aid of the log-scale on the Y-axis, it is now clear the majority of the pores identified are between 0.01 and 10 µm (nanopore to micropore size). Separating the data based on the photomicrograph type, or magnification interval, shows how the two methods of analysis are complementary to provide a more complete data set regarding the pore architecture. The data using the light microscope (LM) (a) is more suitable at capturing the larger pores, while the SEM (b) is more suitable to capturing the size distribution within the micro to nanopore size fraction. A plot of both data sets (c) shows a clear bimodal distribution pattern within the sample set.*

A more detailed graph of the pore sizes identified using the LM and SEM show the majority of the pores identified with the LM are micropores, whereas the majority of the pores identified with the SEM are nanopores (Figure II-17). When the same data are plotted in greater detail within each category, we see from the LM data that there is a bimodal distribution within the micropores (Figure II-18). Looking at the data plotted together, the number of nanopores greatly exceeds the number of micropores identified, which clearly identifies the most common pore size (0.01–10.0 µm) within the nanopore to micropore category but mutes most of the micropore to mesopore data observed in thin sections which overlooks the bimodal distribution that is clear when the data are incorporated together.

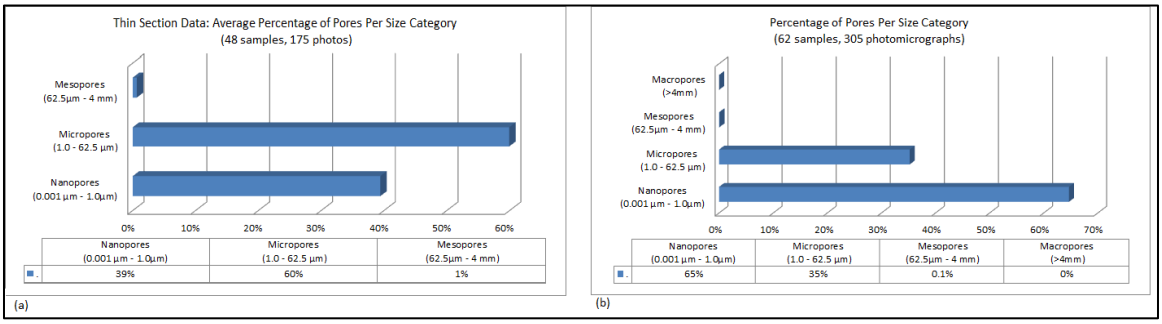

Figure II-17. *Quantified distribution of pore sizes from thin-section data (a) shows the pores are primarily micropores (1–62.5 µm), with secondary nanopores. When the data from SEM photomicrographs are added (b), there is a clear shift to the majority of the pores contained within the nanopore classification.*

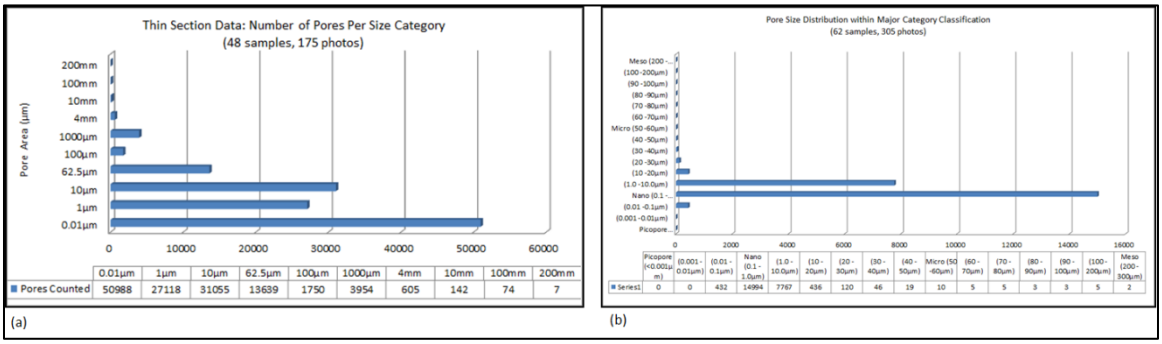

Figure II-18. *(a) A detailed graph showing pore size distribution within each major classification shows a bimodal distribution within the mesopores based on thin-section data. (b) Some of the distribution within the larger pores is muted when the SEM data are added showing a strong skew of the data toward the largest nanopores (0.1–1 µm) and smallest (1.0–10 µm) micropores.*

Pore Shape Relationship to Facies

In conventional carbonates, the pore shape is an indication of pore connectivity where more elongate pores tend to have better connectivity than more spherical pores (Anselmetti et al., 1998). The pore shape was calculated using the methodology outlined by Anselmetti et al. (1998), where the pore shape (ɣ) is calculated using the perimeter (*P*) and area (*A*) resulting in a dimensionless number where a value of 1.0 is equal to perfect circle (Equation II-1). The pore shape for this study varies from 1.20 to 1.96, resulting in an average pore shape of 1.5 and an average pore shape for all facies of 1.53 ± 0.07, which corresponds to a slightly elongate shape.

$$(\gamma) = \frac{P}{2\sqrt{\pi A}}$$

Equaton II-*1. Calculation of pore shape based on Anselmetti et al. (1998), where P = pore perimeter, A = pore area, and ɣ = pore shape. The calculation results in a dimensionless value where the value of 1.0 is a perfect circle and values larger than 1.0 are a reflection of elongation of the pore.*

Pore shape, calculated from both thin-section and SEM photomicrographs, was plotted with laboratory-measured porosity to identify if there is a fundamental relationship that can be identified to predict porosity from shape. Facies 1 does not show any relationship between pore shape and porosity, Facies 2 shows a positive relationship between pore shape and porosity, and Facies 3–7 have an inverse relationship between pore shape and porosity where the largest porosity is associated with more simple pore shapes and the lowest porosity is associated with more elongate pores (Figure II-19).

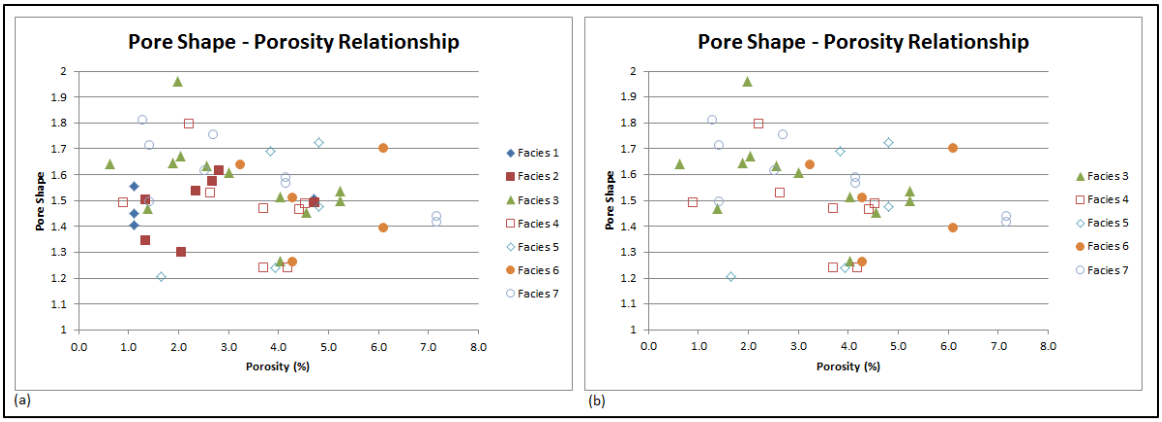

Figure II-19. *(a) The relationship between pore shape and porosity for the data set has no clear relationship when plotted together. (b) However, when data from Facies 1 and 2 are removed, a clear inverse relationship emerges where the highest porosity generally corresponds to the more simple pore shapes. The lack of correlation in Facies 1 and 2 could be due to different pore architecture, or to lack of sufficient data points. In conventional carbonates, the more elongate the pore shape, the greater the connectivity of the pores. In unconventional carbonates, more elongate pores shapes could be an indication of intense diagenetic alteration with complex internal pore architecture resulting in lower total porosity.*

Pore shape was plotted with laboratory-measured permeability to determine if there is a fundamental relationship that can be identified to predict pore connectivity. The relationship between pore shape and permeability has a significant amount of scatter where the overall relationship is either indeterminate or weakly positive (Figure II-11a). The overall trend between pore shape and air permeability compared to pore shape and Klinkenberg-corrected permeability is nearly identical, with the exception that the Klinkenberg values are approximately half the air permeability values (Figure II-11b). The samples with the highest laboratory-measured permeability are both from Facies 5 but do not provide significant clarity or prediction to the data set. The significant scatter and lack of correlation within the carbonate mudrock data is attributed to the complicated internal pore network from postdepositional precipitation of mineral and clay cements that subdivides the internal pore space and inhibits flow pathways. Isolated elongate intraparticle pores and isolated elongate shrinkage pores with poor 2-D connectivity also complicate the expected relationship between pore shape and permeability.

Pore morphology, Porosity, Permeability, and Facies Correlation

Each facies identified has a generally positive correlation between laboratory-measured porosity and permeability with a few notable variances (Figure II-20). On a semilog graph, Facies 4, 6, and 7 have the most predictable grouping of porosity and permeability, whereas Facies 1, 2, 3, and 5 all have several data points that obscure any predictable relationship between porosity and permeability. The highest measured porosity and permeability is in Facies 4 at 20.0% porosity and 1.25 mD Klinkenberg permeability. The second highest permeability is in Facies 2 with 1.7% porosity and 1.05 mD permeability. Facies 1, 3, and 5 also have significant deviations to the positive porosity–permeability relationship with permeability values just over 0.25 mD for porosity values that range from 0.6 to 1.9%. Facies 6 has the lowest and most consistent permeability ranging from 0.001 to 0.01 mD with porosity ranging from 0.3 to 6.1%.

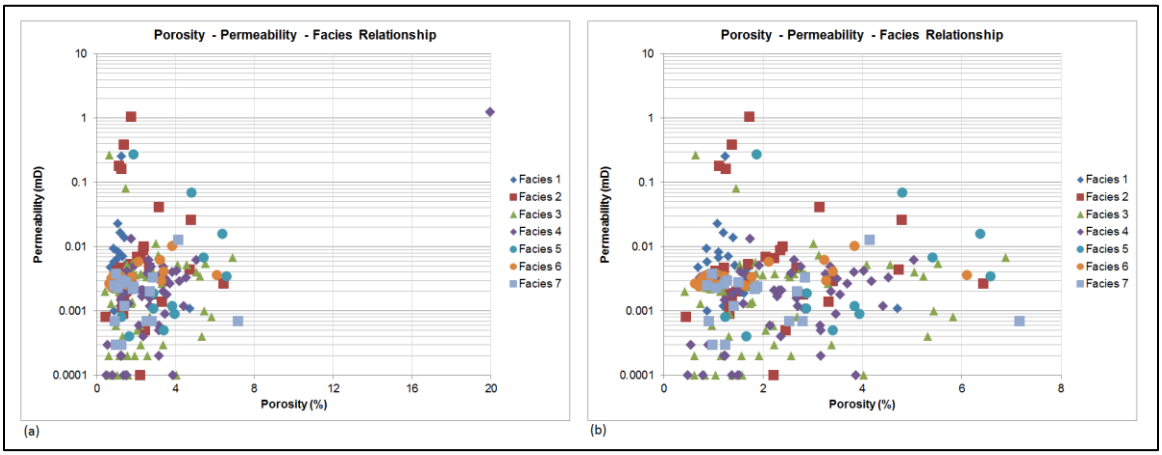

Figure II-20. *Although one data point has a measured porosity value of 20% (a), the majority of the measured porosity and permeability is less than 8% and less than 1mD, respectively (b). As shown, the measured porosity–permeability relationship is generally positive and in at least two facies, Facies 4 and Facies 7, has a predictable correlation. Facies 1 has the greatest deviation with a significant amount of variation in permeability for a given range of porosity values. Facies 6 has the greatest consistency in permeability over a relatively large range of porosity values. Facies 2, 3, and 5 have moderate predictability between porosity and permeability with marked deviations that have relatively high permeability associated with low (<2%) porosity. The difference in the predictability of the porosity and permeability relationship is related to the primary type of porosity and level of complexity observed within the pore space.*

Facies 2, 3, 4, 5, and 7 have moderate to high predictable positive relationship between laboratory porosity and permeability. Each of these facies has a significant amount of interparticle porosity and matrix porosity with pore networks clearly visible in 2-D at 4,000–10,000× magnification. Facies 6, with the least variation in permeability, has primarily matrix porosity with very few intergranular pores with clay occluding cements. Facies 1 has the highest slope with permeability varying from 0.0001 to just over 0.25 mD with porosity remaining primarily between 0.7 and 1.7%. Facies 1 also has the greatest variability in pore types, including intergranular pores with clay occluding cements, matrix porosity, intraparticle porosity with partial pore-filling clays and crystal growth within the pore, intraparticle porosity with currently indeterminate connectivity with other pores, shrinkage pores, and abundant pyrite framboids within the matrix.

Although the focus of this study does not include the contribution of fractures to porosity and permeability, there are several types of microfractures that likely contribute to porosity and permeability in the sample set. Some microfractures have a significant amount of organic staining surrounding the fracture filled with trapped organic (oil) material, whereas open fractures show adjacent staining that could be slowly diffusing into the fracture as a preferential flow path. The open microfractures often have a primary flow path with several smaller microfracture splays extending into the matrix. Microfractures are observed in four settings: (1) in previously opened, cement-filled fractures; (2) as dissolution-enhanced, vuggy void space at randomly spaced intervals adjacent to a primary fracture pathway; (3) parallel to depositional bedding planes; and (4) bisecting, perpendicular to, planes of deposition. Overall, the micro- to nanometer size fractures do not appear to create ideal flow pathways that connect to the matrix porosity, but could be important to the overall flow network by creating a multimodal flow network.

Because of the prominence of macro- to micrometer fractures observed throughout the study, it should be pointed out that deviations to expected trends between porosity, permeability, and facies are likely complicated by the presence or absence of fractures from the nano- to macroscale, as well as the type and density of the fractures present.

<H2>Sequence Stratigraphy, Porosity, and Permeability Correlation

The third-order depositional sequence contains six fourth-order high-frequency sequences that vary in thickness from 5 to 30 m (15–100 ft) with several fifth-order high-frequency cycles identified as 1–5 m thick shallowing upward packages. The highest porosity and highest permeability values are typically aligned together within the regressive phase of the system. Closer examination shows the high porosity, high permeability intervals are often closely aligned with the upper portion of identified fifth-order cycles, which imply the fifth-order cycles have the greatest control on porosity and permeability (Figure II-6). Deviations to this overall trend are highest porosity and permeability values located in the fourth-order transgressive phase toward the base of the core. In this section, these high porosity, high permeability values are located within areas that have undergone hydrothermal brecciation. Therefore, there are two controls on locating zones with relatively higher porosity and permeability. The primary pattern that is likely to be most applicable to other areas within the basin is the association with fifth-order cycles. A secondary pattern to examine is the association with hydrothermal brecciation that will not necessarily be associated with the transgressive phase of deposition.

DISCUSSION OF RESULTS AND APPLICATION TO RESERVOIR STUDIES

The primary contribution of the research presented in this chapter is documentation of the 2-D carbonate mudrock pore architecture and identification of fundamental relationships that are applicable to deciphering both conventional and unconventional carbonate reservoir

systems. The carbonate mudrock pore types observed in this study include interparticle/intergranular, intraparticle, matrix, shrinkage, and fracture (Figure II-10). Complexity of the internal pore network is added from precipitation of clay minerals and crystal growth within the pore space. In most of the pores observed, the internal geometry appears to have a greater control on permeability than the overall pore size. Where minerals subdivide the internal flow network, the total pore architecture becomes a system of nano- to picopore throats that connect nano- to mesopore cavities, or vugs.

Elementary relationships from quantitative data between key measured pore parameters, porosity and permeability, are highlighted to provide a foundation for future analysis of carbonate mudrock systems. Deposition occurred in a platform attached carbonate-dominated environment on a low declivity, or distally steepened ramp, in a tropical epeiric sea. The primary relationships that allow for predictability of permeability from the pore architecture in carbonates with predominately macropores should also be able to be applied to a carbonate mudrock system. However, complexity in the mudrock pore architecture coupled with variability in type and intensity of diagenetic alterations and the influence of a nano- to macrometer fracture network have strong impacts on expected relationships.

Qualitative and quantitative data that describe the pore architecture as observed in thin sections and SEM show the largest cross-sectional areas are in the meso- to nanoscale with smallest measurements in the nano- to picopore scale. By incorporating qualitative observations, this is interpreted as a system of meso- to nanoscale vuggy to moldic pores connected by nano- to picopore throats. Although additional 3-D image analysis or other analytical method (e.g., MICP) is necessary to quantitatively confirm this interpretation, qualitative analysis of the 2-D cross-sectional images, from thin section as well as in SEM, where some topographical features can be viewed in the manually polished parts of the sample,

support this theory. Most pores are irregularly shaped ovals or oblong structures. Photomicrographs using SEM reveals complicated internal pore architecture exists from microcrystalline growth and precipitated clay cements creating complicated flow paths within the pore space. This internal pore texture adds an additional layer of complexity when relating the pore architecture to permeability. Not only is the overall pore size and connectivity important to permeability, but also the internal texture of the pore space has the potential to create tortuous flow pathways independent of pore size and shape.

Quantitative data provide information about the distribution of the pore sizes and can indicate if there is a singular, bimodal, or multimodal distribution of pores that contribute to permeability. Quantification of the pore shape in relation to a circle is an indication of permeability, or pore connectivity, in conventional carbonates but shows only a weak correlation to permeability in carbonate mudrocks used in this study. This weak correlation can be attributed to the complex internal pore architecture created by precipitation of clay cements within the interparticle pores, and quartz and calcite mineral growth that all effectively subdivide the internal pore space and add additional tortuosity to the flow pathway.

The relationship between pore shape and permeability is indeterminate to weakly positive. This is contrary to trends observed in conventional carbonates where pore shape has a significant effect on permeability where more elongate pores have greater connectivity than more spherical pores (Anselmetti et al., 1998). The significant scatter and lack of correlation within the carbonate mudrock data is from the complicated internal pore network created from postdepositional precipitation of mineral and clay cements that subdivides the internal pore space and inhibits flow pathways. Elongate, isolated intraparticle pores and elongate, isolated shrinkage pores with poor 2-D connectivity also complicate the expected relationship between pore shape and permeability. Therefore, in carbonate mudrocks, the more elongate pores could

be an indication of diagenetic alterations that generates complex internal pore geometries through cementation processes and creation of more elongate microfracture porosity from stresses applied postdepositionally.

PORE ARCHITECTURE AND RESERVOIR PROPERTIES

Porosity, Permeability, and Sequence Stratigraphic Framework

The highest porosity and permeability correlate with the upper portion of fifth-order cycles within the fourth-order regressive sequence. The fifth-order cycles were identified by facies stacking patterns and high-resolution sequence stratigraphic analysis. This correlation may be further associated with late stage diagenetic alterations that control the precipitation of clay minerals, quartz, and calcite crystals within the pore space. A secondary indicator of high porosity and permeability intervals is related to postdeposition alteration from hydrothermal brecciation. Within the data set, hydrothermal brecciation affected the lower portion of the core that is in the fourth-order transgressive sequence. However, although predictability associated with the fifth-order cycles appears to be consistent with the fourth-order regressive sequence, hydrothermal brecciation could be associated with several phases of deposition in other parts of the basin.

Although a diagenetic study detailing the type and timing of diagenesis within the data set was outside the scope of the research, a study based on core from this play concluded three to five stages of diagenetic alteration that included replacive dolomite, several stages of calcite cementation within the pore space, and early micritization of lime mud (Ewald, 2015).

Facies Correlation with Pore Types

A predictable, positive relationship between porosity and permeability exists in all facies with minor variations observed in the relationship for Facies 1 and Facies 6. In Facies 1, the porosity and permeability relationship is positive but has a much steeper slope with porosity

remaining less than 2% except for one sample with a porosity of 4.7% and associated permeability ranging from 0.0001 mD to just over 0.25 mD. In Facies 6, this positive relationship has essentially no correlation, where permeability is consistently within the range of 0.001 to 0.01 mD with laboratory-measured porosity as 0.3–6.1%. This lack of correlation could be a result of the predominant pore type being matrix pores that are overall the smallest nanopore to picopores in size. Although the matrix pores have some increased tortuosity in the fluid pathway because of crystal growth within the pores, the overall result of a mostly open network of smaller pores is a consistent, albeit low, average permeability. The highest porosity and highest permeability is within Facies 4 with a positive correlation between porosity and permeability and a visible pore network of interparticle porosity and matrix porosity at a magnification of 4000×. Although the interparticle pores have significant precipitation of clay cements that subdivide the pore space, the total pore space (including that now filled by residual oil/organic matter) allows for good connectivity and flow through the entire section.

Key differences between conventional macropore-dominated carbonates and unconventional carbonate reservoirs with predominately micro- to nanopores is the complex internal pore geometry observed in carbonate mudrocks created through precipitation of cements that subdivide the pore space. Because pore throats have a significant control on the permeability within a reservoir, the average diameter of the pore controlling a flow in a macropore-dominated system can be similar to the average diameter of the pore controlling a micro- to nanopore-dominated system. However, the internal geometry appears to have at least an equally significant effect on the potential permeability within the reservoir, and in a carbonate mudrock system the character of that system is not easily quantified through 2-D digital image analysis or identification of basic pore types (intergranular, moldic, intraparticle). A dual description of the pore architecture using quantitative data and qualitative observations

helps provide insight regarding correlations between facies, pore type, porosity, and permeability. Understanding how the dominant pore type and internal pore network geometry is related within a specific reservoir systems aids in predicting which facies has the greater reservoir potential. For example, in this study, Facies 6 has the most predictable permeability, but Facies 4 and Facies 2 have the greatest potential for the highest permeability for a given porosity value. As noted earlier, additional potential for increased porosity and permeability is the position of each of these facies within the sequence stratigraphic framework. Where any of these facies is located at the top of a fifth-order cycle, the relative porosity and permeability is up to twice the value of porosity and permeability compared with immediately adjacent facies (Figure II-20).

Carbonate Mudrock Acoustic Response

Understanding the relationship between sonic velocity response and porosity provides the potential to further enhance our ability to qualitatively and quantitatively predict permeability in conventional carbonates (Anselmetti et al., 1998; Anselmetti and Eberli, 1999; Thornton and Grammer, 2012). The sonic velocity response and porosity in carbonate mudrocks are inversely related, similar to the relationship observed in conventional carbonates. Upon closer examination, although the relationship has a similar trend, the sonic velocity (V_P) response for the carbonate mudrocks is significantly slower for a given porosity than would be expected based on data from conventional carbonate samples and theoretically calculated values. This shift in the relationship is further evidence of how the pore architecture in carbonate mudrocks is unique from the conventional carbonates and requires an adjusted classification methodology. Although it is clear that integration of several types of data, including facies analysis and identification of the sequence stratigraphic framework, will allow for greater predictability of key petrophysical properties, the foundation of this prediction lies in

accurately describing the variability of the pore architecture and the fundamental relationship between pore architecture, porosity, permeability, facies, and the sequence stratigraphic framework.

CONCLUSIONS

The ability to predict petrophysical properties in carbonate mudrock reservoirs begins with the ability to accurately describe the pore architecture (type, size, shape, spatial distribution, and connectivity). Conventional carbonate pore type descriptions only partially describe the pore architecture in carbonate mudrocks because the overall particle size appears to result in different mechanisms of fluid flow and postdeposition diagenesis that create unique internal pore networks. Analysis of data from the midcontinent Mississippi Lime play provides a classification and understanding how the pore architecture in carbonate mudrocks differs from conventional carbonates with visible macroporosity. Initial results from this study are as follows:

(1) Digital image analysis confirms that carbonate mudrocks have a complex distribution of pore sizes, even within the micro- to picopore scale, that have an impact on the relationship between porosity and permeability.

(2) To obtain a complete suite of data representative of the characteristics of carbonate mudrock pore architecture, analysis should be completed using a light microscope as well as a scanning electron microscope to encompass data from macro- to picopore scales.

(3) Pore shape has a weak relationship with total porosity and total permeability with the greatest correlation observed in Facies 6 and 7. The scatter in the data is a result of the complexity within the internal pore architecture.

(4) The relationship between porosity and sonic velocity response indicates the relationships observed in conventional carbonates are similar to carbonate mudrocks

but not identical in nature. The lower sonic (compressional) velocity response is partly because the complex mudrock pore architecture contained primarily within the micro- to nanopore size fraction produces different elastic properties than properties expected for carbonates with macroporosity. Additionally, the diagenetic alterations of the matrix to a relatively high silica content also impact the elastic properties of the reservoir and the resultant sonic velocity response. This difference in elastic properties associated with the macro- to nanopore architecture correlates with a unique, predictable pattern that has a lower sonic (compressional) velocity for a given porosity, as compared to values expected from the Wyllie time average question. The scatter in the data are still a result of different pore types and permeability that is demonstrated by variations in the range of resultant sonic (compressional) velocity values for a given porosity as well as a range of porosity values for a given sonic (compressional) velocity response.

(5) Microfractures may contribute to the overall porosity and permeability where they are able to provide a less tortuous fluid pathway for water and oil located in the picopores and small nanopore size fraction. Fractures that are currently filled with calcite and dolomite cements likely contributed to migration of fluids and placement of currently observed trapped organic (oil) material, during early and later burial stages. Although not the focus of this study, it is clear the effect of microfracture contribution to porosity and permeability should be considered in additional research relating pore architecture to porosity and permeability in carbonate mudrocks.

(6) Each facies identified has a generally positive correlation between porosity and permeability with notable variances that are a result of the dominant pore type and complex internal pore geometry. The highest porosity and permeability are also often

associated with the upper portion of identified fifth-order cycles within the cored interval. Additional predictability of high porosity and permeability intervals might be associated with specific diagenetic processes. On a broad scale, extreme silicification is most prominent in Facies 5, whereas observed hydrothermal brecciation is primarily within Facies 2. Correlation between type and timing of diagenesis and permeability was beyond the scope of this research.

(7) In carbonate mudrocks quantification of the pore architecture and qualitative descriptions of the pore architecture each provide only part of the information necessary to interpret key relationships between the pore architecture, porosity, permeability, facies, and sequence stratigraphy. The combination of qualitative and quantitative data is recommended to provide a sufficient amount of insight to understand general trends and interpret deviations within these relationships, which in turn allows for enhanced predictability of optimal reservoir conditions and improved horizontal well target selection.

CHAPTER III

QUANTITATIVE EVALUATION OF PORE SYSTEM ARCHITECTURE AND ACOUSTIC RESPONSE OF MICRO- TO NANO-SCALE PORES IN CARBONATE MUDROCKS

ABSTRACT

A qualitative and quantitative analysis has been conducted using data and observations of the macro- to nano-scale pore architecture and the relationship to porosity and permeability for five core from three locations within the Mississippian age North American Mid-Continent region. The qualitative analysis provides insight into variations in the relationship between the pore architecture, porosity, and permeability where differences in the type of diagenetic alteration within the pore space coupled with observations of the dominant pore size can be correlated to relatively high and low porosity and permeability.

The quantitative analysis was performed using regression analysis to identify relationships between geometric measurements of the pore architecture that are extracted using digital image analysis, and laboratory measured porosity, air permeability, and Klinkenberg permeability. The regression analysis was applied to

sub-sets of data groups with a primary focus on the very fine grain, low porosity, low permeability facies. The results of each model identified several statistically significant measurements, but none were statistically valid and able to be used to enhance the predictability of either the porosity, air permeability, or Klinkenberg permeability. The lack of success is presumed to be a result of three primary factors: accuracy in the laboratory measured porosity and permeability data, the need to incorporate semi-quantitative analysis of the contribution or occlusion from macro- to micro-scale fractures, and the need to include semi-quantitative data regarding the extent of the diagenetic alteration.

INTRODUCTION

The Mississippian age limestone of the North American Mid-Continent is a valuable, unconventional reservoir with predominantly very fine grain facies deposited in a mixed carbonate – siliciclastic system. Although there has been oil and gas production from vertical wells for over 50 years, recent advancements in horizontal drilling technology have revitalized the play. This revitalization has highlighted the need to better understand the reservoir architecture and identify tools and methods that can be used to enhance the predictability of key reservoir properties (porosity, permeability). Qualitative and quantitative analysis of the pore architecture in macropore systems has identified a methodology that is able to both qualitative and quantitatively increase the accuracy of predicting high porosity and high permeability intervals. Within carbonates that have predominantly macropore systems, specific geometric measurements (length, width, pore shape) have been identified as key components that can be used as input parameters to statistically define equations that relate the measurements to laboratory measured porosity and permeability data (Anselmetti et al., 1998). It has been shown that in a conventional carbonate system, digital image analysis can be used as input parameters in different analytical models to quantitatively predict permeability with a high level of accuracy. Anselmetti et al. (1998) shows how the relationship to pore type,

pore size, and pore shape can be used to predict permeability. Furthermore the application of an artificial neural network program using several different input values obtained from digital image analysis shows how digital image analysis can be used to predict laboratory measured permeability values with an R-value of 0.842 to 0.982 depending on the number of variables used in the model. Thornton and Grammer (2012) show application of multivariate statistical analysis can also be used to identify the statistically valid input parameters that can be used to quantitatively predict permeability. With identification of the key geometric parameters identified through digital image analysis, laboratory permeability was able to be predicted with an R^2 value of 0.45-0.82 depending on the heterogeneity of the pore system. Although there are several studies where quantitative methodology that describes the pore architecture within a carbonate reservoir with predominantly macropore architecture can be used to predict permeability with reasonable accuracy (Love et al., 1997; Lightenberg and Wansink, 2001; Rogers et al., 1995; Ehrenberg, 2007), it is currently unknown if the same methods can be used to accurately predict permeability in a very fine grained, predominantly micro- to nanopore carbonate mudrock.

Using digital image analysis techniques as outlined by Anselmetti et al. (1998), quantitative data are extracted from thin section and FE-SEM photomicrographs to be used as input values for regression analysis (Davis 1986).

The primary objectives of this study are as follows:

1. To qualitatively and quantitatively characterize the pore architecture observed in each part of the study area and relate these observations to porosity and permeability on a sub-regional to regional scale.

2. To understand how the acoustic response relates to porosity in the very fine grained, low porosity and low permeability, facies in the study area, and how this compares to more “conventional” reservoir facies within the same parts of the study area.

METHODS

Data Set

The data used in this study come from five cores that represent three Mississippian depositional settings and regions within the Mid-Continent, U.S.A.. The cores are from Reno County, Kansas, Logan County, OK, Payne County Oklahoma, and Osage County, Oklahoma (Figure III-1). The facies from North-Central Oklahoma range from very fine grained mudstone to wackestones and packstone deposited in a distal location primarily below wave base, to fine-grained wackestone, packstone, and grainstone deposited in a proximal location primarily below fair weather wave base but within storm wave base. The facies observed in the core from Central Kansas transitional core vary from a fine grain mudstone to a medium to coarse grain packstone, capped by a series of peritidal deposits. The three facies groups have been generically classified within this study as distal facies, transitional facies ,andproximal facies respectively.

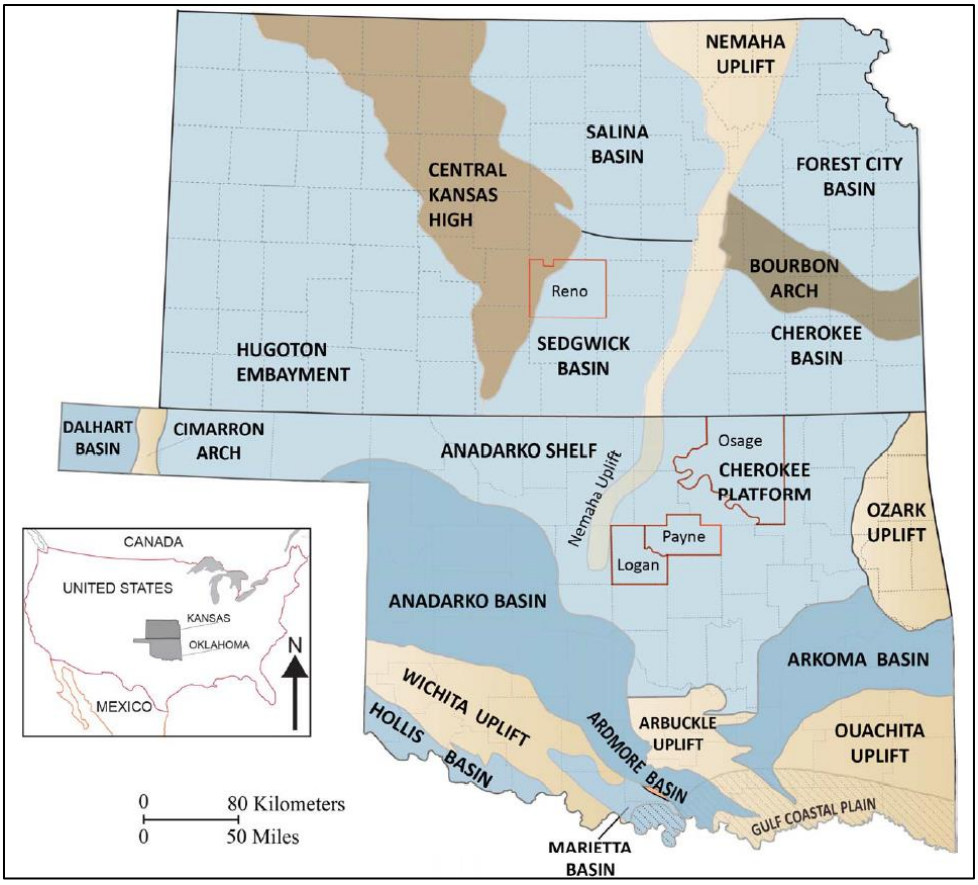

Figure III-1: The study area includes five core from three areas within the North American Mid-Continent area of Kansas and Oklahoma. The core with outer ramp facies preserved is from Osage County, Oklahoma, three cores with middle to inner ramp facies preserved are from Logan and Payne Counties, Oklahoma. A core with facies that vary from a proximal outer ramp to shoreline and peritidal facies is from Reno County, Kansas. During the Mississippian Period, this area was located approximately 30^{o} south of the paleo-equator and was covered by a shallow tropical epeiric sea. Regional tectonics beginning at the end of the Devonian and continuing throughout the Mississippian caused the emergence of the Nemaha Uplift, the Ozark Uplift, the Central Kansas Uplift, and the Ouachita Uplift. The same regional tectonic stress regime created a series of foreland basins including the Arkoma Basin located southeast of the areas included in the study in a paleo-dip direction.

Conventional Laboratory Measured Data

Conventional laboratory measured porosity (%), air permeability (mD), and Klinkenberg permeability (mD) data was available for all five cores used in this study. Two companies were utilized for measure standard petrophysical properties based on the primary owner of the core. Weatherford Laboratory performed the analysis for the three cores in

Logan and Payne Counties, and Special Core Analysis Laboratories (SCAL), Inc. laboratory performed the analysis for the cores in Osage County and Reno County. All measurements were performed using conventional core analysis procedures.

Microscopy

Petrographic analysis of 191 thin sections was performed using a Leica DM 2700P optical, or light, microscope (LM). The micro- to nano-pore architecture was further investigated using 132 ion milled samples using a JEOL IB-19500CP Cross Section Polisher argon ion mill that were viewed and photographed with an FEI Quanta 600F field emission scanning electron microscope (FE-SEM) to view samples from the macro- to pico-scale.

In addition to more accurate facies descriptions, thin section analysis allowed for more accurate description and analysis of the macro- to nanoscale pore sizes, and pore types. Photomicrographs that represent the dominant pore types observed in the samples were captured and analyzed qualitatively and quantitatively. Pores observed in thin section can be accurately characterized quantitatively to approximately 1µm. Pores at and below this size are best quantified and observed using the FE-SEM. As described in Vanden Berg and Grammer (2016), all samples viewed with the FE-SEM were polished using an argon ion mill to provide a clear 2D image of the sample.

Pore Architecture Analysis

The primary goal in the qualitative and quantitative classification of pore architecture is to understand the fundamental features that contribute to permeability. Qualitative analysis included observations related to the density, spatial distribution, dominant pore size, dominant pore type, and diagenetic alteration that could significantly impact the measured porosity or permeability. Pore size classification was completed using the classification scheme of Loucks et al. (2012). Pore morphology is utilized to explain both relationships to

facies and the sequence stratigraphic framework, and discrepancies to trends that appear to otherwise be applicable within the data set. Digital image analysis (DIA) was utilized to quantify the geometric characteristics of the representative pore space within several photomicrographs collected using the LM and FE-SEM. Quantitative analysis included analysis of pore size distribution, pore shape, interpretation of geometric measurements of the pore architecture, and regression analysis to relate the pore geometry to porosity and permeability.

The pore architecture was quantitatively analyzed using regression analysis to identify the most statistically significant relationships between primary geometric measurements of the pore architecture and laboratory measured porosity and permeability (both air and Klinkenberg values). In regression analysis, each laboratory measured value (porosity, air permeability, Klinkenberg permeability) was input as a dependent variable with geometric measurements of the pore architecture that was extracted using DIA, input as independent variable or predictor variables. The model was run using R, version 3.2.4, software designed to perform statistical computations and generate graphical results of the data. Each model used a sub-set of the total data set so the excluded data points could be used to test the applicability of the model within the project data set.

Digital Image Analysis: Quantitative data extraction and compilation

The data used to identify parameters that could be used to enhance the predictability of porosity and permeability within the data set were generated from photomicrographs of thin sections using a light microscope (LM) and of samples viewed with an field emission scanning electron microscope (FE-SEM). A sub-set of all photomicrographs were analyzed using proprietary software from Leica Corporation called “image analysis” that is able to perform either a manual or automated digital image analysis (DIA). The DIA analyzes the photomicrographs by input from the user to identify a specific color, hue, and saturation of

features of interest. Steps within the software allow for iterative calibration to ensure quality of data extracted through feature identification prior to output of measured values into an Excel spreadsheet. The data generated include analysis of a sub-set of photomicrographs collected from both the LM and FE-SEM analysis that are representative of the pore types and sizes observed for each sample.

Data from each photomicrograph analyzed were compiled into a single file to be used as input for the regression analysis to explore correlations and potential for predictability based on relationships between the measured pore architecture geometries, and laboratory measured porosity and permeability. DIA data were compiled into three data sets that were tested using regression analysis.

The first data set incorporates data from four cores that are generically described as 'unconventional' as related to the measured low porosity and permeability, and overall fine-grained sediment and skeletal content. A summary data set of these same four cores is tested to determine if statistically significant correlations could be identified from summary statistics of key geometric features. The second data set included an expanded set of geometric measurements from the same four cores. The third data set is from the transitional core located in Central Kansas that grades from a very fine grain facies with primarily micro- to nanoporosity at the base of the cored interval, to a predominantly silt and sand size matrix with very coarse pebble size clasts that appear to have been brecciated *in-situ*. Summary statistics of the three data sets tested are shown in Table III-1 and III-2.

			Samples	Images analyzed	Data points
Osage County, Oklahoma	Distal ramp, very fine grained facies		90	751	221340
		Thin Sections:	41	157	119612
		ESEM:	49	594	101728
Logan County, Oklahoma	Proximal to middle ramp, fine to very fine grained facies		82	739	177623
		Thin Sections:	59	332	113797
		ESEM:	23	407	63826
Payne County (west), Oklahoma	Proximal to middle ramp, fine to very fine grained facies		31	436	184662
		Thin Sections:	8	66	132319
		ESEM:	23	370	52345
Payne County (east), Oklahoma	Proximal to middle ramp, fine to very fine grained facies		30	1887	60325
		Thin Sections:	19	105	26726
		ESEM:	11	1782	33599
Reno County, Kansas	Outer middle ramp to shoreline and peritidal facies		90	728	758609
		Thin Sections:	64	425	677341
		ESEM:	26	303	81268
All Cores in Study	Unconventional (distal and proximal facies) to transitional	Distal outer ramp	323	4541	1402559
		Thin Sections	191	1085	1069795
		ESEM:	132	3456	332766

Table III-1: There were a total of 191 thin sections available for analysis, 132 samples polished with an argon ion mill and viewed with the ESEM, and 4541 associated number of representative image analyzed with DIA utilized to identify 1,402,559 data points (pores).

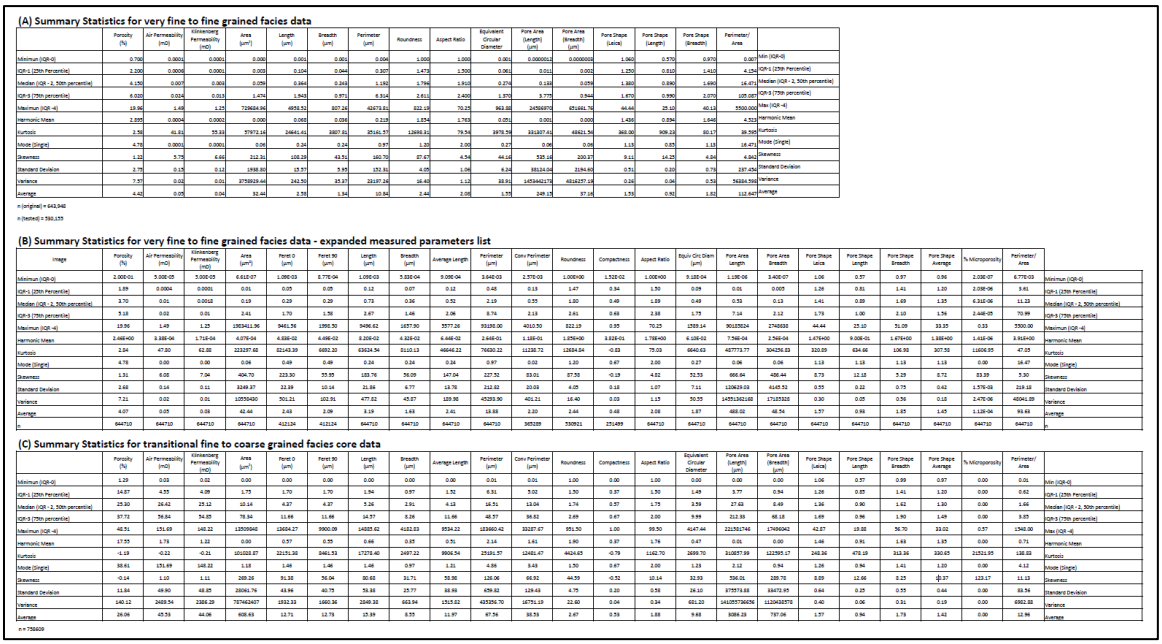

(A) Summary Statistics for very fine to fine grained facies data

	Porosity (%)	Air Permeability (mD)	Klinkenberg Permeability (mD)	Area (µm²)	Length (µm)	Breadth (µm)	Perimeter (µm)	Roundness	Aspect Ratio	Equivalent Circular Diameter	Pore Area (Length) (µm)	Pore Area (Breadth) (µm)	Pore Shape (Lxlca)	Pore Shape (Length)	Pore Shape (Breadth)	Perimeter/ Area	
Minimum (IQR-0)	0.700	0.0001	0.0001	0.000	0.001	0.001	0.004	1.000	1.000	0.001	0.0000013	0.0000003	1.060	0.570	0.970	0.007	Min (IQR-0)
IQR-1 (25th Percentile)	2.200	0.0008	0.0001	0.003	0.104	0.044	0.307	1.473	1.500	0.061	0.011	0.002	1.250	0.310	1.410	4.254	IQR-1 (25th Percentile)
Median (IQR - 2, 50th percentile)	4.150	0.007	0.001	0.059	0.344	0.243	1.192	1.796	1.910	0.274	0.138	0.056	1.380	0.890	1.490	16.471	Median (IQR - 2, 50th percentile)
IQR-3 (75th percentile)	6.020	0.024	0.013	1.474	1.945	0.971	6.314	2.611	2.400	1.370	3.775	0.944	1.670	0.990	2.070	105.087	IQR-3 (75th percentile)
Maximum (IQR -4)	19.96	1.49	1.25	729604.06	4850.52	807.26	42673.61	622.19	70.25	963.88	24556970	4516491.76	44.44	25.10	40.13	5500.000	Max (IQR -4)
Harmonic Mean	2.855	0.0004	0.0001	0.000	0.085	0.036	0.228	1.574	1.759	0.051	0.001	0.000	1.430	0.294	1.640	4.328	Harmonic Mean
Kurtosis	2.36	41.61	55.33	57972.16	24661.41	3807.81	37161.77	13988.21	79.54	3978.59	3313077.61	48621.56	363.00	908.20	80.17	39.598	Kurtosis
Mode (Single)	4.78	0.0001	0.0001	0.00	0.24	0.24	0.97	1.20	2.00	0.27	0.06	0.06	1.13	0.85	1.13	16.471	Mode (Single)
Skewness	1.32	5.75	6.66	212.31	108.29	43.51	160.70	87.47	6.54	44.16	535.16	200.37	9.11	14.25	4.94	4.842	Skewness
Standard Deviation	2.75	0.15	0.12	1938.80	15.37	5.95	152.91	4.05	1.06	6.24	88124.04	2194.80	0.51	0.20	0.79	287.476	Standard Deviation
Variance	7.57	0.02	0.01	3758929.44	242.56	35.37	23387.28	16.40	1.12	38.91	14534462176	4816257.16	0.26	0.04	0.62	54304.596	Variance
Average	4.42	0.05	0.04	32.44	2.59	1.34	10.84	2.46	2.08	1.55	249.15	97.16	1.53	0.92	1.82	112.647	Average

n (original) = 643,940

n (tested) = 592,133

(B) Summary Statistics for very fine to fine grained facies data - expanded measured parameters list

Image	Porosity (%)	Air Permeability (mD)	Klinkenberg Permeability (mD)	Area (µm²)	Feret 0 (µm)	Feret 90 (µm)	Length (µm)	Breadth (µm)	Average Length	Perimeter (µm)	Conv Perimeter (µm)	Roundness	Compactness	Aspect Ratio	Equiv Circ Diam (µm)	Pore Area Length	Pore Area Breadth	Pore Shape Lxlca	Pore Shape Length	Pore Shape Breadth	Pore Shape Average	% Microporosity	Perimeter/ Area	
Minimum (IQR-0)	2.000.01	5.00E-05	5.00E-05	6.61E-07	1.08E-03	8.77E-04	1.09E-03	5.02E-04	9.09E-04	3.04E-03	2.57E-03	1.00E+00	1.52E-02	1.00E+00	9.12E-04	1.13E-06	3.40E-07	1.06	0.57	0.97	0.96	2.03E-07	6.77E-03	Minimum (IQR-0)
IQR-1 (25th Percentile)	1.89	0.0004	0.0001	0.01	0.05	0.05	0.12	0.07	0.12	0.48	0.13	1.47	0.94	1.50	0.09	0.01	0.005	1.26	0.81	1.41	1.20	2.03E-06	5.91	IQR-1 (25th Percentile)
Median (IQR - 2, 50th percentile)	3.70	0.01	0.0018	0.19	0.29	0.29	0.73	0.38	0.52	2.19	0.55	1.90	0.49	1.89	0.49	0.53	0.13	1.41	0.89	1.69	1.35	8.31E-06	11.33	Median (IQR - 2, 50th percentile)
IQR-3 (75th percentile)	5.18	0.02	0.01	2.41	1.70	1.58	2.67	1.48	2.06	8.74	2.13	2.61	0.68	2.38	1.75	7.14	2.12	1.73	1.00	2.10	1.56	2.44E-05	70.99	IQR-3 (75th percentile)
Maximum (IQR -4)	19.96	1.49	1.25	1903411.96	3461.56	1990.50	3496.62	1657.90	3577.26	59100.00	4010.50	922.10	0.95	70.25	1529.14	90135924	2740638	44.44	25.10	51.09	33.35	0.03	5500.00	Maximum (IQR -4)
Harmonic Mean	2.44E+00	3.38E-04	1.71E-04	4.07E-04	4.88E-02	4.49E-02	8.20E-02	4.32E-02	6.44E-02	2.64E-01	1.18E-01	1.25E+00	3.82E-01	1.78E+00	6.10E-02	7.56E-04	2.56E-04	1.47E+00	9.00E-01	1.47E+00	1.38E+00	1.41E-06	3.91E+00	Harmonic Mean
Kurtosis	2.04	47.80	62.86	223297.48	82143.39	6692.20	63624.54	8110.13	46646.22	70630.22	11238.72	12604.04	-0.63	75.03	6640.63	407773.77	304256.33	320.09	634.66	106.90	307.56	11606.95	47.05	Kurtosis
Mode (Single)	4.78	0.00	0.00	0.06	0.49	0.49	0.24	0.24	0.24	0.97	0.02	1.20	0.87	2.00	0.27	0.06	0.06	1.13	1.13	1.13	1.13	0.00	16.47	Mode (Single)
Skewness	1.31	6.08	7.04	404.70	123.30	55.95	183.76	76.09	147.04	227.52	83.01	67.35	-0.19	4.82	52.53	666.64	436.44	8.73	12.18	5.29	8.72	83.39	5.30	Skewness
Standard Deviation	2.68	0.14	0.11	3249.37	22.39	10.14	21.84	6.77	13.70	212.02	20.03	4.05	0.16	1.07	7.11	120629.03	4145.52	0.55	0.22	0.75	0.42	1.57E-03	219.10	Standard Deviation
Variance	7.21	0.02	0.01	10559430	501.21	102.91	477.02	45.87	189.96	45283.90	401.21	16.40	0.03	1.15	50.55	14551302160	17185302	0.30	0.05	0.56	0.18	2.47E-06	48041.09	Variance
Average	4.07	0.05	0.03	42.44	2.43	2.09	3.19	1.63	2.41	13.88	2.20	2.44	0.48	2.08	1.87	488.02	48.54	1.57	0.93	1.85	1.45	1.12E-04	93.69	Average
n	644710	644710	644710	644710	412124	412124	644710	644710	644710	644710	365289	730921	251499	644710	644710	644710	644710	644710	644710	644710	644710	644710	644710	n

(C) Summary Statistics for transitional fine to coarse grained facies core data

	Porosity (%)	Air Permeability (mD)	Klinkenberg Permeability (mD)	Area (µm²)	Feret 0 (µm)	Feret 90 (µm)	Length (µm)	Breadth (µm)	Average Length	Perimeter (µm)	Conv Perimeter (µm)	Roundness	Compactness	Aspect Ratio	Equivalent Circular Diameter	Pore Area (Length) (µm)	Pore Area (Breadth) (µm)	Pore Shape (Lxlca)	Pore Shape Length	Pore Shape Breadth	Pore Shape Average	% Microporosity	Perimeter/ Area	
Minimum (IQR-0)	1.29	0.03	0.02	0.00	0.00	0.00	0.00	0.00	0.00	0.01	0.01	1.00	0.00	1.00	0.00	0.00	0.00	1.06	0.57	0.99	0.97	0.00	0.01	Min (IQR-0)
IQR-1 (25th Percentile)	14.87	4.55	4.09	1.73	1.70	1.70	1.94	0.97	1.51	6.31	5.02	1.50	0.37	1.50	1.49	3.77	0.94	1.26	0.83	1.41	1.20	0.00	0.62	IQR-1 (25th Percentile)
Median (IQR - 2, 50th percentile)	25.30	26.42	25.12	10.14	4.27	4.27	5.26	2.91	4.13	16.51	13.04	1.74	0.57	1.75	3.59	27.43	8.49	1.36	0.90	1.62	1.30	0.00	1.66	Median (IQR - 2, 50th percentile)
IQR-3 (75th percentile)	37.72	56.84	54.35	78.94	11.68	11.68	14.57	8.28	11.68	48.57	36.82	2.69	0.67	2.00	9.99	212.33	68.18	1.69	0.96	1.90	1.49	0.00	8.85	IQR-3 (75th percentile)
Maximum (IQR -4)	40.51	151.69	140.22	13509840	13684.27	9900.09	14025.62	4182.03	9534.22	183660.42	33287.67	951.50	1.00	99.50	4147.44	221581746	17490642	42.87	19.88	56.70	33.02	0.57	1940.00	Max (IQR -4)
Harmonic Mean	17.55	1.79	1.32	0.00	0.57	0.55	0.66	0.35	0.51	2.14	1.61	1.90	0.37	1.76	0.47	0.01	0.00	1.46	0.91	1.43	1.35	0.00	0.71	Harmonic Mean
Kurtosis	-1.19	-0.22	-0.31	101010.87	23191.30	3461.53	17276.40	2497.22	9906.54	27191.57	12481.47	4424.65	-0.79	1162.70	3699.70	310857.99	112395.17	248.36	478.18	313.34	330.65	11251.95	138.33	Kurtosis
Mode (Single)	38.61	151.69	140.22	1.18	1.46	1.46	1.46	0.97	1.21	4.86	3.43	1.50	0.67	2.00	1.23	3.12	0.94	1.26	0.94	1.41	1.20	0.00	4.12	Mode (Single)
Skewness	-0.14	1.10	1.11	269.26	91.30	56.04	90.66	31.71	59.90	126.06	66.92	44.59	-0.52	10.14	32.93	536.01	239.70	8.09	12.66	8.23	9.37	123.17	11.13	Skewness
Standard Deviation	11.84	49.90	48.85	28041.76	48.96	40.75	56.88	25.77	38.99	459.82	129.43	4.75	0.20	0.58	26.10	375579.88	33472.95	0.64	0.25	0.55	0.44	0.00	88.56	Standard Deviation
Variance	140.12	2489.54	2386.29	787462407	1932.33	1660.36	3240.30	663.94	1519.82	435376.70	16751.19	22.60	0.04	0.34	681.20	141055736676	1120430578	0.40	0.06	0.31	0.19	0.00	6982.88	Variance
Average	26.06	43.53	44.06	608.63	12.71	12.78	15.39	8.55	11.97	47.56	38.53	2.47	0.53	1.88	9.68	3086.28	787.06	1.37	0.94	1.73	1.42	0.00	12.96	Average

n = 750609

Table III-2: The data output from the digital image analysis (DIA) was summarized to review primary characteristics of each area included in the study.

Quantitative regression analysis: relationship between pore architecture, porosity, and permeability

Regression analysis was used to identify the relationship between a series of independent variables (geometric features of the pore architecture) and dependent variables (porosity and permeability) to determine which components of the pore architecture could be used to accurately predict porosity or permeability. The regression analysis was performed using three primary data sets in an iterative manner to generate reliable results from a stable model that incorporates parameters that do not have potential redundancies in measurements, missing values or a high degree of co-linearity. Parameters were excluded and data was reduced to derive the most reliable model that could potentially be applicable to other areas within the basin, and other carbonate mudrock reservoirs.

A total of eight models were tested in an attempt to find both statistically significant parameters, and a model that had a valuable level of predictability. Each model tested produced results that identified the most statistically significant variables as well as the applicability of the model to accurately predict unknown data. Variables were removed from subsequent trials if the measured value has a significant amount of redundancy in the measurement (e.g.: area, perimeter/area), or a high degree of co-linearity, which resulted in an unstable model and therefore non-useful results. Covariance values that were used to help identify features with a high degree of co-linearity are shown in Table III-2.

Due to the non-predictive ability of the first two regression models (model #1 and 2) that included a sub-set of all observations from the image analysis, two regression models (model #3 and 4) were processed using reduced data that excluded observations associated with Klinkenberg permeability values less than 0.01mD and air permeability values less than 0.01mD. The cut-off of 0.01mD was applied for two primary reasons. First, the number of

observations in the data set allowed for a reduction in the total number of observations included that did not endanger the potential applicability of the model. Second, the data set is composed of very low porosity, low permeability samples that are composed of very fine grained materials that are generically classified as “unconventional” reservoir rocks. However, the laboratory analysis that quantitatively determined the porosity, air permeability, and Klinkenberg permeability values was done using methods typically applied to samples that have predominantly macropores. Although the data are reported to the ten thousands (0.0001mD) significant digit, the feasibility of this methodology to report data to that accuracy level with repeatable precision is uncertain (Ling et al., 2013; Nooruddin et al. 2014; ASTM Standard D6539-13 2013; ASTM Standard D4525 2013). Because an accuracy of 0.01mD is reportedly a more reliable value, at two orders of magnitude higher, this value was used as the cut-off to identify if uncertainty in the data set was the cause of models that were not highly predictive and therefore not useful. If the data at the lowest reported permeability values had a high degree of uncertainty, the data are effectively noise, which is not statistically feasible to predict using measured pore architecture data.

Due to lack of predictability in the analysis, two regression models (#5 and 6) were tested that incorporated data that measured the length and width of the pores using a slightly different, but more repeatable methodology. The software program that measure the length and breadth values using a methodology that is orientation dependent, whereas the measurements identified as “feret 0” and “feret 90” employ a methodology that is repeatable and independent of the orientation of the object. Because the argument for data reduction has already been applied, the model that utilized the feret 0 and feret 90 data were run using the similarly reduced data with a cut-off value of 0.01mD applied to the air permeability and Klinkenberg permeability observations.

Lastly, two models (model #7 and 8) were tested that incorporated data from the transitional core. The variables used are similar to those included in the previous models that produced stable models and parameters that, confirmed by the covariance values, had the least amount of co-linearity.

Acoustic Response

In conventional carbonate reservoirs, the relationship between porosity and acoustic response (sonic velocity) has a clear inverse relationship that can be approximated by the Wyllie time average equation (Figure III-2a) (Anselmetti et al., 1997). Scatter present and deviations from the fundamental relationship between velocity and porosity is related to the dominant pore type (Figure III-2b) (Anselmetti et al., 1997). Understanding how the dominant pore type affects the velocity response in carbonates can potentially provide information that can be used to predict permeability (Anselmetti and Eberli, 1993; Anselmetti et al., 1997; Anselmetti et al., 1998; Anselmetti and Eberli, 1999). For example, at the same total porosity, a sample with intergranular porosity will typically have a slower velocity than a sample with moldic porosity because of the difference in connectivity of the pores and the effect on the elastic properties of the sample. Because there is typically greater connectivity of the pores in intergranular samples, which indicates a higher permeability, it can be stated that generally if the velocity response is lower than expected, the permeability is relatively higher than in locations where the actual velocity is close to or higher than the value predicted by the Wyllie time average equation.

(a)

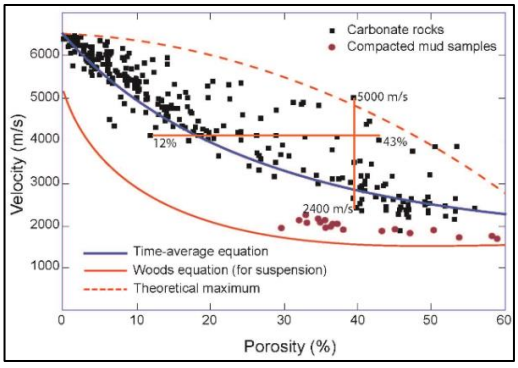

(b)

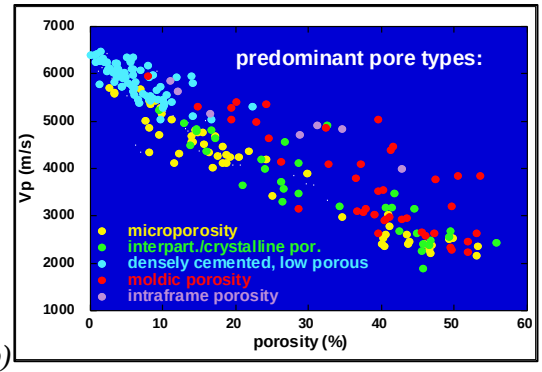

Figure III-2: (a) The relationship between the acoustic response, or velocity, and measured porosity has a predictable inverse relationship. The relationship can be approximated with the Wyllie time average equation with the Woods equation presented as a useful lower boundary to the data. (b) When the data are plotted based on categories of predominant macropore type, there are data groupings observed that can be applied to enhance the predictability of the velocity-porosity relationship in carbonates that predominantly have macroporosity. Figures used with permission from G. Eberli. (Anselmetti and Eberli, 1999; Eberli, 2001).

It has also been shown the percentage of microporosity in carbonate rocks with predominantly macropores affects the velocity response by altering the bulk modulus and elastic properties of the rock (Baechle et al., 2008a). The result of increasing microporosity can result in a lower velocity for a given porosity, but has also been shown to be more consistent with values predicted using the Wyllie time average equation (Baechle et al., 2008b). Examples of how the different bulk modulus and elastic properties of a carbonate mudrock affect the velocity response for carbonate mudrocks, where the pores are predominantly predominantly micro- to picopore size with little to no influence from macroporosity, is currently uncertain but research continues to unveil the primary controlling properties within the pore architecture in carbonates and mixed carbonate – siliciclastic systems as it is related to the acoustic response and mineral composition (Kleipool et al., 2015; Moshier, 1989; El-Husseiny and Vanorio, 2015; Vanorio and Mavko, 2011; Mokhtar et al., 2012; Neto et al., 2014; Neto et al., 2015; Nur et al., 2008; Peltonen et al., 2009; Rafavish et al., 1984; Rasolofosaon et al., 2008, Verwer et al., 2008; Verwer et al., 2010).

Acoustic response for this study was measured on core plugs selected to represent large variations in porosity for a given permeability, and large variations in permeability for given porosity while also being representative of the different facies within each core. The acoustic response was measured using an AutoLab 1000 from New England Research, Inc. that records the travel time through core plugs for one compressional wave (Vp) and two shear waves (Vs) using affixed transducers and receivers. The plugs were measured under dry, non-saturated conditions, saturated in a 35 ppt NaCl brine solution, and then re-measured under saturated conditions at various burial pressures. The internal pore pressure is also adjusted to simulate various burial conditions using a brine liquid with the same concentration used to saturate the samples. For dry samples used in this study, the pore pressure was held constant at ambient conditions and the confining pressure was adjusted to simulate an effective pressure from 2-30MPa, which correlates to a depth of approximately 200m-3000m (650 – 10,000ft.) under normal hydrostatic pressure gradients of approximately 0.45 psi/ft. or 10.20 KPa/m. For saturated samples, the pore pressure was held constant at 3MPa and the confining pressure was adjusted to simulate an effective pressure from 2 - 30 MPa, to easily compare with the conditions the unsaturated samples were tested. For comparison purposes, the data reported are from the acoustic response of the saturated samples at an effective pressure of 20MPa, which correlates with a burial of approximately 2000m (6500ft.), assuming a normal formation pressure (not over-pressured, or under-pressured) and a normal lithostatic gradient. The actual minimum and average minimum depth to the top of the Mississippian section in the cored intervals is 959m (3147ft.) and 1300m (4280ft.) respectively, and the maximum and average maximum depth of the cored interval of samples tested is 1770m (5810ft.) and 1375m (4515ft.) respectively.

The data used to determine these relationships is the brine saturated data from 20MPa effective pressure. Because of the high degree of brine water within the formation, and variability in present day depth, these values are used because they have the greatest applicability. A data specific relationship can be defined with reasonable accuracy (R^2= 0.79) using a simple linear relationship. This best-fit line is necessary to identify to help relate scatter in the velocity-porosity relationship to permeability.

RESULTS

Pore Architecture Analysis

Qualitative Analysis of Pore Architecture: Pore Type, Morphology and relationship to Facies, Porosity and Permeability

The majority of the pores identified in this study are all within a small, nano- to micropore, classification size, as defined by Loucks et al. (2012), and the overall grain size is in the clay/mud (<4μm) to silt fraction (<63μm). The major pore type is a combination of dissolution-enhanced intercrystalline and interparticle porosity, with some samples containing intraparticle porosity, and micro-fracture porosity. Although a quantitative analysis is most straight-forward in the application, integrating qualitative observations can also provide insight into the predictability of potential reservoir porosity or permeability.

Some of the characteristics of the pore architecture are only partially captured through quantitative evaluation methods due to the methodology used that measures two-dimensional geometric features in standardized and repeatable procedures. Supplemental qualitative observations can provide key information when interpreting the relationship between pore architecture, porosity, and permeability.

The majority of the pores viewed in thin section are from the macro- to micropore size. These size pores have a variety of non-geometric shapes but are classified generically as

interparticle, intercrystalline, and intraparticle pores that have variable degrees of dissolution-enhanced pore space. Many of the samples in the data set have pores that are partially to completely filled with trapped organic material, possibly immobile, as well as pore space that was sufficiently connected to be impregnated with an epoxy during the process of making the thin section, herein referred to as open pores or open porosity. Also observed in thin section are areas both connected to the organic filled pores and the open pores that have a significant amount of brown staining that are presumed to have nano- or picopores that area indiscernible with the LM. In general, samples from facies that are more mud-rich appear to have poorly connected interparticle pores and a greater tendency toward highly elongate, fracture-type porosity that parallels the bedding planes. Samples from facies that are more skeletal rich appear to have a greater abundance of open pores, as well as pore space that has been dissolution enhanced. Samples from facies that have had the greatest amount of alteration where the matrix is altered to a crystalline dolomite have the largest pores and the greatest connectivity based on the area observed to be filled by the blue epoxy impregnated into the sample pore space.

Pore morphology as viewed in the FE-SEM provides additional insight into the internal pore network which likely has a direct impact on the permeability (Vanden Berg and Grammer, 2016). Pore sizes that are best viewed with the FE-SEM are those in the micro- to nanopore size range, but can also include the meso- and macropores. As shown in FE-SEM photomicrographs, several of the relatively larger interparticle pores have some type of partial pore filling cement that, based on morphology observed in FE-SEM and compositional information from EDX (energy dispersive x-ray spectroscopy) analysis is typically a type of clay mineral, calcite, or quartz. Based on consistent morphologic features, the clay minerals appear to be either illite, smectite, or kaolinite material (Welton, 1984) and are observed consistently to sub-divide the

pore space into a series of what are effectively smaller, vuggy pores (that are micro-pore to nanopore in size) with even smaller pore throats (that are generally large nanopores in size or small micropores in size). In contrast, pores that are partially filled with a quartz or calcite mineral are consistently observed to have this mineral line the pore walls but not extend into the pore space which results in effectively smaller pore diameter and total void space and smaller pore throats where the crystal extend toward the intersection of the pores, but still retains the open internal flow network. Therefore, the measurements of the pore diameter and shape are similar, but the flow path is significantly different with the quartz and calcite lined pores being easier for a fluid to move through than a series of pores that have highly complicated flow pathways. In some observations of the smaller nanopores, where calcite or quartz is observed in the pore space, the pores are sub-divided in such a way that effectively fills the pore space with the mineral and has a net effect of reducing the total porosity and reducing the permeability. It is noted that with the smaller size pores, it is rare to have any mineral precipitation inside the pore space. The clay minerals are primarily only observed within the large micro- and larger size pores. The only pore type that is observed consistently to have an open internal pore network is the matrix pores which are typically micro- to nanoscale. As defined by Vanden Berg and Grammer (2016) these pores are either preserved or created within the mud matrix but are not specifically associated with any grains. Because these pores are typically in the nanopore size classification the preserved internal pore space could be a result of these pores being part of an the ineffective flow network that were not altered by fluid migration as they were not, and are not, a significant contributing feature to permeability.

Quantitative Analysis of Pore Architecture: Digital Image Analysis

Image analysis was completed using 2,932 images that were most representative of 323 samples from the five cores used in this study. The specific number of samples, images analyzed

and data points/pores are identified in Table III-1. From the photomicrographs that were analyzed, 1,402,559 data points, or pores, were identified. The number of photomicrographs used for each sample varied based on data available, complexity of the pore types, variability in the pore sizes, and variability in the geometric shapes observed. For each identified pore, the following data measurements were included in the output file: area (μm^2), length(μm), breadth(μm), feret 0(μm), feret 90(μm), perimeter(μm), roundness, compactness, Y Max, X Max, Y Min, X Min, X Centroid, Y Centroid, derived orientation, aspect ratio, equivalent circle diameter(μm), curve length, curve width(μm), curve ratio, convex area(μm^2), forks, and joins. Additional parameters used included: area (μm^2), length(μm), breadth(μm), feret 0(μm), feret 90(μm), perimeter(μm), roundness, compactness, aspect ratio, pore shape, equivalent circle diameter(μm), calculated area using the breadth and length measurement, calculated pore shape using the length and breadth measurements, and calculated perimeter/area (P/A). The summary statistics for the data used in this study are included as Table III-2.

Pore Size Distribution

Pore size distribution can be viewed using a variety of graphical methods. A first-glance graphical depiction of the pore size distribution useful for conventional carbonate is obtained by plotting the perimeter/area on the y-axis against the pore area on the x-axis for each point (Weger et al., 2009). In carbonate mudrocks this method also provides a simple at-a-glance method to identify the major pore size in a sample, but does not provide detailed information for the smallest micro- to nano- size pores. As shown in Vanden Berg and Grammer (2016), when the data are plotted using a semi-log scale, the distribution of the micro- to picometer size pores become clearly displayed with a more accurate visual depiction of the pore size distribution in the data set.

Data from this study have been plotted using two types of displays and with four categories as: (1) core with unconventional reservoir facies (fine grain proximal and distal facies) data, (2) unconventional reservoir fine grained distal facies, (3) unconventional reservoir fine grain proximal facies, and (4) transitional reservoir fine to coarse grain facies data (Figure III-3). As shown in Figure III-3, it is clear the core representative of a transitional unconventional to conventional reservoir has the greatest percentage of larger macro- to mesopore size, while the smallest pores are associated with the core that have predominantly unconventional reservoir facies that are fine to very fine grain.

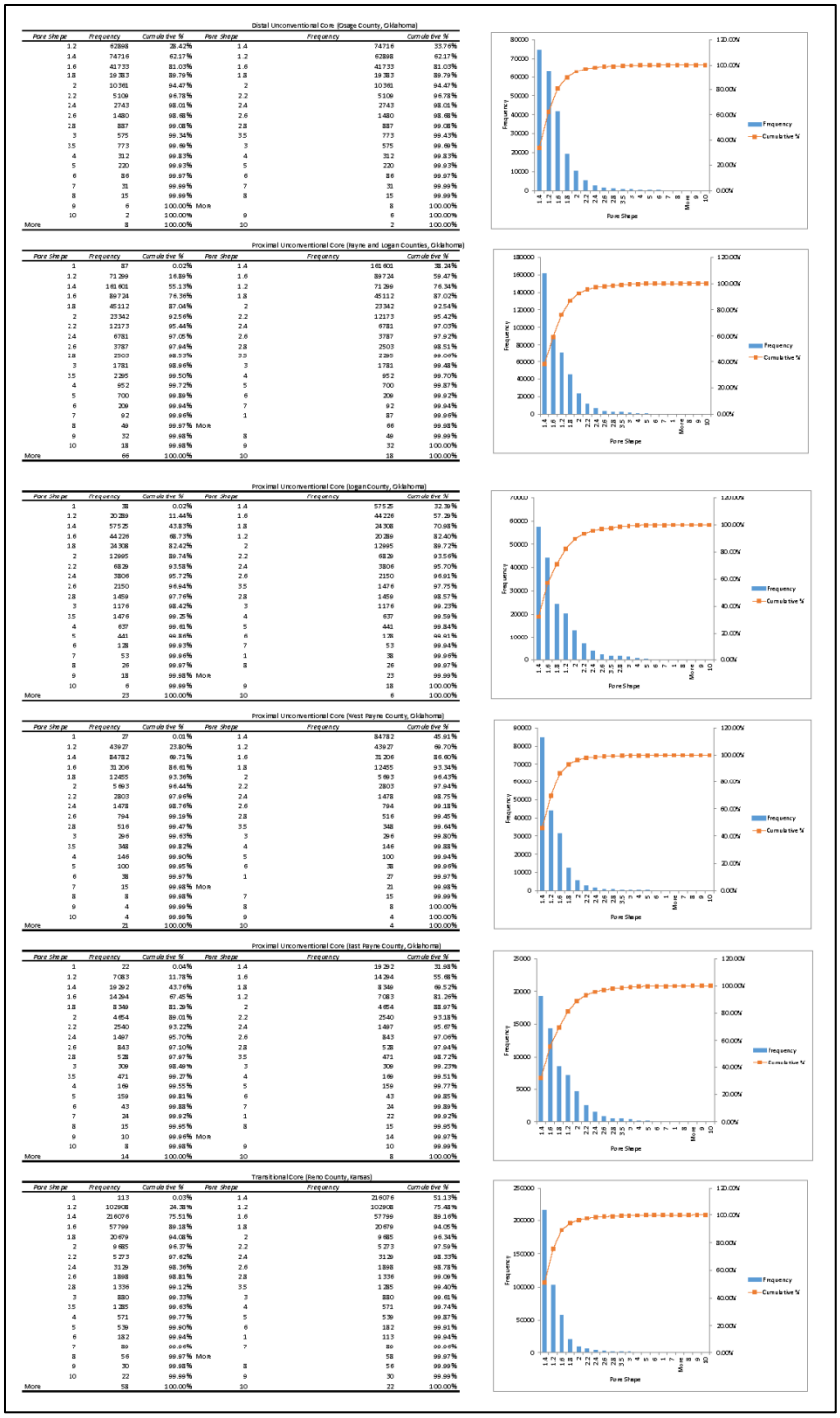

Figure III-3: Pore Shape distribution by core classification and area included in this study. Both graphed by specific core, and by specific area, the pore shape is clearly skewed toward lower values that are generally less than 3.0. A factor of 1.0 is a perfectly spherical pore shape with higher values related to more elongate pores. Based on the graphed data, the majority of the pores are highly spherical to ovoid in shape. What is not shown in the graphed data, are

qualitative observations regarding jagged perimeter boundaries and the highly non-geometric nature of the observed pore shapes.

Pore Shape Distribution

The pore shape is calculated such that a value of 1 is equal to a perfect sphere, and higher values are an indication of more elongation in the pore shape. In carbonate with predominantly macropores, the pore shape is an important characteristic that can be used as an indicator of effective permeability where the more elongate the pore shape, the greater the connected pore space and effective permeability (Anselmetti and Eberli, 1998). As shown in Figure III-4, the overall pore shape for the five cores is strongly skewed toward a value of 1, indicating primarily round or oval shaped pores. Although some of the pores have a pore higher calculated shape values, typically <1% of the data have a pore shape value that is greater than 3 in the data set.

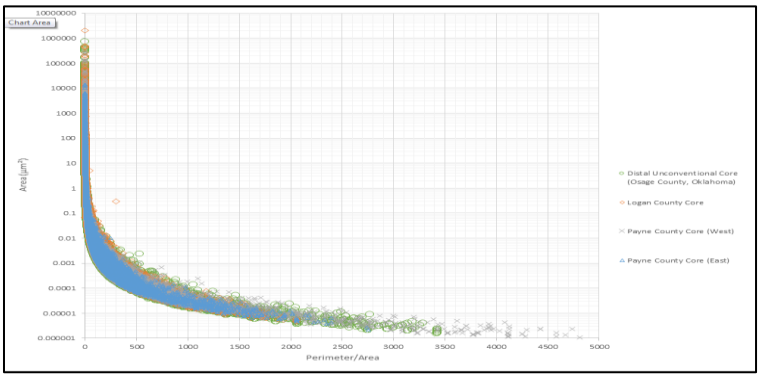

(a)Logan, Payne, and Osage Counties, Oklahoma Pore Size Distribution

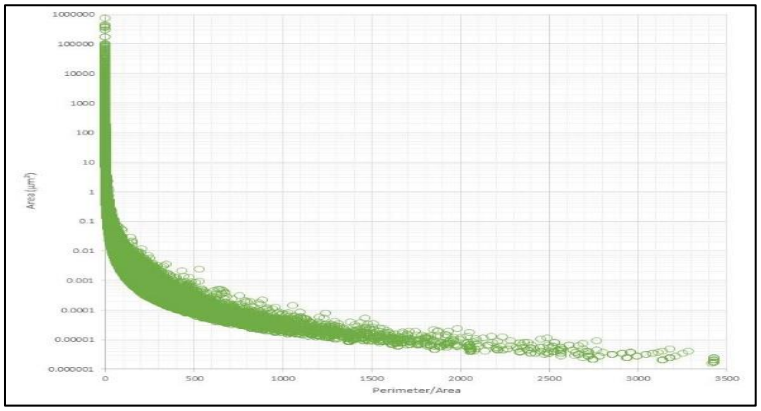

(b) Osage County, Oklahoma core Pore Size Distribution

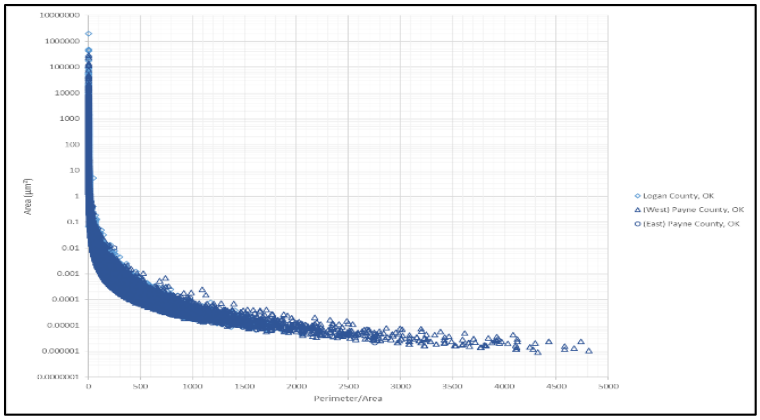

(c) Logan and Payne Counties Core Pore Size Distribution

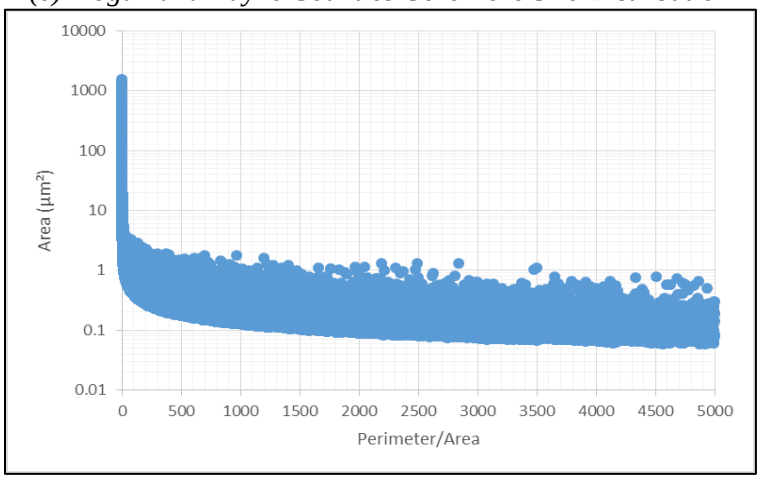

(d) Reno County, Kansas core pore size distribution

Figure III-4: Pore Size distribution plotted by facies type and area included in this study. The measured pore sizes are plotted in a semi-log manner which clearly identifies the distribution from macropores to picopores present in the data set. The data generically plot in such a way that data aligned with the vertical axis are macro- to large micropore size, and data that align with the horizontal axis are micro- to picopore size. The pore size distribution from the four cores with very fine grained facies is nearly identical for each core (a,b,c) with a similar trend but clearly large overall pore sizes measured in the transitional core (d).

Quantitative Regression Analysis: Relationship between porosity, permeability, and pore architecture

Because the size of the data generated is too large to be combined into a single excel spreadsheet that is necessary for input into the statistical software program utilized in this study, and because the primary focus of the research is to enhance the predictability of porosity

or permeability within very fine grained, unconventional reservoirs, the data were separated based on the primary facies observed and classified as unconventional data, and transitional data. The data were further segregated based on results of the models and derivation of data sets to be analyzed that could potentially provide additional information and success of identifying a useful and applicable model.

The regression analysis uses dependent values of porosity, air permeability, and Klinkenberg permeability as reported from the commercial laboratories, and independent variables that were extracted from the photomicrographs using DIA. Eight model trials were analyzed utilizing various inputs of the quantitative pore architecture data to attempt to identify useful parameters that could be used to accurately predict porosity or permeability within the data set. The results of the eight model trials are described below.

Results for the regression models that incorporated a sub-set of all data from the 4 cores from North-Central Oklahoma are shown in Table III-3. Four trials were analyzed that incorporated (1) all data features measured, (2) features that allowed for a stable model analysis, (3) data will lowest Klinkenberg values excluded (<0.01mD), and (4) data with lowest Air Permeability values excluded (<0.01mD). Due to the size of the data set, an additional trial was analyzed using the "Feret 0" and "Feret 90" measurements instead of the "length" and "breadth". The software program was designed so the length and breadth measurements are orientation dependent, but the feret 0 and feret 90 measurements are not orientation dependent and therefore more reliably reproducible measurements.

Significance meaning: 0 '***' 0.001 '**' 0.01 '*' 0.05 '.' 0.1 ' ' 1
The closer the measurement is to 1, the less statistically significant.

(1) Very fine to fine grained facies data with all measurements (unstable model)

Model test for Air Permeability	Estimate	Std. Error	t value	Pr(>|t|)	Significance
(Intercept)	-4.82E+00	0.112	-42.98	< 2e-16	***
Area	-9.02E-01	0.063	-14.39	< 2e-16	***
Length	-2.61E+01	40.770	-0.61	0.995	
Breadth	2.63E+01	17.890	1.47	0.142	
Perimeter	-1.32E-01	0.119	-1.11	0.268	
Roundness	-9.73E-04	0.008	-0.86	0.722	
Aspect Ratio	-6.47E-01	0.032	-20.02	< 2e-16	***
Equivalent Circular Diameter	1.68E-02	0.001	16.95	< 2e-16	***
Pore Area (Length)	9.20E-01	20.380	0.05	0.964	
Pore Area (Breadth)	-1.30E+01	8.944	-1.46	0.145	
Pore Shape (Leica)	-4.79E-01	0.073	-6.53	6.51E-11	***
Pore Shape (Length)	-8.76E-01	0.136	-6.43	1.27E-10	***
Pore Shape (Breadth)	8.27E-01	0.063	13.10	< 2e-16	***
Perimeter/Area	6.05E-04	0.000	20.82	< 2e-16	***

Residual Standard Error	2.502	on 265064 degrees of freedom	
Multiple R-squared:	0.03812		
F-statistic:	808	on 13 and 265064 DF	
p-value	<2.2*10^-16		

Model test for Klinkenberg	Estimate	Std. Error	t value	Pr(>|t|)	Significance
(Intercept)	-6.21E+00	0.121	-51.20	< 2e-16	***
Area	-1.07E+00	0.068	-15.71	< 2e-16	***
Length	-4.70E+01	44.090	-1.07	2.86E-01	
Breadth	5.09E+01	19.350	2.63	8.55E-03	**
Perimeter	1.38E-01	0.129	1.07	2.84E-01	
Roundness	-7.47E-04	0.009	-0.26	7.96E-01	
Aspect Ratio	-6.41E-01	0.035	-18.41	< 2e-16	***
Equivalent Circular Diameter	1.80E-02	0.001	16.83	< 2e-16	***
Pore Area (Length)	2.43E+01	22.050	1.10	2.71E-01	
Pore Area (Breadth)	-2.53E+01	9.674	-2.62	8.89E-03	**
Pore Shape (Leica)	-6.42E-01	0.079	-8.10	5.45E-16	***
Pore Shape (Length)	-6.83E-01	0.147	-4.65	3.37E-06	***
Pore Shape (Breadth)	8.73E-01	0.068	12.83	< 2e-16	***
Perimeter/Area	7.12E-04	0.000	22.68	< 2e-16	***

Residual Standard Error	2.706	on 265064 degrees of freedom	
Multiple R-squared:	0.03675		
F-statistic:	777.9	on 13 and 265064 DF	
p-value	<2.2*10^-16		

Model test for Porosity	Estimate	Std. Error	t value	Pr(>|t|)	Significance
(Intercept)	8.49E+00	0.119	71.17	< 2e-16	***
Area	1.74E+00	0.067	26.13	< 2e-16	***
Length	1.65E+02	43.320	3.80	0.00014	***
Breadth	-1.92E+01	19.010	-1.01	0.31149	
Perimeter	-1.93E+00	0.127	-15.22	< 2e-16	***
Roundness	-7.73E-03	0.003	-2.72	0.00657	**
Aspect Ratio	-2.66E-01	0.034	-7.76	0.00	***
Equivalent Circular Diameter	-3.42E-02	0.001	-32.57	< 2e-16	***
Pore Area (Length)	-8.25E+01	21.660	-3.81	0.00014	***
Pore Area (Breadth)	9.12E+00	9.503	0.96	0.33748	
Pore Shape (Leica)	1.16E+00	0.078	14.83	< 2e-16	***
Pore Shape (Length)	-1.69E+00	0.144	-11.73	< 2e-16	***
Pore Shape (Breadth)	-1.26E-02	0.067	-0.19	0.85	
Perimeter/Area	-3.00E-04	0.000	-9.73	< 2e-16	***

Residual Standard Error	2.658	on 265064 degrees of freedom	
Multiple R-squared:	0.06621		
F-statistic:	1446.00	on 13 and 265064 DF	
p-value	<2.2*10^-16		

(2) Very fine to fine grained facies data with only stable parameters

Model test for Air Permeability	Estimate	Std. Error	t value	Pr(>|t|)	Significance
(Intercept)	-3.9700652	0.056	-71.37	<2e-16	***
Perimeter	-0.1591718	0.004	-42.93	<2e-16	***
Roundness	-0.001795	0.002	-0.94	0.347	
Aspect Ratio	-0.50865	0.026	-19.25	<2e-16	***
Equivalent Circular Diameter	0.0154113	0.001	16.21	<2e-16	***
Pore Shape (Leica)	0.5572243	0.019	29.49	<2e-16	***
Pore Shape (Length)	-2.4122436	0.060	-40.51	<2e-16	***
Pore Shape (Breadth)	0.5471975	0.037	14.62	<2e-16	***
Perimeter/Area	0.0006231	0.000	21.49	<2e-16	***

Residual Standard Error	2.503	on 265064 degrees of freedom	
Multiple R-squared:	0.037		
F-statistic:	1279	on 8 and 265069 DF	
p-value	<2.2*10^-16		

Model test for Klinkenberg	Estimate	Std. Error	t value	Pr(>|t|)	Significance
(Intercept)	-5.16E+00	0.060	-85.79	< 2e-16	***
Perimeter	-1.68E-01	0.004	-41.90	< 2e-16	***
Roundness	-7.47E-03	0.002	-3.62	3.01E-04	***
Aspect Ratio	-4.81E-01	0.029	-16.81	< 2e-16	***
Equivalent Circular Diameter	1.62E-02	0.001	15.73	< 2e-16	***
Pore Shape (Leica)	5.89E-01	0.020	29.00	< 2e-16	***
Pore Shape (Length)	-2.20E+00	0.064	-34.13	< 2e-16	***
Pore Shape (Breadth)	5.35E-01	0.041	13.20	< 2e-16	***
Perimeter/Area	7.41E-04	0.000	23.61	< 2e-16	***

Residual Standard Error	2.710	on 265064 degrees of freedom	
Multiple R-squared:	0.035		
F-statistic:	1217.000	on 8 and 265069 DF	
p-value	<2.2*10^-16		

Model test for Porosity	Estimate	Std. Error	t value	Pr(>|t|)	Significance
(Intercept)	6.87E+00	0.059	115.92	<2e-16	***
Perimeter	3.25E-01	0.004	82.55	<2e-16	***
Roundness	4.62E-03	0.002	22.73	<2e-16	***
Aspect Ratio	-5.26E-01	0.028	-18.67	<2e-16	***
Equivalent Circular Diameter	-2.90E-02	0.001	-28.64	<2e-16	***
Pore Shape (Leica)	-9.01E-01	0.020	-45.08	<2e-16	***
Pore Shape (Length)	-1.59E+00	0.063	-25.06	<2e-16	***
Pore Shape (Breadth)	7.55E-01	0.040	18.94	<2e-16	***
Perimeter/Area	-3.65E-04	0.000	-11.82	<2e-16	***

Residual Standard Error	2.667	on 265064 degrees of freedom	
Multiple R-squared:	0.06339		
F-statistic:	3243.00	on 8 and 265069 DF	
p-value	<2.2*10^-16		

(3) Very fine to fine grained facies data, stablemodel with Air Permeability >0.01mD

Model test for Air Permeability	Estimate	Std. Error	t value	Pr(>|t|)	Significance
(Intercept)	-3.33E+00	0.051	-64.78	< 2e-16	***
Perimeter	-1.31E-01	0.003	-45.48	< 2e-16	***
Roundness	-1.02E-02	0.004	-2.43	0.0152	*
Aspect Ratio	-9.35E-02	0.022	-4.23	2.39E-05	***
Equivalent Circular Diameter	-1.27E-03	0.001	-1.40	0.1629	
Pore Shape (Leica)	-6.62E-02	0.021	-4.04	5.39E-05	***
Pore Shape (Length)	5.53E-01	0.054	10.15	< 2e-16	***
Pore Shape (Breadth)	1.23E-01	0.032	6.86	6.81E-12	***
Perimeter/Area	-1.23E-04	0.000	-10.9020	< 2e-16	***

Residual Standard Error	1.274	on 103267 degrees of freedom	
Multiple R-squared:	0.03879		
F-statistic:	520.1	on 8 and 103267 DF	
p-value	<2.2*10^-16		

Model test for Klinkenberg	Estimate	Std. Error	t value	Pr(>|t|)	Significance
(Intercept)	-4.08E+00	0.060	-68.49	< 2e-16	***
Perimeter	-1.57E-01	0.003	-46.95	< 2e-16	***
Roundness	-1.51E-02	0.005	-3.10	1.93E-03	**
Aspect Ratio	-1.18E-01	0.026	-4.59	4.53E-06	***
Equivalent Circular Diameter	-7.35E-04	0.001	-0.70	4.84E-01	
Pore Shape (Leica)	-6.75E-02	0.025	-2.74	6.11E-03	**
Pore Shape (Length)	6.42E-01	0.063	10.19	< 2e-16	***
Pore Shape (Breadth)	2.69E-01	0.038	7.15	8.99E-13	***
Perimeter/Area	-2.00E-04	0.000	-8.44	< 2e-16	***

Residual Standard Error	1.475	on 103267 degrees of freedom	
Multiple R-squared:	0.04308		
F-statistic:	581.1	on 8 and 103267 DF	
p-value	<2.2*10^-16		

Model test for Porosity	Estimate	Std. Error	t value	Pr(>|t|)	Significance
(Intercept)	6.16E+00	0.125	49.42	< 2e-16 ***	***
Perimeter	4.77E-01	0.007	68.02	< 2e-16	***
Roundness	7.64E-02	0.010	7.50	0.00000	***
Aspect Ratio	3.88E-01	0.054	7.42	0.00	***
Equivalent Circular Diameter	-8.17E-02	0.002	-37.11	< 2e-16	***
Pore Shape (Leica)	-1.83E+00	0.052	-35.40	< 2e-16	***
Pore Shape (Length)	2.70E+00	0.132	20.47	< 2e-16	***
Pore Shape (Breadth)	-2.76E-01	0.079	-3.50	0.00	***
Perimeter/Area	-1.69E-03	0.000	-34.05	< 2e-16	***

Residual Standard Error	3.092	on 103267 degrees of freedom	
Multiple R-squared:	0.1594		
F-statistic:	2448	on 8 and 103267 DF	
p-value	<2.2*10^-16		

(4) Very fine to fine grained facies data, stable model with Klinkenberg Permeability >0.01mD

Model test for Air Permeability	Estimate	Std. Error	t value	Pr(>|t|)	Significance
(Intercept)	-2.06E+00	0.045	-45.25	< 2e-16	***
Perimeter	-6.30E-02	0.003	-31.16	< 2e-16	***
Roundness	3.89E-03	0.003	1.11	0.267724	
Aspect Ratio	-6.49E-02	0.019	-3.38	0.000715	***
Equivalent Circular Diameter	-1.30E-03	0.001	-1.62	0.105088	
Pore Shape (Leica)	-5.67E-02	0.019	-3.03	2.44E-03	**
Pore Shape (Length)	2.43E-02	0.047	0.51	6.08E-01	
Pore Shape (Breadth)	8.41E-02	0.028	2.98	0.00288	**
Perimeter/Area	-4.89E-04	0.000	-28.19	< 2e-16	***

Residual Standard Error	0.9690	on 71273 degrees of freedom	
Multiple R-squared:	0.0187		
F-statistic:	169.9	on 8 and 71273 DF	
p-value	<2.2*10^-16		

Model test for Klinkenberg	Estimate	Std. Error	t value	Pr(>|t|)	Significance
(Intercept)	-2.55E+00	0.051	-49.68	< 2e-16	***
Perimeter	-9.49E-02	0.003	-31.60	< 2e-16	***
Roundness	3.84E-03	0.004	0.97	3.30E-01	
Aspect Ratio	-8.38E-02	0.022	-3.88	1.07E-04	***
Equivalent Circular Diameter	-8.89E-04	0.001	-0.99	3.25E-01	
Pore Shape (Leica)	-5.61E-02	0.021	-2.66	7.84E-03	**
Pore Shape (Length)	1.28E-02	0.053	0.24	8.11E-01	
Pore Shape (Breadth)	1.08E-01	0.032	3.40	6.81E-04	***
Perimeter/Area	-4.95E-04	0.000	-25.30	< 2e-16	***

Residual Standard Error	1.094	on 71273 degrees of freedom	
Multiple R-squared:	0.01826		
F-statistic:	165.7	on 8 and 71273 DF	
p-value	<2.2*10^-16		

Model test for Porosity	Estimate	Std. Error	t value	Pr(>|t|)	Significance
(Intercept)	5.34E+00	0.146	36.64	< 2e-16	***
Perimeter	6.60E-01	0.009	77.20	< 2e-16	***
Roundness	3.22E-02	0.011	2.87	0.00407	**
Aspect Ratio	3.05E-01	0.062	4.96	0.00	***
Equivalent Circular Diameter	-8.45E-02	0.003	-32.91	< 2e-16	***
Pore Shape (Leica)	-2.00E+00	0.060	-33.34	< 2e-16	***
Pore Shape (Length)	3.50E+00	0.152	23.08	< 2e-16	***
Pore Shape (Breadth)	-6.51E-02	0.091	-0.72	0.47	
Perimeter/Area	-1.03E-03	0.000	-18.51	< 2e-16	***

Residual Standard Error	3.112	on 71273 degrees of freedom	
Multiple R-squared:	0.2096		
F-statistic:	2362	on 8 and 71273 DF	
p-value	<2.2*10^-16		

(5) Very fine to fine grained facies data with feret 0 and 90 measurements and Air permeability >0.01mD

Model test for Air Permeability	Estimate	Std. Error	t value	Pr(>|t|)	Significance
(Intercept)	-2.89E+00	0.021	-140.48	< 2e-16	***
Area	6.43E-05	0.000	5.55	2.82E-08	***
Feret 0	-5.59E-03	0.001	-7.78	7.37E-15	***
Roundness	-2.59E-03	0.003	-0.86	0.389	
Aspect Ratio	-4.09E-02	0.003	-11.83	< 2e-16	***
Pore Shape (Leica)	1.31E-01	0.017	7.70	1.42E-14	***
Microporosity	7.37E+00	3.452	2.14	0.0328	*
Perimeter/Area	3.15E-04	0.000	26.53	< 2e-16	***

Residual Standard Error	1.363	on 132710 degrees of freedom	
Multiple R-squared:	0.007009		
F-statistic:	133.8	on 7 and 132710 DF	
p-value	<2.2*10^-16		

Model test for Klinkenberg	Estimate	Std. Error	t value	Pr(>|t|)	Significance
(Intercept)	-3.51E+00	0.024	-147.44	< 2e-16	***
Area	8.03E-05	0.000	5.99	2.08E-09	***
Feret 0	-6.95E-03	0.001	-8.35	< 2e-16	***
Roundness	-1.51E-03	0.003	-0.43	6.64E-01	
Aspect Ratio	-4.41E-02	0.004	-11.02	< 2e-16	***
Pore Shape (Leica)	1.34E-01	0.020	6.83	8.67E-12	***
Microporosity	9.45E+00	3.998	2.36	1.81E-02	*
Perimeter/Area	4.50E-04	0.000	32.71	< 2e-16	***

Residual Standard Error	1.579	on 132710 degrees of freedom	
Multiple R-squared:	0.009479		
F-statistic:	189.3	on 7 and 132710 DF	
p-value	<2.2*10^-16		

Model test for Porosity	Estimate	Std. Error	t value	Pr(>|t|)	Significance
(Intercept)	5.69E+00	0.050	113.097	< 2e-16	***
Area	-4.29E-04	0.000	-15.132	< 2e-16	***
Feret 0	2.77E-02	0.001	23.747	< 2e-16	***
Roundness	-5.65E-02	0.007	-7.676	0.00000	***
Aspect Ratio	-2.10E-01	0.008	-24.791	< 2e-16	***
Pore Shape (Leica)	5.69E-01	0.042	13.699	< 2e-16	***
Microporosity	-3.68E+01	8.448	-4.361	0.00	***
Perimeter/Area	-3.02E-03	0.000	-103.841	< 2e-16	***

Residual Standard Error	3.336	on 132710 degrees of freedom	
Multiple R-squared:	0.08333		
F-statistic:	1837.00	on 7 and 132710 DF	
p-value	<2.2*10^-16		

(6) Very fine to fine grained facies data with feret 0 and 90 measurements and Klinkenberg permeability >0.01mD

Model test for Air Permeability	Estimate	Std. Error	t value	Pr(>|t|)	Significance
(Intercept)	-2.27E+00	0.022	-101.86	< 2e-16	***
Area	8.94E-05	0.000	7.00	2.52E-12	***
Feret 0	-9.71E-03	0.001	-12.02	< 2e-16	***
Roundness	-1.78E-02	0.004	-4.43	9.65E-06	***
Aspect Ratio	-5.93E-03	0.003	-19.14	< 2e-16	***
Pore Shape (Leica)	1.51E-01	0.020	12.75	< 2e-16	***
Microporosity	3.21E+00	3.206	1.00	0.316	
Perimeter/Area	-2.15E-04	0.000	-21.30	< 2e-16	***

Residual Standard Error	1.055	on 97544 degrees of freedom	
Multiple R-squared:	0.01214		
F-statistic:	171.2	on 7 and 97544 DF	
p-value	<2.2*10^-16		

Model test for Klinkenberg	Estimate	Std. Error	t value	Pr(>|t|)	Significance
(Intercept)	-2.77E+00	0.023	-109.46	< 2e-16	***
Area	8.94E-05	0.000	7.38	1.44E-13	***
Feret 0	-1.16E-02	0.001	-12.58	< 2e-16	***
Roundness	-1.76E-02	0.005	-3.86	1.15E-04	***
Aspect Ratio	-6.60E-03	0.004	-18.71	< 2e-16	***
Pore Shape (Leica)	2.68E-01	0.022	11.94	< 2e-16	***
Microporosity	4.52E+00	3.648	1.24	2.16E-01	
Perimeter/Area	-1.76E-04	0.000	-15.38	< 2e-16	***

Residual Standard Error	1.201	on 97544 degrees of freedom	
Multiple R-squared:	0.009282		
F-statistic:	130.3	on 7 and 97544 DF	
p-value	<2.2*10^-16		

Model test for Porosity	Estimate	Std. Error	t value	Pr(>|t|)	Significance
(Intercept)	4.51E+00	0.070	64.83	< 2e-16	***
Area	-4.20E-04	0.000	-13.52	< 2e-16	***
Feret 0	3.77E-02	0.003	14.91	< 2e-16	***
Roundness	-1.41E-01	0.013	-11.18	< 2e-16	***
Aspect Ratio	-2.29E-01	0.010	-23.58	< 2e-16	***
Pore Shape (Leica)	1.06E+00	0.062	17.20	< 2e-16	***
Microporosity	-3.03E+01	10.040	-3.02	0.00	**
Perimeter/Area	-2.46E-03	0.000	-78.12	< 2e-16	***

Residual Standard Error	3.303	on 97544 degrees of freedom	
Multiple R-squared:	0.07811		
F-statistic:	1181.00	on 7 and 97544 DF	
p-value	<2.2*10^-16		

(7) Transitional grain size Core Data

Model test for Air Permeability	Estimate	Std. Error	t value	Pr(>|t|)	Significance
(Intercept)	-1.29E+01	0.373	93.80	< 2e-16	0
Area	7.74E-05	0.000	12.82	< 2e-16	0
Feret 0	5.76E-01	0.020	28.73	< 2e-16	0
Feret 90	6.14E-01	0.021	28.96	< 2e-16	0
Perimeter	-2.15E-03	0.000	-7.30	2.88E-13	0
C Perimeter	-1.91E-01	0.013	-29.11	< 2e-16	0
Roundness	-4.50E-01	0.031	-14.41	< 2e-16	0
Compactness	1.02E+02	0.777	131.74	< 2e-16	0
Aspect Ratio	5.92E-01	0.141	4.20	2.70E-05	0
Equivalent Circular Diameter	-3.21E-02	0.013	-2.53	0.0115	0.05
Pore Shape (Leica)	1.63E+01	0.373	43.60	< 2e-16	0
Microporosity	-4.50E+02	49.070	-9.16	< 2e-16	0
Perimeter/Area	-4.09E-02	0.001	-44.40	< 2e-16	0

Residual Standard Error	47.34	on 379291 degrees of freedom	
Multiple R-squared:	0.09865		
F-statistic:	3459	on 12 and 379291 DF	
p-value	<2.2*10^-16		

Model test for Klinkenberg	Estimate	Std. Error	t value	Pr(>|t|)	Significance
(Intercept)	-3.27E+01	0.353	-94.27	< 2e-16	0
Area	7.56E-05	0.000	12.80	< 2e-16	0
Feret 0	5.64E-01	0.020	28.74	< 2e-16	0
Feret 90	6.00E-01	0.020	29.83	< 2e-16	0
Perimeter	-2.10E-03	0.000	-7.30	2.93E-13	0
C Perimeter	-1.83E-01	0.013	-29.09	< 2e-16	0
Roundness	-4.39E-01	0.031	-14.37	< 2e-16	0
Compactness	1.00E+02	0.761	131.43	< 2e-16	0
Aspect Ratio	5.92E-01	0.138	4.29	1.83E-05	0
Equivalent Circular Diameter	-3.13E-02	0.012	-2.53	1.15E-02	0.05
Pore Shape (Leica)	1.59E+01	0.366	43.51	< 2e-16	0
Microporosity	-4.38E+02	48.050	-9.12	< 2e-16	0
Perimeter/Area	-3.98E-02	0.001	-44.16	< 2e-16	0

Residual Standard Error	46.35	on 379291 degrees of freedom	
Multiple R-squared:	0.09851		
F-statistic:	3454	on 12 and 379291 DF	
p-value	<2.2*10^-16		

Model test for Porosity	Estimate	Std. Error	t value	Pr(>|t|)	Significance
(Intercept)	1.63E+01	0.239	68.15	<2e-16	0
Area	3.75E-05	0.000	25.32	<2e-16	0
Feret 0	3.34E-02	0.005	10.85	<2e-16	0
Feret 90	7.55E-02	0.005	14.87	<2e-16	0
Perimeter	-1.64E-04	0.000	-2.27	0.02320	0.05
C Perimeter	-4.51E-02	0.003	-13.68	<2e-16	0
Roundness	-1.04E-01	0.008	-13.58	<2e-16	0
Compactness	1.20E+01	0.191	63.04	<2e-16	0
Aspect Ratio	-7.39E-01	0.035	-21.33	<2e-16	0
Equivalent Circular Diameter	-3.46E-02	0.003	-11.11	<2e-16	0
Pore Shape (Leica)	3.67E+00	0.093	39.86	<2e-16	0
Microporosity	-1.47E+01	12.040	-1.22	<2e-16	0
Perimeter/Area	-1.51E-02	0.000	-66.81	<2e-16	0

Residual Standard Error	11.62	on 379291 degrees of freedom	
Multiple R-squared:	0.0358		
F-statistic:	1174	on 12 and 379291 DF	
p-value	<2.2*10^-16		

(8) Transitional grain size Core data with High co-linearity measurements removed

Model test for Air Permeability	Estimate	Std. Error	t value	Pr(>|t|)	Significance
(Intercept)	1.75E-01	0.025	7.00	2.63E-12	***
Area	9.99E-07	0.000	8.45	< 2e-16	***
Feret 0	7.80E-04	0.000	9.69	< 2e-16	***
Perimeter	-1.40E-04	0.000	-23.78	< 2e-16	***
Roundness	-1.87E-01	0.001	-23.01	< 2e-16	***
Compact	3.50E+00	0.020	173.84	< 2e-16	***
Aspect Ratio	-1.35E-03	0.004	-0.38	0.705	
Pore Shape (Leica)	5.82E-01	0.010	57.87	< 2e-16	***
Microporosity	-2.23E+01	1.139	-19.57	< 2e-16	***
Perimeter/Area	-2.13E-03	0.000	-88.38	< 2e-16	***

Residual Standard Error	1.749	on 758599 degrees of freedom	
Multiple R-squared:	0.08475		
F-statistic:	7805	on 9 and 758599 DF	
p-value	<2.2*10^-16		

Model test for Klinkenberg	Estimate	Std. Error	t value	Pr(>|t|)	Significance
(Intercept)	7.75E-03	0.026	0.30	7.66E-01	
Area	9.42E-07	0.000	7.66	1.94E-14	***
Feret 0	9.04E-04	0.000	10.80	< 2e-16	***
Perimeter	-1.45E-04	0.000	-23.74	< 2e-16	***
Roundness	-1.93E-02	0.001	-23.83	< 2e-16	***
Compact	3.62E+00	0.021	172.85	< 2e-16	***
Aspect Ratio	-1.09E-03	0.004	-0.29	7.68E-01	
Pore Shape (Leica)	5.78E-01	0.010	57.25	< 2e-16	***
Microporosity	-2.30E+01	1.185	-19.41	< 2e-16	***
Perimeter/Area	-2.22E-03	0.000	-88.41	< 2e-16	***

Residual Standard Error	1.819	on 758599 degrees of freedom	
Multiple R-squared:	0.08413		
F-statistic:	7741	on 9 and 758599 DF	
p-value	<2.2*10^-16		

Model test for Porosity	Estimate	Std. Error	t value	Pr(>|t|)	Significance
(Intercept)	1.56E+01	0.167	93.80	<2e-16	***
Area	3.34E-05	0.000	42.36	<2e-16	***
Feret 0	-2.69E-02	0.001	-50.24	<2e-16	***
Perimeter	-5.23E-04	0.000	-13.40	<2e-16	***
Roundness	-1.14E-01	0.005	-21.10	<2e-16	***
Compact	1.26E+01	0.134	94.11	<2e-16	***
Aspect Ratio	-6.50E-01	0.024	-27.34	<2e-16	***
Pore Shape (Leica)	3.74E+00	0.065	57.51	<2e-16	***
Microporosity	-1.54E+02	7.579	-20.32	<2e-16	***
Perimeter/Area	-1.49E-02	0.000	-92.78	<2e-16	***

Residual Standard Error	11.63	on 758599 degrees of freedom	
Multiple R-squared:	0.03399		
F-statistic:	2966	on 9 and 758599 DF	
p-value	<2.2*10^-16		

*Table III-3: The results from each regression model tested are shown in the above table. The results identify measurements that have a high level of statistical significance, and the ability of the model to predict unknowns based on the p-value. If the p-value is a high number, this indicates the model has a high level of predictability for accurately predicting values for unknown data. The p-value for each model tested is <2.2*10^-16 which indicates the model will not have a high level of accuracy in predicting unknown values.*

The initial model results (models #1 and 2) indicated the area, aspect ratio, equivalent circular diameter, pores shape (calculated using any input values), and the perimeter/area values have the greatest correlation to the laboratory measured porosity, air permeability, and Klinkenberg calculated permeability. Additional statistically significant measurements include whichever is largest between the measured length or breadth value as related to the Klinkenberg permeability or porosity. Secondary statistically significant observations related to the porosity are the pore area, pore perimeter, and roundness measurements.

Additional analysis indicated the model was not stable due to a high degree of co-linearity of measured features within the data set. This is confirmed by the correlation values as shown in Table III-4. As shown in Table III-4, none of the measured parameters have a high degree of co-linearity with the values attempted to be predicted, but several have a high covariance value, and high co-linearity, with other measured parameters. Measured features with the greatest co-linearity and redundancy in other measurements were removed from the model which then produced a stable model and reliable results. However, as noted by the low r^2-value for each additional sub-set of data, the models were unable to identify a useful correlation between the measured pore architecture features and either porosity or permeability.

(A) Correlation matrix for fine to very fine grained facies data

	Porosity	Air Permeability (mD)	Klinkenberg Permeability (mD)	Area (µm²)	Length (µm)	Breadth (µm)	Perimeter (µm)	Roundness	Aspect Ratio	Equiv Circ Diam (µm)	Pore Area (length)	Pore Area (breadth)	Pore Shape (Leica calculation)	Pore Shape (length)	Pore Shape (breadth)	Perimeter/ Area
Porosity	1.00	0.32	0.33	0.22	0.21	0.21	0.20	-0.03	-0.03	0.00	0.21	0.21	-0.06	-0.04	-0.04	-0.18
Air Permeability (mD)		1.00	0.98	-0.15	-0.13	-0.15	-0.14	0.00	0.06	-0.02	-0.13	-0.15	0.03	-0.07	0.05	0.14
Klinkenberg Permeability (mD)			1.00	-0.15	-0.13	-0.15	-0.14	0.00	0.06	-0.01	-0.13	-0.15	0.03	-0.06	0.05	0.14
Area (µm²)				1.00	0.99	0.99	0.99	0.11	-0.09	0.40	0.99	0.99	0.17	0.17	0.00	-0.68
Length (µm)					1.00	0.98	1.00	0.15	0.02	0.40	1.00	0.98	0.26	0.11	0.09	-0.67
Breadth (µm)						1.00	0.99	0.12	-0.16	0.40	0.98	1.00	0.18	0.22	-0.07	-0.67
Perimeter (µm)							1.00	0.17	-0.03	0.42	1.00	0.99	0.28	0.19	0.07	-0.67
Roundness								1.00	0.16	0.28	0.15	0.12	0.74	0.54	0.45	-0.02
Aspect Ratio									1.00	0.00	0.02	-0.16	0.38	-0.46	0.90	0.04
Equiv Circ Diam (µm)										1.00	0.40	0.40	0.34	0.30	0.17	-0.12
Pore Area (length)											1.00	0.98	0.26	0.11	0.09	-0.67
Pore Area (breadth)												1.00	0.18	0.22	-0.07	-0.67
Pore Shape (Leica calculation)													1.00	0.41	0.65	-0.03
Pore Shape (length)														1.00	-0.08	-0.05
Pore Shape (breadth)															1.00	0.03
Perimeter/Area																1.00

(B) Correlation matrix for fine to very fine grained facies data - expanded measured parameters list

	Porosity	Air Permeability (mD)	Klinkenberg Permeability (mD)	Area (µm²)	Feret 0 (µm)	Feret 90 (µm)	Length (µm)	Breadth (µm)	Perimeter (µm)	Roundness	Aspect Ratio	Equiv Circ Diam (µm)	Pore Area (length) (µm²)	Pore Area (breadth) (µm²)	Pore Shape (Leica calculation)	Pore Shape (length)	Pore Shape (breadth)	Calculated % microporosity	Perimeter/ Area
Porosity	1.00	0.26	0.26	-0.01	0.03	0.05	0.04	0.06	0.03	0.04	-0.03	0.06	0.00	-0.01	0.06	0.01	-0.04	0.01	-0.29
Air Permeability (mD)		1.00	1.00	0.00	-0.01	-0.02	-0.01	-0.02	-0.01	0.00	-0.03	-0.02	0.00	0.00	0.01	0.02	-0.03	0.00	-0.01
Klinkenberg Permeability (mD)			1.00	0.00	-0.01	-0.02	-0.01	-0.02	-0.01	0.00	-0.03	-0.02	0.00	0.00	0.00	0.02	-0.03	0.00	0.00
Area (µm²)				1.00	0.82	0.79	0.81	0.74	0.82	0.08	0.01	0.79	0.62	0.86	0.07	0.08	0.05	0.27	-0.01
Feret 0 (µm)					1.00	0.87	0.99	0.72	0.89	0.17	0.02	0.81	0.79	0.57	0.17	0.15	0.08	0.22	-0.06
Feret 90 (µm)						1.00	0.92	0.86	0.94	0.21	0.01	0.93	0.55	0.64	0.21	0.21	0.10	0.26	-0.09
Length (µm)							1.00	0.73	0.91	0.18	0.03	0.84	0.77	0.56	0.18	0.15	0.10	0.23	-0.07
Breadth (µm)								1.00	0.88	0.20	-0.04	0.97	0.22	0.80	0.21	0.27	0.05	0.29	-0.10
Perimeter (µm)									1.00	0.30	0.01	0.92	0.53	0.71	0.24	0.26	0.11	0.30	-0.06
Roundness										1.00	0.34	0.20	0.05	0.07	0.87	0.44	0.54	0.21	-0.12
Aspect Ratio											1.00	-0.02	0.03	0.00	0.44	-0.44	0.94	0.01	-0.07
Equivivalent Circular Diameter												1.00	0.35	0.75	0.20	0.24	0.07	0.29	-0.10
Pore Area (length) (µm²)													1.00	0.23	0.04	0.01	0.04	0.09	0.00
Pore Area (breadth) (µm²)														1.00	0.07	0.10	0.03	0.28	-0.01
Pore Shape (Leica calculation)															1.00	0.35	0.63	0.22	-0.18
Pore Shape (length)																1.00	-0.16	0.21	0.06
Pore Shape (breadth)																	1.00	0.09	-0.06
Calculated % microporosity																		1.00	-0.05
Perimeter/ Area																			1.00

Table III-4: Results from the regression analysis models were interpreted in conjunction with correlation matrixes. The correlation matrix for each data set was alto utilized to identify measurements with a high degree of co-linearity that had the potential to create an unstable model.

Two regression models (model #3 and #4) were analyzed that excluded data associated with Klinkenberg permeability values <0.01mD, and air Permeability values <0.01mD. Of the parameters tested, nearly all showed a high degree of statistical significance (Table III-3). However, as indicated by the low r^2-value, none of the models tested have a useful predictive capability for porosity, air permeability, or Klinkenberg permeability values (Table III-3, #1 and #2, Figure III-5a).

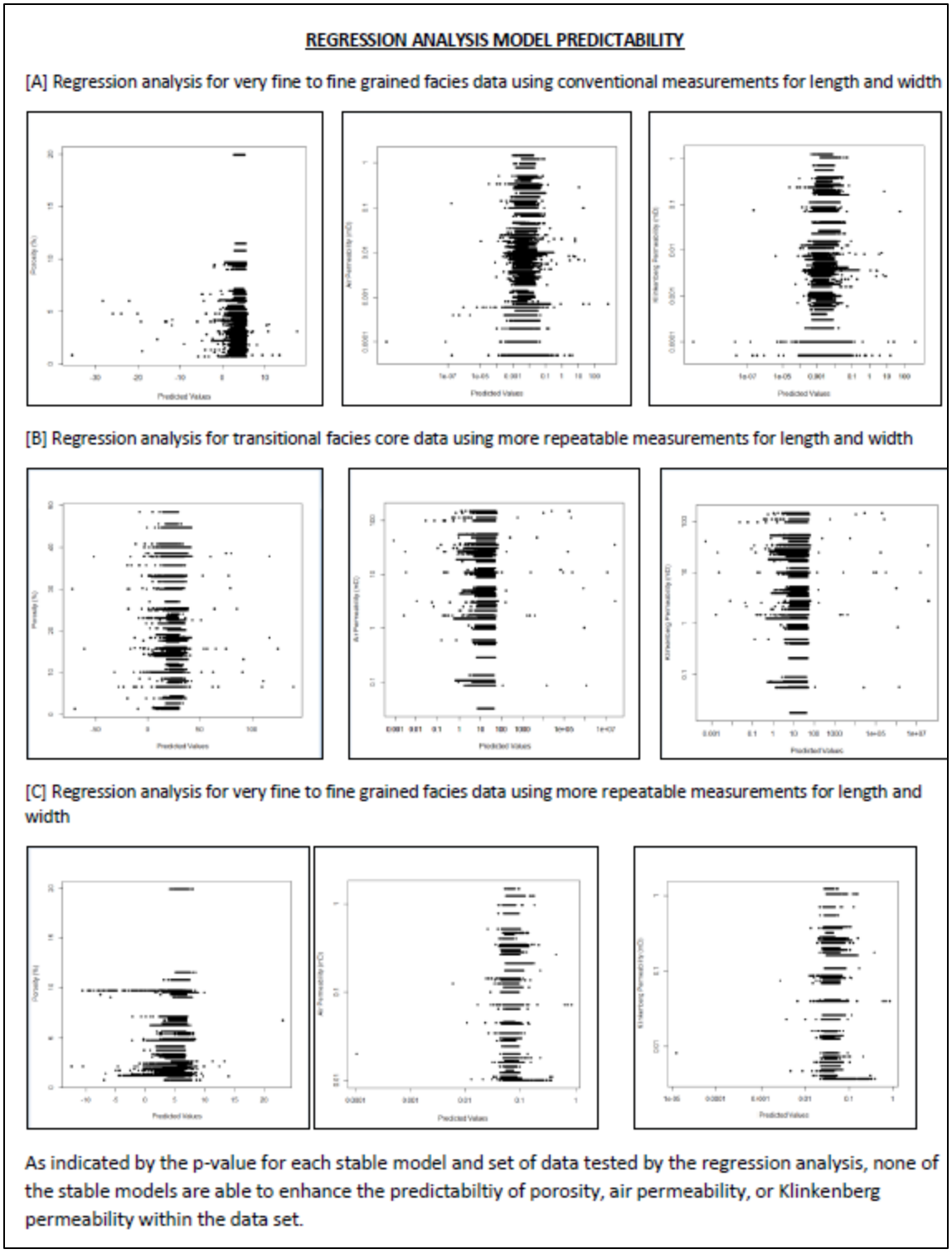

Figure III-5: Regression Analysis Model Predictability. For each of the data sets analyzed using regression analysis, none of the models were able to predict the laboratory measured porosity, air permeability, or Klinkenberg permeability with any applicable level of

accuracy. The inability to identify a useful model is likely due to a combination of (1) a complicated pore architecture, (2) the need to incorporate data that describes the micro- and macro-fracture network, and (3) need to incorporate diagenetic analysis.

Two regression models (model #5 and #6) were analyzed that incorporated data that used length and width measurements that are more repeatable due their lack of dependency on the image orientation. These values are output by the program as the 'Feret 0' and 'Feret 90' which are measurements of the "greatest horizontal distance (width) measured in the horizontal direction" , and the "greatest vertical distance (height) as measured between parallel lines in the vertical direction" (Leica 2013). The models analyzed indicated the area, Feret 0, roundness, aspect ratio, pore shape, calculated percent microporosity, and perimeter/area values. The model results shown in Table III-3, #5 and #6 indicate that for each of the three tests, all parameters except the calculated percent microporosity had the greatest statistical significance. However, although the models are stable, the predictive value as noted in the r^2-value, are all negligible and therefore not useful (Table III-3).

A model was also tested that utilized a data set composed of summary statistics did not identify any statistically significant correlations between the length or width values to the lab measured porosity, air permeability, or Klinkenberg permeability. Although the perimeter/area value did show a possible useful correlation, it was determined the complete data set with observations of each pore identified in the photomicrographs would be most applicable for the purpose of the study.

Due to the lack of predictability of the models that incorporated data from the four cores that are generically classified as "unconventional" due to the overall low porosity and low permeability values, two regression models (model #7 and #8) were tested that incorporated data from the transitional core that has a larger range of both porosity and permeability values

as well as a larger range of pore sizes and pore types. The models incorporated parameters that are most similar to those used in the previous models that also did not indicate a high degree of co-linearity based on the covariance values (Table III-3, #7 and #8). Similar to the other model results, nearly all parameters included have a high statistical significance, but the final model has a very low p-value and r^2 values which indicate the models are not useful in predicting porosity, air permeability, of Klinkenberg permeability within the data set (Table III-3).

Enhanced Predictability via Laboratory Measured Acoustic Response

For this study, the acoustic response data are interpreted relative to other studies that have identified strong correlations between the acoustic response, porosity, pore type, and predictable equations such as the Wyllie time average equation and the Woods equation (Figure III-2) (Anselmetti and Eberli, 1993; Anselmetti et al., 1997). Previous research has shown these relationships can be used to predict permeability either qualitatively or quantitatively where sufficient information regarding the pore type and pore architecture are known and can be incorporated into the analysis (Anselmetti et al., 1997; Thornton and Grammer, 2012). The acoustic response was measured under dry conditions for 181 samples and under 35 ppt NaCl brine saturated conditions for 115 samples. Of the 115 samples tested under brine saturated conditions, 34 samples were from the core with primary distal deposition from Osage County, 47 samples from the three cores with more proximal deposition from Logan and Payne Counties, and 34 samples from the transitional facies core from Reno County. Nearly all of the samples from the four cores with very fine to fine facies (proximal and distal facies) have porosity values less than 10% and permeability values less than 1.0mD. The transitional core includes samples with porosity up to 50% and permeability up to 162mD.

As shown in Figure III-6a, the velocity response (compressional (Vp) and orthogonally oriented shear (Vs)) is inversely related to the porosity in a manner consistent with this

relationship in other carbonate data sets. Because of the similarity in the velocity response for the compression and shear waves, and because relationships between the velocity –porosity trend can be related to pore type and permeability in carbonates with predominantly macropore systems, the focus of this study will be regarding trends observed in the compressional wave response (Vp). As shown in Figure III-6b, there is a pronounced shift in the velocity – porosity relationship that occurs at approximately 10% porosity, but the clear inverse relationship between velocity and porosity remains consistent across the different data sets.

(a) 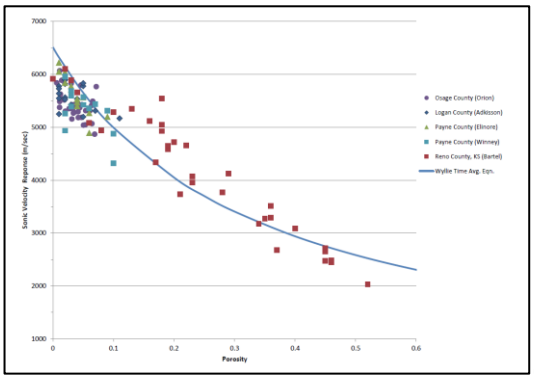

(b) 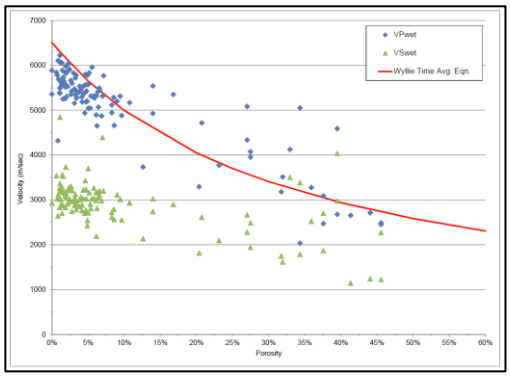

Figure III-6: Laboratory measured acoustic response and porosity data for the areas in the study.

A plot of both the compressional velocity data (Vp) plotted by well location (a), and a plot of the compressional (Vp) and shear wave velocity response (Vs) (b) show an inverse relationship between the measured velocity response and porosity, similar to what has been shown to be a reliably predictive relationship in other carbonate data sets (Anselmetti and Eberli, 1993; Anselmetti and Eberli, 1999, Eberli et al., 2001). The Wyllie time average equation is an adequate approximation for this relationship for samples that have porosity >10%. For samples with <10% porosity, the Wyllie time average equation is the effective upper boundary of the data.

(c) Closer analysis of the data with relatively low measured porosity (<10%), shows a nearly linear relationship between the velocity response and porosity.

(c) 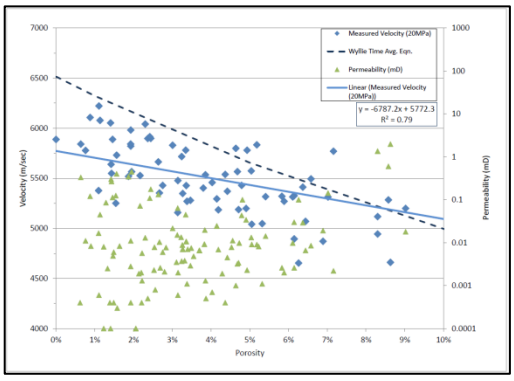

For samples that have a porosity value of 10% or greater, the Wyllie time average equation remains a reasonable approximation of this relationship. For the samples that have

laboratory measured porosity values less than 10%, the recorded acoustic response is slower than the value predicted by the Wyllie time average equation by approximately 500-1000m/sec and faster than the value predicted by the Woods equation. Therefore, for samples with <10% porosity, the Wyllie time average equation and the Woods equation can be utilized as upper and lower data boundaries for the expected velocity response for a given porosity value when the measured porosity is <10% (Figure III-6b).

Closer examination of samples that have <10% porosity shows this shift in the velocity – porosity relationship roughly correlates to samples with permeability values less than 0.5 – 1mD (Figure III-6b). A simple linear relationship can be identified to approximate this relationship with an R^2 value of 0.79. It is interesting to note this relationship shift also correlates to samples that transition from very fine grained facies with predominantly micro- to nanopores, to more coarse grained facies with predominantly meso- to macropores and secondary micro- to nanoporosity. Therefore, the shift in the measured acoustic response compared to predicted acoustic response is likely due to the difference in the pore architecture, where although measured porosity can be <10% in both data sets, within the distal and proximal facies samples the size of the pores are predominantly in the micro- to nanoscale compared to predominantly in the meso- to macroscale for conventional carbonates. This difference in pore size causes a change in the way the acoustic waves are able to propagate through the material. The smaller pores and the overall distribution creates a bulk modulus and elastic properties that are different than expected (Fournier and Borgomano, 2009; El-Husseiny and Vanorio, 2015; Mokhtar et al., 2012; Nur et al., 2008; Rafavich et al., 1984; Verwer et al., 2010)

It is significant to note the relationship between the measured velocity and porosity for samples that have greater than 10% porosity, and are almost exclusively associated with the transitional core that has predominantly meso- to macropores, follows the previously identified

inverse relationship, and more importantly is able to be reasonably approximated using the Wyllie time average equation. This provides additional support for use of this methodology to enhance the predictability of either the velocity or porosity values in carbonate that have conventional predominant pore types and sizes (meso- to macropores).

DISCUSSION OF RESULTS

Qualitative Analysis of Pore Architecture

Qualitative observations and classification of the pore architecture from the macro- to nanoscale indicate a majority of the pores are a form of interparticle, intergranular, or intercrystalline pores, with highly non-geometric shapes due to various levels of dissolution enhancement. The second most abundant pore type are matrix pores, which by definition are not specifically associated with grains but have either formed or been preserved within the very fine grain silt and clay/mud matrix (Vanden Berg and Grammer, 2016). A third common pore type is a moldic or vuggy pore that most often appears to be the result of dissolution of skeletal fragments.

Most significant qualitative observations of the pore architecture are related to the internal pore network, specifically the partial to complete occlusion of the pore space by the growth or precipitation of clay minerals, quartz crystals, or calcite crystal. The presence of any of these partial pore-filling minerals appears to primarily occur in the relatively larger (large micro-, meso- and macropores) pores, which are typically interparticle pores. Where a significant volume of clay mineral precipitation is present within the pore space, the internal pore network appears to be sub-divided into what is effectively a collection of micro- to nanopores with nanopore throats. However, when the pore has either calcite or quartz minerals that have precipitated within the pore space, most often the crystals are observed to line the outer edges of the pore space and only rarely observed to fully occlude the pore.

Therefore, although the presence of quartz or calcite shrinks the total size of the pore, it does not sub-divide the internal area into a series of effectively smaller flow paths.

The associated permeability for samples that have a significant amount of clay minerals precipitated in the pore space is typically lower than for samples that predominantly have quartz or clay minerals lining the pore. The very low permeability within the data set, is a reflection of the predominance of pores to have some form of one or more clay minerals precipitated within the pore space. The porosity value has a similar relationship but is more closely related to the observed density of the void space coupled with the overall size of the pore as observed in 2-dimensional cross-sections rather than the mineral precipitation within the pores.

Quantitative Pore Architecture Analysis: Predictability of Porosity or Permeability using Regression Analysis

Regression model results using quantitative data extracted from photomicrographs from four cores in North-Central Oklahoma that represent an unconventional mudrock reservoir system with very fine grained facies, and one transitional core from Central Kansas, indicate there are statistically significant parameters that have been measured, but no predictive capability to use these parameters to predict porosity, air permeability, or Klinkenberg permeability. Significant co-linearity between several of the measured parameters resulted in the necessary exclusion of select measurements to produce stable models with reliable results. For example, because the length and breadth, or Feret 0 and Feret 90, had a significant level of redundancy with each other only one of the measurements was incorporated into the model. Similarly, measurements that are directly incorporated into other potentially significant measurements (e.g. area is within the perimeter/area value) were also excluded in attempts to produce an applicable and useful model. Data reductions used data that excluded permeability

values that are less than 0.01mD to test if the lower permeability values were effectively creating noise in the data set which would in turn result in a non-predictive model. The model that excluded all permeability values that are less than 0.01mD air permeability value, which corresponds approximately to 0.0044mD for the adjusted Klinkenberg permeability value, still included 207,258 observations in the model analysis. Application of the same cut-off to the Klinkenberg permeability values resulted in a total of 143,117 observations used in the model. The data reduction and exclusion of factors within the model input data set did not result in a more useful or applicable model that could be tested using the same data set, or applied elsewhere, as noted by the very low r^2-value (Table III-3).

The regression analysis trials that used data from the transitional core that grades from a very fine-grained carbonate "mudrock" to a more conventional carbonate with predominantly silt and sand size grains with visible macropores that are mm- to cm-scale in diameter was tested to identify if the high co-linearity and lack of an applicable model was basin-, and possibly also age- specific, or if the results were indicative of a complicated micro- to nanoscale pore architecture. Similar to the trials for the unconventional data, the output from these model trials also indicated that while most measurements are statistically significant, the resultant models are not useful or applicable to enhance the predictability of porosity or permeability within the data set (Table III-3, Figure III-5).

Because the methodology utilized has been proven to be applicable to carbonates that have primarily macropore systems (Anselmetti and Eberli, 2001, Melim et al., 2001; Thornton and Grammer 2012), the cause for the lack of enhanced predictability is likely because of the nature of the carbonates within the data set, with low porosity, low permeability and micro- to nanopore architecture. Secondarily, although the data set comes from five cores that were deposited in a carbonate dominated environment, continued analysis is revealing the

complicated mixed siliciclastic- carbonate deposition within the Mid-Continent Mississippian Period stratigraphic section that is further complicated by a complex diagenetic overprint. Although the application of a generic carbonate ramp, or distally steepened carbonate ramp, is highly applicable to describing the depositional environments observed and relationship to the high resolution sequence stratigraphic framework, the actual composition of the depositional material varies significantly from nearly all carbonate to nearly all siliciclastic (quartz) sediment. This mixed mineralogy coupled with complicated pore architecture has resulted in complex, and currently unpredictable, diagenetic alteration of the section. The diagenetic overprint and alteration becomes part of a complicated narrative in understanding the system as the diagenetic alteration, which remains elusive as to the origins, mechanisms, and how this can be utilized to help guide continued development of the play, has a significant effect on the pore type, total porosity, and permeability. Furthermore, it is locally recognized the play has significant production related to natural fractures within each field. Although fractures were noted within the data set, neither macro- scale or micro- scale fractures were specifically or purposefully included in the pore architecture analysis.

Acoustic Response

Understanding the relationship between acoustic response and porosity provides the potential for further enhanced predictability of permeability in conventional carbonate reservoirs (Anselmetti and Eberli, 1999). Understanding how the quantitative pore architecture is related to the acoustic response may provide additional information that allows for enhanced predictability of permeability in conventional carbonate systems (Anselmetti et al., 1998; Thornton and Grammer, 2012). As shown in this dataset of predominantly very fine grain carbonate samples with some mixed siliciclastic mineralogy, the acoustic response and porosity is inversely related in a similar manner as what is observed in conventional carbonate reservoirs

(Anselmetti and Eberli, 1999). Upon closer examination, although the relationship has a similar trend, the acoustic response for the carbonate mudrocks is significantly slower for a given porosity than would be expected based on data from conventional carbonate samples and theoretically calculated values. It is important to understand the physical reasons for the difference in the details of the relationship so the relationship between other physical properties (porosity, permeability, saturations, strength) can be accurately understood (Nur et al., 1998). Within this study data set, the shift to a slower velocity than what is generally predicted by the Wyllie Time Average equation, which is a useful approximation of the relationship for carbonates with predominantly macroporosity, is likely due to three key properties, and a fourth potentially significant characteristic of the samples, within the current data set. First, the samples tested, especially those with less than 10% measured porosity, have predominantly micro- to nanoscale pore architecture. When the predominant pore architecture is composed of these very small pore sizes, this has a fundamental effect on elastic properties of the sample, including the bulk and shear modulus, which control propagation of sonic velocity waves through the material. The net effect is an observed slower velocity response for a given range of porosity. This micro- to nanoscale pore architecture, although complicated by the presence of several non-geometrically shaped pores, also complicates the relationship between the velocity response, porosity, pore type, and permeability in the how it effects the coupling of the grains, or associations of the grain-to-grain contacts, within the matrix making the relationship between pore shape or pore size with permeability a non-effective predictive tool for micro- to nanopore systems. Both the complicated nature of the pore architecture, and its effect on both the physical properties of the sample and relationships between geometric and laboratory measured properties is important to note due to the potential effect that a significant amount of microporosity could have on the velocity response in a sample set

identified to have a significant amount of macroporosity with the percentage of microporosity overlooked and excluded from the data set. Although the effect observed could arguably be said to be minor (it is within the data boundaries identified for macropore dominated carbonates) when the acoustic response data are used to further predict the primary pore type, and either qualitative or quantitative permeability (Anselmetti and Eberli, 1993; Eberli and Anselmetti and Eberli, 1999) this slower response could be mis-interpreted as a primary producing interval where in fact, there is a relatively lower permeability zone due to the combined effects of the micro- to nanopores on flow within the reservoir. Also in relationship to the micro- to nanoscale pore architecture is the additional complication from precipitation of at least two clay minerals (likely illite and smectite), quartz, and calcite minerals. Although the details of the small variability in mineralogy within the pore space is masked in the available XRD data due to bulk analysis, the observations and analysis from FE-SEM-EDX data should be noted.

Second, the mineralogy of the matrix grains is not pure carbonate for many of the samples used in this study. Whether the mixed mineralogy is a result of original deposition from a mixed carbonate – siliciclastic or due to a complicated diagenetic history is beyond the scope of this paper. However, the resultant mineralogy must be acknowledged with any interpretation to be potentially applicable to other parts of the reservoir system (Kittridge, 2015). Therefore, in relationship to the Wyllie time average equation which is calculated using properties for calcite for greatest application to a pure ($CaCO_3$) carbonate system, at least slight differences in the relationship are expected. When the Wyllie time average equation plotted using properties for average "shale" mineralogy, and quartz mineralogy, it is clear the slower effect observed in the velocity response within the data set are due to the mixed mineralogy with variable amount of quartz/silica or clay materials within the matrix (Figure III-7).

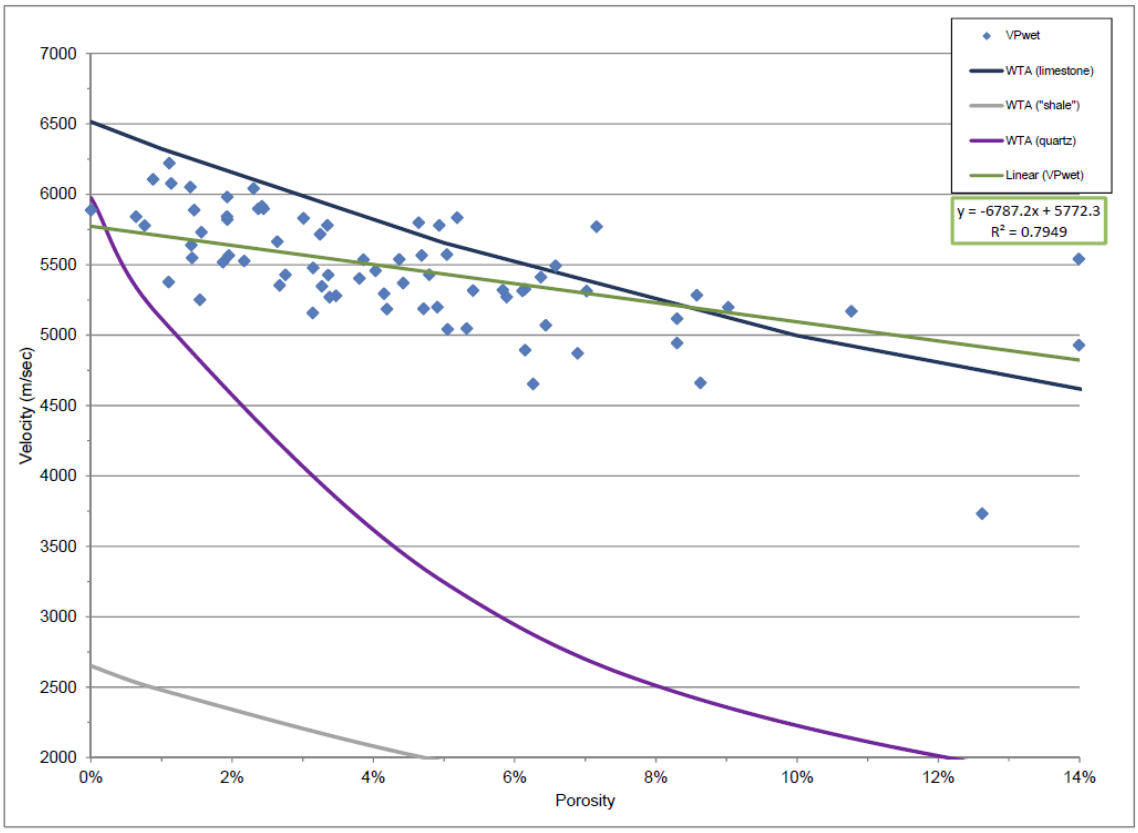

Figure III-7: The shift in laboratory measured sonic velocity response in a mixed carbonate-siliciclastic reservoir system is at least partly attributed to the percentage of silica, or quartz, and clay mineralogy within the sample. As shown above with the Wyllie time average equation plotted for calcite, quartz, and average clay, or shale, mineralogy, show a slower slower velocity response should be expected for samples that have predominantly quarts or clay mineralogy as depicted by the purple and grey lines.

Third, although the integration of micro- or macro- scale fractures was not part of this study, it is recognized that fractures of variable aperture and length will have a potentially significant effect on the porosity, permeability, and elastic properties of the samples. Fourth, and potentially significant as related to original depositional characteristics and/or the diagenetic history, is recognition of the age of the samples as Paleozoic age and potentially unique to the North American Mid-Continent area during the Mississippian Period (Ehrenberg et al., 2009; Bachu and Underschulz, 1992).

As shown in other case studies related to the acoustic response of carbonates and/or mixed siliciclastic-carbonate depositional systems, the acoustic response of samples collected

from a mixed mineralogy composition depositional system should be a reflection of the pore architecture (pore shape, size), the mineralogy, and both original depositional composition and present day mineralogy altered by diagenesis (Kleipool et al., 2015; Anselmetti and Eberli, 1993; Baechle et al., 2008; Kenter et al., 2007; Fournier and Borgomano, 2009; Kittridge, 2015). Also important to acknowledge and incorporate, if feasible, in the interpretation is how heterogeneity in carbonate rocks often results in the lack of applicability of conventional methods (Rasolofosaon et al., 2008). Rasolofosaon et al. (2008) identify several additional conditions where velocity measurements of carbonate samples can be problematic due to the potential for some carbonates to violate basic principles such as: strong ultrasonic attenuation under high differential pressure, anomalous velocity dispersion measurements at low frequency (<5kHz), and an effective violation of the Gassman equation for water saturated samples. One level of heterogeneity that is clearly present within the current data set is presence of secondary porosity formed through the complex diagenetic history.

The results from this study show the relationship between measured acoustic response and measured porosity is similar to what was expected based on previously published data (Anselmetti and Eberli, 1993; Anselmetti and Eberli, 1999; Eberli et al., 2003) where the measured acoustic response has an inverse relationship to porosity. One significant difference in the study data set for samples with porosity less than 10%, is the Wyllie time average equation becomes applicable as an upper data boundary instead of a useful approximation of the velocity – porosity relationship, with the Woods equation still observed to be an applicable and useful lower data boundary. For samples that have greater than 10% porosity, the Wyllie time average equation remains a reasonable approximation of this relationship. This shift in the data is observed in a comparison of data from the five cores, as well as within the transitional core that has both low porosity, low permeability, micro- to nanopores, and

relatively higher porosity, permeability, and meso- to macropores. The shift in the velocity – porosity relationship also has a correlation within the data set to samples with a corresponding permeability of approximately 0.5 -1mD. Although this is helpful and a useful relationship to identify, it is not specifically predictive, nor does it provide a specific relationship to permeability.

SUMMARY

Three areas within the North American Mid-Continent area (Oklahoma and Kansas) with cored intervals from the Mississippian Period stratigraphic section were analyzed to identify qualitative features within the pore architecture with consistent relationships to measured porosity and permeability, and a qualitative analysis to identify statistically significant relationships between geometric measurements of the pore architecture and porosity or permeability.

Qualitative analysis of the pore architecture provided the greatest insight through identification of pore types present in the data set and the relationship between the micro- to nanoscale internal pore space mineral precipitation of clays, quartz, or calcite to permeability. In pores that had a considerable amount of clay mineral precipitation within the pore space, these intervals, regardless of facies, have relatively low measured porosity and permeability. Intervals that have the highest porosity and highest permeability correlate with pores that not only have the greatest density, and are relatively larger in total size, but also have little to no clay mineral precipitation and are lined with calcite or quartz that does not typically sub-divide the flow network. Further insight into the controlling factors will need to incorporate the diagenetic history of the samples as it is clear from this study that extensive diagenetic alterations are not facies specific, but do appear to have a unique relationship to defined sequence stratigraphic architecture.

Qualitative analysis of the pore architecture used data extracted from FE-SEM and thin section photomicrographs to identify key relationships between the pore architecture and laboratory measured porosity, air permeability, and/or Klinkenberg permeability. Regression analysis using sub-sets of data representative from the four cores with distal and proximal unconventional facies identified several statistically significantly measurements but was unable to generate a useful or applicable model that could accurately predict any of the key petrophysical properties. The final models tested to predict porosity, air permeability, or Klinkenberg permeability all have very low predictability as indicated by the very low r^2-values and observed in graphical outputs showing actual vs. predictive values. Trials that attempted to remove potential noise in the data due to possible inaccuracies in the very low reported permeability values did not improve the predictability of any of the models. Regression analysis of data representative of the transitional core, with several facies that have predominantly meso- to macroporosity, had similar results with several statistically significant measurements identified but no model that was able to accurately predict porosity, air permeability, or Klinkenberg permeability. Because the regression analysis was unable to generate a useful model that could be used to predict the key petrophysical parameters with any level of accuracy, it is concluded that additional analysis regarding the fractures, and diagenetic history should be included in the analysis as the lack of enhanced predictability is likely due to the complicated mixed carbonate – siliciclastic deposition, preservation, and diagenetic alteration of the Mid-Continent Mississippian stratigraphic interval.

The acoustic response was measured for samples representative of the facies preserved in each of the five cores used in this study. The measured acoustic response is inversely related to porosity with a significant shift in the overall relationship occurring at approximately 10% porosity, which roughly correlates with a permeability value of 0.5-1.0mD, and facies that are

generically considered unconventional due to their associated low porosity, low permeability, and micro- to nanopore architecture, and more coarse grained, conventional facies with predominantly macroporosity. This shift in the overall velocity-porosity relationship is observed in a comparison of the five cores, as well as within the transitional core that grades upward from very fine grained facies with micro- to nanopores, to coarse-grained facies with meso- to macropores. For samples with less than 10% porosity, and predominantly micro- to nanoporosity, the Wyllie time average equation is applicable as an upper data boundary instead of a good approximation of the data set, with the Woods equation still a useful lower data boundary. For samples with greater than 10% porosity with predominantly meso- to macropore architecture, the Wyllie time average equation remains a reasonable approximation of the velocity – porosity relationship.

CONCLUSIONS

Results from this study indicate the following:

1. Qualitative insight into a correlation between diagenetic alterations of the internal pore network where a high degree of clay precipitation correlates to relatively lower permeability, while a high amount of calcite or quartz precipitation within the pore space correlates to relatively higher permeability values.
2. Quantitative data regarding the pore size and distribution graphed in two unique orientations (pore size vs. P/A, and pore size distribution) provide potentially valuable information regarding the flow network and potential natural rate for fluid extraction or maximum injection rates.
3. A similar inverse relationship with porosity that can be approximated by the Wyllie time average equation is applicable to samples with predominantly conventional reservoir,

with conventional reservoir pore types, pore size ranges (macro- to mesopores) and laboratory measured porosity that is greater than 10%.

4. For unconventional mudrock samples that have predominantly micro- to nanopore sizes in very fine grain sediment and laboratory measured porosity less than 10%, there is a significant shift in the predictable inverse relationship between velocity and porosity. Observations from the data set indicate the Wyllie time average equation is a useful baseline but instead of being applied as an approximation of the relationship between velocity and porosity, it should be applied as an upper data boundary.

CHAPTER IV

A COMPARISON OF THE RELATIONSHIP BETWEEN MEASUREED ACOUSTIC RESPONSE AND POROSITY ACROSS DIFFERENT GEOLOGIC PERIODS, DEPOSITIONAL BASINS, AND WITH VARIABLE MINERAL COMPOSITION

ABSTRACT

Recent work has shown that there is a predictable inverse relationship between laboratory measured sonic velocity response and porosity in carbonates, which can be reasonably approximated using the empirical Wyllie time average equation. The relationship was initially identified in late Cretaceous to Cenozoic age samples collected from the Great Bahama Bank, and the Maiella Platform an exhumed Cretaceous carbonate platform in Italy. This study provides a comparison of "older" carbonate samples from different basins and different geological ages to determine the applicability of this relationship, and subsequent correlations to key petrophysical properties, to other carbonate basins and other geologic time periods. The data set used for the comparison shows this relationship to be relatively consistent in other depositional basins (Michigan Basin, Paradox Basin) and from samples from older geologic periods (Pennsylvanian, Ordovician, Mississippian). However, this basic relationship is also observed to vary significantly within a reservoir system and within a depositional basin in

samples from different geologic periods (e.g. Silurian vs. Ordovician age rocks in the Michigan Basin).

While the empirical Wyllie time average equation can generally be applied as a first-order estimate across a wide range of sample ages in carbonates, limited data suggest the relationship between velocity and porosity in unconventional carbonate reservoirs characterized by predominantly micro- to nano-scale porosity is at least moderately more complex, such that the Wyllie time average equation should be applied as an upper data boundary. In addition, this study has shown that the relationship to dominant pore type is less direct than in a macropore system where it can be assumed that the dominant pore type also has the greatest effect on the effective permeability.

INTRODUCTION

In conventional carbonate reservoirs, where the predominant pore type is in the macro- to mesopore size range, as defined by Loucks et al. (2012), the relationship between porosity and acoustic response (velocity) has a clear inverse relationship that can be approximated by the Wyllie time average equation (Figure IV-1) (Anselmetti and Eberli 1993). Although there is significant scatter in the data, it has been shown to be directly related to the dominant pore type (Figure IV-2) (Anselmetti and Eberli 1993) which can in turn be related to the relative permeability (Anselmetti et al. 1997). Understanding how this relationship can vary when applied to different depositional basins and through geologic time periods can provide insight into the potential relationship to the dominant pore type and potential relationship to permeability (Anselmetti and Eberli, 1993; Anselmetti et al., 1997; Anselmetti et al., 1998; Anselmetti and Eberli, 1999). For example, it can be assumed that within a carbonate system, if two samples with the same total porosity, one with intergranular porosity and one with moldic

porosity, the sample with the intergranular porosity will more consistently have the higher permeability. These same two samples show distinct relationships regarding the velocity response and subsequent relationship to the Wyllie time average equation (WTA). At the same porosity, the sample with intergranular porosity and relatively higher permeability will have a slower velocity than the average predicted velocity, and the sample with moldic porosity with the lower permeability will have a higher than average predicted velocity. Based on these observations and correlation to both pore type and permeability values, it can be generally assumed that when the actual velocity is slower than what is predicted by the WTA equation, that sample will have a relatively higher permeability in comparison to a sample that plots as the WTA equation would predict, or at a velocity higher than predicted. The identification of this fundamental relationship and subsequent relationships to pore type and permeability has significant potential to improve understanding and predicting key reservoir properties, including the development of proxies for interpreting permeability from the knowledge of pore type and corresponding sonic velocity response.

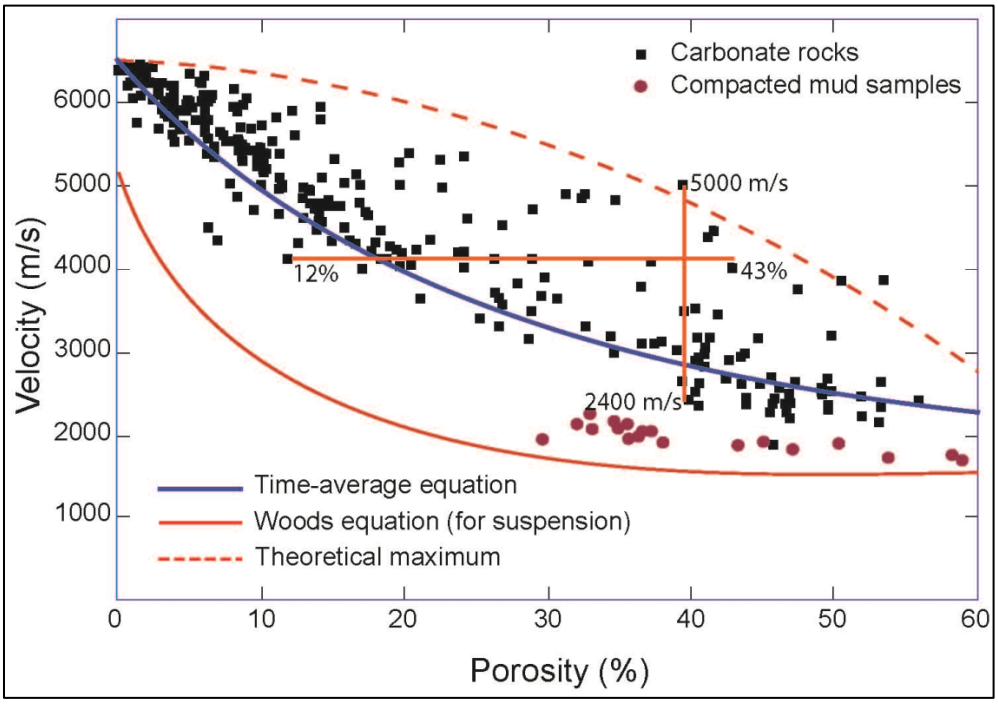

Figure IV-1: The baseline data set for this study measured the velocity response for Cenozoic to early Mesozoic age pure carbonates from the Great Bahama Bank, Maiella (Italy), and Florida Bay. When plotted with porosity, there is a clear inverse relationship with higher porosity values correlated to lower/slower velocity response and low porosity values correlated to high/faster velocity response. Although there is a significant amount of scatter in the data set, the overall relationship is reasonably approximated by the Wyllie time average equation (blue line). (Figure modified from Anselmetti and Eberli, 1993 and used with permission from G. Eberli)

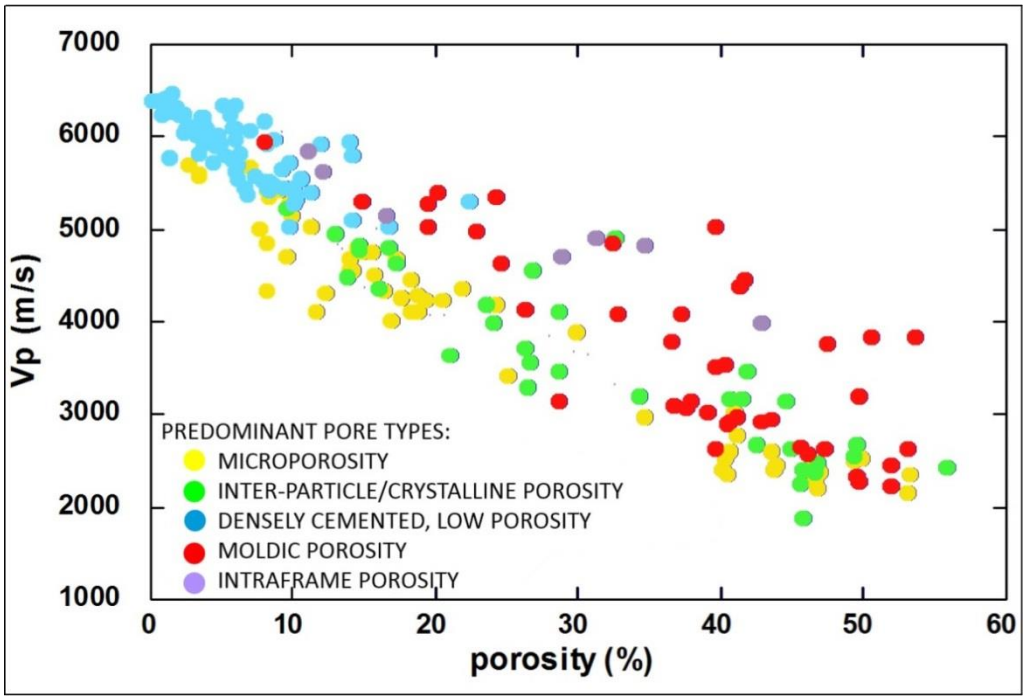

Figure IV-2: The scatter within the Cenozoic to early Mesozoic data set is explained clearly when the data are plotted based on the predominant pore type. As shown in the figure, when the velocity – porosity relationship is classified by pore type, the relationship becomes significantly more precise and therefore more applicable as a useful predictive tool. (Figure modified from Anselmetti and Eberli, 1993 and used with permission from G. Eberli).

These relationships and trends, however, are based primarily on a data set of "young" rocks that are late Cretaceous to Cenozoic in age. For this reason, a fundamental question remains to be addressed regarding the applicability of these relationships and trends to (1) older rocks, (2) carbonates from different depositional basins, and (3) carbonates that have a mixed mineral composition either from original depositional dynamics or from diagenetic alteration. With these questions in mind, the goal of this paper is to:

3. Identify how the relationship between velocity response and porosity compares to the baseline data from different basins, and from different geologic time periods (Ordovician and Silurian of the Michigan Basin, Pennsylvanian of the Paradox Basin, and Mississippian of the North American Mid-Continent).
4. Identify how the relationship between velocity response, porosity, and permeability changes with different fundamental pore system architectures, specifically between a macro- to mesopore dominated system and a micro- to nano-meter scale pore dominated system, when pore size is classified using the proposed classification scheme by Loucks et al. (2012).

These goals were adressed through a series of observations and analyses of laboratory measured velocity response data, and the associated laboratory measured porosity values. Where available, this data was also compared to laboratory measured permeability data to identify relationships, or lack thereof, to the velocity-porosity trend and infer the potential for this to be related to the pore type, and ideally be applied to accurately predict permeability.

DATA SET AND METHODS

Cenozoic Conventional Carbonates: Baseline

The baseline data, as referenced in this study, include relationships identified from a fundamental inverse relationship between velocity and porosity as measured from conventional carbonate samples collected from the Great Bahama Bank, Florida Bay, and the Maiella Platform, an exhumed Cretaceous carbonate platform in Central Italy (Anselmetti and Eberli 1993). Subsequent analysis included defining additional controls and applications of the fundamental relationship between velocity and porosity including the identification of dominant pore type, relationship to relative permeability, and application to seismic interpretation (Anselmetti et al. 1997, Anselmetti and Eberli 1999, Anselmetti and Eberli 2001, Anselmetti et al.

1998, Eberli and Anselmetti 2003). The velocity response was measured using a pulse transmission technique (Birch 1960) where samples are water or brine-saturated, placed inside a rubber jacket and placed into the machine apparatus. The confining pressure and the pore pressure are adjusted independently so *in situ* conditions can be mirrored by the analysis. The transducers are configured so one compressional wave (Vp) and two orthogonally polarized shear waves (Vs) are generated and transmitted through the sample. The wave signals are computer filtered and analyzed so the velocity response at different effective pressure steps can be defined. As noted by Anselmetti and Eberli (1993), the quality of the data is directly related to the quality of the sample and the clarity of the first clear peak. The most clear first peak typically occurs with highly cemented samples and allows for a velocity measurements with an error of less than 1%. The least clear first peak typically occurs with samples that are highly friable. When the first arrival peak is unclear, the error in the velocity measurements could be up to approximately 5% (Anselmetti and Eberli 1993).

Comparative data sets:

The data sets used for the comparative analysis come from two Ph.D. theses and two M.Sc. theses. In each study, the research incorporated a variable number of laboratory measured velocity responses as it related to porosity and the wider research topic. The four studies provide data grouped by five classifications based on basin, age, and represented facies. The comparative data sets, in order from youngest to oldest, include:

(1) A Pennsylvanian age, mixed carbonate-siliciclastic-evaporite system with samples collected from three outcrop locations within the Paradox Basin in southeast Utah, U.S.A. Facies include a quartz sandstone, black laminated carbonate mudstone, carbonate skeletal wackestone and packstone, and evaporite facies. The data for 362 samples are reported for an effective pressure of 50MPa (Nussbaumer 1999).

(2) A Mississippian age, unconventional to transitional, mixed carbonate – siliciclastic reservoir with 34 samples from a single well in Reno County, located in Central Kansas. The facies include a fine grain carbonate mudstone to diagenetically altered packstone to grainstone, and a sequence of peritidal deposits. The data are reported for an effective pressure of 20MPa.

(3) A Mississippian age, unconventional mixed carbonate-siliciclastic reservoir, with 81 samples collected from four cores located in North-Central Oklahoma. The facies include very fine grain carbonate mudstone, wackestones, and skeletal packstone facies. The facies have variable amounts of quartz, and clay minerals mixed in with the original deposition as well as different grades of chert from diagenetic alterations. The data are reported for an effective pressure of 20MPa.

(4) A Silurian age, conventional carbonate reservoir with 16 samples analyzed from one well, and supplementary velocity data derived from wire line sonic logs for two wells in the Michigan Basin. The wells include reef facies that include muddy bioherm, framework reef wackestone, packstone and grainstones, and cyanobacterial mat facies. The data are specifically Niagaran age with core collected from Niagaran reef reservoirs that spatially outline the Michigan Basin. The data for 16 samples are reported with an effective pressure of 20MPa (Noack 2008).

(5) An Ordovican age, conventional carbonate reservoir with data for 37 samples are reported from within the study area which includes analysis of samples and core from three well locations in the Michigan Basin. Facies include a carbonate mudstone, but are primarily carbonate wackestone to carbonate grainstone facies. Samples were collected from three well locations in the Albion-Scipio trend in the South-Central area of the Michigan Basin. The specific effective pressure for the data used in this study is

unknown. However, the analysis included a measurement at 20MPa and did not exceed 30MPa so it is likely the data correspond to either a 20MPa or 30MPa effective pressure (Thornton 2011).

The laboratory measured velocity response for each of the data sets was performed using a pulse transmission methodology, the same as what was used by the baseline study described above. Additionally, laboratory analysis was performed using the same equipment with assistance from laboratory personnel at the University of Miami – Rosenstiel School of Marine and Atmospheric Sciences (UM-RSMAS) comparative sedimentology laboratory (CSL). One minor difference in the specific steps followed relates to the measured velocity response for the Mississippian age samples. The specific machine utilized was a newer model with slightly modified specific steps to complete the analysis, but the fundamental methodology using a pulse transmission to propagate a compressional wave and two orthogonal shear-waves with the ability to replicate *in situ* conditions by independently adjusting the specific pore pressure and confining pressure conditions was the same as what was used in the other studies.

Minor differences regarding the specific measurements are noted in each study regarding the maximum effective pressure which varied from a maximum of 30MPa to 100MPa. The specific range of measurements was related in each study to the purpose of the research and conditions that would encompass the average present day burial depth. Each of the analyses included a collection of measurements from a series of increasing and decreasing pressure steps using both dry and brine-saturated samples. The data reported by each study is associated with a specific effective pressure that is most applicable to the representative data set. However, the major trends observed should not change significantly at the reported effective pressures, and for the purpose of this study are considered to be within a reasonable, comparative effective pressure range.

RESULTS

Cenozoic Conventional Carbonate Reservoir types: Baseline

The results from the study using Cenozoic samples from the Great Bahama Bank, Lower Cretaceous to Cenozoic samples from the exhumed Maiella carbonate platform in Italy, and modern, compacted mud samples from Florida Bay, show a clear inverse relationship between velocity and porosity (Figure IV-1) (Anselmetti and Eberli 1993). This inverse relationship is further referenced within this paper as a baseline, or reference, relationship that is reasonably approximated by the Wyllie time average equation. The one exception to this was observed in the modern compacted mud samples collected from Florida Bay which naturally plot just above the Wood equation as calculated using values for water and calcite reported as $4.06*10^{-10}m^2/N$ and $1.34*10^{-11}m^2/N$ respectively (Figure IV-1) (Anselmetti and Eberli 1993).

In addition to identifying a baseline relationship between velocity and porosity, the study also showed the velocity response can be reasonably approximated with the empirical Wyllie time average equation. Additional controls on the velocity response have been identified as related to the dominant pore type, have slight differences when grouped into specific velocity ranges based on sample location (Florida Bay, Great Bahama Bank, or Maiella), and that the mineral composition of a "pure carbonate" as related to the difference between calcite, dolomite, and aragonite is insignificant compared to primary controlling petrophysical features. The study also showed the velocity response is not predictable based on the depth or age. However, samples can be correlated to the original depositional environment where generally samples collected from areas with relatively more shallow water conditions, such as on the top of a platform or in a near-shore environment, typically have a higher average velocity than samples deposited in relatively deep water environments such as along the slope or in a basin. Ultimately, the primary controlling feature on this baseline relationship between velocity and

porosity is identified to be the total porosity of the sample which is the primary control on the elastic properties. As shown in Figure IV-2 (Anselmetti and Eberli 1993), when the velocity response is plotted based on the dominant pore type, this enhances the predictability of the relationship by minimizing the scatter.

Comparative Data Sets:

Pennsylvanian Paradox Basin: Conventional Mixed Carbonate-Siliciclastic-Evaporite reservoir types

A plot of the published data from the Paradox Basin indicates that a consistent inverse relationship exists between the velocity response and porosity (Figure IV-3a). The mineralogy of the data set indicates there is highly variable mineral composition that ranges from 0-100% pure carbonate (calcium carbonate) as determined from X-ray diffraction (XRD) mineral identification of quartz, calcium carbonate, dolomite, potassium feldspar, albite, and anhydrite. Although the minimum pure carbonate is 0%, this is a measure of the current percentage of calcium carbonate ($CaCO_3$) and not an indication of the original composition. As a Pennsylvanian age system, several of the samples have a significant (0-100%) amount of dolomite identified as part of the mineral composition. The maximum amount of quartz identified in the samples is 78%, and the maximum amount of potassium feldspar is 11% by composition. Therefore, in consideration of the XRD analysis, the "quartz sandstone facies", identified as 50% quartz silt, 20% dolomite cement and 30% calcite cement could also be classified as a highly carbonaceous facies with a significant amount of carbonate mineralogy. The data associated with this facies is included in the analysis to identify if this change in mineral composition significantly, or minimally, impacts the relationship between velocity and porosity or if can be considered a minimal impact on the interpretation. It is however important to analyze the mineral composition so changes that are a result of a high percentage of a specific mineral can be readily

identified and either noted so the interpretation is not influenced, or removed from the data set. In this study, it is noted that the mineral composition of the Pennsylvanian data set is highly variable but the data are included to make observations of how the relationship between velocity and porosity changes in a mixed mineralogy reservoir system. Furthermore, based on the mineral composition, even though this is a mixed depositional system that has undergone diagenetic alteration, the mineralogy indicates most samples are generally classified as a carbonate. As shown in Figure IV-3b, when the data are plotted based on the facies type, which presumably have similar dominant pore types, there is a grouping of the data that significantly reduces the scatter, similar to what is observed in the baseline data by pore type. When the data are overlain with associated permeability values (Figure IV-4), although there is a wide range of measured permeability, the overall relationship to the WTA equation is consistent with the results from the baseline study in that a plot of the data by facies type shows clear grouping of the data which enhances the predictability. The difference between this graph from the baseline data set is the data are grouped by facies compared to being graphed by predominant pore (Anselmetti and Eberli 1999).

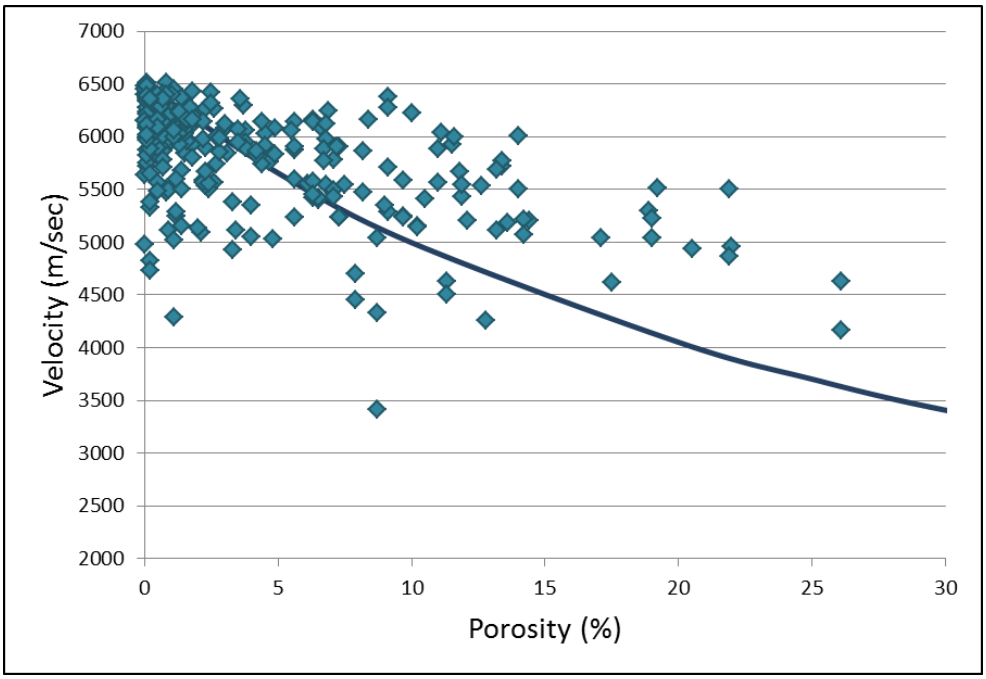

Figure IV-3a: Pennsylvanian age samples from the Paradox Basin in southeast Utah (U.S.A.) show a similar inverse relationship between velocity and porosity that is reasonably approximately by the Wyllie time average equation as shown in the figure. Although the data set includes samples with mixed mineralogy, the majority of the samples are composed predominantly of carbonate or dolomite mineralogy with conventional macro- to mesopore architecture. (data from Nussbaumer, 1999)

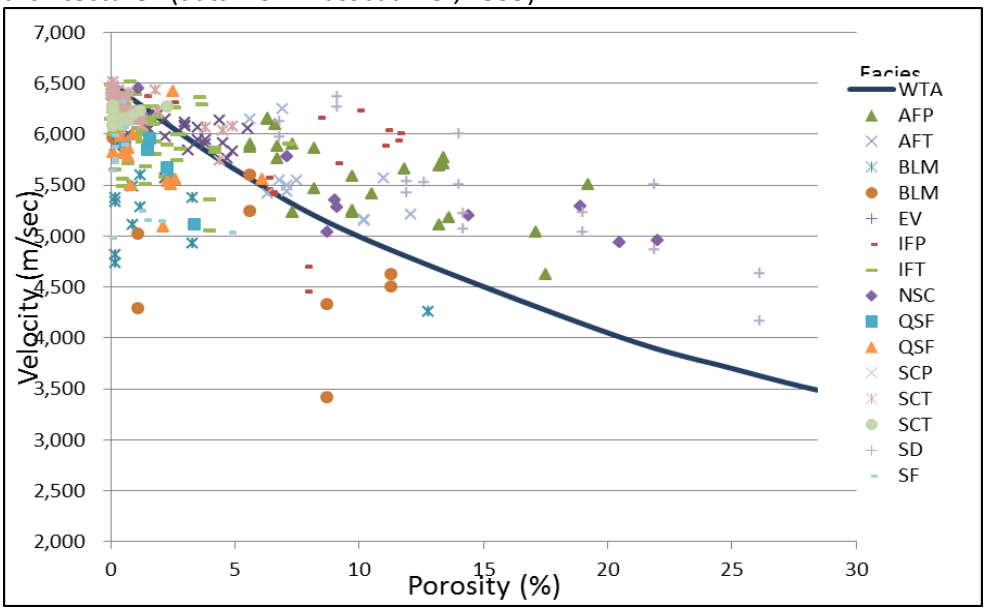

Figure IV-3b: The Pennsylvanian data are plotted based on the identified facies in the system which is assumed to be a reflection of the original depositional environment and primary pore type. As shown in the figure, similar to the baseline data set, there is a grouping of the data based on facies which increases the applicability of the identified relationships for use as a predictive tool.
(data from Nussbaumer, 1999)

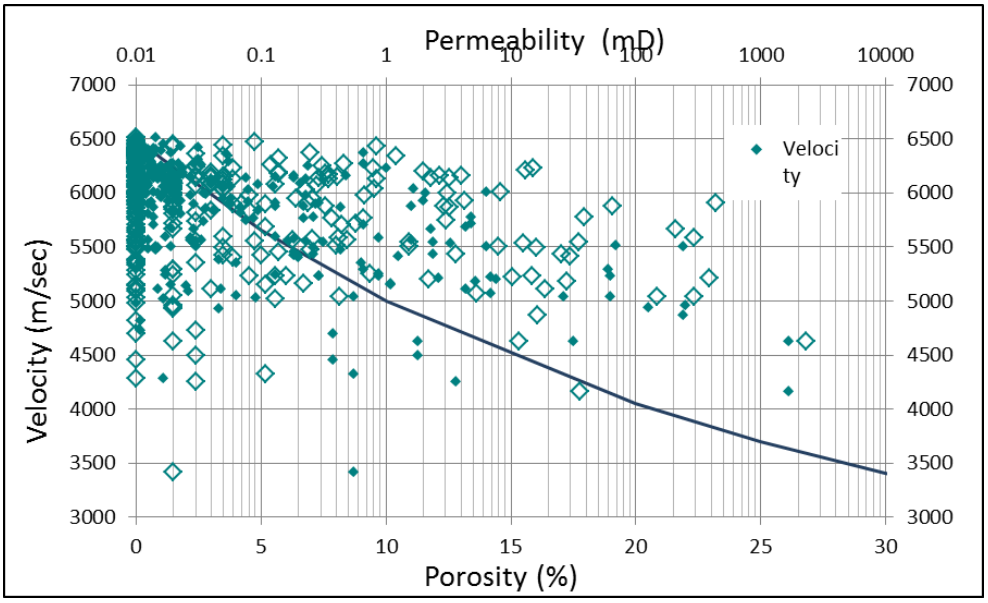

Figure IV-4: When the Pennsylvanian Paradox Basin velocity – porosity relationship is overlain with permeability data, we see how Wyllie time average equation not only approximates the velocity relationship to porosity, but is likely to be applicable in the relationship to permeability variation based on pore type. (data from Nussbaumer, 1999)

Mississippian North American Mid-Continent: Unconventional Mixed Carbonate – Siliciclastic reservoir types

The velocity response and porosity for samples taken from five locations within the North American Mid-Continent Basin (Mid-Continent) are shown in Figure IV-5. As shown, there is a predictable inverse relationship between the velocity response and measured porosity. The Wyllie time average equation is a reasonable approximation for a significant portion of the graphed area, but there is a unique shift in the overall pattern associated with samples that have less than approximately 10%. For these samples, the Wyllie time average equation is more applicable as an upper data boundary than an approximation of the velocity/porosity relationship, indicating a more specific mathematical relationship should be identified for these data. When measured permeability is overlain on the graph (Figure IV-6) a correlation between samples with relatively high permeability values and lowest velocity response can be observed.

There appears to be a nearly L-shaped curve that follows the permeability values as they relate to velocity, however this is partly due to the scales used to display the data. This becomes apparent when only data associated with both low porosity and low permeability values are shown. The cut-off applied to porosity values is 10%, based on where the relationship shift occurs as related to the Wyllie time average equation. The associated permeability cut-off used is a value of 10mD which is where most of the permeability data are clearly associated with the lowest velocity response measurements. With this adjusted displayed focus (Figure IV-7) a best fit line applied to the data show an overall behavior that is expected of a conventional carbonate where data plot both above and below a line that approximate the velocity – porosity relationship based on the dominant pore type and related permeability. Although a unique best fit line may be necessary to identify for a specific study area or data set within a basin, if the fundamental behavior is assumed to be the same with the velocity response related to the total measured porosity and dominant pore type, then mathematically defining this line should improve the ability to enhance the predictability of the velocity and porosity, and potentially relate to the dominant pore type and relative permeability.

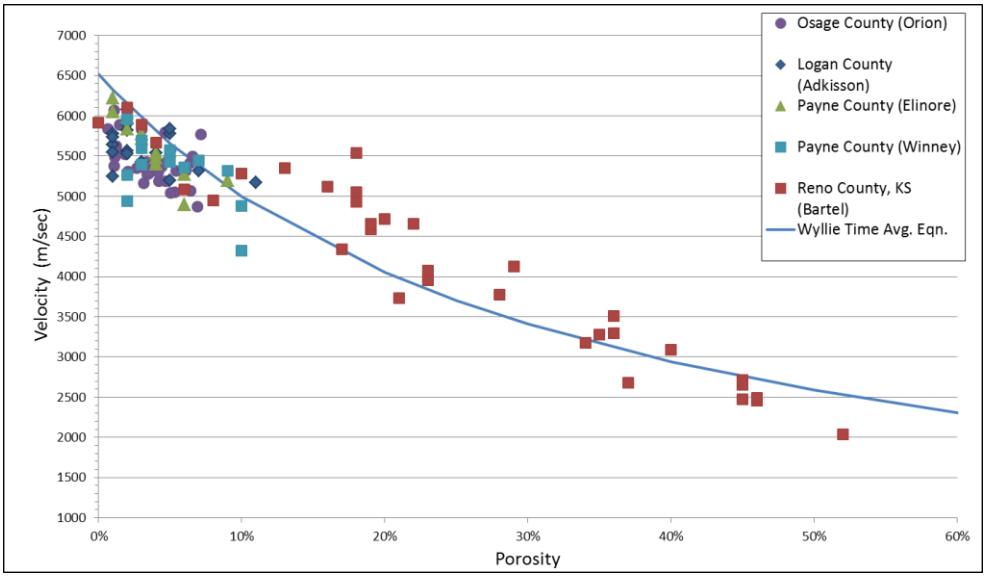

Figure IV-5: Mississippian age data from the North American Mid-Continent area show a predictable inverse relationship between the velocity response and measured porosity. The

Wyllie time average equation provides a reasonable approximation of this relationship for samples that have a porosity greater than 10% and predominately meso- to macropore architecture, and is an approximate upper boundary for samples with porosity less than 10% and with predominately micro- to nanopore architecture. (data from Vanden Berg 2016).

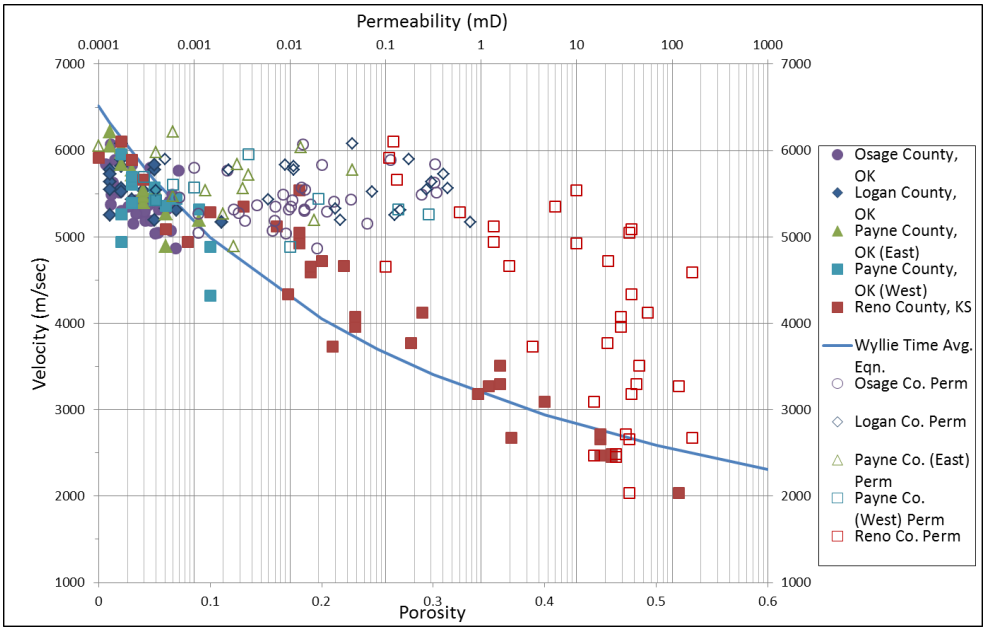

Figure IV-6: The Mississippian age velocity and porosity data are overlain with permeability data to identify potential relationships that can be applied to other areas of the reservoir. Because the majority of the associated permeability values plot above the average best-fit line, it is likely that specific mathematical relationships between velocity and porosity for each major category of pore architecture (macro- and mesopores vs. micro- to nanopores) will provide more accurate estimates of associated petrophysical properties in this reservoir.
(data from Vanden Berg, 2016)

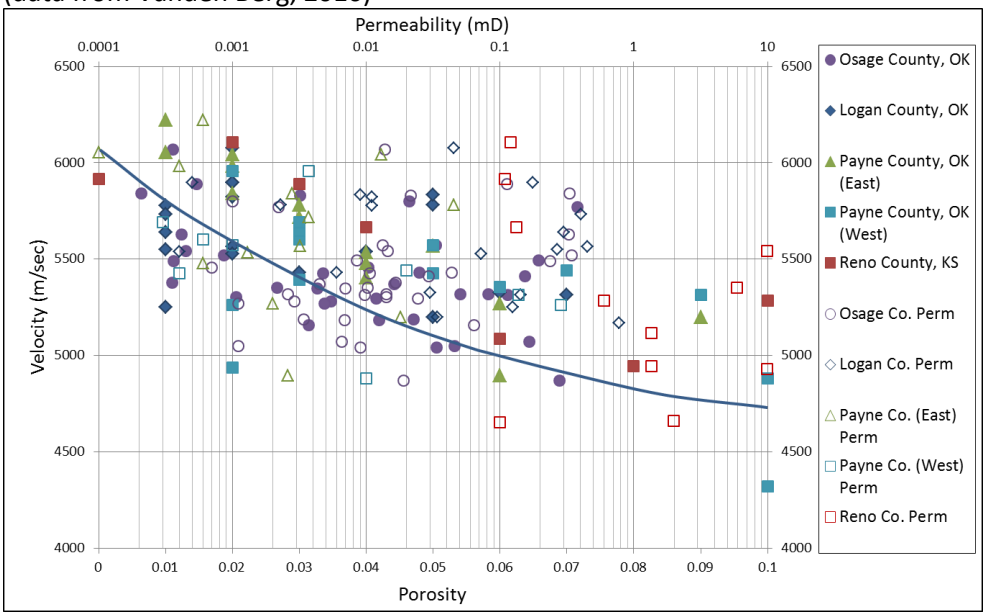

Figure IV-7: The Mississippian age velocity and porosity data for only the samples with predominantly micro- to nanoporosity are overlain with permeability data to identify how the relationship between velocity and porosity compares to associated permeability values. Within this sub-set of Mississippian age data we see that a best-fit line can be applied to the overall velocity – porosity relationship where the permeability values plot in a manner similar to what is observed for conventional carbonates and is likely related to the predominant pore type that is associated with the effective permeability.
(data from Vanden Berg, 2016)

Silurian and Ordovician Michigan Basin: Conventional Carbonate reservoir types

Ordovician and Silurian data from the Michigan Basin are plotted together in Figure IV-8 which highlights the potential for significantly different laboratory measured velocity response for carbonates within the same basin but from different geologic time periods. The Ordovician data has a clear inverse relationship between velocity and porosity but the maximum velocity response is observed to be 500-1000 m/sec faster than observed in either the baseline data or the Paradox Basin data. Although not specifically highlighted in the original study, closer examination of the Ordovician data set (Figure IV-9) clearly shows distinct velocity – porosity relationships based on the well location. It is noted the Ordovician data set comes from an interval that has been subjected to hydrothermal dolomitization. Although the relative timing of the alteration would be similar on a geologic time scale, differences due to facies thickness and effective impact of the diagenetic alteration appears to have been sufficient to result in the slight differences in the elastic properties and therefore the velocity response in specific parts of the study area. The overall behavior for the Ordovician samples is sufficiently similar to the baseline data so that the Wyllie time average equation reasonably approximates the relationship between velocity and porosity. However, if a best-fit line was identified based on a more specific location or impact from diagenetic alteration, the predictability of associated petrophysical properties would likely become more accurate and useful. As noted with the Mississippian data reported in Figure IV-6, data plotted based on the three well locations clearly identifies three similar, but unique relationships between measured velocity and porosity.

When the data are overlain with measured permeability (Figure IV-10), it becomes clear that two areas (data set 2 and 3) have either preserved or enhanced permeability while one area appears to either have lowered permeability, or may have been by-passed by the hydrothermal diagenetic alterations.

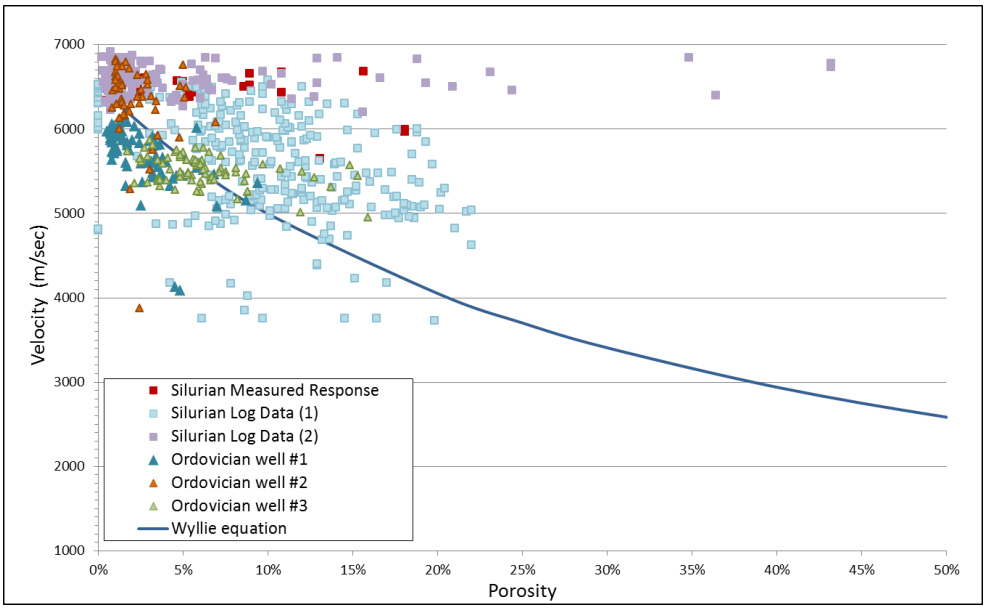

Figure IV-8: Silurian and Ordovician data from the Michigan Basin show a predictable inverse relationship between the velocity response and measured porosity. The Wyllie time average equation provides a reasonable approximation of this relationship with primary deviations related to the two data sets that are derived from the wireline sonic log response. (Silurian data from Noack, 2008; Ordovician data from Thornton, 2011)

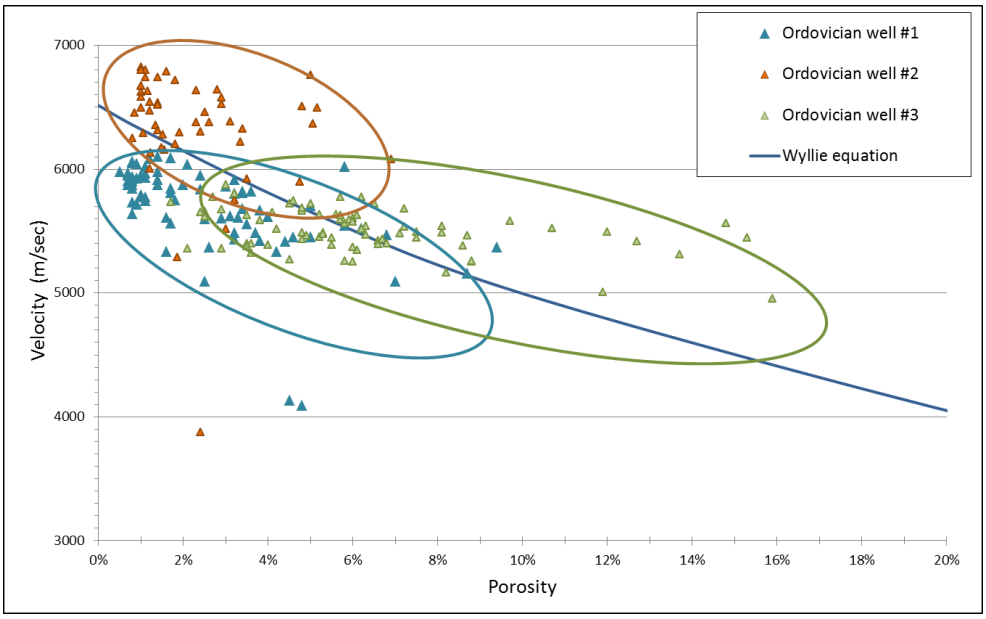

Figure IV-9: When the Ordovician age Michigan Basin data are plotted alone, we see a distinct grouping of the data based on well location. Although the Wyllie time average equation provides a nice approximation for this data set, by plotting the data based on spatial location an additional level of predictability can be applied by applying a best-fit line to each area. Additional, and likely more accurate, information related to the predominant pore type, permeability, and diagenetic alteration should also be feasible. (data from Thornton, 2011)

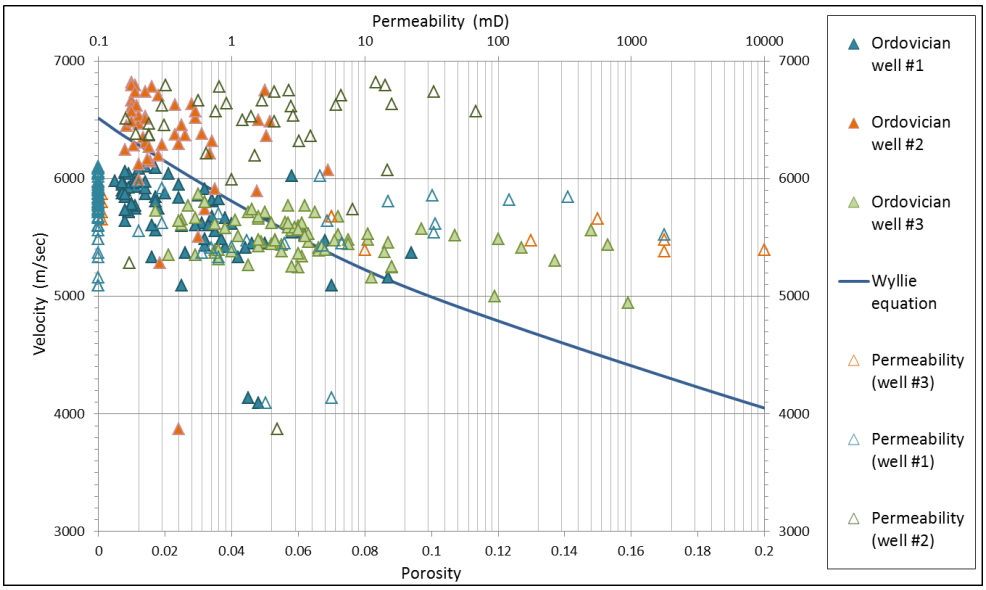

Figure IV-10: The Ordovician velocity and porosity data from the Michigan Basin are overlain with permeability data to identify potential relationships that can be applied to other areas of the reservoir. Because the majority of the associated permeability values plot above the average best-fit line, it is likely that well, or area specific mathematical relationships between velocity and porosity will provide more accurate estimates of associated petrophysical properties in this reservoir. (data from Thornton, 2011)

In comparison to the Michigan Basin Ordovician data, the Silurian data set has an even higher (faster) velocity response overall (Figure IV-8). When the Silurian data are plotted alone, the deviation to an expected inverse relationship that can be approximated by the Wyllie time average equation becomes readily apparent (Figure IV-11). The relationship between velocity and porosity is not consistent between the three sub-sets of data where there is only one group with a clear inverse relationship between velocity and porosity (log data (1)). The other data exhibit a moderately inverse relationship for the laboratory measured response data, and what appears to be a nearly consistent range of velocity response of 6200-7000m/sec for a wide

range of porosity values from 0-45%, from a second location with values derived from a wireline sonic log (log data (2)).

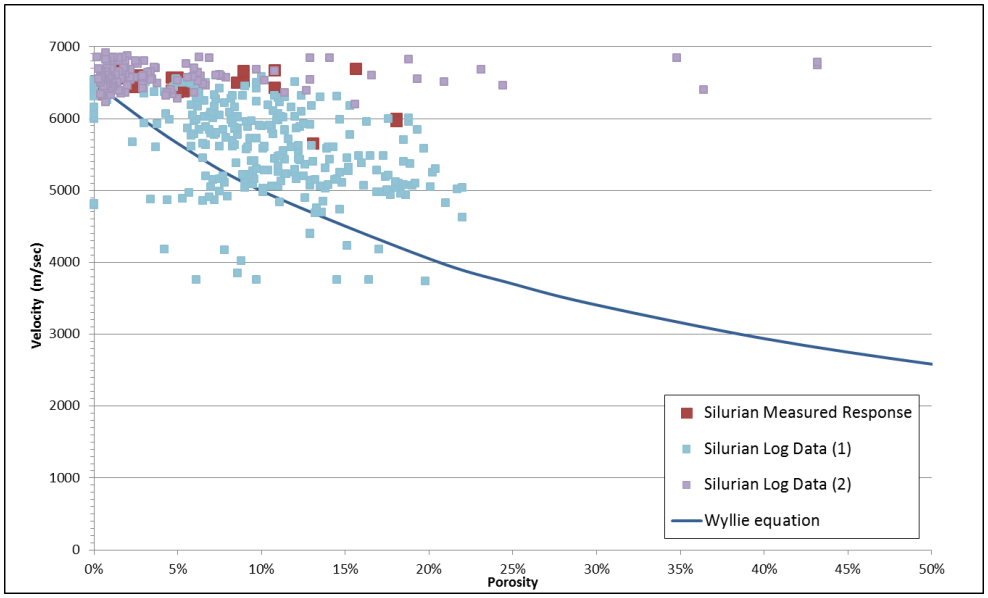

Figure IV-11: When the Silurian age Michigan Basin data are plotted alone, we see a distinct deviation from the Wyllie time average equation that for this data set is not a reasonable approximation. The data derived from a wireline log response in one location does have a clear inverse relationship between velocity and porosity but the measured data show only a weak inverse relationship and data from a second well and wireline log response appears to have no clearly defined relationship. (data from Noack, 2008)

Measured permeability, available for only two of the data sets, was overlain on the velocity-porosity graph (Figure IV-12). From this figure, it is clear a best fit line should be identified for both locations because of the different, and wide range of porosity and permeability values. For the log derived velocity data sets, the velocity, porosity, and permeability data points are each clustered into narrow data groups of 6200-6500m/sec velocity, 0-5% porosity, and 1-10mD permeability with scatter in the data indicating a much larger range of values. Focusing only where these clusters overlap shows the extent of the scatter within the narrow data ranges, and also shows that a best-fit line can be applied that might be applicable to predicting the predominant pore type and associated permeability value (Figure IV-11). Because of the wide degree of scatter within this data set, caution should be

utilized when predicting petrophysical properties from this data set, based on this limited information with relationships that do not follow expected trends.

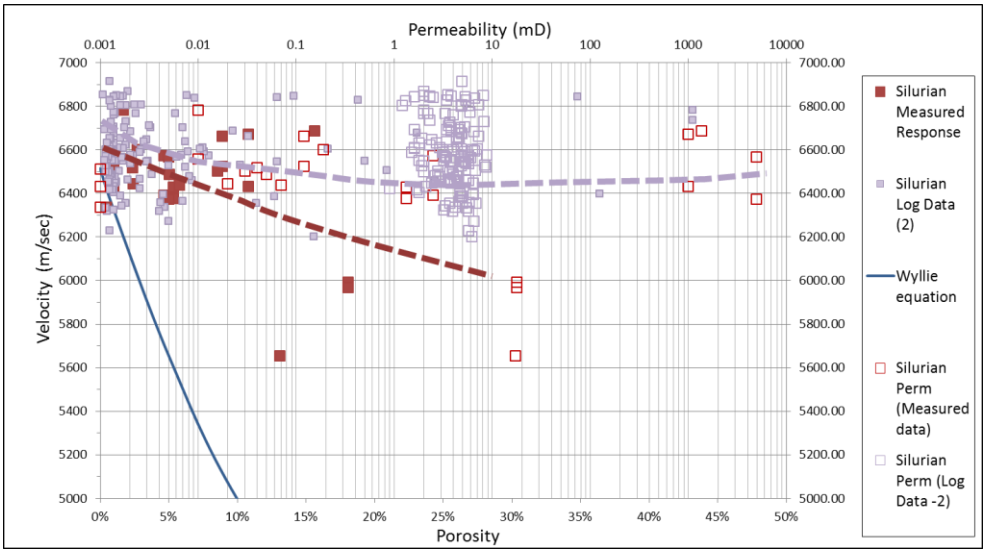

Figure IV-12: The Silurian velocity and porosity data from the Michigan Basin are overlain with permeability data to identify potential relationships that can be applied to other areas of the reservoirs and potential predictable relationships. Only two of the data sets have associated permeability data, one associated with the laboratory measured velocity response, and one associated with wireline log response. As shown in the figure, when a best-fit line is approximated for each velocity – porosity relationship, there also appears to be a basic relationship to permeability with some values plotted above, and some values plotted below the line which likely relate to the primary pore type. This relationship with the log derived data set is quite weak, but this data set also has the weakest relationship between velocity and porosity. (data from Noack, 2008)

DISCUSSION

The relationship between velocity and porosity is compared using data that represent five geologic time periods (Cenozoic, Pennsylvanian, Mississippian, Silurian, and Ordovician), three unique types of mineralogy classifications (pure carbonates, mixed carbonate-siliciclastic-evaporites, mixed carbonate –siliciclastic), and three types of reservoir classifications (conventional with predominantly macro- to mesopores, unconventional with predominantly micro- to nano-meter scale pores, and transitional with macro- to nano-meter scale pores). The correlations identified from Cenozoic data are used as a baseline relationship between velocity

and porosity. This comparative study is based upon two primary predictable components regarding the relationship between velocity and porosity: (1) there is an inverse relationship between velocity response and porosity, and (2) that relationship can be reasonably approximated by the Wyllie time average equation. Additional interpretations related to pore type and permeability assume the above are applicable.

The first question addressed in this study is the inquiry of applicability of this velocity – porosity relationship to different basins and to samples from different time periods. A comparison of data from three basins that represent four geologic time periods (from Paleozoic to Cenozoic) has shown this relationship to be moderately true and applicable to conventional carbonate reservoir systems from different geologic periods, including reservoirs system with variable mineralogy either due to variations in the primary depositional composition or due to diagenetic alteration. The inverse relationship between velocity and porosity is observed in all of the data sets, but only partially within the Silurian age data where much of the sonic velocity data was calculated from old sonic tools. The applicability of the Wyllie time average equation to reasonably approximate the relationship is shown to be generically true, but in all examples, except for the Pennsylvanian data set, a more accurate mathematically defined equation can, and should, be identified prior to extrapolation or application within a reservoir system to more accurately predict associated petrophysical properties. The primary reason for the lack of applicability of a generic equation is likely due to the fundamental controls identified by Anselmetti and Eberli (1993) as being related to the dominant pore type, as well as effects from the percentage of micro- to nano-meter scale porosity as this can have a significant effect on the sample elastic properties (Eberli et al. 2003; Baechle et al. 2008; Verwer et al. 2008; Weger et al. 2009; Verwer et al. 2010) and as a final point, the effects of a mixed mineral composition either

due to diagenetic alterations or from original mixed composition (Nussbaumer 1999; Kittridge 2015; Kleipool 2015).

The second question addressed in this comparison is how the fundamental relationship between velocity and porosity changes in relation to the dominant pore architecture, specifically between a macro- to mesopore dominated system and a micro- to nano-meter scale pore dominated system. As noted above, the largest deviation of the applicability of the Wyllie time average equation based on these data sets is for two sub-sets of Silurian data that are primarily based on a wireline sonic log response, and for the Mississippian data that are representative of an unconventional mixed composition carbonate system with predominantly micro- to nano-scale porosity. Based on these observations, although it is recommended to always define the reservoir specific velocity – porosity relationship, if the reservoir is predominantly carbonate in composition, and more importantly consists predominantly of a macro- to mesoporosity, application of the Wyllie time average equation should result in a reasonable estimate or the relationship between porosity and velocity. For unconventional reservoir systems characterized by very low porosity and permeability values, the limited data from this comparative study indicates the Wyllie time average equation can still be applicable, but will provide a maximum estimated value.

SUMMARY AND CONCLUSIONS

This study has performed a comparison of five unique data sets that represent five geologic time intervals and six basins, to identify the potential for variability within the relationship between laboratory measured velocity and porosity with subsequent implications for the relationship to permeability within both pure and mixed carbonate reservoir systems. The laboratory analysis was performed by five different researchers but each followed the same

methodology and utilized equipment from the same laboratory. Primary conclusions based on the comparative analysis are as follows:

1. The Wyllie time average equation is often, but not always, able to provide a reasonable approximation of the relationship between laboratory measured velocity and porosity in both pure carbonate and mixed carbonate depositional systems.
2. Where the Wyllie time average equation is not a suitable representation, a best fit line should be applied to the data so the relationship, and potential for enhanced predictability of primary pore type, or permeability, can be determined.
3. Even within a basin, intervals of different ages can potentially have a significantly different relationship between velocity and porosity. Although it is likely to be an inverse relationship, the specific character should be identified before empirical equations, or equations derived from a single borehole, are used to predict petrophysical properties within a reservoir interval.
4. In a mixed carbonate-siliciclastic-evaporite system, it is reasonable to expect similar trends and relationships as identified for pure carbonate systems, assuming the primary mineral composition is a carbonate, or diagenetically altered carbonate.
5. In a mixed carbonate- siliciclastic mudrock system, it is reasonable to expect an inverse relationship exists between the velocity and porosity. However, the correlation to primary pore type and permeability may be complicated if there exists more than one characteristic best-fit data line to data from the same reservoir system.
6. Plotting the data in a manner based on the dominant pore type, or the well location can aid in enhanced predictability by further defining the fundamental velocity – porosity relationship.

7. Limited data indicate an unconventional carbonate mudrock system with predominantly micro- to nanoporosity has a modified relationship between velocity and porosity. The data presented indicate a unique relationship exists for unconventional, or transitional reservoirs that primarily have low porosity values that are equal or less than 10%.
8. At minimum, the Ordovician data set from the Michigan Basin, and the Mississippian data set from the Mid-Continent area have undergone extensive diagenetic alteration. Both data sets show a predictable inverse relationship with velocity and porosity, but they also show different ways this relationship can be shifted such that if a mathematically defined relationship is defined that is either basin specific, or region and geologic time specific, this will be the most applicable to understanding how to interpret subsequent correlations to pore type, facies, and permeability.

CHAPTER V

INTEGRATED RESERVOIR CHARACTERIZATION TO PROVIDE INSIGHT INTO POROSITY AND PERMEABILITY IN A MIXED CARBONATE-SILICICLASTIC RESERVOIR

ABSTRACT

The Mississippian age limestone of the North American Mid-Continent is a valuable unconventional, very fine grained, low porosity and low permeability mixed carbonate – siliciclastic reservoir in Oklahoma and Kansas. Although over 14,000 vertical wells have been producing oil and gas from these Mississippian age reservoirs for over 50 years, recent horizontal activity has illustrated how crucial it is to understand the petrophysical and depositional characteristics associated with producing intervals. High resolution sequence stratigraphic architecture determined for five cores in three areas of the basin have been integrated with key petrophysical data (porosity and permeability), a qualitative and quantitative analysis of the pore architecture, and the acoustic response from representative samples from each core to better understand the distribution of reservoir facies in this

unconventional carbonate reservoir and provide insight into how to enhance the predictability of key reservoir intervals within the study area.

The very fine grained, unconventional reservoir facies within the sample set have a horizontal porosity that ranges from 0.1-12.5% (avg. 2.5%), although porosity values may be as high as 20% locally within these facies. Correlative permeability ranges from 0.0001mD to 3.4mD (avg. 0.05 mD). Horizontal porosity from coarse grained facies in the "conventional" reservoir facies range from 13% to 45% (avg. 31%) porosity with correlative permeability ranging from 5.92mD to 163mD (avg. 43mD). The variability within the facies provides insight to key characteristics and measurements that allow for enhanced predictability of key petrophysical features (porosity and permeability). The qualitative and quantitative analysis of the pore architecture, completed using an Environmental Scanning Electron Microscope (SEM) and digital image analysis, shows the pores are mostly oblong to oval shaped, interparticle and intercrystalline to vuggy, meso- (4mm-62.5 μm) to nanopore (1μm-1nm) size, while pore throat measurements are consistently in the nanopore range. Acoustic response measurements are inversely related to porosity, which is consistent with published case studies using conventional carbonate. A notable difference in the acoustic response from the data set, is a significant shift in the velocity-porosity relationship that is likely a result of the complex micro- to nanopore architecture and post-depositional diagenesis within the basin

Detailed facies analysis from five cores support the suggestion that deposition in the North American Mid-Continent area during the Mississippian Period occurred on an attached, low-declivity, carbonate ramp, or possibly distally steepened carbonate ramp system. Facies preserved in the core used in this study range from very fine grain carbonaceous mudstone and wackestones deposited in an outer ramp environment to moderate to highly bioturbated wackestone to grainstones deposited in middle ramp environments, and near-shore wackestone

to packstones capped by a series of peritidal deposits. All facies exhibit significant overprinting by diagenesis, including weathering and karst development due to subaerial exposure. Each core shows a shallowing, or shoaling, upward succession of facies which is in agreement with published eustatic sea-level during this period. The sequence stratigraphic architecture determined from detailed facies analysis reveals a similar hierarchy preserved throughout the basin which is shown to be the foundation to predicting key reservoir intervals.

The high resolution sequence stratigraphic architecture is the foundation to predict intervals with high porosity and high permeability. The highest order sequences (2nd or 3rd order) have a high level of correlation to conventional wire line logs, specifically the gamma-ray log. Augmenting this data with the acoustic response, and qualitative characterization of the macro- to nanoscale pore architecture, provides an example of how integrated studies can enhance predictability of key reservoir facies and producing intervals within unconventional carbonate reservoirs.

INTRODUCTION

Unconventional, low porosity and low permeability, resources have steadily taken a prominent place in oil and gas exploration within the last decade. As oil and gas exploration continues to advance technologically to more accurately identify key hydrocarbon-rich zones, and develop methods for more efficient extraction, the need to better understand these low porosity and low permeability reservoirs remains a fundamental necessity.

The “Mississippi Lime” play, which extends throughout North-Central Oklahoma and Southern Kansas, has seen oil and gas production from vertical wells for over 50 years. However, the “Mississippi Lime” has recently undergone a revival in production through advances in horizontal drilling technology. With this renewed interest, it is increasingly important to understand the complexity of this reservoir system to target the highest producing

intervals. To accomplish this, it is necessary to understand fundamental depositional and petrophysical characteristics from facies identification at the meter-scale to the larger reservoir-scale units.

The goal of this study is to provide insight into possible depositional environments found within the study area, and to identify possible methods and tools that aid in understanding reservoir conditions and exploration potential when related to a high resolution sequence stratigraphic analysis. With several other on-going research projects related to the Mississippian Limestone reservoir (this volume), this study provides one component of a very complicated depositional and diagenetic history found in the Oklahoma and Kansas area.

The primary objectives of the study are:

1. To define the high-resolution sequence stratigraphic framework through detailed facies analysis from core and thin section data from five cores in three areas of the basin.
2. To integrate the sequence stratigraphic hierarchy with wireline log signatures and conventional, petrophysical laboratory data (porosity, air permeability, and Klinkenberg permeability) to identify trends that can potentially be applicable to other parts of the basin, as well as other similar unconventional carbonate – siliciclastic reservoir systems.
3. To understand how the acoustic response relates to porosity in the very fine grain, low porosity and low permeability, facies in the study area, and how this compares to relationships and correlations in the medium to coarse grained facies with predominantly macroporosity and relatively high porosity and permeability.

Identifying relationships between common well log data, traditional laboratory measured petrophysical data and a detailed sequence stratigraphic framework increases the predictability of reservoir-quality units in the subsurface, allows for an enhanced understanding of reservoir and seal geometries and distributions, and ultimately leads to enhanced hydrocarbon

production. The results from this study should be applicable to other areas within the "Mississippian Limestone" play outside of the areas included in this study and also be applicable as an analog for other carbonate – siliciclastic systems deposited in similar environmental conditions on an attached carbonate ramp or attached, distally steepened carbonate ramp, adjacent to an actively subsiding foreland basin. Understanding how the acoustic response relates to porosity within the basin, and how the response compares to other published trends for conventional carbonates, and conventional siliciclastics, is a supplemental characteristic that can be integrated to provide further enhanced predictability of porosity within the basin.

Geologic Background

During the Mississippian Period, present day southern North America was covered by a shallow, tropical, epeiric sea that established a broad carbonate depositional system (Gutschick and Sandberg, 1983). Paleogeographic reconstruction indicates the present day North American mid-continent area straddled the paleoequator, which placed most of North American within 5-30^{o} North or South of the equator (Lane and DeKeyser, 1980; Scotese, 1999; Gutschick and Sandberg, 1983). Recent research has indicated that regional paleogeographic deposition occurred on a low declivity carbonate ramp, or a distally steepened carbonate ramp, with a combination of sediment sources that range from pure carbonate, to pure siliciclastic, to a mixed carbonate – siliciclastic depositional system (Childress, 2015; Price, 2014; LeBlanc and Grammer, 2014).

It is generally agreed that during Late Mississippian or Early Pennsylvanian time the Nemaha Uplift or Nemaha Ridge, a north-south trending structural high extending from Kansas into Oklahoma, was active (Gay, 2003; Gay, 1999). Faulting associated with the Nemaha Uplift is believed to have affected Mississippian deposition creating a potentially significant sediment source, additional accommodation space, and variable bathymetric geometry. This localized

tectonism is also a likely primary cause of some of the complex lateral and vertical distribution observed in Mississippian age reservoir units due to localized changes in depositional activity as a result of nearby tectonic movements (Gay, 2003; Gay, 1999; Meckel et al., 1992).

The Mississippian Period represents an overall 2nd order sequence characterized by numerous (20-30), 3rd order eustatic sea level fluctuations as illustrated in Figure V-1 Haq and Schutter, 2008; Vail et al., 1977). Higher order depositional cyclicity correlative to 4th order or 5th order packages are likely preserved in several locations within the basin, but many of these higher frequency packages are likely to have been influenced by localized allocyclic and autocyclic processes from localized depositional and Paleogeographic conditions (Haq and Schutter, 2008; Ross and Ross, 1988; Cecil, 2003).

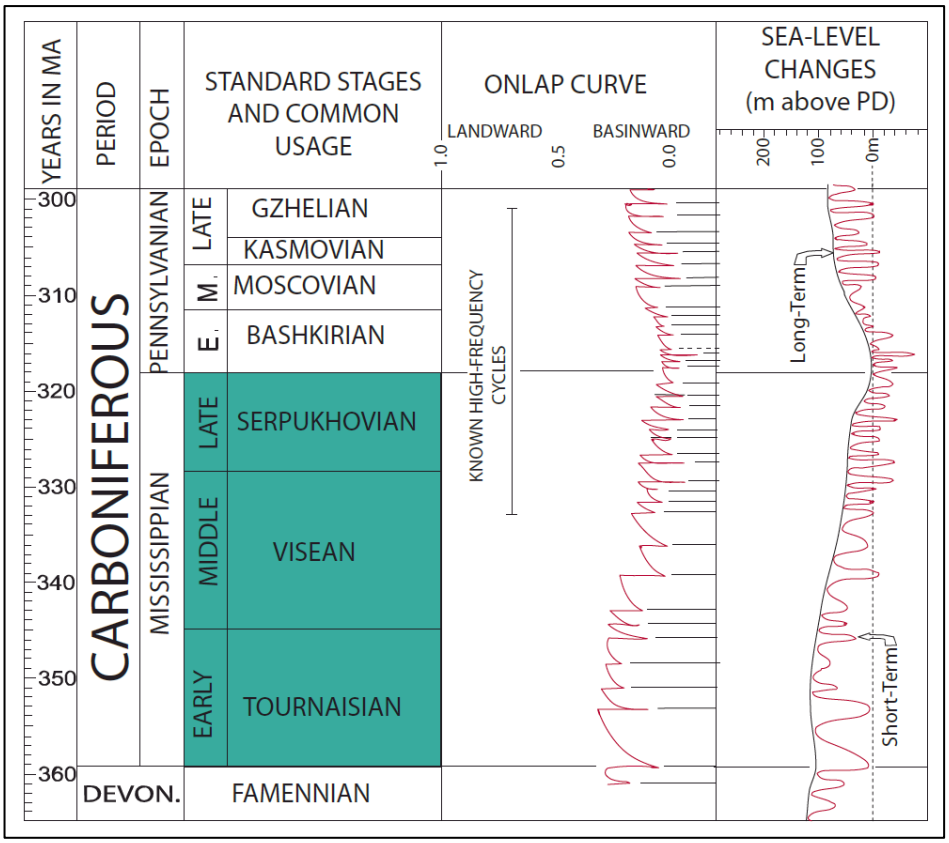

Figure V-1: Eustatic sea level curves applicable to the Early Carboniferous Period: Mississippian Epoch. On-lap curves and sea-level curves provide insight into the rate of sea-level change and estimated change in water depth throughout the Mississippian. Absolute changes to water

depth were basin specific and would have exaggerated or muted the identified Eustatic changes based on local changes to basin geometry and rate of subsidence or adjacent uplift. Figure modified from Haq and Schutter (2008).

Study Area and Depositional Environments

The Mid-Continent Mississippian age carbonate system has several unique depositional environments that, coupled with diagenetic and structural alterations, have resulted in several different lithologies that are credited as the primary reservoir faces. Depositional environments varied from high-energy near-shore beaches, sand shoals and tidal complexes to aerially extensive, low energy, sheltered middle-ramp and outer-ramp carbonate mud deposition with localized bioherms, reefs, and muddy lagoons (Curtis and Chapman, 1959). The regional tectonic regime resulted in continuous changes to both regional and local basin geometries and, along with the realization of the effect of multiple eustatic sea level oscillations, continue to be studied from outcrop and subsurface data sets to better understand and predict reservoir and facies distributions in the sub-surface throughout the Mid-Continent area (Boardman et al., 2013a,b; Grammer et al., 2013; LeBlanc and Grammer, 2014; Mazzullo et al., 2009; Mazzullo et al., 2011; Mazzullo, 2011; Morris et al., 2013; Price, 2014; Watney et al., 2001).

The data set includes five cores that represent three different depositional settings within the basin. The cores are from Reno County, Kansas, Logan County, OK, Payne County Oklahoma, and Osage County, Oklahoma. Within these areas, deposition is assumed to have occurred in a relatively shallow, tropical to subtropical epeiric sea environment located 20-30° south of the paleoequator (Curtis and Champlin, 1959; Gutschick and Sandberg, 1983; Witzke, 1990). It is currently accepted that deposition occurred on a low declivity (<1^{o}) ramp to a distally steepened ramp environment, with strike trending roughly east-west adjacent to actively subsiding foreland basins (Mazzullo et al., 2011a). Current research indicates the ramp system was regionally extensive and deposited carbonate and siliciclastic sediment across

hundreds of square kilometers in portions of Colorado, Nebraska, Kansas, Oklahoma, Arkansas, Missouri, Iowa, and Illinois (Gutschick and Sandberg, 1983; Lane, 1978; Childress, 2015; Price 2014; LeBlanc and Grammer, 2014; Bertallott, 2015). Proximal, shallow water conditions were present to the north, and deeper water with sediment starved conditions existed to the south (Gutschick and Sandberg, 1983; Lane and DeKyser, 1980). The entire ramp system was bounded to the north and northwest by the Transcontinental Arch, to the east by the Ozark Uplift, and to the south by the deep water settings of the ancestral Anadarko and Arkoma Basins (Lane and DeKyser, 1980). Local influences from the Nemaha Uplift and the Central Kansas Uplift have also been observed in recent studies (Bertallott, 2015; Doll, 2015).

DATA SELECTION AND ANALYTICAL METHODS

Data Set

The data used in this study come from five cores that represent three different areas of the basin (Figure V-2). Data analysis and interpretation integrates qualitative data with quantitative data to identify major and minor trends that can be utilized to identify key reservoir intervals with greatest hydrocarbon production potential. Qualitative data includes visual observations of the five cores and includes detailed facies analysis, generation a high resolution sequence stratigraphic framework, analysis of thin section and SEM photomicrographs, and correlation to conventional wireline log signatures. Quantitative data includes conventional laboratory analysis for porosity and permeability from core plugs and sections of whole core, pore architecture geometrical attributes extracted from thin section and SEM photomicrographs using digital image analysis, and laboratory measured sonic velocity response.

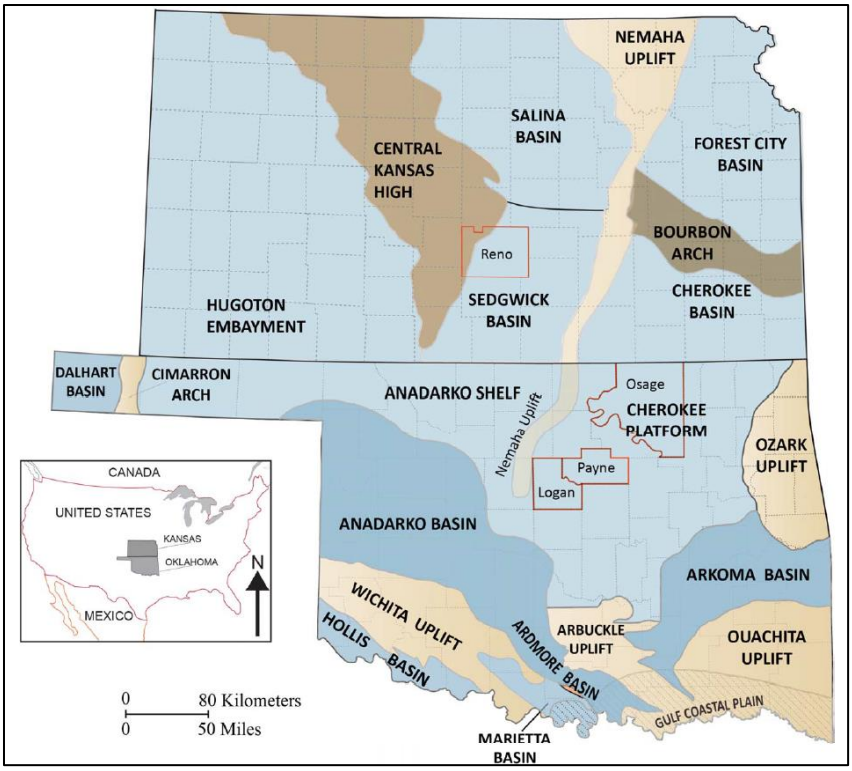

Figure V-2: The study area includes five core from three areas within the North American mid-continent area of Kansas and Oklahoma. An unconventional core with outer ramp facies is from Osage County, Oklahoma, three unconventional cores with middle to inner ramp facies are from Logan and Payne Counties, Oklahoma. A transitional core with proximal outer ramp to shoreline and peri-tidal facies is from Reno County, Kansas. During the Mississippian Period, this area was located approximately 30^{o} south of the paleo-equator and was covered by a shallow tropical epeiric sea. Regional tectonics beginning at the end of the Devonian and continuing throughout the Mississippian caused the emergence of the Nemaha Uplift, the Ozark Uplift, the Central Kansas Uplift, and the Ouachita Uplift. The same regional tectonic stress regime created a series of foreland basins including the Arkoma Basin located southeast of the areas included in the study in a paleo-dip direction.

The cores utilized in this study were selected for three specific reasons common to all cores:

1) Completeness of cored interval:

    a. The 3 cores from Logan and Payne County are continuous throughout the entire Mississippian section, showing contacts with both the

underlying and overlying formations. From west to east, the cores are nearly 100m (324ft.), 58m (190ft), and 44m (143ft) thick.

b. The core from Osage County is a continuously cored section of nearly 85m (278ft.) with 3 missing intervals associated with Mississippian age deposition. Sections missing from this core include the uppermost and lowermost sections, including the contact with the Pennsylvanian and Devonian, and an interval near the base of the core that was unable to be extracted with current drilling technology.

c. The core from Reno County Kansas is a continuously cored 69m (225ft) section through the majority of the Mississippian section with the Pennsylvanian and Devonian contacts approximated from wireline log signatures.

2) Availability of conventional wireline log suites (i.e. – gamma-ray, caliper, density and neutron porosity, and resistivity logs) and petrophysical data (porosity, permeability, mineralogy from XRD, grain density and bulk density).

3) The varying distribution of cores from more proximal to the north (Kansas core) moving more distal to the south, proximity to the Nemaha ridge (Osage core), and the relative spacing of the Payne and Logan county cores along depositional strike.

Core Descriptions and Facies Analysis

Total core footage from the 5 wells in this study is 357m (1173ft). Facies were defined based on the texture, grain type, sedimentary structures, environmental indicators such as type and intensity of bioturbation, and color. Facies analysis using the Dunham classification (Dunham, 1962) and interpretation of depositional environments were utilized to create an

idealized facies stacking pattern, which in turn was used as the foundation for developing the sequence stratigraphic framework (Loucks and Sarg, 1993; Emery and Myers, 1996; Catuneanu, 2006). Facies colors were identified using a wetter surface and comparison to the closest match from the GSA Rock-Color Chart, composed of a subset of Munsell color chips (Munsell 1995), or using the 2009 Munsell Soil Colorbook (Soil Survey Staff, 1993).

Classification of the macro- to meso-scale pore types observed in hand sample and thin sections utilized the classification scheme outlined by Choquette and Pray (1970). Classification of the meso- to nanoscale pores visible only by the SEM utilized the classification scheme outlined by Choquette and Pray (1970) where feasible, and where exceptions were noted other proposed descriptive terminology was utilized as applicable (Loucks et al., 2012; Milliken 2014; and Vanden Berg and Grammer, 2016).

High-Resolution Sequence Stratigraphic Analysis

The sequence stratigraphic framework applicable to the Mississippian section for each of the cores used in this study was determined through detailed facies analysis that defined an idealized vertical stacking pattern with subsequent application of the idealized stacking pattern to help define key sequence and cycle boundaries. The idealized facies succession for each core identifies the pattern of deposition that grades from either the deepest interpreted water depths, or most restricted water circulation, upward to the most shallow interpreted water depths, or least restricted environment. This gradation of most restricted to least restricted or deepest water to most shallow water environment is assumed to represent a single transgressive to regressive pattern of deposition as applicable to each specific location. A hierarchy of sequence and cycle boundaries are proposed for each core based on the idealized stacking pattern and observations from hand samples. It is important to note that currently there is no biostratigraphic control available that can be applied to the sequence stratigraphic framework, so discussions and

interpretations of the sequence stratigraphic hierarchy are relative. Although the specific time intervals are not able to be identified at this time, as shown in this study, identification of the depositional hierarchy based on a detailed facies analysis is still useful when key patterns and relationships allow for the application to other areas of the basin (Grammer et al., 2004).

Wireline Logs

A standard suite of wireline logs were available for each of the cores used in this study. The wireline log signature that was most useful and applicable for enhancing predictability within the data set is the gamma ray log. Other wireline logs that were integrated into the analysis if available include: the density-porosity, neutron- porosity, sonic porosity, bulk density, spontaneous potential, resistivity (shallow, medium and/or deep), compositional analysis, and permeability. The use of wireline logs in combination with core and petrographic analyses can serve as a powerful tool that helps to constrain the high frequency sequence stratigraphic framework and allow for correlation of high frequency sequence and cycle boundaries in areas where core and thin section data may be missing or otherwise unavailable.

Microscopy

Petrographic analysis of 323 available thin sections was performed using a Leica DM 2700P optical, or light, microscope (LM). The micro- to nanopore architecture was further examined using 132 a FEI Quanta 600F field emission environmental scanning electron microscope (SEM) to view samples from the micro- to pico-scale.

In addition to more accurate facies descriptions, thin section analysis also allowed for more accurate description and analysis of the macro- to nano-meter scale pore sizes, and pore types. Photomicrographs that represent the dominant pore types observed in the samples were captured and analyzed qualitatively and quantitatively. As described in Vanden Berg and

Grammer (2016), all samples viewed with the SEM were polished using an argon ion mill to provide an accurate representation of the pores within a 2D cross section of the sample.

Conventional Laboratory Measured Data

Conventional laboratory measured porosity (%), air permeability (mD), and Klinkenberg permeability (mD) data was available for all five cores used in this study. Other data available for some of the cores include discrete analysis for: oil saturation (%), water saturation (%), grain density (g/cm^3), and fluorescence, ambient and NCS porosity, mineralogy classified by percentage as clay (chlorite, kaolinite, illite/mica, marcasite), carbonate (calcite, iron-rich dolomite, dolomite, siderite), or other (quartz, feldspar, plagioclase, pyrite, apatite, marcasite, halite, barite) via XRD analysis, and TOC (%). For core without a suite of XRD analysis, bulk mineralogy was determined using samples representative of the facies within the core. It is important to acknowledge results from the bulk mineralogy analysis are significantly less specific and therefore less reliable when applied to the identification of trends and patterns that could be used to predict key reservoir intervals and therefore not highly utilized in identification of potentially useful patterns.

Two companies were utilized for measure standard petrophysical properties based on the primary owner of the core. Weatherford Laboratory performed the analysis for the three cores in Logan and Payne Counties, and Special Core Analysis Laboratories (SCAL), Inc. laboratory performed the analysis for the cores in Osage County and Reno County. All measurements were performed using conventional core analysis procedures. Laboratory measured porosity, air permeability, and Klinkenberg permeability data were utilized to identify potentially significant relationships between reservoir quality, position within the overall sequence stratigraphic framework, and variations within the pore architecture.

Pore Architecture Analysis

The primary goal in the qualitative and quantitative classification of pore architecture is to understand the fundamental features that correlate to laboratory measured porosity and permeability. Qualitative analysis included observations related to the density, spatial distribution, dominant pore size, dominant pore type, and diagenetic alteration that could significantly impact the measured porosity or permeability. Pore size classification was completed using the classification scheme of Loucks et al. (2012). Pore morphology is utilized to explain both relationships to facies and the sequence stratigraphic framework, and discrepancies to trends that appear to otherwise be applicable within the data set. Digital image analysis (DIA) was utilized to quantify the geometric characteristics of the pore space representative within several photomicrographs collected using the LM and SEM. Quantitative analysis was performed using the program R to identify relationships between laboratory measured porosity, air permeability, and Klinkenberg permeability with geometric features of representative pores. For a thorough description of the qualitative and quantitative analysis of the pore architecture, please see Vanden Berg (2016).

Acoustic Response

Acoustic response for this study was measured on core plugs selected to represent large variations in porosity for a given permeability, and large variations in permeability for given porosity while also being representative of the different facies within each core. The acoustic response was measured using an AutoLab 1000 from New England Research, Inc. that records the travel time through core plugs for one compressional wave (Vp) and two shear waves (Vs) using affixed transducers and receivers. The plugs were measured under dry, non-saturated conditions, saturated in a 35 ppt NaCl brine solution, and then re-measured under saturated conditions at five effective pressures at both increasing and decreasing pressure steps, where

the confining pressure and pore pressure are both adjusted independently. The data reported are the brine saturated samples at 20MPa effective pressure. Because of the high degree of brine water within the formation, and variability in present day depth, these values are used because they have the greatest applicability. For a more detailed analysis of the methodology followed to measure the acoustic response please refer to Vanden Berg (2016).

RESULTS

Core Descriptions: Facies analysis, and interpreted depositional environments

Unconventional reservoir core. Distal ramp, low-energy depositional environments (Osage County, Oklahoma)

The facies preserved in the core from Osage County, OK represents an unconventional reservoir with deposition located in distal, outer ramp environments, with moderate to highly restricted environments (Figure V-3). The contact with the underlying Devonian and overlying Pennsylvanian are both missing from the cored interval, but are both easily identified based on wireline log signatures. Seven facies were identified based on visual analysis of the core and thin sections with specific observations and descriptive methods followed noted in Table V-1a and Figure V-4a. Observations from slabbed sections of the core were supplemented with data from other sources as shown in Table V-2. Additional supplementary data included bulk XRD analysis from representative facies as shown in Table V-3. The interpreted depositional environments transition from a low-energy, highly restricted outer ramp below storm wave base, to a pore proximal location on the ramp that remains restricted and is a low-energy environment below storm wave base (Figure V-3).

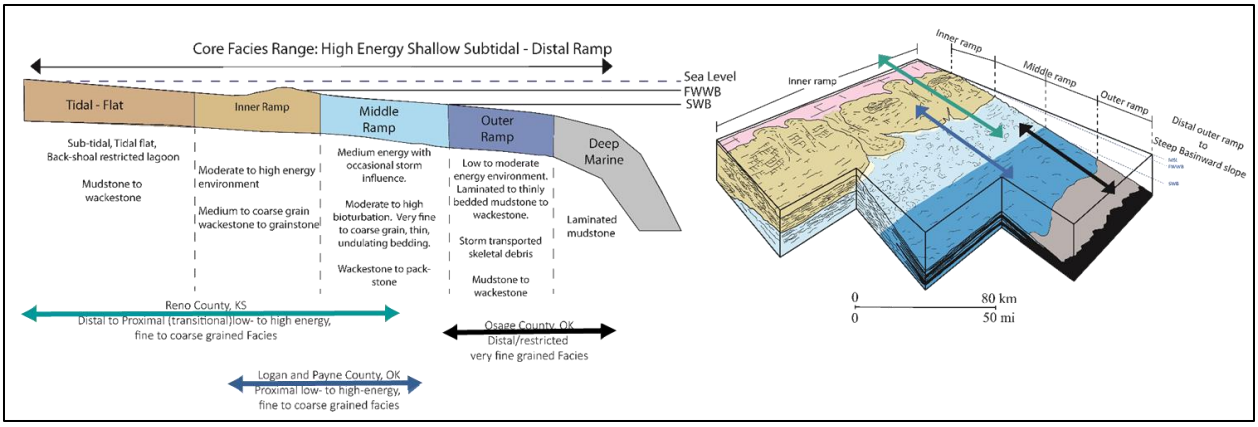

Figure V-3: The facies preserved within the Mississippian stratigraphic section from the three areas of the Mid-Continent included in this study represent distal, relatively deep water, and low energy conditions, to nearshore, relatively shallow water and high energy conditions, to shoreline and peritidal depositional environments. (Figure modified from Handford, 1986).

(a)

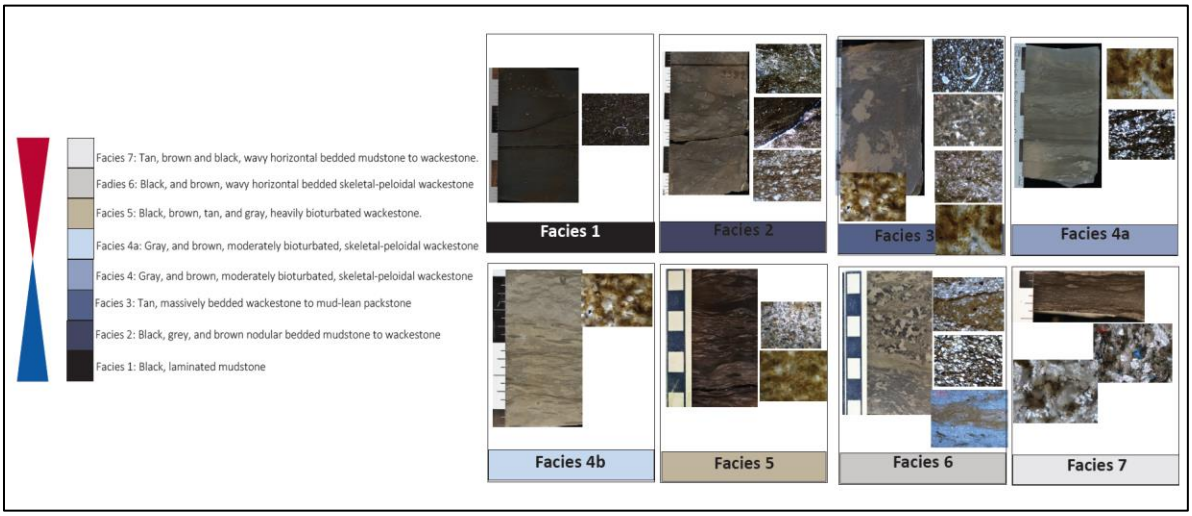

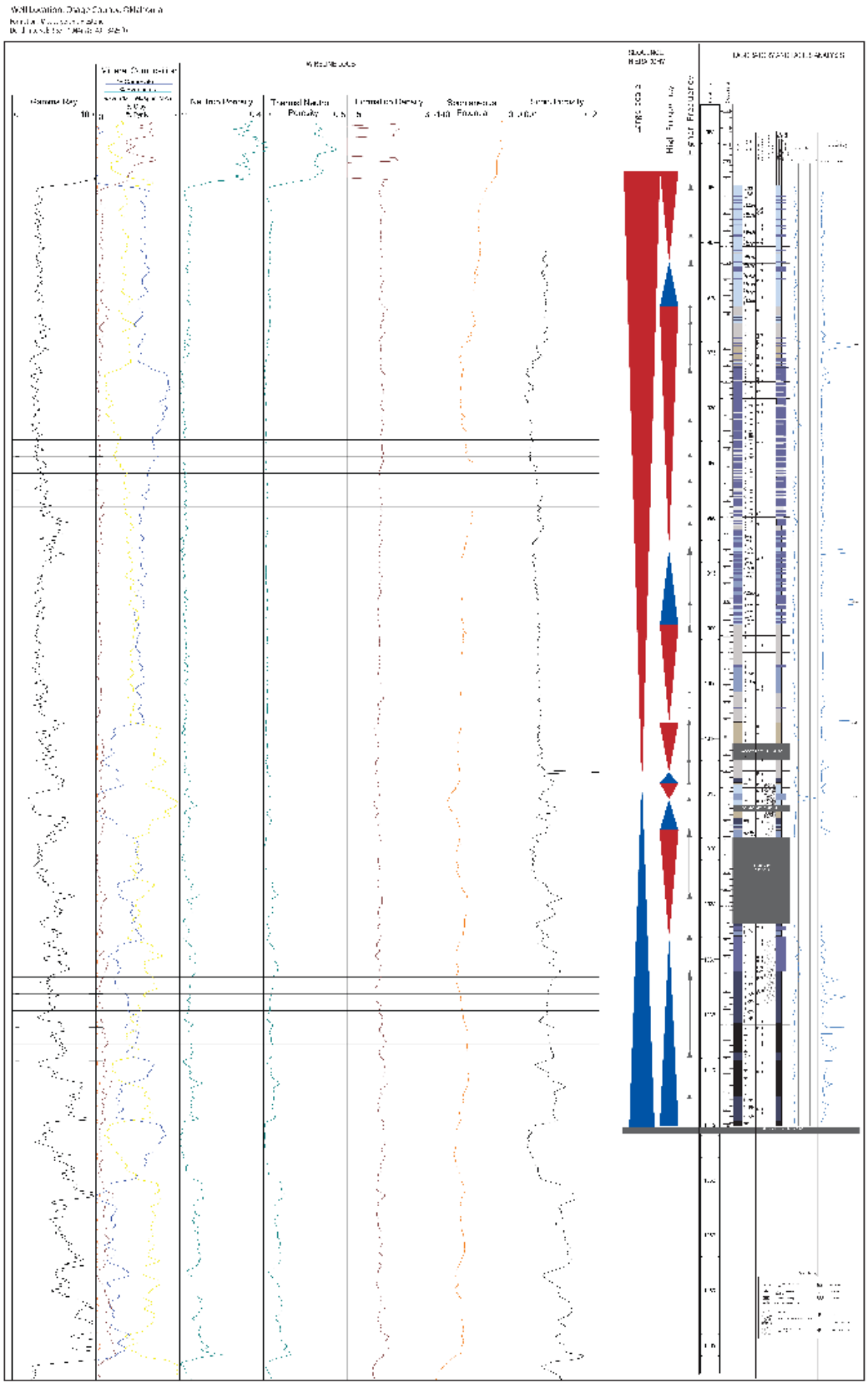

(b)

Figure V-4: The core from Osage County, Oklahoma is composed of facies deposited predominately in a distal outer ramp to middle ramp position in relatively deep water or a low energy environment. The length of core recovered from the Mississippian section is approximately 85m. [A] Seven facies were identified based on subtle variations in observed texture, composition, grain size, and level of bioturbation. Facies are named according to the Dunham Classification Scheme (1962). Although an idealized facies stacking pattern was applied to the core, the transition from Facies 1 to Facies 7 is more accurately described as a transition from a highly restricted, low-energy environment to depositional environments that have nearly normal marine circulation close to, but still beneath, storm wave base. A proximal facies, Facies 4, is interpreted to be deposited within the stratigraphic succession due to transportation from significant storm events. [B] Although the data set does not include biostratigraphic data that would allow to time constrain the core, a prominent exposure interval near the base of the core provides support for a theory that deposition in this location began in the early Mississippian Period and captures the earliest globally correlated eustatic sea level fall. As shown, the sequence stratigraphic framework was used to identify trends in wire line log signatures and laboratory measured petrophysical data.

(a) Osage County, OK Core: Unconventional Reservoir Facies

Facies I.D.	Rock Classification (Dunham, 1962)	Sedimentary Structures	Environmental Indicators (Trace fossils identified with MacEachern et al., 2009)	Color	Primary Pore Type (Thin Section) (Choquette and Pray, 1970)	Primary Pore Type (SEM) (Choquette and Pray, 1970; Vanden Berg and Grammer, 2016)	Acoustic Response (Vp)	Acoustic Response (Vs)	Depositional Environment
1	Mudstone	Laminated bedding	Crinoids	black	Interparticle, cemented	matrix, cemented	5560.878	3119.81	Outer ramp below storm wave base
2	Mudstone - wackestone	Nodular bedding	Crinoids	black to grey	Interparticle, moldic, cemented	matrix, cemented, interparticle	5300.541667	3135.766667	Outer ramp below storm wave base
3	Wackestone - packstone	Massive bedding	Crinoids, peloids, brachiopods, ooids, skeletal debris	tan	Interparticle, cemented, moldic	cemented, interparticle, matrix	5396.276667	3089.29	Outer ramp below storm wave base
4	Skeletal-peloidal wackestone	Horizontal bedding	Crinoids, peloids	grey and brown	Interparticle, cemented	matrix, interparticle, cemented	5366.966	3087.438	Outer to inner ramp, transported from proximal inner ramp location
5	Wackestone	Horizontal bedding	Crinoids, peloids	black, brown, tan, grey	Interparticle, cemented	interparticle, cemented, matrix	5434.895	3049.0225	Distal inner ramp
6	Skeletal-peloidal wackestone	Horizontal bedding	Sponge spicules	black, brown	cemented, interparticle	cemented, matrix, moldic, interparticle	5486.993333	3239.156667	Proximal inner ramp
7	Mudstone to Wackestone	Horizontal bedding	Crinoids, peloids, brachiopods, skeletal debris	tan, black, brown	Interparticle, cemented	interparticle, cemented, moldic	5532.175	2980.95	Restricted, muddy, lagoon

(b) Logan County, OK and Payne County, OK Cores: Unconventional Reservoir Facies

Facies I.D.	Rock Classification (Dunham, 1962)	Sedimentary Structures	Environmental Indicators (Trace fossils identified with MacEachern et al., 2009)	Color	Primary Pore Type (Thin Section) (Choquette and Pray, 1970)	Primary Pore Type (SEM) (Choquette and Pray, 1970; Vanden Berg and Grammer, 2016)	Acoustic Response (Vp)	Acoustic Response (Vs)	Depositional Environment
1	Glauconitic sandstone	Massive bedded, burrowed	brachiopod fragments	Dark greenish grey	n/a	n/a	n/a	n/a	Distal outer ramp, low-energy environment below storm wave base
2	Burrowed calcareous mudstone-wackestone	Planar laminations, local bioturbation	brachiopod, sponge spicules	Brownish black to greyish black	Interparticle	matrix	5602.44	3185.86	Middle ramp
3	Bioturbated wackestone-packstone	Bioturbated and burrowed, local thin bedding	crinoid, brachiopod fragments, sponge spicules	Dusky yellowish brown	Interparticle	Matrix, interparticle, intraparticle	5406.40	2951.45	Proximal ramp
4	Peloidal packstone-grainstone	Massive bedded, bioturbated	peloids, crinoids, sponge spicules, brachiopod fragments	Olive grey	Interparticle	matrix, intraparticle	5570.18	3490.82	Proximal ramp
5	Skeletal packstone-grainstone	Cross-bedded skeletal debris	crinoid, brachiopod, bryozoan fragments, sponge spicules, peloids	Medium to dark gray and dark yellowish brown	Interparticle	matrix, interparticle	5749.95	2964.71	Proximal ramp, high-energy shoal, above fair weather wave base

(c) Reno County, KS Core: Unconventional Reservoir to Conventional Reservoir Facies

Facies I.D.	Rock Classification (Dunham, 1962)	Sedimentary Structures	Environmental Indicators (Trace fossils identified with MacEachern et al., 2009)	Color	Primary Pore Type (Thin Section) (Choquette and Pray, 1970)	Primary Pore Type (SEM) (Choquette and Pray, 1970; Vanden Berg and Grammer, 2016)	Acoustic Response (Vp)	Acoustic Response (Vs)	Depositional Environment
1	Mudstone-wackestone	horizontal laminated silt and clay with horizontal layers of skeletal debris	crinoid fragments, skeletal debris	light grey to black	Interparticle	matrix	6106.91	3116.11	Inner ramp, below storm wave base
2	Crinoidal wackstone - packstone	alternating 1-3cm thick laminated silt and clay with fine to coarse grain sand and skeletal debris	crinoids, bivalves	grey with black laminations	Interparticle	matrix	5914.97	2962.15	Inner ramp, below storm wave base
3	Mudstone - peloidal/skeletal wackestone	Fine to coarse silt and sand with up to 90% skeletal debris	peloids, crinoids, skeletal debris	grey and greyish green	n/a	n/a	n/a	n/a	Inner ramp, between fair weather and storm wave base
4	Mudstone - skeletal wackestone	horizontal bedding with wavy laminations	crinoids, peloids, skeletal debris	brown and grey	Interparticle	Intercrystalline, matrix	5103.346667	2628.926667	Inner ramp, between fair weather and storm wave base
5	Crinoid-skeletal wackestone	horizontal bedding	crinoids, skeletal debris	dark to light brown	n/a	n/a	n/a	n/a	Inner ramp below fair weather wave base
6	Mudstone - Skeletal wackestone	large-scale cross-bedding, stacked fining upward sequences	indeterminate skeletal debris	light brown	Interparticle	Intercrystalline, matrix	5271.866	2798.766	Inner ramp, above fair weather wave base
7	Dolomitized mudstone - wackestone	horizontal, laminated, wavy bedding	n/a	light brown to grey-brown	Intercrystalline	organic, moldic	4626.96	2602.268	tidal flat
8	Mudstone	laminated	n/a	grey-brown, dark olive brown	Intercrystalline	Interparticle	4196.535	2349.12	tidal flat
9	Mudstone	wavy horizontal laminations	n/a	light olive green	Interparticle	Interparticle	4015.585	2215	tidal flat
10	Laminated Mudstone	laminated	sponge spicules	black and brown	Intercrystalline	Interparticle	3771.18	2093.84	tidal flat
11	Bioturbated Mudstone	horizontal, wavy bedding	n/a	light olive brown to dark grey brown	Interparticle	Interparticle	4123.79	3501.73	tidal flat
12	Spiculitic mudstone	horizontal, wavy bedding	n/a	rose-pink to greyish green	Interparticle, moldic	Interparticle	2452.64	2270.95	tidal flat

Table V-1: Seven facies were identified in the core from Osage County, Oklahoma, four common faces were identified in the cores from Logan and Payne Counties, Oklahoma, and twelve facies were identified in the core from Reno County, Kansas. A summary description of the identified facies is shown in the table above. 1a – Osage County, Oklahoma; 1b – Logan and Payne Counties, Oklahoma; 1c – Reno County, Kansas.

		Thin Sections	Ion polished samples viewed with SEM	Acoustic Reponse (dry)	Acoustic Response (brine saturated)	Cored Interval (m, ft.)
Osage County, Oklahoma	Distal ramp deposition (Unconventional reservoir)	50	67	93	34	85m., 278ft.
Logan County, Oklahoma	Proximal ramp deposition (Unconventional reservoir)	94	36	19	19	99m., 324ft.
Payne County (west), Oklahoma	Proximal ramp deposition (Unconventional reservoir)	69	38	16	14	58m., 190 ft.
Payne County (east), Oklahoma	Proximal ramp deposition (Unconventional reservoir)	22	37	14	14	44m., 143ft.
Reno County, Kansas	Proximal ramp to shoreline deposition (Transitional from unconventional to conventional reservoir)	87	30	39	34	70m, 230ft.
All Cores in Study	Distal outer ramp to shoreline deposition	322	208	181	115	356m., 1165ft.

Table V-2: Observations from the slabbed sections of core were supplemented with qualitative and quantitative observations from thin sections, ion milled samples, and laboratory measured acoustic response data as shown in the table above.

(a)

Core	Sample Number	Depth (ft)	Facies #	Air Permeability (mD)	Klinkenberg Permeability (mD)	Porosity %	Grain Density (g/cm^3)	Sw %	So %	quartz	calcite, syn	ankerite	calcite, magnesium, syn
Osage County, OK	233	3,379.10	1.00	0.0034	0.0011	4.71	2.67	33.5	0.0	82	11	7	
Osage County, OK	250	3,396.10	1.00	0.0166	0.0083	1.1	2.61	40.9	0.0	71	25	4	
Osage County, OK	263	3,409.30	1.00	0.0144	0.0071	1.30	2.65	33.6	0.0	60	34	6	
Osage County, OK	240	3,386.10	2.00	0.0042	0.0016	1.34	2.60	48.3	0.0	75	25		
Osage County, OK	274	3,420.20	2.00	0.0142	0.0069	2.05	2.61	39.1	0.0	73	24	3	
Osage County, OK	234	3,380.10	2.00	0.0066	0.0027	6.44	2.79	34.4	0.0	78	18	4	
Osage County, OK	243	3,389.05	2.00	0.0175	0.0088	2.35	2.77	47.4	0.0	77	23		
Osage County, OK	8	3,154.05	3.00	0.0007	0.0001	4.03	2.74	45.5	0.0	54	37	9	
Osage County, OK	232	3,378.10	3.00	0.0081	0.0035	5.23	2.66	40.5	0.0	75	19	6	
Osage County, OK	220	3,366.10	3.00	0.0004	0.0001	1.39	2.67	39.0	0.0	61	39		
Osage County, OK	180	3,326.10	4.00	0.0066	0.0027	3.70	2.58	38.2	0.0	100			
Osage County, OK	29	3,175.10	4.00	0.0057	0.0021	2.22	2.72	35.2	0.0	49	44	7	
Osage County, OK	48	3,194.10	5.00	0.1001	0.0695	4.81	2.79	33.6	6.9	77	19	4	
Osage County, OK	51	3,197.10	5.00	0.0034	0.0012	3.84	2.60	36.3	4.3	86	14		
Osage County, OK	47	3,193.10	6.00	0.0098	0.0036	6.11	2.72	46.1	9.2	61	25	14	
Osage County, OK	175	3,321.10	6.00	0.0019	0.0006	4.29	2.65	24.0	10.7	79			21
Osage County, OK	59	3,205.10	7.00	0.0244	0.0128	4.15	2.69	33.3	17.1	87	13		
Osage County, OK	62	3,208.10	7.00	0.0035	0.0012	1.41	2.68	40.0	0.0	89	11		
Osage County, OK	98	3,244.10	7.00	0.0069	0.0030	1.28	2.67	37.1	0.0	59	37	4	

Well Location	CLAYS				CARBONATES				OTHER MINERALS								TOTALS			Porosity (%)		Permeability (mD)		TOC	Facies
	Chlorite	Kaolinite	Illite/Mica	Mx I/S*	Calcite	Fe-Dol[1]	Dolomite[1]	Siderite	Quartz	K-spar	Plag.	Pyrite	Apatite	Marcasite	Halite	Barite	Clays	Carb.	Other	Ambient	NCS	To Air	Klinkenberg	(%)	Number
Logan County, OK	Tr	Tr	9	3	23	7	0	Tr	45	3	6	3	1	Tr	N/A	0	12	30	58	1.54	1.38	0.125	0.075	0.8	2
Logan County, OK	Tr	Tr	9	4	20	4	0	Tr	49	4	7	3	Tr	0	N/A	0	13	24	63	0.00			0	0.97	2
Logan County, OK	1	Tr	15	6	11	1	0	Tr	49	4	9	3	1	0	N/A	0	22	12	66	0.00			0	0.935	2
Logan County, OK	1	Tr	8	7	33	1	0	Tr	38	1	5	3	2	1	N/A	0	16	34	50	2.17			0	1.508	2
Logan County, OK	1	Tr	8	1	42	1	0	Tr	36	3	5	2	1	Tr	N/A	0	10	43	47	0.00			0	1.468	2
Logan County, OK	Tr	Tr	8	2	55	3	0	Tr	26	1	1	1	2	1	N/A	0	10	58	32	0.00			0	1.413	2
Logan County, OK	Tr	Tr	1	Tr	20	5	0	Tr	71	2	1	0	0	0	N/A	0	1	25	74	0.18	0.10		0.00001	0.1219	3
Logan County, OK	Tr	Tr	1	1	21	17	0	Tr	54	3	2	1	0	0	N/A	0	2	38	60	4.91	4.75	0.034	0.016	1.37	3
Logan County, OK	Tr	Tr	1	Tr	29	7	0	Tr	58	2	2	1	0	Tr	N/A	0	1	36	63	1.67			+	0.5617999	3
Logan County, OK	Tr	Tr	3	1	45	8	0	Tr	40	1	1	1	0	0	N/A	0	4	53	43	1.08	0.95	0.0012	0.0002	0.1802	3
Logan County, OK	Tr	Tr	1	Tr	72	Tr	0	Tr	24	1	1	1	0	0	N/A	0	1	72	27	0.59	0.41		<0.0001	0.16	3
Logan County, OK	Tr	Tr	1	1	71	1	0	Tr	23	1	1	1	0	0	N/A	0	2	72	26	0.23	0.14		<0.0001	0.1166	3
Logan County, OK	Tr	Tr	Tr	Tr	86	1	0	Tr	9	1	3	Tr	0	Tr	N/A	0	Tr	87	13	0.87	0.71	0.0001	<0.0001	0.14	3
Logan County, OK	Tr	Tr	2	Tr	80	1	0	Tr	13	1	2	1	0	0	N/A	0	2	81	17	0.19	0.10	0.0005	0.0001	0.106	3
Logan County, OK	Tr	Tr	1	1	65	8	0	Tr	20	1	3	1	0	0	N/A	0	2	73	25	2.48	2.31	0.0008	0.0001	0.34	3
Logan County, OK	Tr	Tr	2	5	41	9	0	Tr	37	1	3	2	0	Tr	N/A	0	7	50	43	2.17	2.00	0.072	0.04	0.5141	3
Logan County, OK	Tr	Tr	2	1	61	3	0	Tr	27	2	3	1	0	Tr	N/A	0	3	64	33	0.94	0.76		<0.0001	0.59	3
Logan County, OK	Tr	Tr	5	2	43	7	0	Tr	37	1	3	2	0	0	N/A	0	7	50	43	1.32	1.15		+	0.6837	3
Logan County, OK	Tr	Tr	1	Tr	87	Tr	0	Tr	9	Tr	2	1	0	0	N/A	0	1	87	12	0.45	0.28	0.0002	<0.0001	0.16	3
Logan County, OK	Tr	Tr	5	2	50	7	0	Tr	28	1	4	2	1	Tr	N/A	0	7	57	36					0.36	3
Logan County, OK	Tr	Tr	Tr	Tr	63	2	0	Tr	30	1	3	1	0	0	N/A	0	Tr	65	35	1.21	1.03	0.0002	<0.0001	0.27	3
Logan County, OK	Tr	Tr	4	1	45	3	0	Tr	40	1	2	1	2	1	N/A	0	5	48	47	0.57	0.43	0.0002	<0.0001	0.1431	3
Logan County, OK	Tr	Tr	4	1	51	6	0	Tr	34	1	2	1	0	Tr	N/A	0	5	57	38	0.45	0.30	0.0001	<0.0001	0.13	3
Logan County, OK	Tr	Tr	3	2	30	3	0	Tr	51	3	6	2	Tr	Tr	N/A	0	5	33	62	1.43	1.26	0.267	0.178	0.14	3
Logan County, OK	Tr	Tr	2	1	44	5	0	Tr	40	2	5	1	Tr	0	N/A	0	3	49	48	1.45	1.27	0.0003	<0.0001	0.13	3
Logan County, OK	Tr	Tr	1	Tr	73	2	0	Tr	21	1	2	Tr	0	0	N/A	0	1	75	24	0.42	0.28	0.0001	<0.0001	0.09	3
Logan County, OK	Tr	Tr	1	1	48	5	0	Tr	39	2	3	1	Tr	0	N/A	0	2	53	45	2.25	2.09	0.0002	<0.0001	0.17	3
Logan County, OK	Tr	Tr	2	1	49	4	0	Tr	41	1	2	Tr	Tr	0	N/A	0	3	53	44	2.18	2.03	0.0006	0.0001	0.43	3
Logan County, OK	Tr	Tr	8	2	33	6	0	Tr	39	4	6	2	Tr	Tr	N/A	0	10	39	51	2.47			+	0.7	3
Logan County, OK	Tr	Tr	2	1	45	4	0	Tr	41	2	4	1	Tr	Tr	N/A	0	3	49	48	1.40	1.25	0.0011	0.0002	0.107	3
Logan County, OK	1	Tr	9	5	32	4	0	Tr	41	1	3	2	1	1	N/A	0	15	36	49	1.95	1.82	0.45	0.322	0.547	3
Logan County, OK	1	Tr	5	3	34	5	0	Tr	41	1	3	3	3	1	N/A	0	9	39	52	1.42	1.29	0.301	0.203	0.816	3
Logan County, OK	Tr	Tr	8	3	19	1	0	Tr	54	3	6	3	3	Tr	N/A	0	11	20	69	2.75	2.58	0.006	0.0018	2.475	3
Logan County, OK	Tr	Tr	1	Tr	29	2	0	Tr	62	2	3	1	Tr	0	N/A	0	1	31	68	3.05	2.89	0.0008	0.0001	0.157	3
Logan County, OK	Tr	Tr	3	1	27	2	0	Tr	63	1	2	1	0	Tr	N/A	0	4	29	67	2.47	2.36	0.0026	0.0006	0.154	3
Logan County, OK	Tr	Tr	1	1	32	2	0	Tr	59	2	3	Tr	Tr	0	N/A	0	2	34	64	2.83			+	0.089	3
Logan County, OK	Tr	Tr	3	1	45	4	0	Tr	42	1	3	1	Tr	Tr	N/A	0	4	49	47	0.76	0.65	0.011	0.0041	0.137	3
Logan County, OK	1	Tr	8	4	30	2	0	Tr	43	2	6	3	1	Tr	N/A	0	13	32	55					0.711	3
Logan County, OK	Tr	Tr	3	2	56	1	0	Tr	33	1	2	2	Tr	Tr	N/A	0	5	57	38	0.94	0.82	0.0015	0.0003	0.544	3
Logan County, OK	Tr	Tr	Tr	Tr	23	1	0	Tr	72	3	1	Tr	0	0	N/A	0	Tr	24	76	0.95	0.80	0.0001	<0.0001	0.0742	4
Logan County, OK	Tr	Tr	Tr	Tr	79	Tr	0	Tr	16	2	3	Tr	0	0	N/A	0	Tr	79	21	0.84	0.66	0.0002	<0.0001	0.12	4
Logan County, OK	Tr	Tr	2	1	26	6	0	Tr	56	3	4	1	Tr	1	N/A	0	3	32	65	1.42	1.25	0.0001	<0.0001	0.07	4
Logan County, OK	Tr	Tr	4	1	34	13	0	Tr	38	1	6	2	1	Tr	N/A	0	5	47	48	2.91	2.76	0.0002	<0.0001	0.17	4
Logan County, OK	Tr	Tr	Tr	Tr	73	2	0	Tr	22	1	2	Tr	0	Tr	N/A	0	Tr	75	25	0.38	0.27	0.0002	<0.0001	0.08	4
Logan County, OK	Tr	Tr	1	1	51	3	0	Tr	39	1	3	1	0	Tr	N/A	0	2	54	44	1.18	1.03	0.0001	<0.0001	0.13	4
Logan County, OK	Tr	Tr	1	Tr	36	3	0	Tr	53	2	4	1	Tr	0	N/A	0	1	39	60	0.76	0.63		<0.0001	0.15	4
Logan County, OK	Tr	Tr	1	Tr	39	3	0	Tr	51	2	3	1	0	0	N/A	0	1	42	57	0.99	0.85	0.0001	<0.0001	0.15	4
Logan County, OK	Tr	Tr	1	1	37	2	0	Tr	53	2	3	1	0	0	N/A	0	2	39	59	1.01	0.85	0.0006	0.0001	0.14	4
Logan County, OK	Tr	Tr	1	1	54	2	0	Tr	37	1	3	1	0	0	N/A	0	2	56	42	1.27	1.11		<0.0001	0.11	4
Logan County, OK	Tr	Tr	1	Tr	47	3	0	Tr	40	3	5	1	Tr	0	N/A	0	1	50	49	1.14	0.96		<0.0001	0.12	4
Logan County, OK	Tr	Tr	1	Tr	72	2	0	Tr	22	1	2	Tr	0	0	N/A	0	1	74	25	0.50	0.36	0.0001	<0.0001	0.08	4
Logan County, OK	Tr	Tr	1	1	43	3	0	Tr	46	2	3	1	Tr	0	N/A	0	2	46	52	1.83	1.66	0.0002	<0.0001	0.14	4
Logan County, OK	Tr	Tr	2	2	41	3	0	Tr	44	2	5	1	0	Tr	N/A	0	4	44	52	1.40	1.29	0.0005	0.0001	0.067	4
Logan County, OK	Tr	Tr	4	1	28	3	0	Tr	51	3	8	1	1	0	N/A	0	5	31	64	2.41	2.27	0.0002	<0.0001	0.115	4
Logan County, OK	Tr	Tr	1	Tr	78	1	0	Tr	16	1	3	Tr	Tr	0	N/A	0	1	79	20	0.91	0.77		<0.0001	0.014	4
Logan County, OK	Tr	Tr	2	1	35	3	0	Tr	50	2	4	2	1	Tr	N/A	0	3	38	59	2.18	2.03	0.0002	<0.0001	0.147	4
Logan County, OK	Tr	Tr	1	Tr	60	5	0	Tr	28	1	4	Tr	1	Tr	N/A	0	1	65	34	1.35	1.19	0.0002	<0.0001	0.01	4
Logan County, OK	Tr	Tr	1	1	64	5	0	Tr	25	1	2	1	Tr	Tr	N/A	0	2	69	29	2.37	2.24	0.0005	0.0001	0.074	4
Logan County, OK	Tr	Tr	1	Tr	64	3	0	Tr	29	1	2	Tr	Tr	Tr	N/A	0	1	67	32	2.57	2.42	0.0002	<0.0001	0.01	4
Logan County, OK	Tr	Tr	4	Tr	28	22	0	Tr	36	2	6	Tr	1	1	N/A	0	4	50	46	3.08	2.92	0.0003	<0.0001	0.01	4
Logan County, OK	Tr	Tr	1	Tr	84	Tr	0	Tr	10	1	3	1	Tr	Tr	N/A	0	1	84	15	1.14	1.02	0.045	0.023	0.03	4
Logan County, OK	Tr	Tr	1	Tr	53	0	16	Tr	27	1	2	Tr	0	Tr	N/A	0	1	69	30	6.22	6.05	0.0058	0.0018	1.33	5
Logan County, OK	Tr	Tr	1	Tr	79	3	0	Tr	12	1	2	Tr	1	1	N/A	0	1	82	17	6.14	5.96	0.03	0.014	4.2	5
Logan County, OK	Tr	Tr	1	Tr	82	2	0	Tr	12	1	2	Tr	0	0	N/A	0	1	84	15	1.07	0.92	0.0003	<0.0001	0.1	5
Logan County, OK	Tr	Tr	Tr	Tr	21	0	7	Tr	71	1	Tr	Tr	0	0	N/A	0	Tr	28	72	1.56	1.39	0.402	0.282	0.12	5
Logan County, OK	Tr	Tr	1	Tr	37	4	0	Tr	56	1	1	Tr	0	0	N/A	0	1	41	58	0.47	0.35	0.0001	<0.0001	0.15	5
Logan County, OK	Tr	Tr	1	Tr	69	13	0	Tr	16	Tr	1	Tr	0	0	N/A	0	1	82	17	5.18	5.03	0.009	0.0031	0.97	5
Logan County, OK	Tr	Tr	1	Tr	68	5	0	Tr	21	2	3	Tr	0	0	N/A	0	1	73	26	7.02	6.86	0.143	0.087	2.34	5
Logan County, OK	Tr	Tr	Tr	Tr	67	2	0	Tr	27	1	2	1	Tr	Tr	N/A	0	Tr	69	31	0.76	0.60		<0.0001	0.1	5
Logan County, OK	Tr	Tr	1	Tr	77	2	0	Tr	17	Tr	3	Tr	0	0	N/A	0	1	79	20	0.38	0.25	0.0002	<0.0001	0.09	5

Well Location	CLAYS				CARBONATES				OTHER MINERALS								TOTALS			Porosity (%)		Permeability (mD)		TOC	Facies
	Chlorite	Kaolinite	Illite/Mica	Mx I/S*	Calcite	Fe-Dol[1]	Dolomite[1]	Siderite	Quartz	K-spar	Plag.	Pyrite	Apatite	Marcasite	Halite	Barite	Clays	Carb.	Other	Ambient	NCS	To Air	Klinkenberg	(%)	Number
Logan County, OK	Tr	Tr	Tr	Tr	49	2	0	Tr	45	2	2	Tr	0	0	N/A	0	Tr	51	49	0.66	0.50		<0.0001	0.1	5
Logan County, OK	Tr	Tr	Tr	Tr	31	1	0	Tr	66	2	Tr	Tr	0	0	N/A	0	Tr	32	68	2.44	2.31	0.175	0.11	0.1	5
Logan County, OK	Tr	Tr	1	Tr	31	1	0	Tr	64	1	2	Tr	0	0	N/A	0	1	32	67	1.08			+	0.11	5
Logan County, OK	Tr	Tr	1	Tr	59	1	0	Tr	36	1	2	Tr	Tr	0	N/A	0	1	60	39	4.93	4.76	0.0023	0.0005	0.64	5
Logan County, OK	Tr	Tr	3	2	33	4	0	Tr	52	2	3	1	Tr	Tr	N/A	0	5	37	58	7.73			+	0.5	5
Logan County, OK	Tr	Tr	Tr	Tr	16	1	0	Tr	80	2	1	Tr	0	0	N/A	0	Tr	17	83	1.93	1.77	0.011	0.004	0.139	5
Logan County, OK	Tr	Tr	1	Tr	31	1	0	Tr	63	2	2	Tr	Tr	0	N/A	0	1	32	67	0.93	0.80	0.0003	<0.0001	0.086	5
Logan County, OK	Tr	Tr	1	Tr	17	1	0	Tr	73	4	2	2	0	0	N/A	0	1	18	81	0.13	0.05	0.0002	<0.0001	0.098	5
Logan County, OK	Tr	Tr	Tr	Tr	50	9	0	Tr	38	1	1	1	Tr	0	N/A	0	Tr	59	41	10.77	10.60	0.777	0.553	0.44	5
Logan County, OK	Tr	Tr	1	Tr	77	1	0	Tr	15	Tr	5	Tr	1	0	N/A	0	1	78	21	1.33	1.15	0.0001	<0.0001	0.009	5
Logan County, OK	Tr	Tr	1	Tr	34	1	0	Tr	58	2	4	Tr	Tr	0	N/A	0	1	35	64	1.63	1.48	0.0002	<0.0001	0.025	5
Logan County, OK	Tr	Tr	3	1	33	3	0	Tr	53	1	5	1	0	Tr	N/A	0	4	36	60	1.88	1.76	0.0005	0.0001	0.074	5
Logan County, OK	Tr	Tr	1	Tr	71	1	0	Tr	22	1	4	Tr	Tr	0	N/A	0	1	72	27	2.03	1.88	0.0006	0.0001	0.01	5
Logan County, OK	Tr	Tr	1	Tr	47	7	0	Tr	42	1	2	Tr	Tr	Tr	N/A	0	1	54	45	4.37	4.19	0.0004	0.0001	0.227	5
Logan County, OK	Tr	Tr	1	Tr	71	Tr	0	Tr	22	1	4	Tr	1	Tr	N/A	0	1	71	28	0.78	0.62		<0.0001	0.009	5
East Payne County, OK	Tr	Tr	11	9	13	9	0	Tr	49	2	3	3	1	Tr	N/A	0	20	22	58	9.47	9.34	0.016	0.0062		1
East Payne County, OK	Tr	Tr	5	3	28	19	0	Tr	36	2	5	2	Tr	Tr	N/A	0	8	47	45	2.99	2.84	0.0002	<0.0001		3
East Payne County, OK	Tr	Tr	5	3	42	12	0	Tr	29	3	4	1	1	Tr	N/A	0	8	54	38	4.17	4.03	0.0034	0.0009		3
East Payne County, OK	Tr	Tr	1	Tr	66	1	0	Tr	26	1	4	1	Tr	0	N/A	0	1	67	32	1.41	1.26	0.0001	<0.0001		4
East Payne County, OK	Tr	Tr	1	Tr	75	1	0	Tr	19	1	3	Tr	0	0	N/A	0	1	76	23	1.93	1.79	0.0004	<0.0001		4
East Payne County, OK	Tr	Tr	1	Tr	54	4	0	Tr	40	Tr	1	Tr	Tr	Tr	N/A	0	1	58	41	3.35	3.21	0.045	0.023		5
East Payne County, OK	Tr	Tr	Tr	Tr	27	2	0	Tr	66	2	3	Tr	Tr	0	N/A	0	Tr	29	71	1.52	1.40	0.0003	<0.0001		5
East Payne County, OK	Tr	Tr	1	Tr	84	1	0	Tr	11	1	2	Tr	0	0	N/A	0	1	85	14	3.24	3.10	0.0037	0.001		5
East Payne County, OK	Tr	Tr	Tr	Tr	47	2	0	Tr	48	1	2	Tr	Tr	0	N/A	0	Tr	49	51	1.17	1.03	0.0001	<0.0001		5
East Payne County, OK	Tr	Tr	1	Tr	53	2	0	Tr	41	1	2	Tr	Tr	0	N/A	0	1	55	44	5.40	5.27	0.345	0.238		5
East Payne County, OK	Tr	Tr	1	Tr	33	Tr	0	Tr	61	2	3	Tr	0	0	N/A	0	1	33	66	3.02	2.89	0.0002	<0.0001		5
East Payne County, OK	Tr	Tr	1	Tr	37	1	0	Tr	56	2	3	Tr	Tr	0	N/A	0	1	38	61	3.15	3.00	0.0006	0.0001		5
East Payne County, OK	Tr	Tr	1	Tr	31	2	0	Tr	61	2	2	1	0	0	N/A	0	1	33	66	9.02	8.89	0.018	0.0074		5
East Payne County, OK	Tr	Tr	1	Tr	26	3	0	Tr	65	2	3	Tr	Tr	0	N/A	0	1	29	70	11.52	11.38	0.046	0.023		5
East Payne County, OK	Tr	Tr	1	Tr	45	Tr	0	Tr	51	1	2	Tr	Tr	0	N/A	0	1	45	54	5.89	5.75	0.002	0.0004		5
East Payne County, OK	Tr	Tr	1	Tr	85	0	0	Tr	10	1	3	Tr	0	0	N/A	0	1	85	14						5
West Payne County, OK	Tr	Tr	21	5	11	2	0	Tr	47	2	5	5	2	Tr	0	0	26	13	61	9.69	9.56	0.969	0.71	1.3	1
West Payne County, OK	Tr	Tr	10	5	28	10	0	Tr	37	1	5	3	1	Tr	0	0	15	38	47	3.47			0	0.745	2
West Payne County, OK	Tr	Tr	7	4	45	5	0	Tr	31	1	3	3	1	Tr	0	0	11	50	39	0.00			0	3.13	2
West Payne County, OK	1	Tr	15	4	25	2	0	Tr	45	1	4	2	Tr	1	0	0	20	27	53	0.00			0	1.82	2
West Payne County, OK	Tr	Tr	10	3	41	2	0	Tr	34	Tr	5	2	3	Tr	0	0	13	43	44	1.89	1.75	0.284	0.191	1.61	2
West Payne County, OK	Tr	Tr	9	3	23	17	0	Tr	42	1	2	2	1	0	0	0	12	40	48	1.92	1.78	0.0001	0.00001	0.574	2
West Payne County, OK	1	Tr	11	3	29	2	0	Tr	44	1	4	4	1	0	0	0	15	31	54	0.00			0	1.91	2
West Payne County, OK	1	Tr	17	5	17	1	0	Tr	47	2	5	4	1	0	0	0	23	18	59	0.00			0	1.98	2
West Payne County, OK	1	1	27	5	7	0	0	Tr	48	2	3	3	2	1	0	0	34	7	59	0.00			0	2.05	2
West Payne County, OK	Tr	Tr	1	1	55	15	0	Tr	23	1	2	1	1	0	0	0	2	70	28	3.26	3.11	0.0036	0.0009	0.426	3
West Payne County, OK	Tr	Tr	1	Tr	83	1	0	Tr	12	1	2	Tr	Tr	0	0	0	1	84	15	0.56	0.43	<0.0001	<0.0001	0.079	3
West Payne County, OK	Tr	Tr	2	2	65	3	0	Tr	25	1	2	Tr	0	0	0	0	4	68	28	0.84	0.69		<0.0001	0.179	3
West Payne County, OK	1	Tr	9	4	25	9	0	Tr	41	3	5	3	Tr	0	0	0	14	34	52	3.79	3.66	0.517	0.369	0.641	3
West Payne County, OK	Tr	Tr	8	4	26	10	0	Tr	45	1	4	2	Tr	0	0	0	12	36	52	2.52	2.40	0.072	0.039	0.847	3
West Payne County, OK	Tr	Tr	2	Tr	74	3	0	Tr	17	1	3	Tr	Tr	0	0	0	2	77	21	1.07	0.96		<0.0001	0.125	3
West Payne County, OK	Tr	Tr	12	5	22	8	0	Tr	43	1	5	3	Tr	1	0	0	17	30	53					0.391	3
West Payne County, OK	1	Tr	5	3	30	2	0	Tr	50	2	5	2	Tr	0	0	0	9	32	59	1.75	1.63		<0.0001	0.627	3
West Payne County, OK	Tr	Tr	6	3	45	9	0	Tr	32	1	2	1	1	0	0	0	9	54	37	2.50			+	1.29	3
West Payne County, OK	1	Tr	6	2	19	2	0	Tr	48	1	7	1	13	0	0	0	9	21	70	3.17	3.01	0.0025	0.0006	0.572	3
West Payne County, OK	Tr	Tr	24	9	10	1	0	Tr	45	2	5	4	Tr	0	0	0	33	11	56					0.789	3
West Payne County, OK	Tr	Tr	11	6	31	5	0	Tr	36	1	5	2	3	Tr	0	0	17	36	47	4.56			+	1.91	3
West Payne County, OK	Tr	Tr	8	4	38	4	0	Tr	30	1	6	3	6	0	0	0	12	42	46	2.21			+	2.49	3
West Payne County, OK	Tr	Tr	Tr	Tr	83	Tr	0	Tr	13	Tr	3	Tr	1	0	0	0	Tr	83	17	0.84	0.71	<0.0001	<0.0001	0.047	4
West Payne County, OK	Tr	Tr	1	Tr	80	4	0	Tr	12	Tr	3	Tr	Tr	0	0	0	1	84	15	2.36	2.22	0.0018	0.0004	0.146	4
West Payne County, OK	Tr	Tr	1	Tr	77	2	0	Tr	17	1	2	Tr	Tr	0	0	0	1	79	20	1.03	0.89		<0.0001	0.034	4
West Payne County, OK	Tr	Tr	1	Tr	76	0	2	Tr	17	1	3	Tr	Tr	0	0	0	1	78	21	1.68			+	0.071	4
West Payne County, OK	Tr	Tr	1	Tr	51	0	0	Tr	47	1	Tr	Tr	Tr	0	0	0	1	51	48	1.84	1.70	0.0006	0.0001	0.031	4
West Payne County, OK	Tr	Tr	1	1	59	3	0	Tr	26	2	6	1	1	0	0	0	2	62	36	2.26	2.13	0.0004	<0.0001	0.379	4
West Payne County, OK	Tr	Tr	8	2	26	9	0	Tr	47	1	5	2	Tr	0	0	0	10	35	55	2.79	2.64	0.0006	0.0001	0.154	4
West Payne County, OK	Tr	Tr	1	1	78	2	0	Tr	14	1	3	Tr	Tr	0	0	0	2	80	18	1.70	1.57	0.0006	0.0001	0.084	4
West Payne County, OK	Tr	Tr	Tr	Tr	78	1	0	Tr	17	1	3	Tr	Tr	0	0	0	Tr	79	21	1.88	1.72	0.0002	<0.0001	0.053	4
West Payne County, OK	Tr	Tr	1	Tr	81	Tr	0	Tr	14	1	3	Tr	Tr	0	0	0	1	81	18	0.83	0.70	0.0001	<0.0001	0.054	4
West Payne County, OK	Tr	Tr	1	1	58	Tr	0	Tr	34	1	4	Tr	1	0	0	0	2	58	40	1.33	1.19	0.0002	<0.0001	0.091	4
West Payne County, OK	Tr	Tr	2	1	39	4	0	Tr	51	1	1	1	Tr	Tr	0	0	3	43	54	3.07	2.92	0.0013	0.0003	0.233	5
West Payne County, OK	Tr	Tr	2	1	61	10	0	Tr	22	1	3	Tr	Tr	0	0	0	3	71	26	5.56	5.43	0.0037	0.001	0.57	5
West Payne County, OK	Tr	Tr	1	Tr	42	3	0	Tr	50	1	1	1	1	0	0	0	1	45	54	1.69	1.57	<0.0001	<0.0001	0.176	5
West Payne County, OK	Tr	Tr	1	Tr	73	0	0	Tr	22	1	3	Tr	Tr	0	0	0	1	73	26	0.93	0.78	0.0003	<0.0001	0.053	5
West Payne County, OK	Tr	Tr	2	1	46	2	0	Tr	43	1	3	1	1	Tr	0	0	3	48	49	3.46	3.31	0.0001	<0.0001	0.186	5
West Payne County, OK	Tr	Tr	2	1	35	3	0	Tr	51	2	4	1	1	Tr	0	0	3	38	59	2.68	2.55	0.0003	<0.0001	0.18	5

(b)

Well Location	CLAYS				CARBONATES				OTHER MINERALS								TOTALS			Porosity (%)		Permeability (mD)		TOC	Facies
	Chlorite	Kaolinite	Illite/Mica	Mx I/S*	Calcite	Fe-Ca*	Dolomite*	Siderite	Quartz	K-spar	Plag.	Pyrite	Apatite	Marcasite	Halite	Barite	Clays	Carb.	Other	Ambient	NCS	To Air	Klinkenberg	(%)	Number
West Payne County, OK	Tr	Tr	2	Tr	52	3	0	Tr	40	1	2	Tr	Tr	0	0	0	2	55	43	2.37	2.22	0.0003	<0.0001	0.192	5
West Payne County, OK	Tr	Tr	2	Tr	37	3	0	Tr	53	1	3	1	Tr	0	0	0	2	40	58	2.78	2.65	0.0024	0.0005	0.112	5
West Payne County, OK	Tr	Tr	1	Tr	74	1	0	Tr	21	1	2	Tr	Tr	0	0	0	1	75	24	0.87	0.74	0.0002	<0.0001	0.074	5
West Payne County, OK	Tr	Tr	Tr	Tr	73	1	0	Tr	22	1	3	Tr	Tr	0	0	0	Tr	74	26					0.09	5
West Payne County, OK	Tr	Tr	Tr	Tr	69	1	0	Tr	27	1	1	Tr	1	0	0	0	Tr	70	30	1.86	1.72	<0.0001	<0.0001	0.193	5
West Payne County, OK	Tr	Tr	1	Tr	51	Tr	0	Tr	42	2	3	1	Tr	0	0	0	1	51	48	1.16	1.01	0.0002	<0.0001	0.07	5
West Payne County, OK	Tr	Tr	1	Tr	26	1	0	Tr	68	1	Tr	3	Tr	0	0	0	1	27	72	1.54			+	0.216	5
West Payne County, OK	Tr	Tr	1	Tr	41	6	0	Tr	50	1	1	Tr	Tr	Tr	0	0	1	47	52	0.24	0.12	<0.0001	<0.0001	0.042	5
West Payne County, OK	Tr	Tr	2	1	26	2	0	Tr	66	1	2	Tr	Tr	0	0	0	3	28	69	3.32	3.18	0.0001	<0.0001	0.291	5
West Payne County, OK	Tr	Tr	1	1	62	1	0	Tr	31	1	3	Tr	Tr	0	0	0	2	63	35	1.65	1.51	0.0001	<0.0001	0.077	5
West Payne County, OK	Tr	Tr	1	Tr	62	9	0	Tr	25	1	2	Tr	Tr	0	0	0	1	71	28	5.46	5.30	0.137	0.083	0.461	5
West Payne County, OK	Tr	Tr	1	Tr	57	10	0	Tr	30	1	1	Tr	Tr	0	0	0	1	67	32	5.27	5.12	0.125	0.075	0.431	5
West Payne County, OK	Tr	Tr	1	Tr	54	7	0	Tr	36	1	1	Tr	Tr	0	0	0	1	61	38	3.09	2.95	0.0009	0.0001	0.076	5
West Payne County, OK	Tr	Tr	3	1	33	7	0	Tr	50	1	3	1	1	Tr	0	0	4	40	56						5
West Payne County, OK	Tr	Tr	1	Tr	81	1	0	Tr	13	1	3	Tr	Tr	0	0	0	1	82	17	2.46	2.33	0.0007	0.0001	0.069	5
West Payne County, OK	Tr	Tr	1	1	38	5	0	Tr	47	2	5	1	Tr	0	0	0	2	43	55	2.93	2.77	0.0007	0.0001	0.263	5
West Payne County, OK	Tr	Tr	1	Tr	55	3	0	Tr	35	1	3	1	1	0	0	0	1	58	41	4.44			+	0.245	5
West Payne County, OK	Tr	Tr	2	1	30	Tr	0	Tr	53	1	5	Tr	3	0	0	0	8	30	62	2.93	2.78	0.0002	<0.0001	0.064	5
West Payne County, OK	Tr	Tr	1	Tr	39	0	0	Tr	58	1	1	Tr	Tr	0	0	0	1	39	60	2.87	2.72	0.0004	<0.0001	0.192	5
West Payne County, OK	Tr	Tr	1	Tr	78	Tr	0	Tr	17	1	2	1	Tr	0	0	0	1	78	21	1.74	1.61	0.0002	<0.0001	0.041	5
West Payne County, OK	Tr	1	1	Tr	52	Tr	0	Tr	43	1	2	Tr	Tr	0	0	0	2	52	46	6.64	6.48	0.02	0.0082	0.229	5
West Payne County, OK	Tr	Tr	Tr	Tr	48	Tr	0	Tr	50	1	1	Tr	0	0	0	0	Tr	48	52	0.89	0.78	<0.0001	<0.0001	0.055	5
West Payne County, OK	Tr	Tr	1	Tr	79	Tr	0	Tr	17	1	1	Tr	1	0	0	0	1	79	20	3.25			+	0.05	5
West Payne County, OK	Tr	1	2	Tr	53	Tr	0	1	39	1	1	Tr	2	0	0	0	3	54	43	4.72	4.58	0.001	0.0002	0.163	5
West Payne County, OK	Tr	1	3	Tr	41	Tr	0	1	48	2	2	Tr	2	0	0	0	4	42	54	5.92			+	0.266	5
West Payne County, OK	Tr	1	2	Tr	Tr	0	0	Tr	93	2	1	Tr	1	0	Tr	0	3	Tr	97	4.78	4.69	0.0004	<0.0001	0.062	5
West Payne County, OK	Tr	1	6	Tr	Tr	0	0	1	85	2	2	1	2	0	Tr	0	7	1	92	9.67	9.52	0.01	0.0037	0.329	5
West Payne County, OK	Tr	2	2	Tr	0	0	0	6	87	2	1	Tr	0	0	0	0	4	6	90	2.96			+	0.179	5
West Payne County, OK	13	7	26	2	Tr	0	0	1	35	2	14	Tr	Tr	0	0	0	48	1	51	6.02			+	0.64	5

(c)

Table V-3: bulk X-ray diffraction (XRD) data was measured for select samples from the core in Osage County, OK (Table V-3a) and detailed XRD data was available for the three cores located in Logan and Payne Counties, OK (Table V-3b).

(a) XRD Data measured for samples from the Osage County, OK core were selected based on their facies associated to provide insight into the mineral variability within the cored interval.

(b) The data available for the core in Logan and Payne Counties, OK include approximations of the percent and type of clays, the percent and composition of carbonate minerals, and an estimate of the percent of quartz and other primary components including potassium feldspar (K-spar), plagioclase feldspar (Plag.), pyrite, apatite, marcasite, halite and barite. Each of the primary groups (Clay, Carbonate, Other) is summarized and compared to the measured porosity, permeability, total organic carbon (TOC) and identified facies.

Unconventional reservoir core. Proximal ramp, medium-energy depositional environments (Logan and Payne County, Oklahoma)

The three cores located in Logan and Payne Counties in Oklahoma have been grouped based on lateral proximity and orientation to paleo-stratigraphic strike, as well as similarity in facies observed in each core. Each of the three cores includes the stratigraphic contact with the underlying Devonian Woodford Shale and the overlying Pennsylvanian stratigraphy. Four facies were identified based on visual analysis of the core and thin sections with specific observations and descriptive methods followed noted in Table V-1b and Figure V-5a. Observations from slabbed sections of the core were supplemented with data from other sources as shown in Table

V-2. The interpreted depositional environments transition from a position on the inner ramp position below storm wave base to a more proximal position above fair weather wave base in a high-energy shoal environment (Figure V-3).

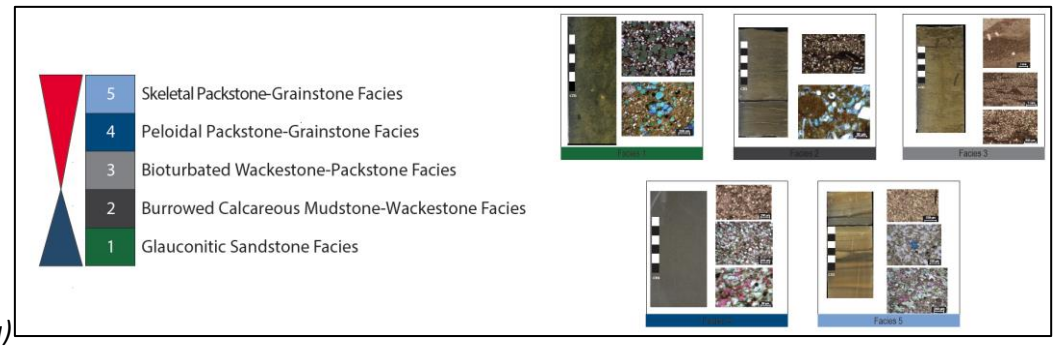

(a)

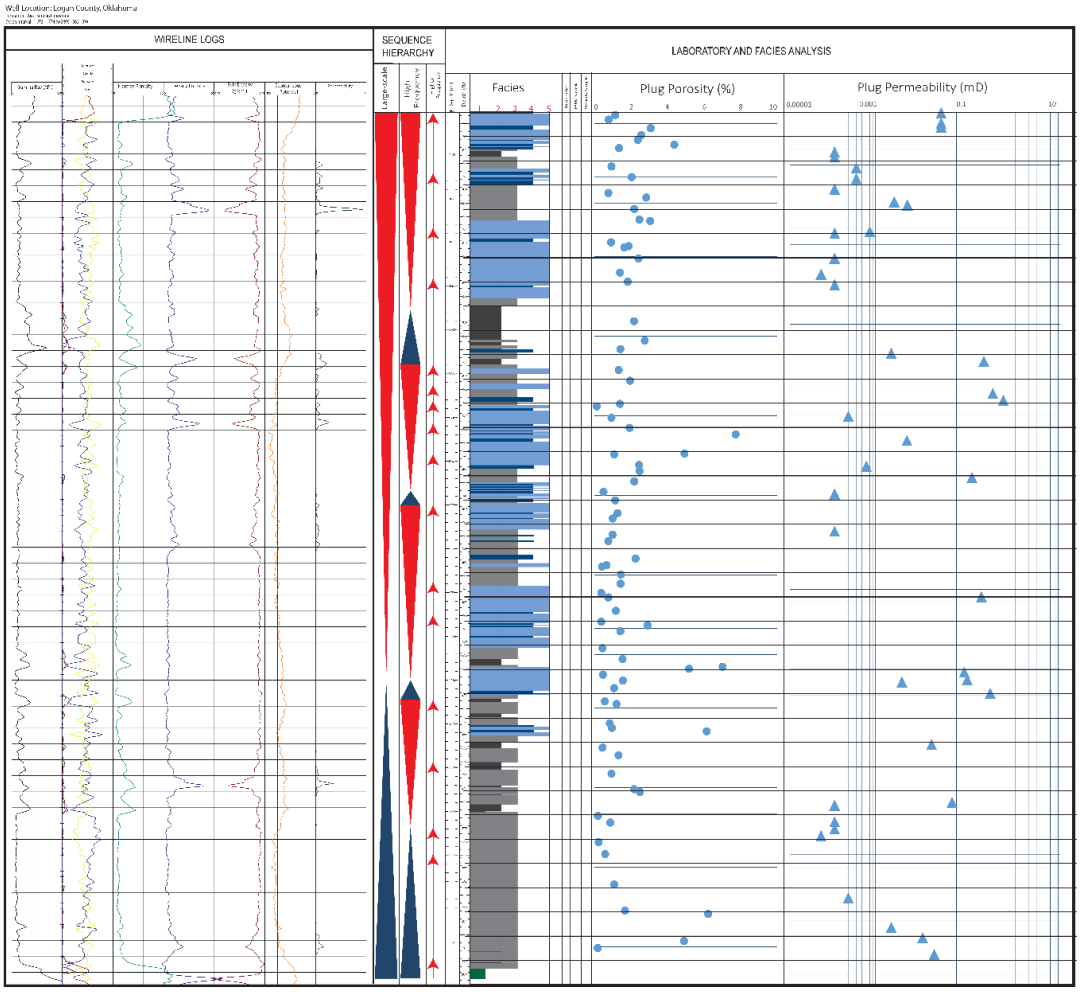

(b)

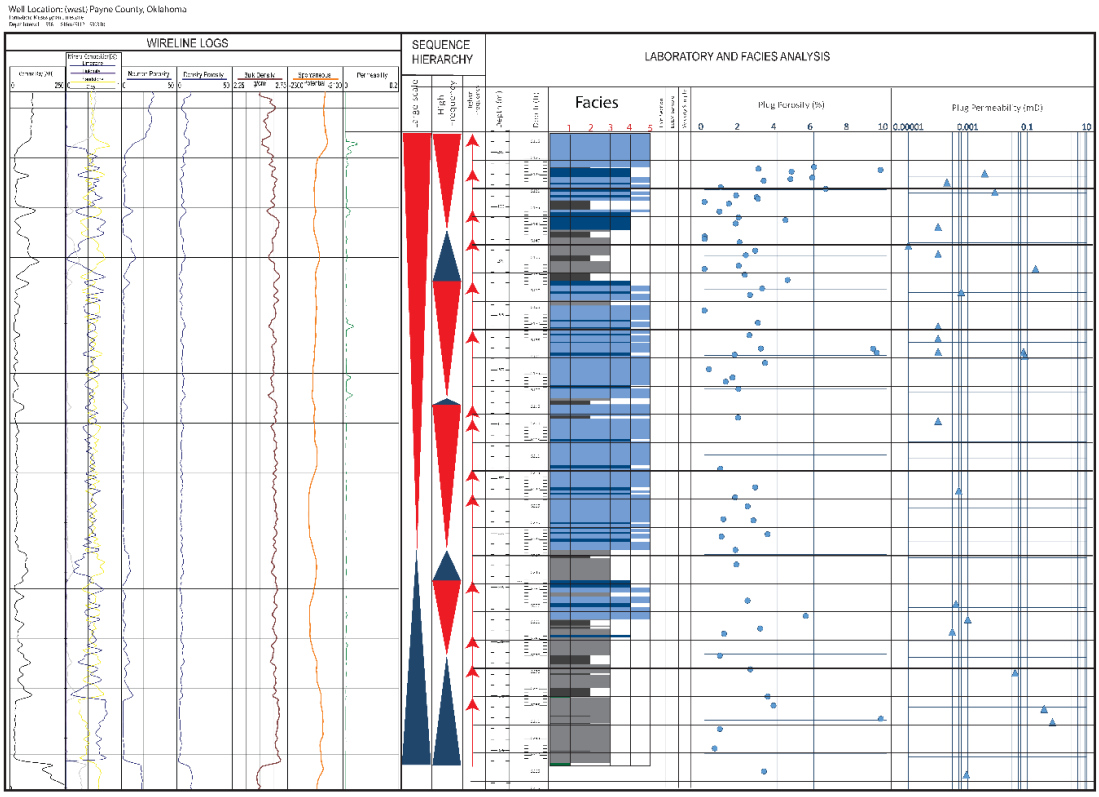
Well Location: (west) Payne County, Oklahoma
WIRELINE LOGS
SEQUENCE HIERARCHY
LABORATORY AND FACIES ANALYSIS
Facies
Plug Porosity (%)
Plug Permeability (mD)

(c)

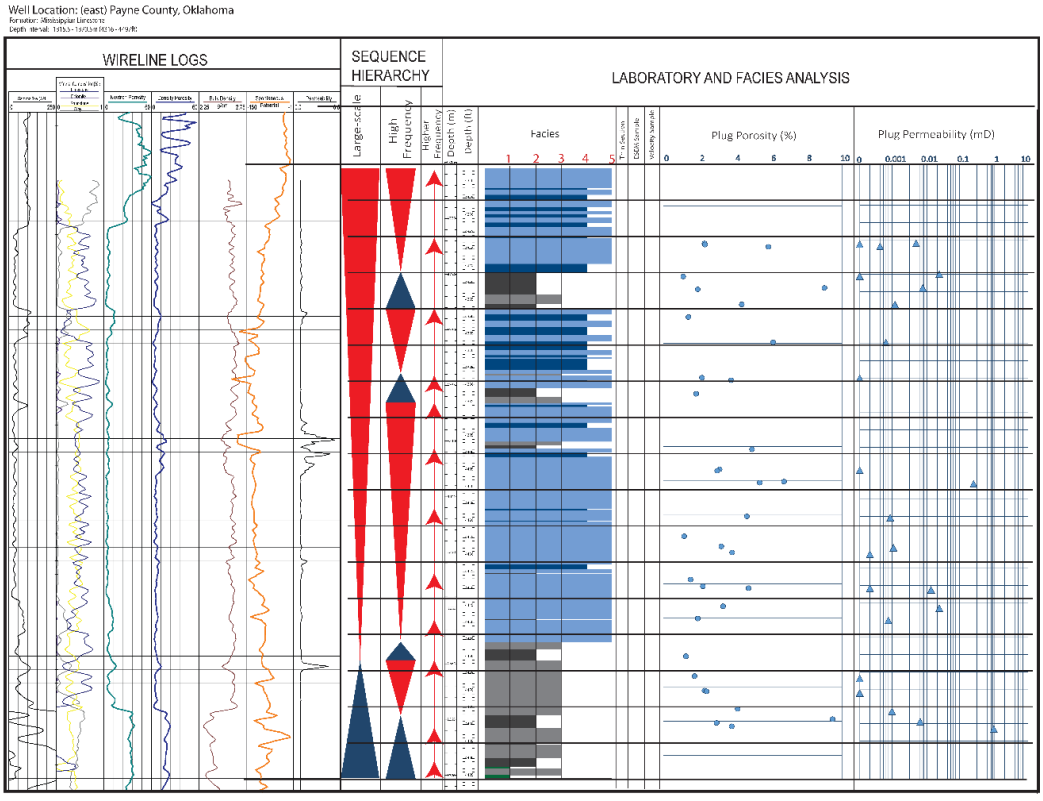
Well Location: (east) Payne County, Oklahoma
WIRELINE LOGS
SEQUENCE HIERARCHY
LABORATORY AND FACIES ANALYSIS
Large-Scale
High Frequency
Higher Frequency
Facies
Plug Porosity (%)
Plug Permeability (mD)

(d)

Figure V-5: The unconventional reservoir core from Payne County (East), Payne County (West), and Logan County, Oklahoma has preserved facies that were deposited predominantly in a middle to inner ramp position on a low-declivity ramp system. Total recovered core from the three locations is approximately 200m (657ft). Five facies were identified based on visual observations of texture, composition, grain size, and level of bioturbation. Facies are named according to the Dunham Classification Scheme (1962). The facies were placed into an idealized facies stacking pattern and utilized to define the sequence stratigraphic framework (b,c,d).

Because biostratigraphic data is unavailable the time interval represented is undefined. Due to the lack of alteration from major exposure intervals or other globally correlated features, placement within the Mississippian Period is not feasible at this time. As shown, the sequence stratigraphic framework was used to identify trends in wire line log signatures and laboratory measured petrophysical data. [b] Logan County, OK Sequence Stratigraphic Framework and wireline log response data. [c] (West) Payne County, OK Sequence Stratigraphic Framework and wireline log response data. [d] (East) Payne County, OK Sequence Stratigraphic Framework and wireline log response data.

Transitional reservoir core. Proximal ramp to shoreline, low-energy to high energy to shoreline depositional environments (Reno County, Kansas).

The facies preserved in the core from Reno County, Kansas represent an unconventional reservoir with low porosity, low permeability and predominantly micro- to nanoporosity at the base that transitions into a conventional reservoir with higher porosity and permeability with predominantly macro- to mesoporosity in the top portion of the core. The contact with the underlying Devonian and overlying Pennsylvanian are not present in the cored interval but are easily identified from the wireline log signature. Twelve facies were identified based on visual analysis of the core and thin sections with specific observations and descriptive methods followed noted in Table V-1c and Figure V-6a. Observations from slabbed sections of the core were supplemented with data from other sources as shown in Table V-2. The interpreted depositional environments transition from a position on the inner ramp, below storm wave base, to shoreface and tidal flat environments (Figure V-3).

(a)

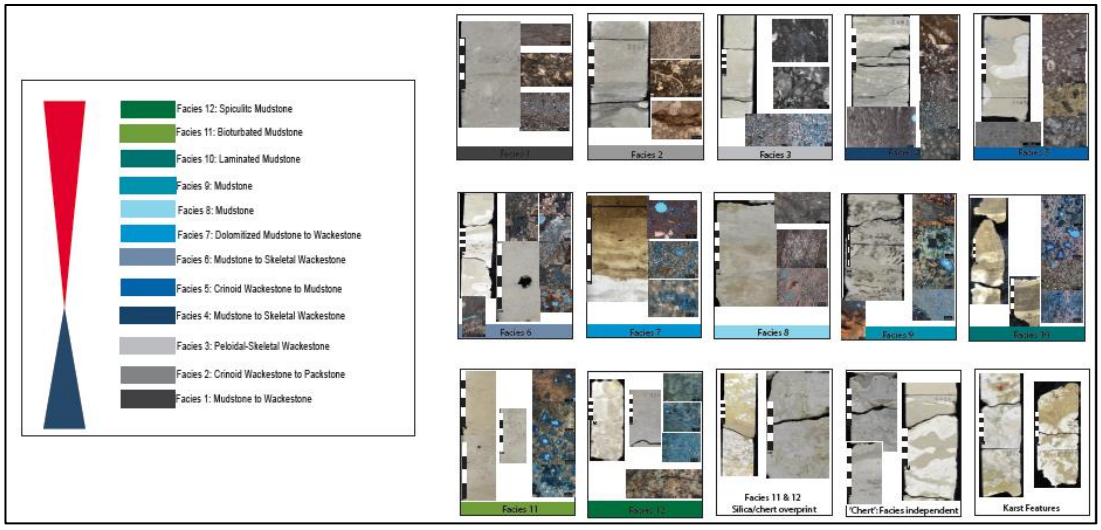
Facies 12: Spiculitic Mudstone
Facies 11: Bioturbated Mudstone
Facies 10: Laminated Mudstone
Facies 9: Mudstone
Facies 8: Mudstone
Facies 7: Dolomitized Mudstone to Wackestone
Facies 6: Mudstone to Skeletal Wackestone
Facies 5: Crinoid Wackestone to Mudstone
Facies 4: Mudstone to Skeletal Wackestone
Facies 3: Peloidal-Skeletal Wackestone
Facies 2: Crinoid Wackestone to Packstone
Facies 1: Mudstone to Wackestone
Facies 1
Facies 2
Facies 3
Facies 6
Facies 7
Facies 8
Facies 9
Facies 11
Facies 11 & 12
Silica/chert overprint
'Chert': Facies independent
Karst Features

(b)

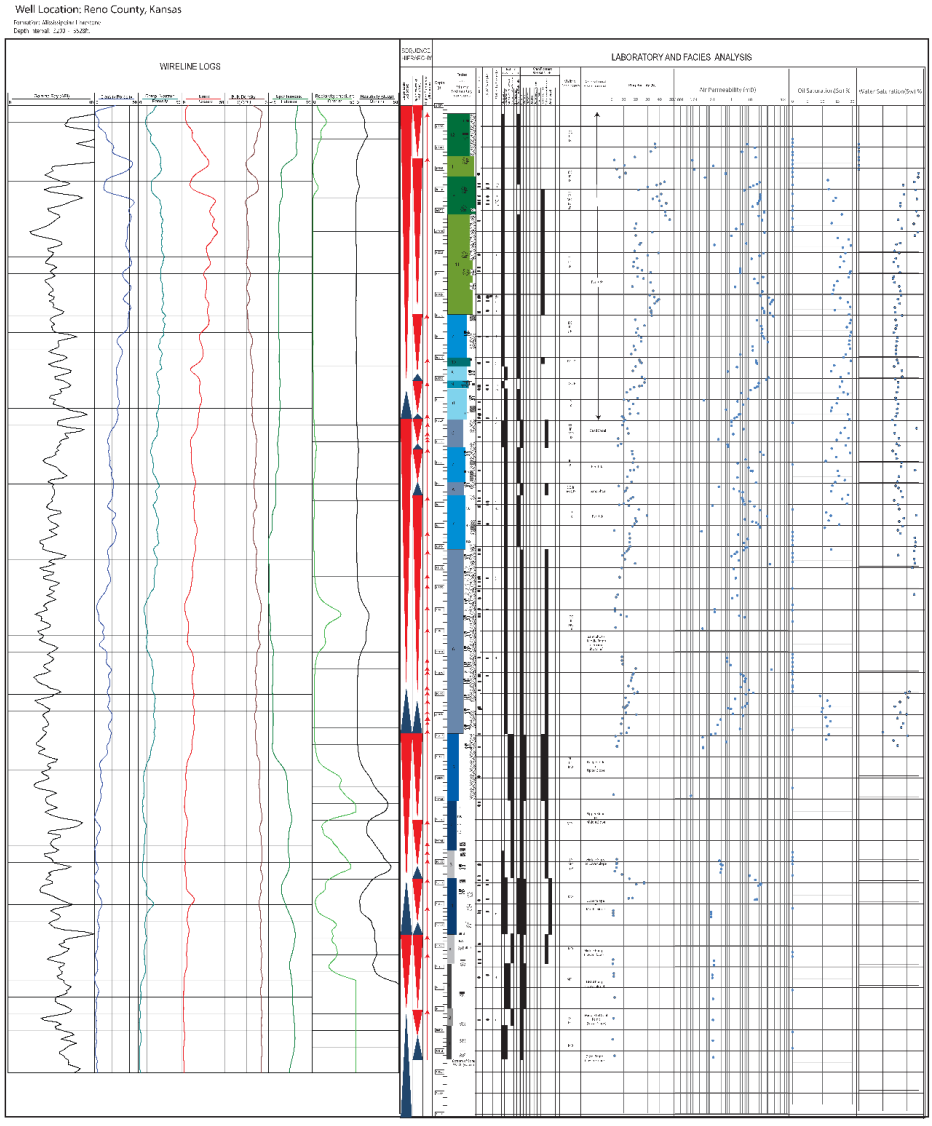
Well Location: Reno County, Kansas
WIRELINE LOGS
LABORATORY AND FACIES ANALYSIS

Figure V-6: The core from Reno County, Kansas is composed of a shallowing upward sequence of facies that were deposited in a middle ramp environment to near-shore and peri-tidal environment. Total recovered core from this location is approximately 72m (238ft). [A] Twelve facies were identified based on visual observations of texture, composition, grain size, and level of bioturbation. Facie are named according to the Dunham Classification Scheme (1962). The facies are placed into an idealized stacking pattern that was utilized to define the sequence stratigraphic framework. [B] Although biostratigraphic data is unavailable, a prominent exposure interval that impacts the upper portion of the core supports deposition in this location culminated at the end of the Mississippian and captures the latest globally correlated eustatic sea level fall and hiatus between the Mississippian and Pennsylvanian Periods. As shown, the sequence stratigraphic framework was used to identify trends in wire line log signatures and laboratory measured petrophysical data.

High Resolution Sequence Stratigraphic Framework

The interpreted depositional environments for each core was utilized to place the facies into an idealized stacking pattern following principles of Walther's Law. The interpreted depositional environments indicate deposition occurred on an attached, low-declivity ramp with deposition transitioning from a distal position below storm wave base to a slightly more proximal position that remains below fair weather wave base. The sequence stratigraphic framework was determined using the idealized vertical stacking pattern of facies. In each core the idealized facies succession exhibits a shallowing-upwards profile that correlates to a single large-scale transgressive and regressive phase which also represents a relative shallowing upward sequence from deeper to more shallow water with increasingly improved water circulation and oxygenation. The idealized stacking pattern was used as a foundation to identify the sequence stratigraphic framework (Figure V-4b, 5b.c.d., 6b).

Based on the identified facies, the largest scale sequence, interpreted as either a 2nd or 3rd order sequence, includes the entire cored interval. Within this sequence are two higher order frequency sequences that are likely either 3rd or 4th order sequences and 4th or 5th order cycles. Because there is no biostratigraphic control, the exact time intervals and therefore precise temporal definitions of the cyclicity cannot be ascertained unequivocally. For purposes

of detailed results and discussion, the sequences will be referenced, from largest to smallest, as a second-, third- and fourth-order sequence.

Each of the cores have a single second-order sequence that is assumed to be correlative within the Mid-Continent region. Each of the second order sequences show an overall shallowing upward, regressive depositional character, which is consistent with global sea level curves that show a gradual fall in eustatic sea level throughout the Mississippian (Haq and Schutter, 2008). The cores from Reno County, KS, Logan County, OK, and Payne County, OK have 4 identified third-order sequences, and the core from Osage County, OK has 6 identified third-order sequences. Each of these sequences has slight to obvious asymmetry with a longer regressive phase than transgressive phase preserved in the core. There is a significant amount of variability in the number of fourth-order sequences identified in each core which represents the impact of autocyclic and allocyclic processes on preserved facies with the tectonically active region.

Sequence stratigraphic framework, porosity, permeability, and wireline log relationship

As observed in the wireline logs available for use in this study, the gamma ray log signature consistently has an approximate correlation to the identified third-order sequence (Figures V-7a,b,c,d,e). Although this relationship should be verified by facies observations, use of the gamma ray log can provide a first-order identification of the number and thickness of third-order sequences within the Mississippian stratigraphic interval. Wireline log correlation with higher resolution depositional sequences are not sufficiently consistent to be used with accuracy. However, there is a consistent relationship observed between the fourth-order sequences and intervals that have the highest laboratory measured porosity and permeability. Where both the measured porosity and permeability are relatively high, these interval correlate with the top of the fourth order sequences. Additionally, this correlation is observed to be most consistent

within the regressive phase of preserved deposition both on the second- and third-order scale. Although there are some fourth-order sequences within each of the five core used in the study that defy this relationship, the consistency of this relationship within each of the study areas indicates this type of observation could be used as a first-order approximation to identify intervals worthy of closer analysis of other key reservoir properties (TOC, %water, %oil, brittleness, etc…).

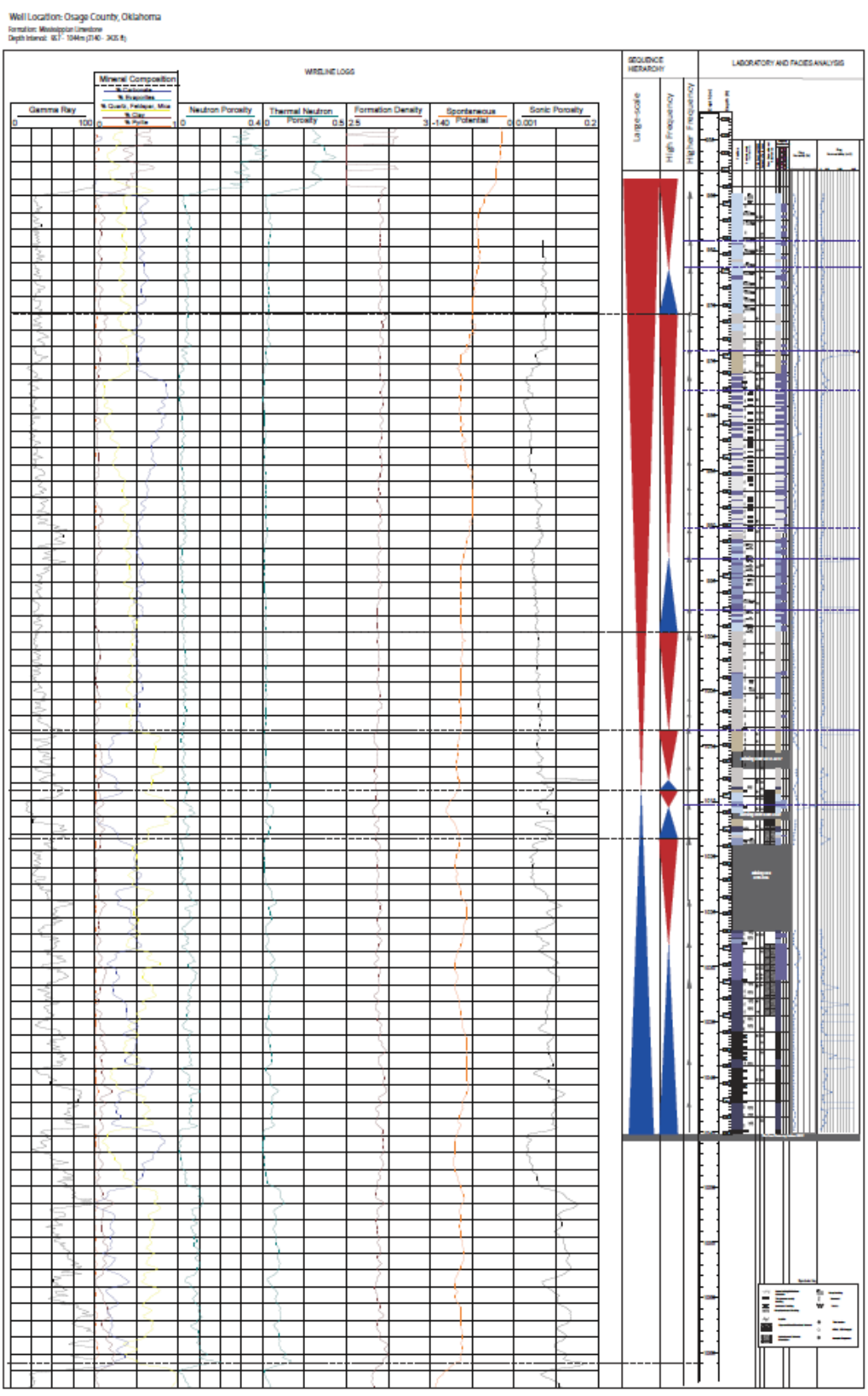
Well Location: Osage County, Oklahoma
WIRELINE LOGS
Mineral Composition
Gamma Ray
Neutron Porosity
Thermal Neutron Porosity
Formation Density
Spontaneous Potential
Sonic Porosity
SEQUENCE HIERARCHY
Large-scale
High Frequency
Higher Frequency
LABORATORY AND FACIES ANALYSIS

(a)

(b)

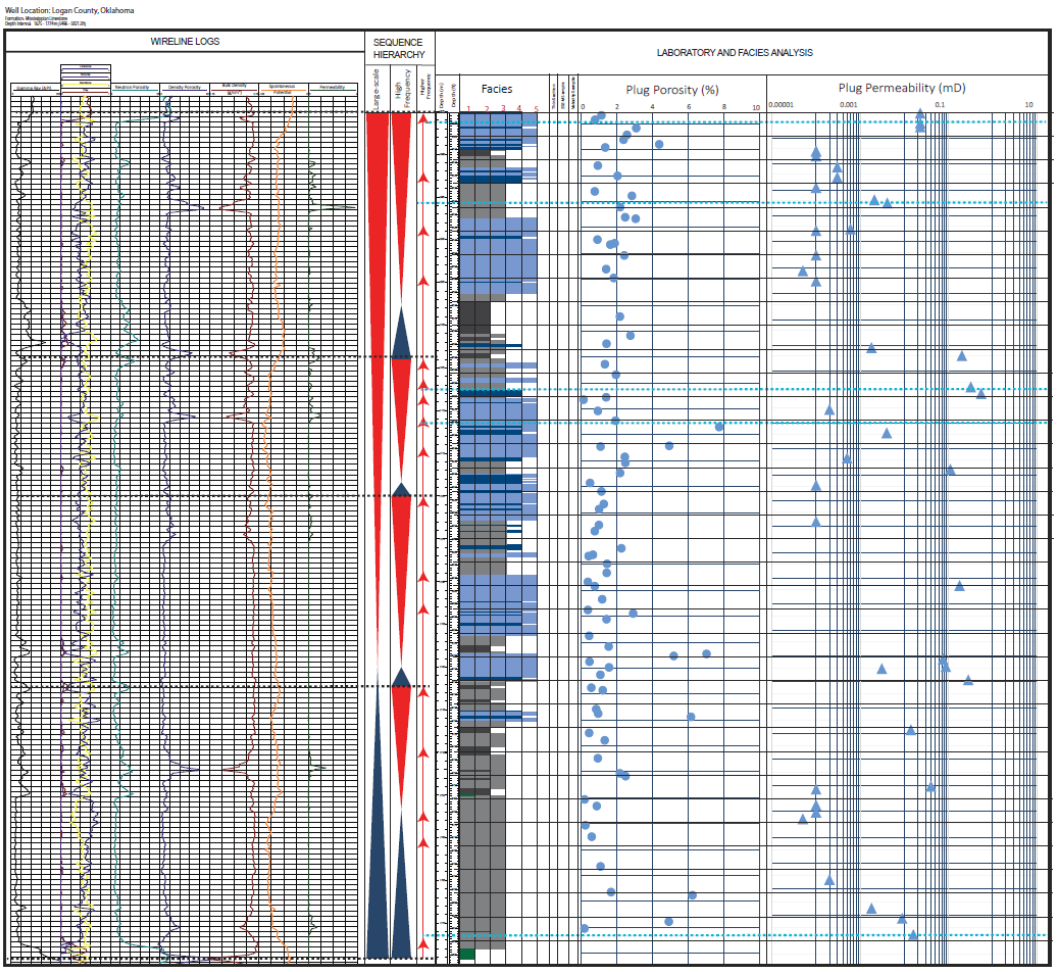
Well Location: Logan County, Oklahoma
WIRELINE LOGS
SEQUENCE HIERARCHY
LABORATORY AND FACIES ANALYSIS
Facies
Plug Porosity (%)
Plug Permeability (mD)

(c)

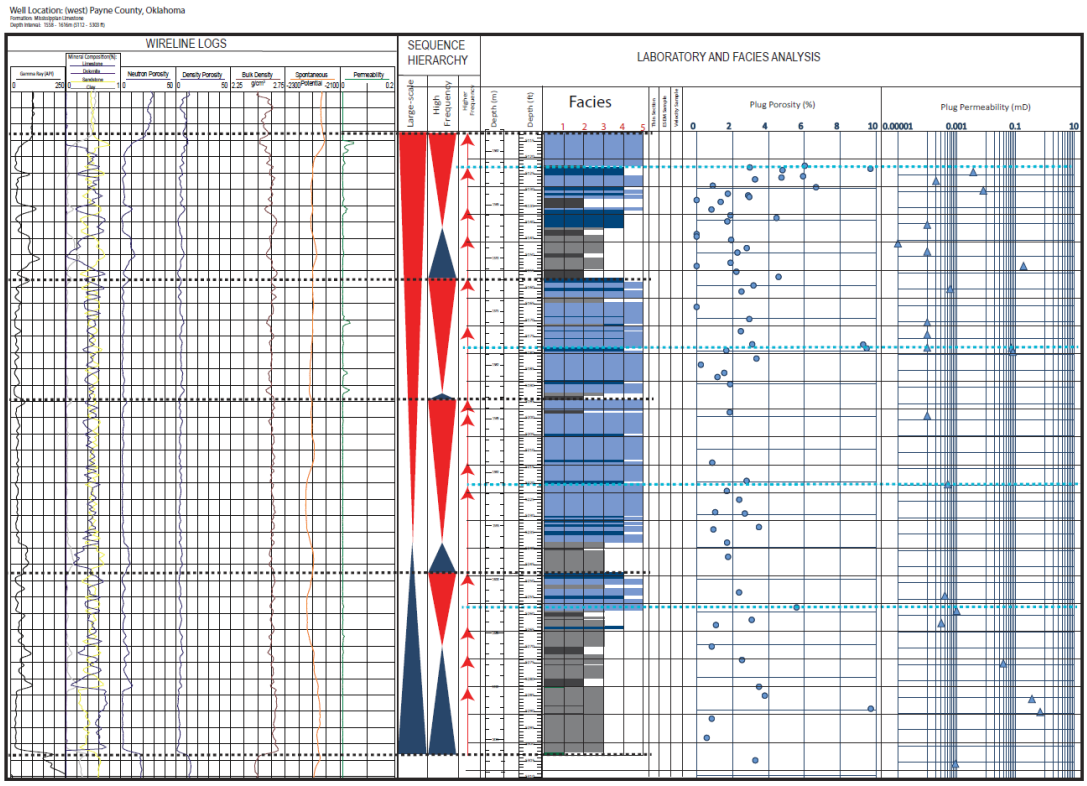
Well Location: (west) Payne County, Oklahoma
WIRELINE LOGS
SEQUENCE HIERARCHY
LABORATORY AND FACIES ANALYSIS
Facies
Plug Porosity (%)
Plug Permeability (mD)

(d)

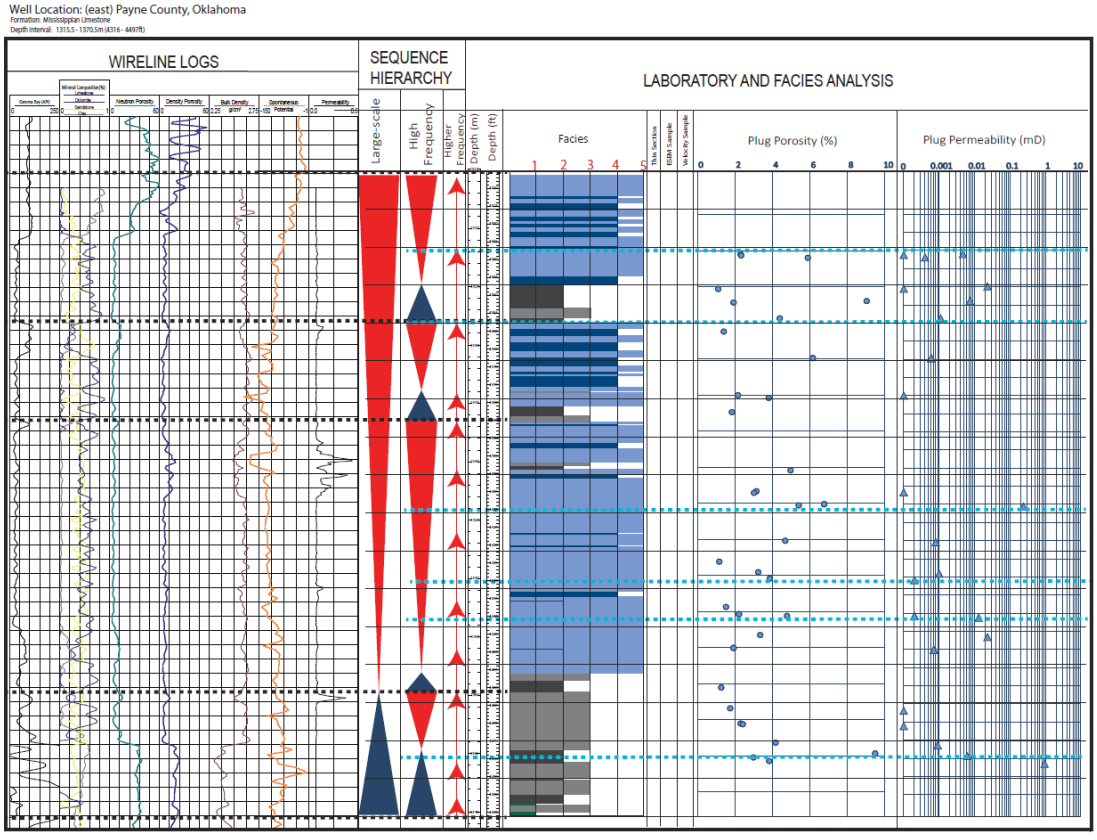
Well Location: (east) Payne County, Oklahoma
WIRELINE LOGS
SEQUENCE HIERARCHY
LABORATORY AND FACIES ANALYSIS
Facies
Plug Porosity (%)
Plug Permeability (mD)

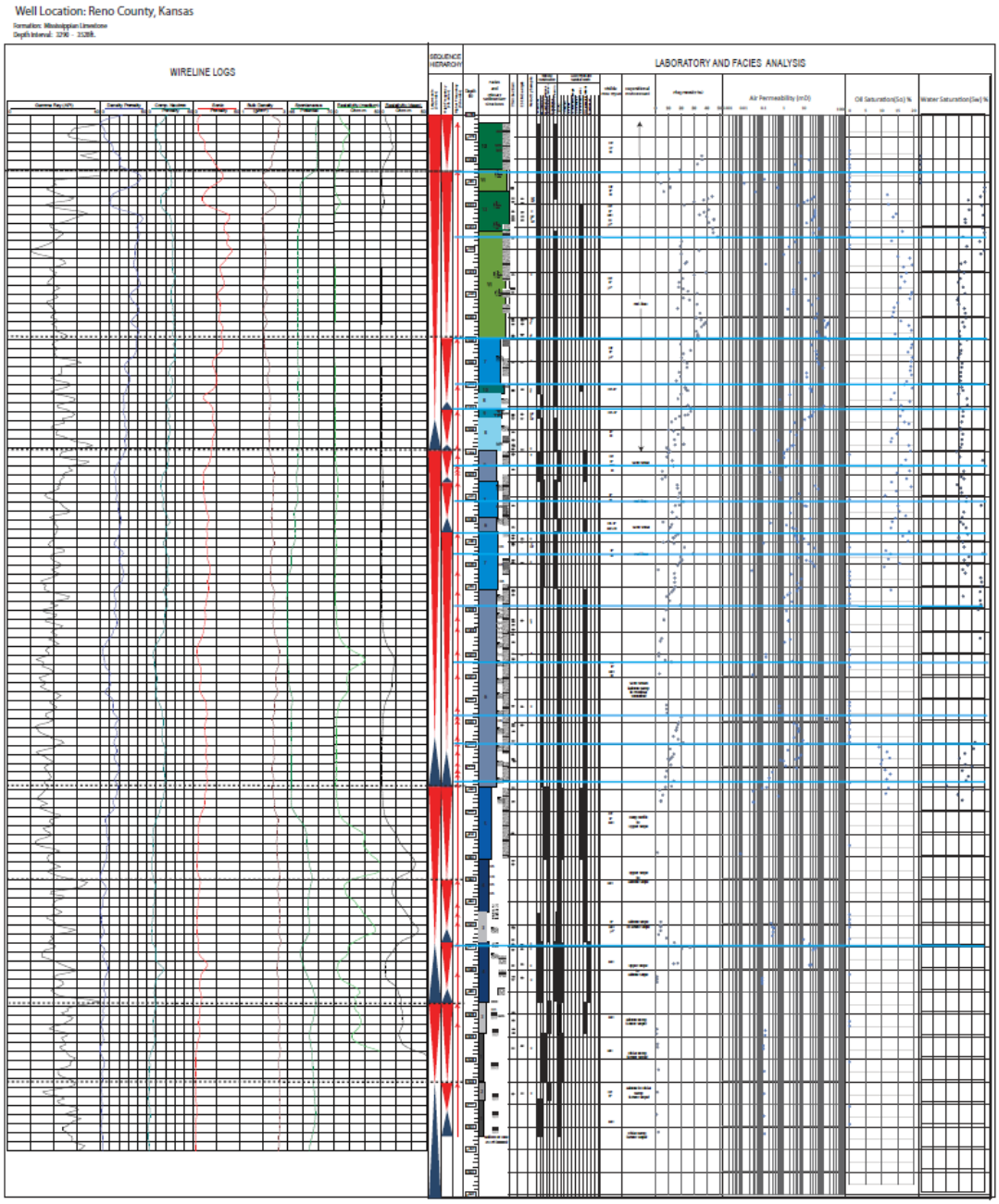

(e)

Figure V-*7a,b,c,d,e: Highlighted by the dashed black lines, the depositionally defined "third order" sequences are shown to correlate approximately with the gamma ray log response for each of the cores within the research. Additionally, highlighted by the dashed blue lines, there is an approximate correlation between the uppermost portion of the "fourth order" sequences and the intervals with the highest porosity and permeability which are consistently within the regressive depositional phases of system. One core, from Osage County, Oklahoma, shows a correlation between relatively high porosity and permeability within the transgressive phase of the system. However, this appears to be a secondary relationship that is related to hydrothermal alteration of the lowermost section of the strata. [a – Osage County, Oklahoma; b – Logan*

County, Oklahoma; c – Payne County, Oklahoma (west); d – Payne County, Oklahoma (east); e-Reno County, Kansas]

A second pattern was observed in the Osage County, OK core with the most distal depositional facies preserved. In the second order transgressive phase of the interval a moderate correlation exists between intervals with both relatively high porosity and permeability and the top of the fourth order sequences that are within the second- and third-order transgressive phase (Figure V-7a). Because this was only core with this relationship observed to have any consistency within the largest transgressive phase, it is possibly related to specific diagenetic alteration that has occurred in this part of the region, as well as related to observations of hydrothermal brecciation present only within this section of the core.

Mineralogy

The three unconventional cores that represent proximal to distal depositional environments have the greatest detailed mineralogy data. Data for these cores was determined by Weatherford Laboratories using bulk x-ray diffraction with detailed results shown in Table V-3. Examination of the detailed mineral composition, as well as mineralogy inferred from wireline logs for the other two cores highlights the nature of the mixed carbonate-siliciclastic sediment composition during the Mississippian in this part of the North American Mid-Continent region. Some of the variability noted in the mineral composition is a direct consequence of several phases of diagenetic alteration in this region, including alteration to porous and non-porous chert. However, based on observations from thin section analysis, there was also a significant amount of original siliciclastic deposition in some intervals and time periods. With the exception of the alteration to chert or other significant silicification of facies, the percentage of original siliciclastic input varies based on specific facies classification and associated depositional environment.

Both the detailed laboratory measured mineralogy indicates there is up to 15% illite or mixed-layer illite/smectite clay content, and the wireline log data estimates a similar composition of clay mineralogy with some intervals indicating up to 45% clay content. This percentage of clay mineralogy is most likely a representation of the amount of clays within the matrix and not a true a representation of the clay precipitation within the pore space that has been shown to have a qualitative relationship to the measured porosity and permeability (Vanden Berg, 2016). Similarly, the amount of quartz is estimated to be up to 100% from laboratory measured samples, and up to 80% composition from wireline log estimates. This estimated composition similarly does not have a consistently predictable relationship with relatively high porosity and permeability even though there is a qualitative relationship between quartz or calcite within the pore space and measured porosity and permeability (Vanden Berg, 2016).

Enhanced Predictability via Laboratory Measured Acoustic Response

The acoustic response data were measured for samples representative of primary facies and depositional environments observed within the data set that also had a large variability in the porosity and permeability to identify end-member relationships that could be applied to other carbonate mudrock reservoir data sets. As observed in Figure V-8, the samples have porosity from 0-nearly 50% with associated compressional velocity of 2000 m/sec to 6400 m/sec, and associated shear wave velocity of 1000 m/sec to 5000 m/sec.

Figure V-8: The laboratory measured sonic velocity (acoustic response)data for samples from the Mid-Continent, Mississippian age samples shows a clear inverse relationship between the velocity and porosity for both compressional (Vp) and shear wave (Vs) responses. The relationship between the Vp response and the Wyllie time average equation plotted for values consistent with pure carbonate samples shows a distinct shift in the response for low porosity (<10%) samples. This is due to a difference in the mudrock mineral composition, the complicated micro- to nanoscale pore architecture, and the different type of grain coupling within a carbonate mudrock compared to conventional carbonates with predominantly macro- to mesopores.

As noted in Figure V-8, the Wyllie time average equation is plotted as a reference line for comparison to other data sets. The Wyllie time average equation is plotted using values for calcite for comparison to pure carbonate systems, but could also be shown using values for quartz or clay mineralogy shown in Figure V-9, which also identifies the effect both significant clay and quartz mineralogy within the matrix affect the sonic velocity response.

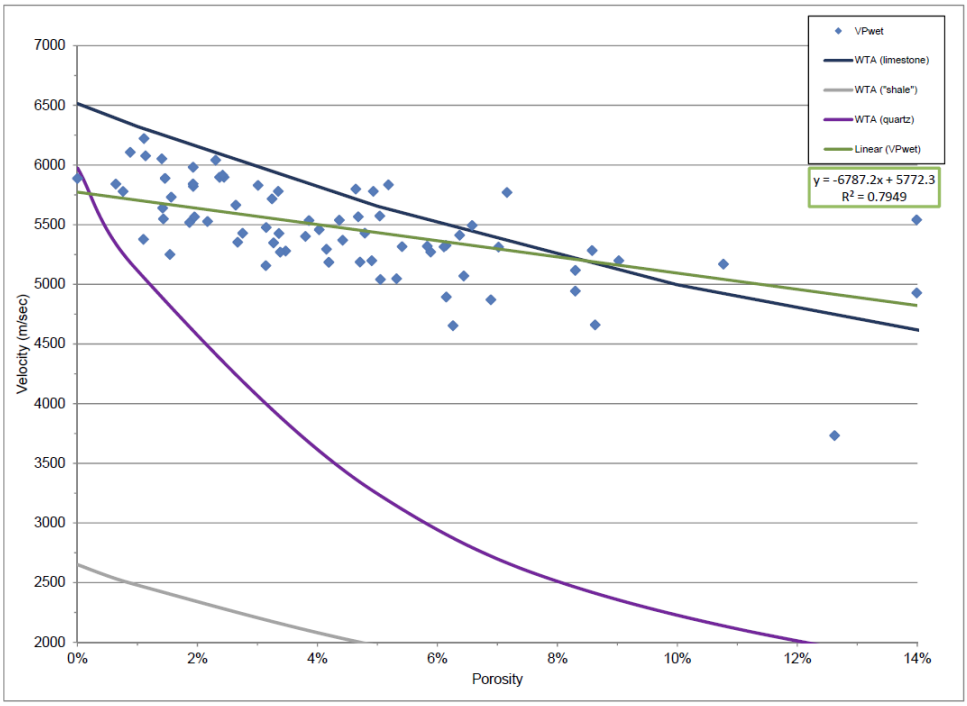

Figure V-9: When the Mississippian data with the low porosity values are plotted in comparison to the Wyllie time average equation plotted using values for quartz or clay ("shale"), it is clear the shift in the relationship is at least partially because of the mixed mineralogy of the data set.

In a pure carbonate system the Wyllie time average equation is both a good approximation of the relationship between sonic velocity and porosity, but also a useful baseline that can be used to qualitatively predict the permeability within the data set (Anselmetti and Eberli 1999). As shown in the data for the Mid-Continent Mississippian stratigraphic interval, the Wyllie time average equation is a reasonable approximation of the relationship between sonic velocity and porosity for samples that have a measured porosity that is greater than 10%. For the samples with a measured porosity that is less than 10%, which is the majority of the data set that is representative of unconventional reservoir facies, a different best fit line needs to be identified. A data specific relationship can be defined with reasonable accuracy (R^2= 0.79) using a simple linear relationship. This best-fit line is necessary to identify to help relate scatter in the velocity-porosity relationship to permeability.

DISCUSSION OF RESULTS

Facies Analysis and Sequence Stratigraphic Framework

As noted in the introduction, the five cores were chosen to be included in this research for several reasons including the variety of facies represented that provide insight into possible depositional environments preserved within the North American Mid-Continent Mississippian age stratigraphic section (Figure V-3). Facies from the Osage County, Oklahoma core are primary representative of a distal ramp environment, or a highly restricted, low-energy environment in the inner to outer ramp area. Facies preserved in the cores from Logan and Payne Counties, Oklahoma are primarily representative of a middle ramp to inner ramp environment and are also oriented along the paleo-strike. Facies preserved in the core from Reno County, Kansas are primarily representative of a proximal outer ramp to shoreline and peri-tidal depositional environments. Understanding how the sequence stratigraphic framework varies in each area and how this correlates to variability in mineral composition, pore architecture, and correlation to wireline log responses, are all key observations that can potentially provide insight into predicting key reservoir intervals within the oil and gas play, and can also provide insight into the application to other similar reservoir systems.

A comparison of the sequence stratigraphic framework from the three areas highlights the potential depositional variability within the system but also indicates the sequence stratigraphic framework fundamentally has a high degree of similarity within the region. There is a consistent correlation observed in each core between the relative 3rd order sequences and the gamma ray log signature indicates this is a useful tool for a first-order approximation of the number and thickness of these units. As shown with the three cores from Logan and Payne County, OK that are within relatively close lateral proximity, and are also located along paleodepositional strike, the third-order sequence can also be used to identify localized patterns

in deposition and associated local geometric patterns of deposition (Figure V-10). Additionally, a similar pattern exists in each core that can be used to predict intervals with the t highest porosity and permeability within the N.A. Mid-continent Mississippian section. As shown in Figure V-7a,b,c,d,e, at each interval where there is a relatively high measurement of both porosity and permeability, this interval corresponds to the highest level of depositional hierarchy identified from facies analysis, which occasionally also correlates to an increased reading from the wireline logs. Additionally, these intervals are typically at the top of the fourth-order sequences that are within the regressive phase of both the third-order and second-order depositional sequences. Although there are exceptions to this observation, the general observation can be used as an initial estimate of where the highest porosity and permeability intervals are located with additional laboratory measurements used to confirm the feasibility of use for either extraction of fluids or gasses present, or for the injection of fluids or gasses.

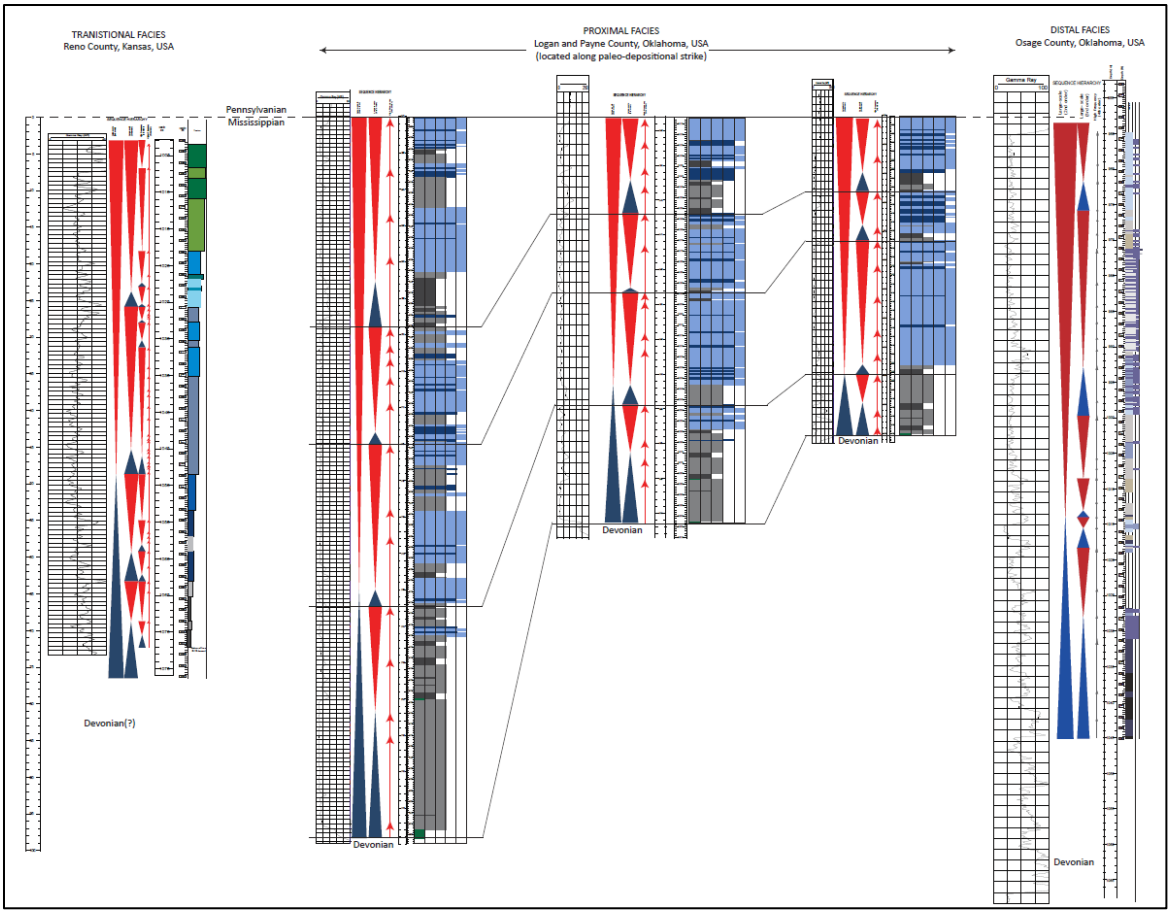

Figure V-10: The similarity observed in the depositionally defined sequence stratigraphic framework provides support for confidence in correlation between closely spaced well locations. As shown in the figure above, correlations between the "third order" sequences for the three cores located along depositional strike in Logan and Payne Counties, Oklahoma, can be used with confidence to provide enhanced predictability of stratigraphic intervals with the highest porosity and permeability within the Mississippian stratigraphic interval.

Comparison to Modern Depositional Environments

The assumptions related to the geometry of the depositional system observed in the five cores used in this study is consistent with other recent research using date from this area and time period (e.g.: Price, 2015; LeBlanc, 2015; Childress, 2015; Bertallot, 2015; Doll, 2015) as well as previously published research that describes typical depositional environments, geometry of the deposits as related to fundamental albeit generalized bathymetry features, and potential diagenetic alterations. The North American Mid-Continent area in the Mississippian Period is an example of a low-declivity ramp system that abuts an actively subsiding foreland

basin created by regional tectonism. As noted by Burchette and Wright (1992) in their analysis of carbonate ramp depositional systems and how the authors are unique and similar to other carbonate depositional system, they highlight several key potential depositional features that are possible, and unique, to a ramp environment due to the natural tendency to develop into flat-topped depositional environments. For example, shoal deposits in a ramp setting have a tendency to form "sheet-like grainstone units" that "migrate or prograde rapidly" as linear belts that parallel a distal foreland basin depocenter. Within this setting sedimentation that has been isolated by foredeep areas are noted to typically be absent of siliciclastics due to very low quantities of terrigenous sediment able to be transported to these locations. Another generic depositional feature that is applicable and observed in the current data set is the observation that carbonate ramps associated with foreland basins, as with the Ouchita Orogeny and resultant series of foreland basins that includes the Oklahoma Anadarko and Arkoma Basins (Figure V-2), are often subject to repetitive episodes of uplift and drowning. Some of this uplift creates complicated karsted unconformities within the middle and inner ramp areas that are only locally present. With a ramp that has a very low declivity slope the inner ramp areas can be several hundreds of kilometers along strike which can potentially further complicate the depositional and diagenetic history through local tectonism and differential rates in both carbonate and terrigenous sediment supplies.

As noted in the facies descriptions with interpreted depositional environments, a low-declivity carbonate ramp or distally steepened carbonate ramp adjacent to a foreland basin is best described through divisions generically termed the inner, middle and outer ramp area (Figure V-3). Loosely defined, the carbonate ramp is gently sloping with an overall slope of less than 1^{o} that can locally be significantly steeper. The inner ramp includes deposition from the upper shoreface (beach, lagoons) and fair weather wave base where there is nearly constant

wave activity that has a lasting effect on deposition and sedimentologic features. The middle ramp extends between the fair weather wave base to normal storm wave base with potentially significant variability in the water depths and frequent re-working of sediment by larger storm waves. The outer ramp is defined as the area below normal storm wave base where there is little to no storm deposition and has a significant amount of mud/clay sedimentation. A slight modification to these classically defined areas includes observations from the Florida shelf and specifically Florida Bay where areas close to the shoreline have a greater amount of eolian deposited quartz, and are likely to have low-energy depositional areas with a high percentage of very fine grain silt, clay and carbonate mud sedimentation in areas where water circulation is restricted due to local changes in bathymetry due to the location of mud banks or restriction from islands located in a windward direction (Harris et al. 1985).

Facies from an additional geometrically defined slope environment located between the outer ramp and the basin in distally steepened ramps are also observed is several ancient systems (Burchette and Wright 1992). This type of depositional environment can occur in several types of sedimentary basins, but are largest and most common "where subsidence is flexural and slow and gradients are slight over large areas", such as the North American Mid-Continent area during the Mississippian Period. Also similar to what is observed in the study areas are observations that diagenesis on a carbonate ramp system is often significantly different from what occurs on flat-topped carbonate platforms and steep-slope depositional environments. Observations of different carbonate ramps systems provide the conclusion that "early marine cementation is less pronounced and seawater dolomitization driven by processes such as Kohout convection is absent." Also potentially significant is the observation that due to the low declivity slope in a ramp system, "the meteoric zone may extend for significant distances offshore so that mixing zone dolomitization and leaching are important processes"

observed in diagenesis. Several other observations from Burchette and Wright (1992) are consistent regarding deposition including the potential for peritidal sediments to be microbially laminated and extend for significant distances, as inferred from thickness preserved in the transitional core.

Modern Depositional Analogs

Comparing ancient deposits to modern depositional environments is a valuable practice to help conceptualize the potential spatial distribution and geometry of identified reservoir facies during a single time slice (Grammer et al., 2004). A modern analog that seem to be most applicable to the three different parts of the study area from most distal to most proximal deposition are is the Arabian-Persian Gulf where carbonate deposition can be observed in an arid environment close to the equator, on an attached gently sloping ramp system. A comparison between the observations from core and this depositional system should provide useful perspective related to the potential 3-D facies distribution and heterogeneity in the subsurface. Although the current paleodepositional models (Lane and Dekyser 1980, Childress 2015) are useful, they do not highlight the potential affects that can result from bathymetric changes within a basin or region, and are also too generalized to be used for predictions of reservoir units.

The Arabian - Persian Gulf is a northwest-southeast trending body of water that is bordered by Oman, the United Arab Emirates (USE), Qatar, and Saudi Arabia to the south and southwest, and Kuwait, Iraq, and Iran to the northwest and north. The Arabian - Persian Gulf carbonate ramp is part of the gently sloping Saudi Arabian shield where water depths range from largely exposed sabkhas to depths greater than 80m (260ft) in the Zagros Mountain foredeep in Iran (Wilkinson and Drummond 2004). Holocene sediments have accumulated over an area that is 500km (310 miles) long and up to 60km (37 miles) wide (Alsharhan and Kendall,

2003). Sedimentation in the Arabian - Persian Gulf is believed to be controlled by a number of factors including an arid climate, wave energy, orientation with respect to NW prevailing winds, and offshore barriers (Alsharhan and Kendall, 2003). General facies types include supratidal sabkha deposits, various types of bioclastic carbonate sands composed of skeletal fragments, peloids, and ooids, muddy carbonate sands, and carbonate mud (Figure V-11) (Alsharhan and Kendall, 2003; Wilkinson and Drummond 2004). Bioclastic and oolitic sands are deposited in high-energy settings located predominantly on the southern margin of the Arabian coast (Alsharhan and Kendall, 2003). These bioclastic sediments are found as deep as 20m, suggesting that storm wave base is at least this deep (Alsharhan and Kendall, 2003). Generalized facies types occur in wide facies belts paralleling the shoreline, with the highest energy facies (carbonate sands) being deposited closest to the shore (Alsharhan and Kendall, 2003).

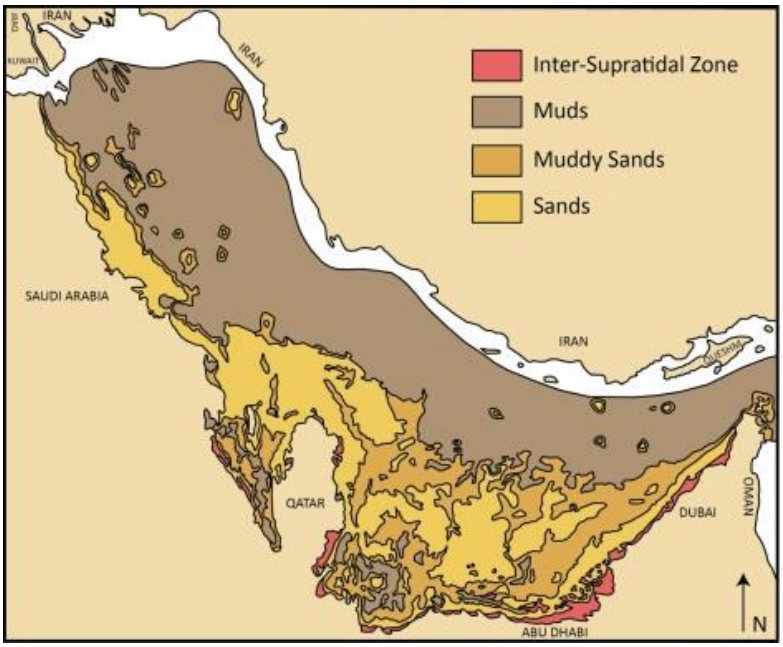

Figure V-11: Deposition in the Arabian-Persian Gulf is one modern analogue to Missippian age deposition in the North American mid-continent region. Deposition in the Arabian-Persian Gulf occurs on an attached ramp system with significant variability in facies deposited in relatively deep water transitioning to shoreline, tidal flat and restricted tidal flat lagoon environments. The facies map shown above identified general strike elongate trends that mirror the shoreline based on water depth. Facies within this modern system are generically classified, from deepest

water (brown) to most shallow water depth (yellow): carbonate mud, muddy carbonate sand and mud, bioclatic carbonate sand, and peloidal and skeletal packstones to grainstones. This facies mosaic is similar to what is observed in core used in this study when placed into generic depositional environments and facies classifications. Image modified from Wagner and Togt,1973.

Comparison of North American Mid-Continent Mississippian age facies to those observed in the Arabian - Persian Gulf allows for a first order interpretation of the spatial distribution of facies and possible water depths at the time of deposition. Similar to the facies observed in the study area, facies being deposited in the Arabian – Persian Gulf are directly related to physical location on the outer, middle or inner ramp area, are spatially distributed in a manner that is a direct result of the water depth, wave base, and wave energy in the depositional environment, in a pattern that is primarily strike elongate, more or less parallel to the coastline but with a high degree of correlation to water depth contours (Gischler and Lomando, 2005). Within the modern depositional system, facies range from low-energy marls or muds, to wackestone, packstones, and grainstones deposited toward higher energy, shallower water, inner ramp environments, and peritidal sediments that are capped by sabkha deposits in the coastal areas in the northern part of the Arabian - Persian Gulf (Gischler and Lomando, 2005; Evans, 1966). Application of the Arabian - Persian Gulf depositional system as an analog, it is possible the peloidal and skeletal packstone and grainstone facies observed in the North American Mid-Continent area during the Mississippian Period were deposited in 1-20m (3-65ft) water depth, are mostly strike elongate but certainly paleo-depositional elongate, and decrease in thickness in a basinward direction. It is also a plausible assumption the carbonate mudstone facies were deposited in water depths that were greater than 20m (65ft), where there is very low energy in the depositional environment, but are also deposited in generally strike elongate geometry that parallels the paleo-shoreline with increasing thickness in a basin-ward direction (Esrafili-Dizaji and Rahimpour-Bonab, 2009).

Where this modern analog has the greatest potential to deviate significantly from depositional patterns in the North American Mid-Continent during the Mississippian Period is the presence of both large and small-scale bathymetric changes due to a tectonically active margin, tectonically active interior within the areas of deposition, and the presence of actively subsiding basins adjacent to the carbonate ramp (Arkoma Basin and Anadarko Basin). Because the North American continent was partially inundated with an epeiric sea, both large and small-scale bathymetric changes would have potentially significant effects on the resultant facies mosaics due to small scale changes to the eustatic sea level enhanced or muted by local subsidence or uplift. Despite these differences, it is clear the distribution of facies observed in the Arabian - Persian Gulf area can easily be extrapolated to areas within the North American Mid-Continent area to provide an additional level of predictability of facies along what is currently understood to be the paleo-strike and paleo-dip directions.

Another modern analog that can provide potential insight into depositional geometries is the Florida Bay where interior muds are deposited in sheltered areas with variable energy and variable siliclastic input. The Florida Bay is another example of a low-declivity shelf that has potentially significant differences in depositional environments and amount of siliciclastic or carbonate deposition depending on which part of the region is being studied. For example, a lateral transect from Florida Bay to the west along the current low-declivity depositional 'shelf' would likely have greater similarity in depositional features than a lateral transect that begins in Florida Bay and moves toward the south or to the east. This is also observed in the variability of depositional environments preserved and observed in the study area where a relatively short lateral distance between Payne and Osage County, OK have significantly different depositional facies preserved that could be related to different time periods within the Mississippian, but

could also be an indication of how quickly the bathymetry changed in some parts of the Mid-Continent region during the Mississippian.

Acoustic Response

In conventional carbonates, the relationship between porosity and acoustic response (sonic velocity) has a clear inverse relationship that can be approximated by the Wyllie time average equation (Figure V-12a) (Anselmetti et al., 1997). Scatter present and deviations from the fundamental relationship between velocity and porosity are related to the dominant pore type (Figure V-12b) (Anselmetti et al., 1997). Understanding how the dominant pore type affects the velocity response in carbonates can potentially provide information that can be used to predict permeability (Anselmetti and Eberli, 1993; Anselmetti et al., 1997; Anselmetti et al., 1998; Anselmetti and Eberli, 1999).

(a) 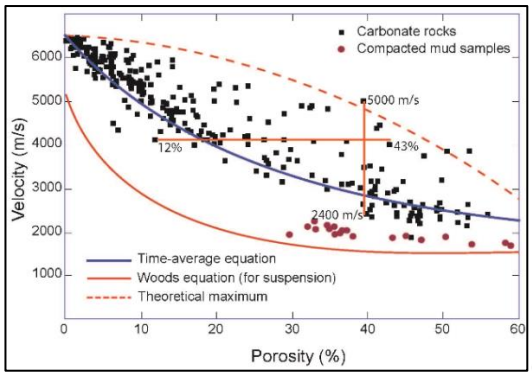

(b) 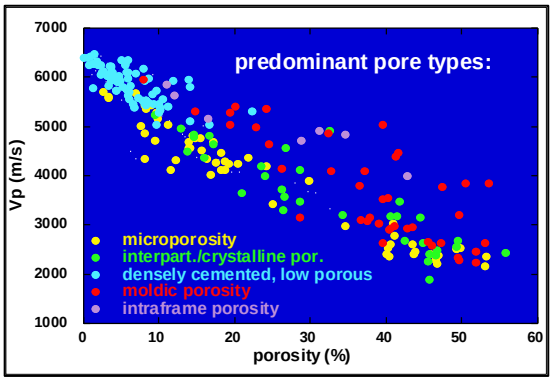

Figure V-12: (a) The relationship between the acoustic response, or velocity, and measured porosity has a predictable inverse relationship. The relationship can be approximated with the Wyllie time average equation with the Woods equation presented as a useful lower boundary to the data. (b)] When the data are plotted based on categories of predominant macropore type, there are data groupings observed that can be applied to enhance the predictability of the velocity-porosity relationship in carbonates that predominantly have macroporosity. Figures used with permission from G. Eberli. (Anselmetti and Eberli 1999; Eberli 2001).

Understanding the relationship between acoustic response and porosity provides the potential for further enhanced predictability of permeability in conventional carbonates (Anselmetti and Eberli, 1999). As shown in this dataset, the acoustic response and porosity is

inversely related similar to what is observed in conventional carbonates (Anselmetti and Eberli, 1999). However, although the relationship has a similar trend, the acoustic response for the carbonate mudrocks is significantly slower for a given porosity than would be expected based on data from conventional carbonate samples and theoretically calculated values. The reason for this is because the samples are from a mixed carbonate – siliciclastic system with a significant amount of quartz and clays in the mineral composition, and the pore architecture is predominately micro- to nano-scale pores. The combination of these two important factors results in a slower wave propagation through the samples due to differences in the elastic properties of the samples as compared to pure carbonates ($CaCO_3$ composition) with predominantly macro- to meso-scale pores. For additional information please reference Vanden Berg, 2016.

SUMMARY

Three areas within the North American Mid-Continent region (Oklahoma and Kansas) with cored intervals from the Mississippian Period stratigraphic section were analyzed to identify the variability in preserved facies, high resolution sequence stratigraphic framework, pore architecture, and relationship to conventional wireline log signatures, conventional laboratory measured porosity and permeability, and laboratory measured sonic velcoity to identify key relationships and predictable trends that provide insight into enhanced prediction of primary reservoir intervals and petrophysical properties (porosity, permeability). Detailed facies analysis of five cores from these areas within the basin highlight the variability in facies deposited within the basin from very fine grained mudstone with little to no skeletal material or bioturbation in outer ramp environments, to wackestone and packstones deposited with moderate to extensive bioturbation and skeletal grains deposited in middle ramp environments, to coarse grained carbonate sand shoals and peri-tidal deposits in the inner ramp and shoreline

environments. Despite the differences in facies preserved in different parts of the basin, a relative high-resolution sequence stratigraphic hierarchy is shown to be applicable throughout the study area. Wireline logs are able to be used as a first-order definition of third-order sequences, and fourth-order sequences identified through detailed facies analysis can be used as a first-order approximation of intervals with relatively high porosity and permeability.

Qualitative analysis revealed a relationship between pores with a significant amount of clay mineral precipitation within the pore space and relatively low laboratory measured porosity and permeability. Conversely, intervals that have the highest laboratory measured porosity and highest permeability correlate with pores that not only have the greatest density as observed in a 2-D cross section, and are relatively larger in total size, but also have little to no clay mineral precipitation in the pore space.

The regression analysis was unable to generate a useful model that could be used to accurately predict key petrophysical parameters which highlights the need to verify the applicability of analytical methodology when used to interpret or define properties in samples with significantly different petrophysical features (e.g.: macro- to mesoporosity vs. micro- to nanoporosity).

The laboratory measured acoustic response shows a clear inverse relationship to porosity. In comparison to pure carbonates ($CaCO_3$) that can be approximated using the Wyllie time average equation, the mixed carbonate- siliciclastic samples have a slower, or lower, response than predicted for pure carbonates with similarly low porosity values. The primary cause of the slower acoustic response is related to the mixed mineralogy with a significant amount of quartz and clay mineralogy, as well as the effect of the micro- to nanoscale poro architecture. Both the non-carbonate mineralogy and the small scale pore architecture combine

to have a significant effect on the elastic properties of the samples which translates into the slower acoustic response in a carbonate mudrock data set.

CONCLUSIONS

Results from this study indicate the following:

The sequence stratigraphic framework identified for three areas within the North American Mid-Continent show the show:

1. Even without biostratigraphic data, a relative hierarchy is a key tool to predict the intervals with the best reservoir quality as determined by measured porosity and permeability values. Within a localized area, the third order sequences can be used for reliable correlations. Variability observed at the fourth order sequence scale can be used with limited reliability to predict the intervals with the highest porosity and permeability at each specific location, but have too much variability in depositional features to correlate between well locations that are not immediately adjacent.
2. Although the facies observed in different parts of the basin vary significantly from one area to another, the basic sequence stratigraphic architecture defined in one area has a high degree of similarity to the depositional architecture in other areas of the basin. Although caution is advised for correlation at a sequence scale more detailed than the 2nd order scale across long distances, the similarity observed can be used as a foundation for defining the sequence stratigraphic hierarchy in unexplored areas of the basin.

The acoustic response measured from core plugs shows:

1. A similar inverse relationship with porosity that can be approximated by the Wyllie time average equation is applicable to samples with predominately conventional types and laboratory measured porosity that is greater than 10%.

2. For unconventional mudrock samples that have predominantly micro- to nanopore sizes in very fine grain sediment and laboratory measured porosity less than 10%, there is a significant shift in the predictable inverse relationship between velocity and porosity. Observations from the data set indicate the Wyllie time average equation remain an applicable relationship, however instead of being utilized as an approximation of the relationship it should be applied as an upper data boundary.

CHAPTER VI

SUMMARY AND CONCLUSIONS

Research Focus #1: 2-D Pore Architecture Characterization of a Carbonate Mudrock Reservoir: Insights from the Mid-Continent "Mississippi Lime"

The first focused research topic was to understand the fundamental geometry of the pore system architecture within a mixed carbonate-siliciclastic mudrock. As shown in chapter/publication 1 titled "2-D Pore Architecture Characterization of a Carbonate Mudrock Reservoir: Insights from the Mid-Continent 'Mississippi Lime'", a specific pore type classification such as intergranular or moldic, does not fully describe the pore system. The predominantly very fine grain size within the reservoir, coupled with a complicated diagenetic history which has altered the internal pore network, has a significant impact on physical factors that affect fluid flow and of therefore any measured porosity or permeability. However, a first-order classification and understanding how the pore architecture in carbonate mudrocks differs from conventional carbonates with visible macroporosity, can aid in understanding conventionally measured petrophysical properties and how these relate to the potential for economic reservoir development. Analysis of the carbonate mudrock pore architecture has led to the following key observations:

1. Digital image analysis confirms that carbonate mudrocks have a complex distribution of pore sizes, even within the micro- to pico-meter scale pores, that have an impact on the relationship between porosity and permeability.
2. To obtain a complete suite of data representative of the characteristics of carbonate mudrock pore architecture, analysis should be completed using a light microscope as well as a scanning electron microscope to encompass data from macro- to picometer-scale pores.
3. Pore shape has a weak relationship with total porosity and total permeability with the greatest correlation observed in Facies 6, a skeletal-peloidal wackestone, and Facies 7, a mudstone-wackestone. The scatter in the data is a result of the complexity within the internal pore architecture.
4. The relationship between porosity and sonic velocity response indicates the relationships observed in conventional carbonates are similar to carbonate mudrocks but not identical in nature. The lower sonic (compressional) velocity response is partly because the complex mudrock pore architecture contained primarily within the micro- to nanometer-scale pore size fraction produces different elastic properties than properties expected for carbonates with macroporosity. Additionally, the diagenetic alterations of the matrix to a relatively high silica content also impact the elastic properties of the reservoir and the resultant sonic velocity response. This difference in elastic properties associated with the macro- to nano-scale pore architecture correlates with a unique, predictable pattern that has a lower sonic (compressional) velocity for a given porosity, as compared to values expected from the Wyllie time average equation. The scatter in the data are still a result of different pore types and permeability that is demonstrated by variations in the range of

resultant sonic (compressional) velocity values for a given porosity as well as a range of porosity values for a given sonic (compressional) velocity response.

5. Micro-fractures may contribute to the overall porosity and permeability where they are able to provide a less tortuous fluid pathway for water and oil located in the picopores and small nanopore size fraction. Fractures that are currently filled with calcite and dolomite cements likely contributed to migration of fluids and placement of currently observed trapped organic material, during early and late burial stages. Although not the focus of this study, it is clear the effect of micro-fracture contribution to porosity and permeability should be considered in additional research relating pore architecture to porosity and permeability in carbonate mudrocks.
6. Each facies identified has a generally positive correlation between porosity and permeability with notable variances that are a result of the dominant pore type and complex internal pore geometry. The highest porosity and permeability values are often associated with the upper portion of the identified "5^{th} order" cycles within the cored interval. Additional predictability of high porosity and permeability intervals might be associated with specific diagenetic processes. On a broad scale, extreme silicification is most prominent in Facies 5 while observed hydrothermal brecciation is primarily within Facies 2. Correlation between type and timing of diagenesis and permeability was beyond the scope of this research.
7. In carbonate mudrocks quantification of the pore architecture and qualitative descriptions of the pore architecture each provide only part of the information necessary to interpret key relationships between the pore architecture, porosity, permeability, facies, and sequence stratigraphy. The combination of qualitative and quantitative data is

recommended to provide a sufficient amount of insight to understand general trends and interpret deviations within these relationships, which in turn allows for enhanced predictability of optimal reservoir conditions and improved horizontal well target selection.

Research Focus #2: A quantitative evaluation of the pore system architecture and acoustic response of micro- to nanometer-scale pores in carbonate mudrocks.

The second focused research topic expands the image data set to include observations from five cores from three locations within the Mid-Continent Mississippian basin. This research integrates qualitative and quantitative observations from representative photographs collected using thin sections with a magnification of 5x-40x, and ion milled samples viewed with an ESEM with a magnification of 100x-1,000,000x to identify useful trends that can applied in other areas of the basin to increase the predictability of key petrophysical properties. Key observations from this expanded image data set include the following:

1. Qualitative analysis of the pore architecture provides the greatest insight to trends in porosity and permeability through identification of pore types present in the data set and the relationship between the micro- to nano-meter scale internal pore space and the mineral precipitation of clays, quartz, or calcite to permeability.
2. Within the micro- to nano-meter scale pore types, pores that had a considerable amount of clay mineral precipitation within the pore space have relatively low measured porosity and permeability. Intervals that have the highest porosity and highest permeability correlate with pores that not only have the greatest spatial density, and are relatively larger in total size, but also have little to no clay mineral precipitation but are often

observed to have the pore walls lined with either calcite or quartz crystals which do not typically sub-divide the flow network.

3. Extensive diagenetic alterations have resulted in porosity and permeability trends that are not facies specific, but do have a unique and predictable relationship to defined sequence stratigraphic architecture.
4. Quantitative analysis using multi-linear regression with inputs from sub-sets of data representative of the four cores with very fine grained facies with predominantly micro- to nano-meter scale porosity, identified several statistically significantly measurements but was unable to generate a useful or applicable model that could accurately predict any of the key petrophysical properties.
5. Quantitative data regarding the pore size and distribution graphed in two unique orientations (pore size vs. perimeter/area (P/A), and pore size distribution) provide valuable insight to pore size controls on potential fluid flow from the natural pore system.
6. A quantitative analysis that is able to mathematically define key relationships that can be used to enhance the predictability of porosity and permeability require additional data. Some common types of data that could increase the predictive potential of the models include: fracture density at the macro- and micro-scale with a semi-quantitative classification scale related to the potential to increase or decrease permeability, NMR response, 3-D CT scans of the pore architecture at meso- and nanoscales, and mercury-injection capillary pressure data (MICP).

Research Focus #3: Testing the applicability of identified relationships between velocity response and permeability in Cenozoic and Mesozoic carbonates to Paleozoic carbonates from multiple depositional basins.

The third goal of the research was to perform a comparative analysis of laboratory measured acoustic response data from samples collected from different basins, and that represent different geologic time periods, to identify the applicability of identified trends and relationships from Cenozoic carbonate samples to older Mesozoic and Paleozoic carbonates. The data used for the comparative analysis are from two Ph.D. theses and two M.Sc. theses that incorporated laboratory measured velocity response into broader research projects. The laboratory measurements from each data set were performed (with one exception) using the same methodology, and the same equipment. The data set that utilized a different machine followed the same analytical procedure and performed the analysis using the same fundamental process and procedure. The primary conclusions based on the comparative analysis are as follows:

9. The Wyllie time average equation is often, but not always, a suitable representation of the relationship between laboratory measured velocity and porosity in both pure carbonate and mixed carbonate depositional systems.
10. Even within a basin, intervals of different ages can potentially have a significantly different relationship between the velocity and porosity. Although it is likely to be an inverse relationship, the specific character should be identified before empirical equations, or equations derived from a single borehole, are used to predict petrophysical properties within a reservoir interval.

11. Where the Wyllie time average equation is not a suitable representation, a best fit line should be applied to the data so the relationship, and potential for enhanced predictability of primary pore type, or permeability, can be determined.
12. In a mixed carbonate-siliciclastic-evaporite system, it is reasonable to expect similar trends and relationships as identified for pure carbonate systems, assuming the major mineralogical composition is a carbonate, or diagenetically altered carbonate.
13. In a mixed carbonate- siliciclastic mudrock system, it is reasonable to expect a similar inverse relationship between the velocity and porosity, but the relationship to permeability may become additionally complicated within a reservoir system if there exists more than one characteristic best-fit data line.
14. Plotting the data in a manner that identifies either or both the dominant pore type, and/or the well location can aid in enhanced predictability by further defining the fundamental velocity – porosity relationship.
15. Limited data indicate an unconventional carbonate mudrock system with predominantly micro- to nano-meter scale porosity has a modified relationship between velocity and porosity. The data presented indicate a unique relationship exists for unconventional, or transitional reservoirs that primarily have low porosity values that are equal to or less than 10%.

<u>Research Focus #4: Integrated reservoir characterization to provide insight into porosity and permeability in a mixed carbonate- siliciclastic reservoir</u>

The fourth focused research topic incorporated the expanded data set to identify predictable relationships between the facies defined sequence stratigraphic framework applicable to each of

the five cores to test whether results can be applied to other areas in the basin to enhance the predictability of relatively higher porosity and permeability intervals within the Mid-Continent Mississippian age reservoir. Additional data incorporated into the analysis included wireline logs (especially the gamma-ray), conventional laboratory measured porosity, permeability, and sonic velocity response, and qualitative integration of the effects from diagenetic alteration events on otherwise predictable trends and relationships.

Key observations from comparative analysis of the facies defined sequence stratigraphic framework for five cores from three areas within the Mid-Continent Mississippian basin include the following:

1. Even without biostratigraphic data, a relative hierarchy is a key tool to predict the intervals with the best reservoir quality as determined by measured porosity and permeability values.
2. Although the facies observed in different parts of the basin vary significantly from one area to another, the basic sequence stratigraphic architecture defined in one area has a high degree of similarity to the depositional architecture in other areas of the basin.

Key observations from the laboratory measured acoustic response shows:

3. The inverse relationship with porosity that has been previously defined for conventional carbonate reservoirs that can be approximated by the Wyllie time average equation is applicable to samples with predominantly macroporosity and laboratory measured porosity that is greater than 10%.
4. For unconventional carbonate mudrock samples, characterized by predominantly micro- to nano-meter scale pore sizes in very fine grained sediment with laboratory measured porosity less than 10%, there is a significant shift to the predictable inverse relationship

between velocity and porosity. Observations from the data set indicate the Wyllie time average equation remains an applicable relationship, however instead of being utilized as a first order approximation of the porosity-permeability relationship, it should be applied as an upper data boundary.

5. For unconventional mudrock samples, the very fine grained matrix with predominately micro- to nano-meter scale pore architecture results in an ambiguous relationship between the velocity – porosity relationship and permeability. As identified with quantitative image analysis, additional data related to the diagenetic history should be incorporated into the analysis to provide additional clarity to this relationship.

REFERENCES

Abouelresh, 2015, Quantitative and Qualitative Evaluation of Micro-Porosity in Qusaiba Hot Shale, Saudi Arabia, Extended Abstract for paper presented at the Unconventional Resources Technology Conference, Denver, Colorado, August 25-27, DOI 10.15530/urtec-2015-2154081.

Alsharhan, A.S., and Kendall, C.G.St.C., 2003, Holocene Coastal Carbonates and Evaporites of the Southern Arabian Gulf and Their Ancient Analogues, Elsevier Earth-Science Reviews v. 61, p. 191-243.

Andrews, J. E., 1991, Geochemical indicators of depositional and early diagenetic facies in Holocene carbonate muds, and their preservation potential during stabilization: Chemical Geology, v. 93, p. 267–289.

Anselmetti, Flavio S., and Eberli, Gregor P., 1993, Controls on Sonic Velocity in Carbonates, Pure and Applied Geophysics, v141, p. 287-323. DOI:

Anselmetti,F.S., G.A. von Salis, K.J. Cunninghan, G.P. Eberli, 1997, Acoustic properties of Neogene carbonates and siliciclastics from the subsurface of the Florida Keys: implications for seismic reflectivity, Marine Geology, v. 144, p. 9-31.

Anselmetti, Flavio S., Stefan Luthi, and Eberli, Gregor P.,1998, Quantitative characterization of Carbonate Pore Systems by Digital Image Analysis, AAPG Bulletin, V. 82, pg. 1815-1836.

Anselmetti, Flavio S., and Eberli, Gregor P., 1999, The velocity-deviation log: a tool to predict type and permeability trends in carbonate drill holes from sonic and porosity or density logs, AAPG Bulletin, V. 83, pg.450-466.

Anselmetti, Flavio S., and Gregor P. Eberli, 2001, Sonic velocity in carbonates- a combined product of depositional lithology and diagenetic alterations, p. 192 – 216 *in* SEPM Special Publication No. 70: Subsurface Geology of a Prograding Carbonate Platform Margin, Great Bahama Bank: Results of the Bahamas Drilling Project, ed.: Robert N. Ginsburg, 207 pp.

Anselmetti, Flavio S., and Gregor P. Eberli, 2001, Sonic velocity in carbonates- a combined product of depositional lithology and diagenetic alterations, p. 192 – 216 *in* SEPM Special Publication No. 70: Subsurface Geology of a Prograding Carbonate Platform Margin, Great Bahama Bank: Results of the Bahamas Drilling Project, ed.: Robert N. Ginsburg, 207 pp.

Archie, G. E., 1952, Classification of carbonate reservoir rocks and petrophysical considerations: AAP Bulletin, v. 36, p. 278–298.

ASTM Standard D6539-13, 2013a, " Standard test method for measurement of the permeability of unsaturated porous materials by flowing air," ASTM International, West Conshohocken, PA, 2013, DOI: 10.1520/D6539, www.astm.org.

ASTM Standard D4525-13e1, 2013b, "Standard test method for measurement of the permeability of unsaturated porous materials by flowing air," ASTM International, West Conshohocken, PA, 2003, DOI: 10.1520/D4525, www.astm.org.

Bachu, Stefan and J.R. Underschultz, 1992, Regional-scale porosity and permability variations, Peace River Arch Area, Alberta, Canada, AAPG Bulletin, V. 76, p. 547-562.

Baechle, G.T., A. Colpaert, G.P. Eberli, and R.J. Weger, 2008a, Modeling sonic velocity in carbonate using thin sections, AAPG Search and Discovery Article #40313.

Baechle, G.T., A. Colpaert, G.P. Eberli, and R.J.Weger, 2008b, Effects of microporosity on sonic velocity in carbonate rocks, The Leading Edge, v.27, p. 1012-1018.

Bathurst, R. G. C., 1970, Problems of lithification of carbonate muds: Proceedings of the Geologists' Association, v. 81, p. 429–440.

Bertalott, Johnny, 2014, Core and log-based stratigraphic framework of the Mississippian limestone in portions of north-central Oklahoma, Master's Thesis, Oklahoma State University, Stillwater, Oklahoma,132 p.

Boardman, D. R., T. L. Thompson, C. Godwin, B. W. Wilhite, and B. T. Morris, 2013a, High-resolution conodont zonation for Kinderhookian (Middle Tournaisian) and Osagean (Upper Tournaisian–Lower Visean) strata of the eastern edge of the Ozark Plateau: North America, v. 64, p. 98–151.

Boardman, D. R., W. L. Watney, J. Victorine, J. Doveton, and T. Thompson, 2013b, Gulf Oil P & M 12 Core Near-Surface Analog to the Mississippian Tripolitic Petroleum Reservoirs in Southern Kansas: Mid-Continent Core Workshop: From Source to Reservoir to Seal, Mid-Continent Section AAPG, Wichita, KS October 13, 2013, p. 191-212.

Burchette, T.P., and V.P. Wright, 1992, Carbonate ramp depositional systems, Sedimentary Geology V.79, p. 3-57.

Buggisch, W., M. M. Joachimski, G. Sevastopulo, and J. R. Morrow, 2008, Mississippian $d^{13}C_{carb}$ and conodont apatite d ^{18}O records: Their relation to the Late Paleozoic Glaciation: Palaeogeography, Palaeoclimatology, Palaeoecology, v. 268, p. 273–292.

Camargo, O., and L. Fons, 1965, Logging considerations for Mississippi Lime evaluations in Oklahoma: The Log Analyst, v. 6, p. 55–61.

Catuneanu, O., 2006, Principles of sequence stratigraphy: Oxford, United Kingdom, Elsevier, 375 p.

Cecil, Blaine C., 2003, The concept of autocyclic and allocyclic controls on sedimentation and stratigraphy, emphasizing the climate variable, p. 13-20. *in* Cecil, Blaine C., and Terence Edgar eds., SEPM Special Publication No. 77: Climate Controls on Stratigraphy, 275pgs.

Childress, Miranda, 2015, High resolution sequence stratigraphic architecture of a Mid-Continent Mississippian outcrop in Southwest Missouri Master's Thesis, Oklahoma State University, Stillwater, Oklahoma, 268p.

Choquette, P. W., and L. C. Pray, 1970, Geologic nomenclature and classification of porosity in sedimentary carbonates: AAPG Bulletin, v. 54, p. 207–250.

Curtis, D. M., and S. C. Champlin, 1959, Depositional environments of Mississippian limestones of Oklahoma: Tulsa Geological Society Digest, University of Oklahoma, p. 90–103.

Dae-Choul, K., H. M. Manghnani, and S. O. Schlanger, 1985, The role of diagenesis in the development of physical properties of deep-sea carbonate sediments: Marine Geology, v. 69, p. 69–91.

Davis, John C., 1986, Statistics and Data Analysis in Geology, Second Edition, John Wiley and Sons, New York, 646p.

Davies, D. K., W. R. Bryant, R. K. Vessell, and P. J. Burkett, 1991, Porosities, permeabilities and microfabrics of Devonian shales, *in* R. H. Bennett, W. R. Bryant, and M. H. Hulbert, eds., Microstructure of fine-grained sediments: From mud to shale: New York, Springer-Verlag, p. 109–119.

Davis, John C., Statistics and Data Analysis in Geology, Second Edition, John Wiley and Sons, New York, 646 pgs.

Dewhurst, D. N., Y. Yang, and A. C. Aplin, 1999, Permeability and fluid flow in natural mudstones, *in* A. C. Aplin, A. J. Fleet, and J. H. S. Macquaker, eds., Muds and mudstones: Physical and fluid flow properties: Geological Society of London: Special Publication 158, p. 23–43.

Dix, G. R., and C. S. Nelson, 2006, Diagenetic potential for lithification of cool-water carbonate shelf mud: Sedimentary Geology, v. 185, p. 41–58.

Doll, Preston, 2015, Determining structural influence on depositional sequences in carbonates using core-calibrated wireline logs: Mississippian carbonates, Midcontinent U.S.A., Master's Thesis, Oklahoma State University, Stillwater, Oklahoma,156 p.

Dorsch, J., 1995, Determination of effective porosity of mudrocks – A feasibility study, Oak Ridge National Laboratory, ORNL/GWPO-019, p. 60.

Dunham, R. J., 1962, Classification of carbonate rocks according to depositional texture: AAPG Memoir 1: Classification of Carbonate Rocks – A Symposium, p. 108–121.

Eberli, Gregor P., Flavio S. Anselmetti, Michael L. Incze, 2003, Factors controlling elastic properties in carbonate sediments and rocks, Society of Exploration Geophysicists: The Leading Edge, V.22, p. 654-660. DOI: 10.1190/1.1599691

Ehrenberg, S.N., P.H. Nadeau, and Ø. Steen, 2009, Petroleum reservoir porosity versus depth: Influence of geological age, AAPG Bulletin, V. 93, p. 1281-1296.

Ehrenberg, S.N., 2007, Whole core versus plugs: scale dependence of porosity and permeability measurements in platform carbonates, AAPG Bulletin: GEohorizons, v.91, p.835-846.

El-Husseiny, Ammar El, and Tiziana Vanorio, 2015, The effect of micrite cement on the acoustic velocity of carbonate rocks, Geophysics, v. 80, pg. L45-L55. DOI: 10.1190/GEO2014-0599.1

Embry, A. F., and J. E. Klovan, 1971, A Late Devonian reef tract on Northeastern Banks Island, N.W.T.: Society of Canadian Society of Petroleum Geologists, v. 19, p. 730–781.

Emery, D., and K. J. Myers, 1996, eds., Sequence stratigraphy: Malden, Massachusetts, Blackwell Publishing, 297 p.

Esrafili-Dizaji, B., and H. Rahimpour-Bonab, 2009 Effects of depositional and diagenetic characteristics on carbonate reservoir quality: a case study from the South Pars gas field in the Persian Gulf, Petroleum Geoscience, V. 15, p.325-344. DOI: 10.1144/1354-079309-817

Evans, G., 1966, The Recent Sedimentary Facies of the Persian Gulf Region, *Philosophical Transactions of the Royal Society of London. Series A, Mathematical and Physical Sciences, v.* 259, No. 1099, A Discussion Concerning the Floor of the Northwest Indian Ocean (Apr. 7, 1966), pp. 291-298. Published by: Royal Society, DOI: http://www.jstor.org/stable/73293

Ewald, T., 2015, Integrated diagenesis and high-resolution sequence stratigraphy of the Mississippian Lime, North-Central Oklahoma, Master's Thesis, Oklahoma State University, Stillwater, Oklahoma, 75 p.

Folk, R. L., 1959, Practical petrographic classification of limestones: AAPG Bulletin, v. 43, p. 1–38.

Folk, R. L., 1962, Spectral subdivision of limestone types, *in* Ham, W. E., ed., Classification of carbonate Rocks-A Symposium: AAPG Memoir 1, p. 62–84.

Fournier, F., and J. Borgomano, 2009, Critical porosity and elastic properties of microporous mixed carbonate – siliciclastic rocks, Geophysics, v. 74, p. E93-E109. DOI: 10.1190/1.3043727

Freund, D., 1992, Ultrasonic compressional and shear velocities in dry clastic rocks as a function of porosity, clay content, and confining pressure, Geophysical Journal International, v. 108, p. 125-135. DOI: 10.1111/j.1365-246X.1992.tb00843.x

Gay, Parker S. Jr., 1999, Strike-Slip, Compressional Thrust-Fold Nature of the Nemaha System in Eastern Kansas and Oklahoma, Kansas Geological Society, Transactions of the 1999 American Association of Petroleum Geologists Midcontinent Section Meeting (Geoscience for the 21st Century), p. 39-50.

Gay, Parker S. Jr., 2003, The Nemaha Trend – A System of Compressional Thrust-Fold, Strike-Slip Structural Features in Kansas and Oklahoma, Part 1, Shale Shaker, July-August, p. 9-49.

Ginsburg, R. N., 1956, Environmental relationships of grain size and constituent particles in some South Florida carbonate sediments: AAPG Bulletin, v. 40, p. 2384–2427.

Gischler, Eberhard, and Anthony Lomando, 2005, Offshore sedimentary facies of a modern carbonate ramp, Kuwait, northwestern Arabian-Persian Gulf, Facies, v.50, p. 443-362. DOI: DOI 10.1007/s10347-004-0027-4.

Gischler, E., S. Dietrich, D. Harris, J. M. Webster, and R. N. Ginsburg, 2013, A comparative study of modern carbonate mud in reefs and carbonate platforms: Mostly biogenic, some precipitated: Sedimentary Geology, v. 292, p. 36–55.

Grammer, M., D. Boardman, J. Puckette, J. Gregg, P. Jaiswal, M. Childress, B. Price, B. Vanden Berg, and S. LeBlanc, 2013, Integrated reservoir characterization of Mississippian-Age Mid-Continent carbonates: AAPG Search and Discovery #30297.

Grammer, G. M., C. M. Crescini, D. F. McNeill, and L. H. Taylor, 1999, Quantifying rates of syndepositional marine cementation in deeper platform environments—New insights into a fundamental process: Journal of Sedimentary Research, v. 69, p. 202–207.

Grammer, G. M., P. M. Harris, and G. P. Eberli, 2004, Integration of modern and outcrop analogs for reservoir modeling – Overview and examples from the Bahamas, *in* G. M. Grammer et al., eds., Integration of outcrop and modern analogs in reservoir modeling: AAPG Memoir 80, p. 1–22.

Grützner, J., and J. Mienert, 1999, Physical property changes as a monitor of pelagic carbonate diagenesis: An empirically derived diagenetic model for Atlantic Ocean basins: AAPG Bulletin, v. 83, p. 1485–1501.

Gutschick, R., and C. A. Sandberg, 1983, Mississippian continental margins of the conterminous United States: SEPM Special Publication 33, p. 79–96.

Han and Batzle 2004; Haq, B. U., and S. R. Schutter, 2008, A chronology of Paleozoic sea-level changes, Science v. 322, p. 64-68.

Handford, C.R., 1986, Facies and bedding sequences in shelf-storm-deposited carbonates Fayetteville shale and Pitkin Limestone (Mississippian), Arkansas: Journal of sedimentary petrology, v. 56, p. 123-137.

Harris, P.M., C.H. Moore, and J.L. Wilson, 1985, Carbonate Platforms *in* in P.M. Harris and C.H. Moore, 1985, Modern and Ancient Shelf Carbonates - Facies, Diagenesis, and Petroleum Potential: The Modern of South Florida and the Bahamas, The Ancient of the U. S. Gulf Coast: Colorado School of Mines Short Course Notes, 172 p. and *in* AAPG Search and Discovery Article #60032, Posted May 15, 2009.

Harris, Paul M., 2009, Depositional Environments of Carbonate Platforms, AAPG Search and Discovery Article #60032

Haq, B. U., and S. R. Schutter, 2008, A chronology of Paleozoic sea-level changes: Science, v. 322, p. 64–68.

Husseiny, Ammar El, and Tiziana Vanorio, 2015, The effect of micrite cement on the acoustic velocity of carbonate rocks, Geophysics, v. 80, pg. L45-L55. DOI: 10.1190/GEO2014-0599.1

Jordan, Clifton F. Jr., and James Lee Wilson, 1994, Carbonate Reservoir Rocks, AAPG Memoir 60: The petroleum system – from source to trap, pgs. 141-158.

Kammer, T. W., and D. L. Matchen, 2008, Evidence for eustasy at the Kinderhookian-Osagean (Mississippian) boundary in the United States: Response to late Tournasian glaciation, *in* C. R. Fielding, T. D. Frank, and J. L. Isbell, eds., Resolving the Late Paleozoic Ice Age in time and space: Geological Society of America Special Paper 441, p. 261–274.

Kump, L. R., and M. A. Arthur, 1999. Interpreting carbon-isotope excursions: Carbonates and organic matter: Chemical Geology, v. 161, p. 181–198.

Kenter, J.A.M.m F.S. Anselmetti, P.H. Kramer, H. Westphal, and M.G.M. VanDamme, 2002, Acoustic properties of "Young" carbonate rocks, ODP Leg 166 and Boreholes Clino and Unda, Western Great Bahama Bank, Journal of Sedimentary Research, v. 72, p.129-137. DOI: 1527-1404/02/072-129

Kittridge, Mark G., 2015, Investigating the influence of mineralogy and pore shape on the velocity of carbonate rocks: Insights from extant global data sets, Interpretation, V.3, N.1, p. SA15-SA31.

Kleipool, L.M., J.J.G. Reijmer, B. Badenas, M. Aurell, 2015, Variations in petrophysical properties along a mixed siliciclastic carbonate ramp (Upper Jurassic, Ricla, NE Spain), Marine and Petroleum Geology, V.68, p. 158-177.

Lak, Razyeh, Ali Mohammadi, Reza Behbahani, and Majid Moeini, 2010, Verification of the Persian Gulf Sea Level changes in Holocene through sedimentary core obtained from sea floor of Bushehr neighboring area, 1st International Applied Geological Congress, Department of Geology, Islamic Azad University – Mashad Branch, Iran, April 26-28, 7 pgs. 2010.

Lane, H. R., 1978, The Burlington Shelf (Mississippian, North-Central United States): Geologica et Palaeontologica, v. 12, p. 165-175.

Lane, H. R., and T. L. De Keyser, 1980, Paleogeography of the late Early Mississippian (Tournasian 3) in the central and southwestern United States, Paleozoic paleogeography of the West-central United States: Rocky Mountain Paleogeography, p. 149–162.

LeBlanc, S., 2014, High resolution sequence stratigraphy and reservoir characterization of the "Mississippian Limestone" in North-Central Oklahoma, Master's Thesis, Oklahoma State University, Stillwater, Oklahoma, 481 p.

LeBlanc, Stephanie L. and Michael Grammer, 2014, High resolution sequence stratigraphy and reservoir characterization of the Mississippian Lime in Northeastern Oklahoma, AAPG Search and Discovery Article #90189, AAP ACE – Houston, April 6-9, 2014.

Lightenberg, J.H., and A.G. Wansink, 2001, Neural network prediction of permeability in the El Garia Formation, Ashtart Oilfield, Offshore Tunisia, Journal of Petroleum Geology, v. 24, p.389-404.

Ling, Kegang, Jun He, Peng Pei, Guoqing Han, and He Zhang, 2013, Determining the permeability of tight rock with gas transient flow, Journal of Natural Gas Science and Engineering, v. 15, p. 1-7. DOI: http://dx.doi.org/10.1016/j.jngse.2013.07.003

Loucks, R. G, and J. F. Sarg, eds., 1993: Carbonate sequence stratigraphy: AAPG Memoir 57, Tulsa, Oklahoma, 545 p.

Loucks, R. G., R. M. Reed, S. C. Ruppel, and D. M. Jarvie, 2009, Morphology, genesis, and distribution of nanometer-scale pores in siliceous mudstones of the Mississippian Barnett Shale: Journal of Sedimentary Research, v. 79, p. 848–861.

Loucks, R.G., R. M. Reed, S.C. Ruppel, and U. Hammes, 2012, Spectrum of pore types and networks in mudrocks and a descriptive classification for matrix-related mudrock pores, AAPG Bulletin, v. 96, p. 1071-1098.

Loucks and Rowe, 2014, Upper Cretaceous Niobrara Chalk in Buck Peak Field, Sand Wash Basin, NW Colorado: Depositional Setting, Lithofacies, and Nanopore Network, Extended Abstract, Extended Abstract for paper presented at the Unconventional Resources Technology Conference, Denver, Colorado, August 25-27, DOI 10.15530/urtec-2014-1918913.

Love, K.M., C. Strohmenger, A. Woronow, and K. Rockenbauch, 1997, Predicting reservoir quality using linear regression models and neural networks, AAPG Memoire 69: Reservoir Quality Prediction in Sandstones and Carbonates, J.A.Kupecz, J. Gluyas, and S. Bloch eds., p. 47-60.

Lucia, F. J., 1983, Petrophysical parameters estimated from visual description of carbonate rocks: a field classification of carbonate pore space: Journal of Petroleum Technology, v. 35, p. 626–637.

Lucia, F. J., 1995, Rock-fabric/petrophysical classification of carbonate pore space for reservoir characterization: AAPG Bulletin, v. 79, p. 1275–1300.

Lucia, F. J., 1999, Carbonate reservoir characterization: New York, Springer-Verlag, 226 p.

MacEachern, J. A., K. L. Bann, M. K. Gingras, and S. G. Pemberton, 2009, eds., Applied Ichnology: SEPM Short Course Notes 52, SEPM, 380 p.

Marion, D.P. 1990. Acoustic, mechanical, and transport properties of sediments and granular materials. PhD dissertation, Stanford University, Palo Alto, California.

Mazzullo, S. J., 2011, Mississippian oil reservoirs in the Southern Midcontinent: New exploration concepts for a mature reservoir objective: AAPG Search and Discovery #10373.

Mazzullo, S. J., B. W. Wilhite, and D. R. Boardman, March 2011, Lithostratigraphic architecture of the Mississippian Reeds Spring Formation (Middle Osagean) in S. W. Missouri, N. W. Arkansas, and N. E. Oklahoma: Outcrop analog of subsurface petroleum reservoirs: Shale Shaker, v. 61, p. 254–269.

Mazzullo, S. J., B. W. Wilhite, and W. Woolsey, 2009, Rhythmic carbonate versus spiculite deposition in Mississippian hydrocarbon reservoirs in the Midcontinent USA: Causative factors and resulting reservoir petrophysical attributes, AAPG Search and Discovery #10209.

McNeill, D.F., K.J. Cunningham, L.A. Guertin, and F.S. ANselmetti, 2005, Depositional Themes of Mixed Carbonate-siliciclastics in the South Florida Neogene: Application to Ancient Deposits, *in* Integration of outcrop and modern analogs in reservoir modeling: AAPG Memoir 80, p. 23-43.

Meckel, L. D., D. G. Smith, and L. A. Wells, 1992, Ouachita foredeep basins: Regional paleogeography and habitat of hydrocarbons, *in* R. W. Macqueen, and D. A. Leckie, eds., Foreland basins and fold belts: Tulsa, Oklahoma: American Association of Petroleum Geologists Memoir 55, p. 427–444.

Melim, Leslie A., Flavio S. Anselmetti, and Gregor P. Eberli, 2001, The Importance of Pore Type on Permeabity in Noegene Carbonates, Great Bahama Bank, SEPM Special Publications No. 70, p. 217-238.

Michaels and Budd, 2014, Pore Systems of the B-Chalk Zone in the Niobrara Formation, Denver-Julesburg Basin, Colorado, Extended Abstract for paper presented at the Unconventional Resources Technology Conference, Denver, Colorado, August 25-27, DOI 10.15530/urtec-2014-1922247.

Miller, M. F., and S. E. Smail, 1997, A semi-quantitative field method for evaluation bioturbation on bedding planes: PALAIOS, v. 12, p. 391–396.

Milliken, K., 2014, A compositional classification for grain assemblages in fine-grained sediments and sedimentary rocks: Journal of Sedimentary Research, v. 84, p. 1185-1199. http://doi.org/10.2110/jsr.2014.92.

Mokhtar, El Amin, Sandra Vega, Ahmed Abed Hassan, and Mariam Al Baloushi, 2012, Porosity and heterogeneity effect on Vp/Vs ratio in carbonate rocks from a reservoir in the Middle East, AAPG Search and Discovery Article #40880.

Moore, David S., and George P. McCabe, 1999, Introduction to the Practice of Statistics, Third Edition, W.H. Freeman and Company, New York, 825pgs.

Morris, B., S. Mazzullo, and B. White, 2013, Potential reef reservoir objectives in the Lower Mississippian St. Joe Group (Kinderhookian to Basal Osagean) in Southern Kansas: AAPG Search and Discovery #50889.

Moshier, Stephen O., 1989, Microporosity in micritic limestones: a review, Sedimentary Geology, V.63, pg. 191-213.

Munsell, C., 1995, Geological Society of America Rock-Color Chart with genuine Munsell color chips, 8th printing.

Nath, Prabir Kumar, Sunil Kumar Singh, Reyad Abu-Taleb, Raghav Prasad, Badruzzaman Khan, Sara Bader, and Awani W. Jaradat, 2012, Characterization and modeling of tight fractured carbonate reservoir of Najmah-Sargelu Formation, Kuwait, AAPG Search and Discovery Article #41059

Nelson, P. H., 2009, Pore throat sizes in sandstones, tight sandstones, and shales: American Association of Petroleum Geologists, Bulletin, v. 93, p. 1–13.

Neto, Irineu A.Lima, Roseane M. Miss ágia, Marco A. Ceia, Nathaly L. Archilha, and Lucas C. Oliveira, 2014, Carbonate pore system evaluation using the velocity-porosity-pressure relationship, digital image analysis, and differential effective medium theory, Journal of Applied Geophysics, v. 110, p. 23-33. DOI: http://dx.doi.org/10.1016/j.jappgeo.2014.08.013

Neto, Irineu A.Lima, Roseane M. Miss ágia, Marco A. Ceia, Nathaly L. Archilha, and Cathy Hollis, 2015, Evaluation of carbonate pore system under texture control for prediction of microporosity aspect ratio and shear wave velocity, Sedimentary Geology, v. 323, p. 43-65. DOI: http://dx.doi.org/10.1016/j.sedgeo.2015.04.011

Noack, Amy Kathryn, 2008, Analysis of Pore architecture and correlation to sonic velocity values in Silurian (Niagaran) reefs of the Michigan Basin, Masters Thesis, Department of Geosciences, Western Michigan University, 153 pgs.

Nooruddin, Hasan A., M. Enamul Hossain, Hasan AL-Yousef, and Taha Okasha, 2014, Comparison of permeability models using mercury injection capillary pressure data on carbonate rock samples, Journal of Petroleum Science and Engineering, v. 121, p. 9-22. DOI: http://dx.doi.org/10.1016/j.petrol.2014.06.032

Norbisrath, Jan H., Gregor P. Eberli, Ben Laurich, Guillaume Desbois, Ralf J. Weger, and Janos L. Urai, 2015, Electrical and fluid flow properties of carbonate microporosity types from multiscale digital image analysis and mercury injection, AAPG Bulletin V. 99, p.2077-2098.

Nur, Amos, Gary Mavko, Jack Dvorkin, and Doron Galmudi, 1998, Critical porosity: A key to relating physical properties to porosity in rocks, The Leading Edge, March 1998, Vol. 17, No. 3 : pp. 357-362. DOI:10.1190/1.1437977

Nur, Amos, Gary Mavko, Jack Dvorkin, and Doron Galmudi, 2008, Critical porosity: a key to relating physical properties to porosity in rocks, The Leading Edge, v. 17, p. 357-362.

Nussbaumer, Christophe Damien Pascal, 1999, Petrophysical and petrographic characterization, mixed carbonate - siliciclastic - evaporite cyclic system, upper Desmoinesian (Middle Pennsylvanian) of the Paradox Basin (SE Utah, U.S.A.), Thèse (doctoral) Université de Genève no 2971. Terre & environnement v. 17, 259 pgs. ISBN: 2940153167, 9782940153169, Call Number QE500.T48 F V.17

Peltonen, Christer, Øyvind Marcussen, Knut Bjørlykke, and Jens Jahren, 2009, Clay mineral diagenesis and quartz cementation in mudstones: The effects of smectite to illite reaction on rock properties, Marine and Petroleum Geology, v. 26, p. 887-898. DOI: 10.1016/j.marpetgeo.2008.01.021

Pittman, E. D., 1992, Artifact porosity in thin sections of sandstones: Journal of Sedimentary Research, v. 62, p. 734–737.

Price, B., 2014, High resolution sequence stratigraphic architecture and reservoir characterization of the Mississippian Burlington/Keokuk Formation, Northwestern Arkansas, Master's Thesis, Oklahoma State University, Stillwater, Oklahoma, 143 p.

Rafavich, F., Kendall, C., and Todd, T. 1984. The relationship between acoustic properties and the petrographic character of carbonate rocks. Geophysics 49 (10): 1622-1636. http://dx.doi.org/10.1190/1.1441570.

Rasolofosaon, Patrick, Nathalie Lucet, and Bernard Zinszner, 2008, Petroacoustics of carbonate reservoir rocks, The Leading Edge, v. 27, p.1034-1039.

Read, J. F., 1995, Depositional sequences, parasequences and systems tracts, *in* Milankovitch sea-level changes, cycles, and reservoirs on carbonate platforms in greenhouse and icehouse worlds: SEPM Special Publication SC35, p. 23–32.

Reed, R. M., and R. G. Loucks, 2007, Imaging nanoscale pores in the Mississippian Barnett Shale of the northern Fort Worth Basin (abs): American Association of Petroleum Geologists, Annual Convention, Abstracts Volume, v. 16, 115 p.

Robin, L., M. Cocks, and T. H. Torsvik, 2011, The Palaeozoic geography of Laurentia and western Laurussia: A stable craton with mobile margins: Earth-Science, v. 106, p. 1–51.

Rogers, S.J., H.C. Chen, D.C.Kopaska-Merkel, and J.H. Fang, 1995, Predicting permeability from porosity using artificial neural networks, AAPG Bulletin, v. 79, p. 1786-1796.

Ross, C. A., and Ross, J. R., 1988, Late Paleozoic Transgressive-Regressive Deposits, in Wilgus, Cheryl K., Hastings, Bruce S., Posamentier, Henry, Wan Wagoner, John, Ross, Charles A., and Kendall, Christopher G. St. C., eds., Sea-Level Changes - An Integrated Approach, SEPM Special Publication No. 42, p. 227-247.

Rouquerol, J., D. Avnir, C. W. Fairbridge, D. H. Everett, J. H. Haynes, N. Pernicone, J. D. F. Sing, and K. K. Unger, 1994, Recommendations for the characterization of porous solids: Pure and Applied Chemistry, v. 66, p. 1739–1758.

Rude, P. D., and R. C. Aller, 1991, Fluorine mobility during early diagenesis of carbonate sediment: AN indicator of mineral transformations, Geochimica et Cosmochimica Acta, v. 55, p. 2491–2509.

Ruppel, S. C., and R. G. Loucks, 2008, Black mudrocks: Lessons and questions from the Mississippian Barnett Shale in the southern Midcontinent: The Sedimentary Record, v. 6, p. 4–8.

Saltzman, M. R., 2002, Carbon and oxygen isotope stratigraphy of the Lower Mississippian (Kinderhookian–early Osagean), western United States: Implications for seawater chemistry and glaciation: Geological Society of America Bulletin, v. 114, p. 96–108.

Saltzman, M. R., E. Groessen, and A. V. Zhuravlev, 2004, Carbon cycle models based on extreme changes in $\delta^{13}C$: An example from the lower Mississippian: Palaeogeography, Palaeoclimatology, Palaeoecology, v. 213, p. 359–377.

Saner, Salih, and Ali Sahin, 1999, Lithological and Zonal Porosity-Permeability Distributions in the Arab-D Reservoir, Uthmaniyah Field, Saudi Arabia, AAPG Bulletin, V. 83, p. 230-243.

Sarkisyan, S.G., 1972, Origin of authigenic clay minerals and their significance in petroleum geology, Sedimentary Geology, v.7, p. 1-22.

Schieber, J., J. B. Southard, P. Kissling, B. Rossman, and R. Ginsburg, 2013, Experimental deposition of carbonate mud from moving suspensions: Importance of flocculation and implications for modern and ancient carbonate mud deposition: Journal of Sedimentary Research, v. 83, p. 1025–1031.

Schlager, W., J. Austin, A. Palmer, P. Comet, A. Droxler, G. P. Eberli, and C. Williams, 1985, The rise and fall of carbonate platforms: Leg 101 of the Ocean Drilling Program: Nature, v. *315*, p. 632–633.

Schlager, W., F. Bourgeois, G. Mackenzie, and J. Smit, 1988, Boreholes at Great Isaac and Site 626 and the history of the Florida Straits: Proceedings of the Ocean Drilling Program, Scientific Results, v. 101, p. 425–437.

Scotese, C. R**.**, A. J. Boucot, and W. S. McKerrow, 1999, Gondwanan palaeogeography and palaeoclimatology: Journal of African Earth Sciences, v. 28, p. 99–114.

Slatt, E. M., and N. R. O'Neal, 2011, Pore types in the Barnett and Woodford gas shale: Contribution to understanding gas storage and migration pathways in fine-grained rocks (abs.): AAPG Search and Discovery Article #80166.

Snedden, J. W., and C. Liu, 2010, A compilation of Phanerozoic sea-level change, coastal onlaps and recommended sequence designations, 2010, AAPG Search and Discovery #40594.

Soil Survey Staff, 1993, Soil Survey Manual, USDA Soil Conservation Service, Agricultural Handbook No.18, U.S. Gov. Print. Office, Washington, D.C., Munsell Soil Color Charts 2009, 2013 Production.

Sondergeld, C. H., R. J. Ambrose, C. S. Rai, and J. Moncrieff, 2010, Microstructural studies of gas shales: Society of Petroleum Engineers Unconventional Gas Conference, Pittsburgh, Pennsylvania, February 23–25, 2010, SPE Paper 131771, 17 p.

Thornton, John E., 2011, Prediction of Petrophysical Properties of Trenton-Black River (Ordovician) Reservoirs by Comparing Pore Architecture and Permeability to Sonic Velocity, Master of Science Thesis, Department of Geosciences, Western Michigan University, 417 pgs.

Thornton, John, and G. Michael Grammer, 2012, Enhanced reservoir characterization and permeability prediction of heterogeneous carbonate reservoirs from sonic velocity and digital image analysis, AAPG Search and Discovery #50689, AAPG Annual Convention and Exhibition, Long Beach, CA, April 22-25, 2012.

Thyne, Geoffrey, Mark Tomasso, David Budd, Sharon Bywater-Reyes, and Brian Reyes, 2011, Characterization of Petrophysical Properties for CO2 Sequestration Models in the Mississippian Madison Group, Moxa Arch-La Barge Platform, Southwestern Wyoming,

AAPG Search and Discovery Article #80182, Adapted from oral presentation at AAPG Rocky Mountain Section meeting, Cheyenne, Wyoming, USA, June 25-29, 2011.

Vail, P. R., R. M. J. Mitchum, R. G. Todd, J. M. Widmier, S. J. Thompson, J. B. Sangree, J. N. Bubb, and W. G. Hatlelid, 1977, Seismic stratigraphy and global changes of sea-level: The American Association of Petroleum Geologists, Memoir 26: Tulsa, The American Association of Petroleum Geologists, p. 49–212.

Vanden Berg, Beth, and G. Michael Grammer, Accepted, Qualitative and Quantitative Characterization of Carbonate Mudrock Pore Architecture: An example from the Mid-Continent "Mississippian" Limestone, AAPG Memoir X: Imaging Unconventional Reservoirs, T. Olson (ed).

Vanden Berg, Beth, 2016, An integrated analysis of carbonate mudrocks and mixed carbonate-siliciclastic reservoirs to define the effects of micro- to nano-scale pore architecture on the ability to predict porosity or permeability, Ph.D. Dissertation, Oklahoma State University, Stillwater, Oklahoma.

Vanorio, Tiziana and Gary Mavko, 2011, Laboratory measurements of the acoustic and transport properties of carbonate rocks and their link with the amount of microcrystalline matrix, Geophysics, V. 76, p. E105-E115. DOI: 10.1190/1.3580632

Verwer, Klaas, Hendrick Braaksma, and Jeroen A.M. Kenter, 2008, Case History: Acoustic properties of carbonates: Effects of rock texture and implications for fluid substitutions, Geophysics, V. 73, p. B51-B65. DOI: http://dx.doi.org/10.1190/1.2831935.1

Verwer, Klaas, Gregor Eberli, Gregor Baechle, and Ralf Weger, 2010, Effect of carbonate pore structure on dynamic shear moduli, Geophysics, V. 75, p. E1-E8. DOI: 10.1190/1.3280225

Wagner, C.W, and Togt, C. Van Der, 1973, Holocene Sediment Types and Their Distribution in the Southern Persian Gulf, In: Purser, Burce H. (ed), The Persian Gulf, Springer-Verlag, Berlin, Heidelberg, New York, p. 123-155.

Wang, Z., Hirsche, W.K., and Sedgwick, G. 1991. Seismic Velocities *In* Carbonate Rocks. Journal of Canadian Petroleum Technology v.30, p. 110-122. DOI: http://dx.doi.org/10.2118/91-02-09.

Watney, W. L., W. J. Guy, and A. P. Byrnes, 2001, Characterization of the Mississippian chat in south-central Kansas: AAPG Bulletin, v. 85, p. 85–113.

Welton, Joann E., 1984, re-printed 2003, SEM Petrology Atlas, AAPG Methods in Exploration Series No. 4, American Association of Petroleum Geologists, Tulsa, Oklahoma, 240pgs.

Weger, R. J., G.P. Eberli, G.T. Baechle, Jose L. Massaferro, and Yue-Feng Sun, 2009, Quantification of pore structure and its effect on sonic velocity and permeability in carbonates, AAPG Bulletin, v. 93, p. 1297-1317.

Wilkinson, Bruce H., and Carl N. Drummond, 2004, Facies mosaics across the Persian Gulf and around Antigua – Stochastic and deterministic products of shallow-water sediment accumulation, Journal of Sedimentary Research (SEPM), V. 74, p. 513-526.

Witzke, B. J., 1990, Paleoclimatic constraints for Paleozoic paleolatitudes of Laurentia and Euramerica, W. S. McKerrow and C. R. Scotese, eds. Paleogeography and biogeography: Geological Society (London) Memoir 12, p. 57-73.

Wold, Jessica, 2008, SEQUENCE STRATIGRAPHY AND 3-D RESERVOIR CHARACTERIZATION OF A SILURIAN (NIAGARAN) REEF - RAY GAS STORAGE FIELD,MACOMB COUNTY,MICHIGAN, Degree of Master of Science, Department of Geosciences Western Michigan University, Kalamazoo, Michigan, December 2008, 121pp.

APPENDICES

Appendix I: EXTENDED ABSTRACT

The primary focus of this research has been to increase the understanding of carbonate mudrocks by providing some of the first insight into the nature of micro- to nano-meter scale pore systems in these types of carbonates. In particular, this study has focused on the pore systems in carbonate mudrocks and their three dimensional architecture, how the pore systems relate to permeability in the reservoirs and how that permeability may be predicted based upon acoustical properties of the rock, as well as how this ties to overarching geological parameters such as the depositional environment and the sequence stratigraphic framework.

Over the last decade unconventional resources, defined by low porosity and low permeability, have taken a prominent place in oil and gas exploration. This change in focus for exploration and reservoir development has created a need to better understand shale and mudrock depositional environments and their reservoir characteristics. Much of the research on shale and mudrock reservoirs has been focused on siliciclastic shale and mudrocks such as the Barnett Shale (Mississippian) in the Fort Worth Basin, and the Utica Shale (Ordovician) in the Appalachian Basin. A fundamental control on reservoir systems and production capabilities is often linked to facies types and their corresponding geometrical attributes derived from interpretation of the primary depositional environments, as well as petrophysical characteristics that are identified through facies analysis of cored intervals at meter-scale down to the micro- and nano-meter scale.

Facies interpretation and development of a high resolution sequence stratigraphic-based depositional architecture in Mississippian-age carbonates from three regions of the Mid-Continent have been integrated with key petrophysical data (porosity and permeability), analysis of the pore system architecture, and acoustic response data to provide insight into primary reservoir controls

and trends that can be successfully applied to other areas of these Mississippian age strata as well as to carbonate mudrocks on a global scale.

Detailed facies analysis indicate deposition occurred on an attached, low-declivity, carbonate ramp, or possibly distally steepened carbonate ramp system. Facies observed in the cores range from very fine grain carbonaceous mudstone, wackestones, and grainstones to near-shore wackestone to packstones capped by a series of peritidal deposits. The fine grained facies have a horizontal porosity that ranges from 0.1 to12% (avg.2.5%) with a correlative permeability range of 0.0001mD to 3.4mD (avg. 0.05mD). Horizontal porosity from coarse grain facies range from 13% to 45% (avg.31%) porosity with a correlative permeability range from 5.92mD to 163mD (avg. 43mD). Each core shows a shallowing upward succession of facies throughout the cored interval, and a similar sequence stratigraphic framework. Within this overall regressive system, the highest porosity and highest permeability intervals are most commonly located within the regressive phase of large-scale sequences. Qualitative analysis shows a relationship between mineral precipitation within the pore space and the measured porosity and permeability in the intervals with predominantly micro- to nano-meter size pores. Where clay minerals (illite/smectite, kaolinite) are observed in the pore space, a significant portion of the area is sub-divided in smaller pores and pore throats. Where either calcite or quartz are precipitated inside the pore space, the crystals grow primarily only along the pore wall. This different growth morphology reduces the overall size of the pore and pore throat but does not sub-divide the pore. Samples that have a significant amount of clay minerals precipitated within the pore space correlate with low porosity, and low permeability. Samples with predominantly calcite or quartz precipitated within the pore space correlate with the relatively higher porosity and permeability values.

Quantitative analysis shows the relationships between measured geometric parameters of the pore systems and how porosity and permeability transforms may differ significantly in carbonate mudrocks with micro- to nano-meter scale porosity (<62µm diam.) compared to conventional carbonate reservoirs with primarily macro-porosity (256-4mm diam.). The complex pore architecture in carbonate mudrocks equates to the inapplicability of standard methods and analyses applied to macropore systems to identify and predict key reservoir properties. A complicated diagenetic and structural over-print within the data set causes additional complications in interpreting trends that are observed consistently within the data set.

Acoustical response (velocity) data are inversely related to porosity, with a clear shift in the relationship as related to the empirical Wyllie time average equation. The shift in this mathematically defined relationship is attributed to the complexity within the micro- to nanopore

architecture and the effects this has on the elastic properties of the samples. A comparison of the velocity – porosity relationship using data from different basins and geological ages shows the inverse relationship is a reasonable expectation, but that caution is suggested before application of the Wyllie time average equation as a baseline to interpret the primary pore type or relative permeability, especially in micro- to nano-scale pore systems. Specific measurements from the reservoir or interval of interest should be used to identify the reservoir specific relationship between velocity and porosity to have greater confidence in the development of proxies to predict permeability from the combination of pore architecture and associated acoustical response.

Appendix II: SUPPLEMENTARY SEM IMAGES FOR 2-D PORE ARCHITECTURE CHARACTERIZATION OF A CARBONATE MUDROCK RESERVOIR: INSIGHTS FROM THE MID-CONTINENT "MISSISSIPPI LIME"

Supplemental SEM images of observed pore architecture in used in data set for a first-order characterization of the pore in a carbonate mudrock reservoir.

Note: not all pores are identified in each image. Images are arranged by order of facies.

Select SEM images that are representative of the samples analyzed in this study have been grouped by facies classification to highlight the complex pore structure at the micro- to nanometer pore scale. The internal pore architecture adds an additional layer of complication to predict permeability due to the precipitation of different clays and minerals within the pore space. Although many of the pores can be generically classified as interparticle or intergranular pores, most are effectively moldic and vuggy in relationship to their connection to other void space and in their relationship to the flow network. The matrix pores, defined within this paper, are observed and common in each facies with a variety of geometric (oval, circular) and non-geometric shapes. Pyrite framboids, also common in several facies, have the least amount of precipitation observed within the structure, but are also observed to have intraparticle pore space that in a two dimensional cross section does not appear to have significant connection to other pore space within the samples.

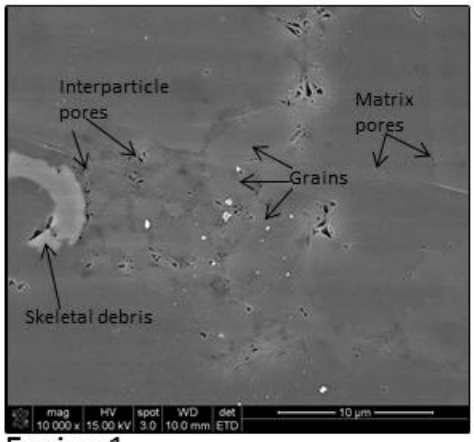

Facies 1

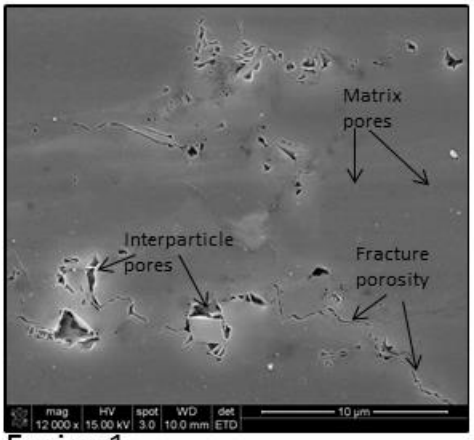

Facies 1

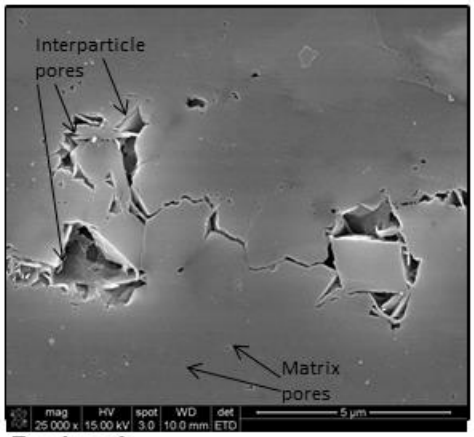

Facies 1

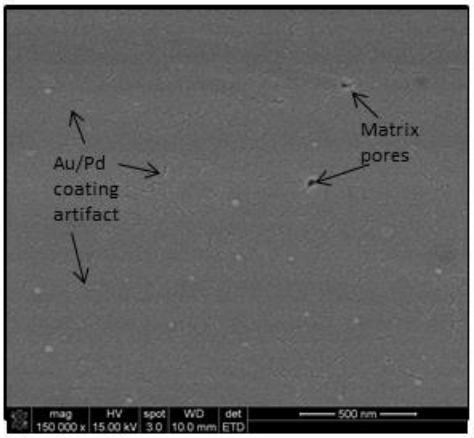

Facies 1

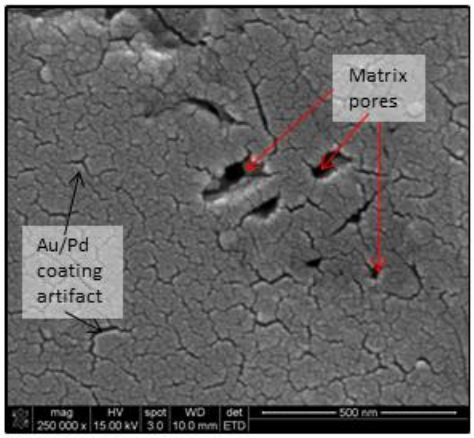

Facies 1

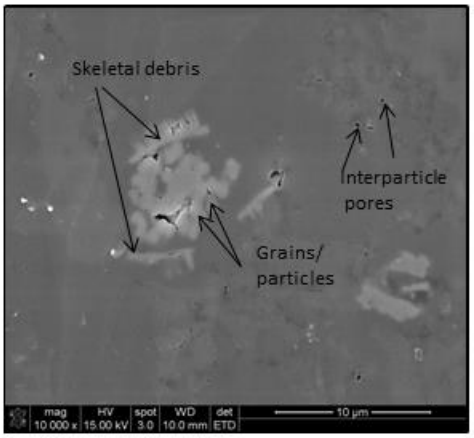

Facies 1

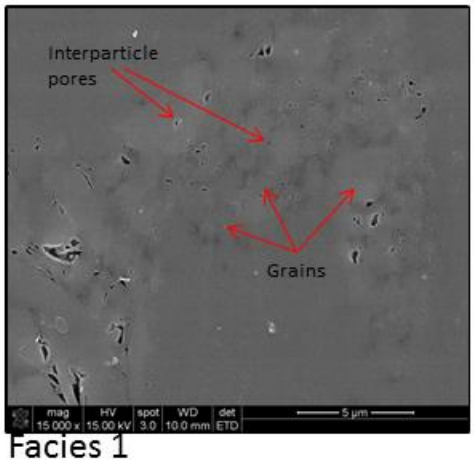

Facies 1

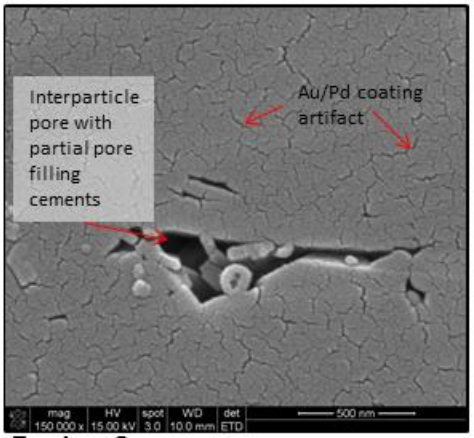

Facies 2

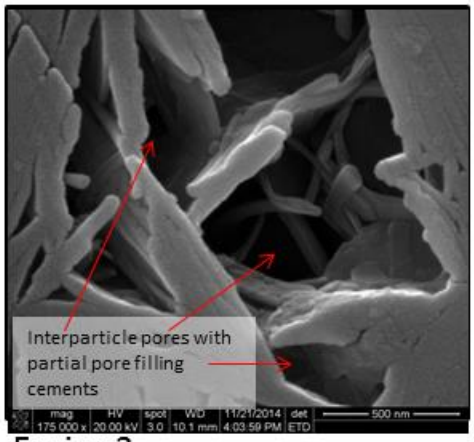

Facies 3

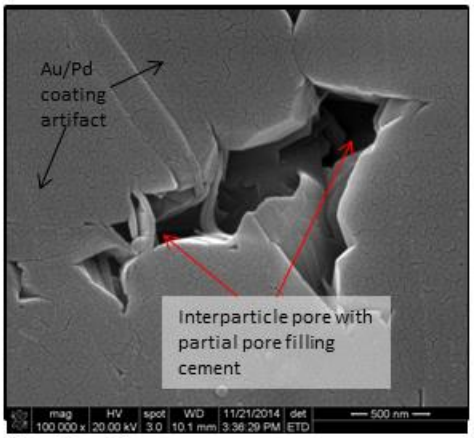

Facies 3

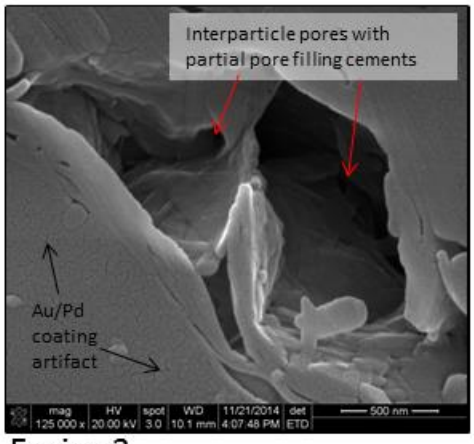

Facies 3

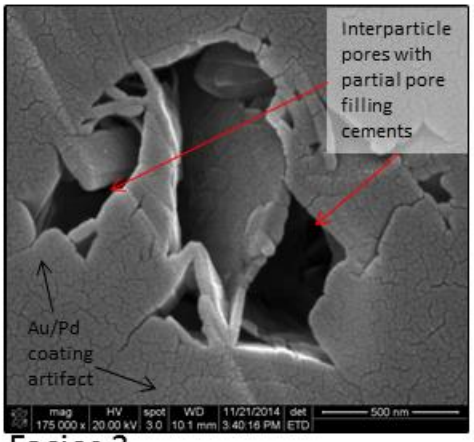

Facies 3

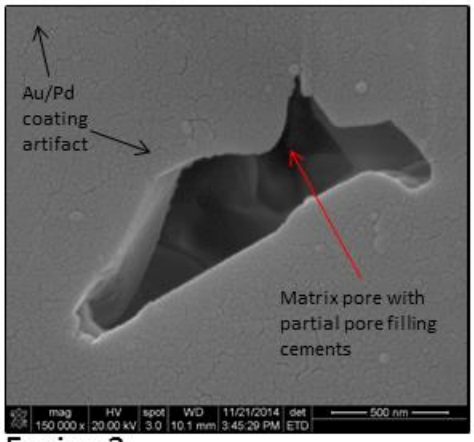

Facies 3

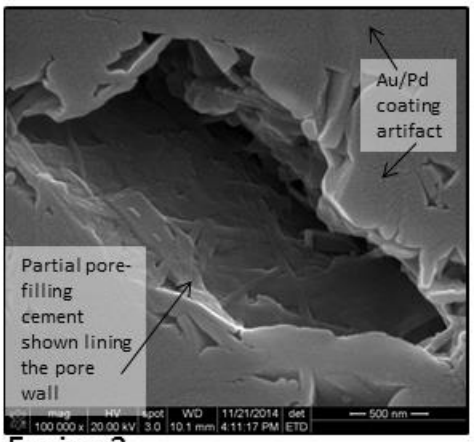

Facies 3

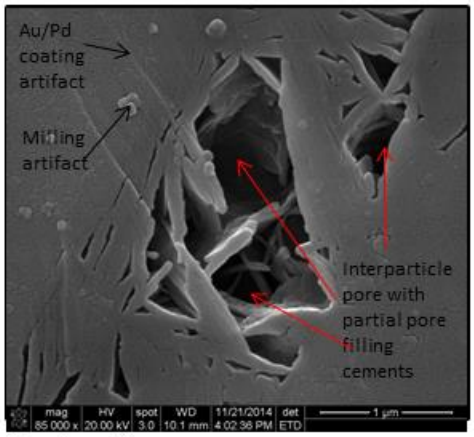

Facies 3

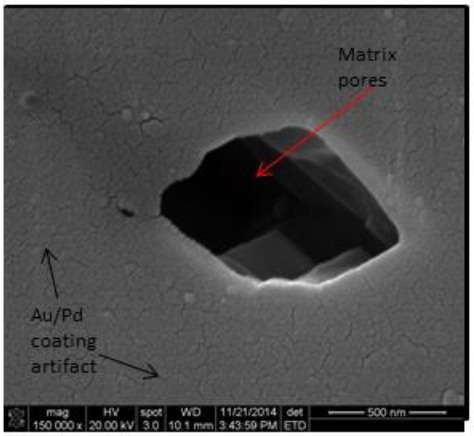

Facies 3

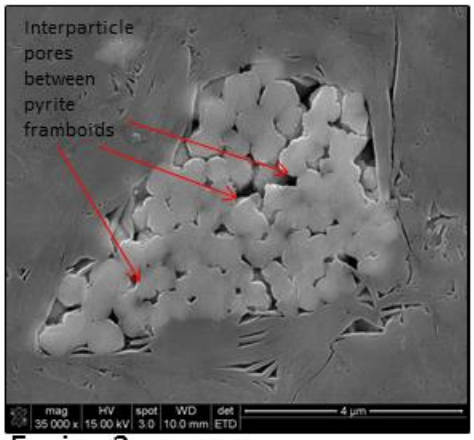

Facies 3

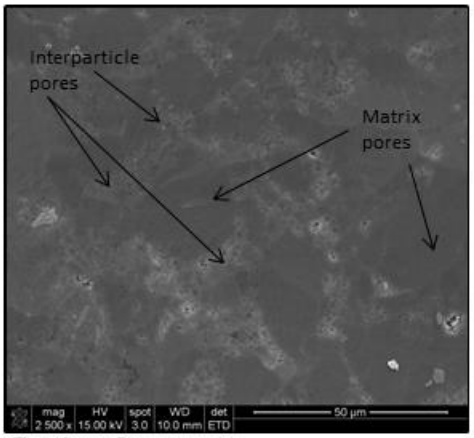

Facies 3

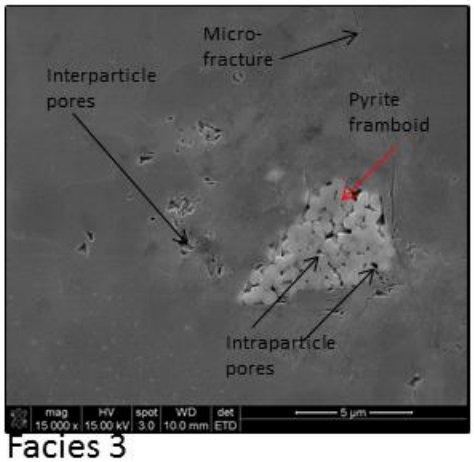

Facies 3

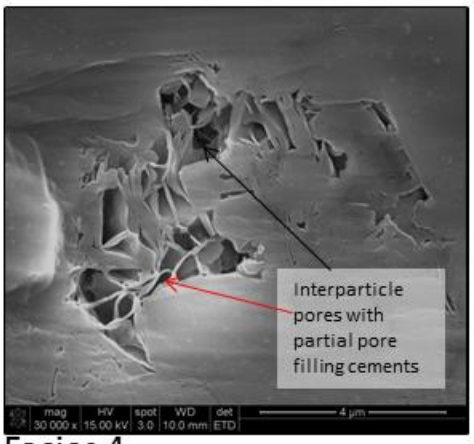

Facies 4

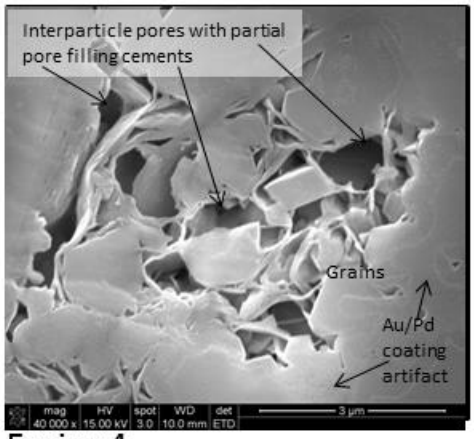

Facies 4

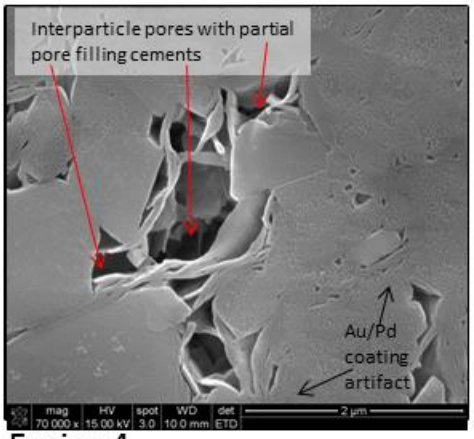

Facies 4

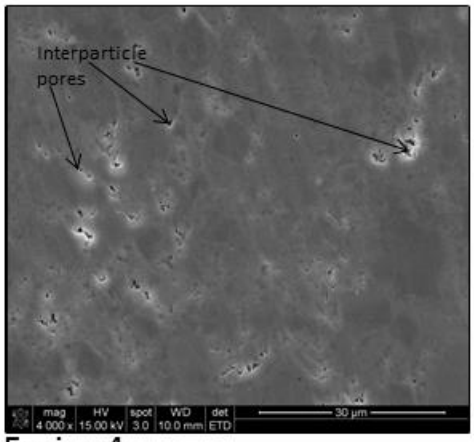

Facies 4

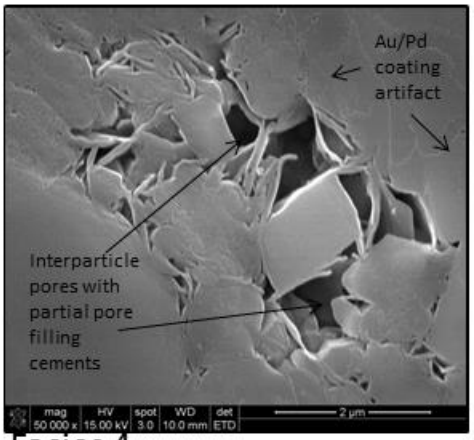

Facies 4

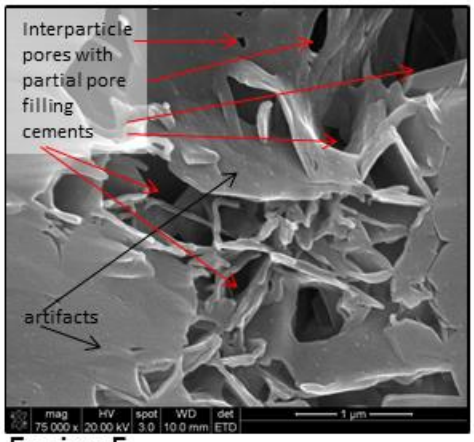

Facies 5

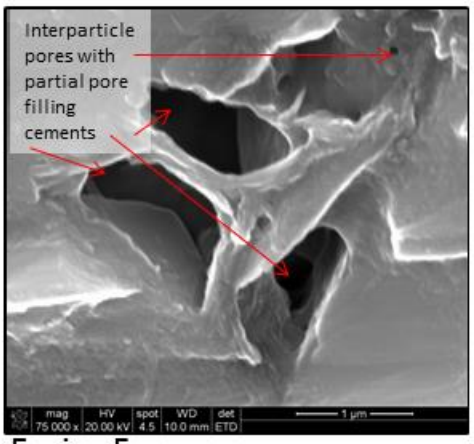

Facies 5

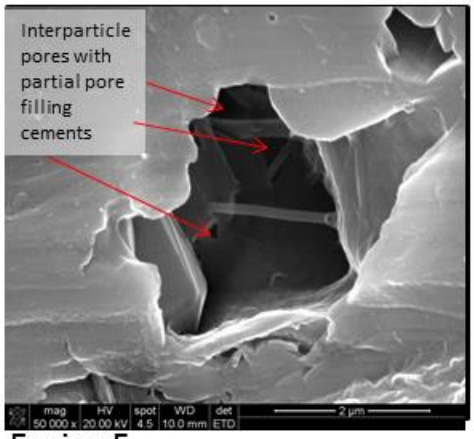

Facies 5

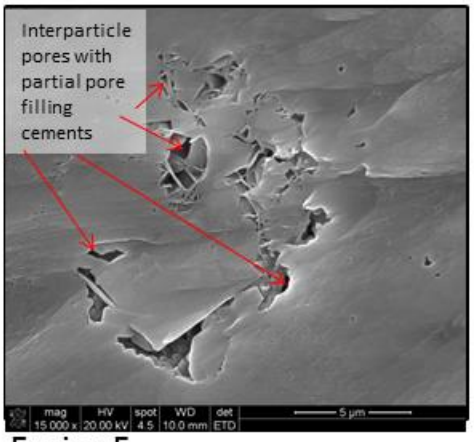

Facies 5

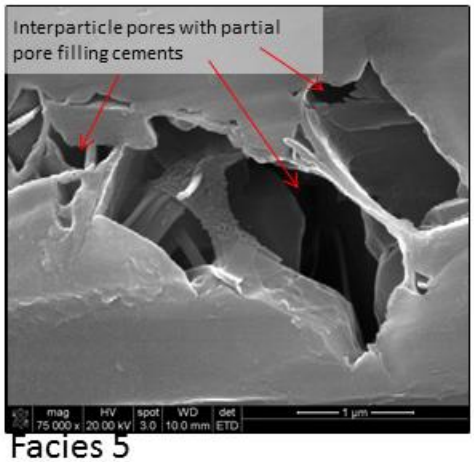

Facies 5

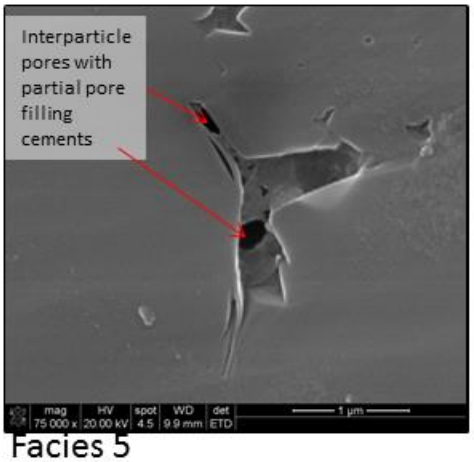

Facies 5

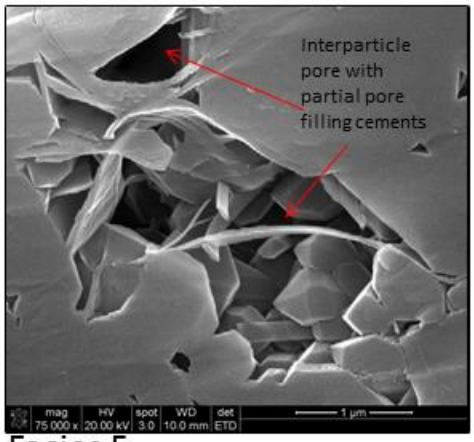

Facies 5

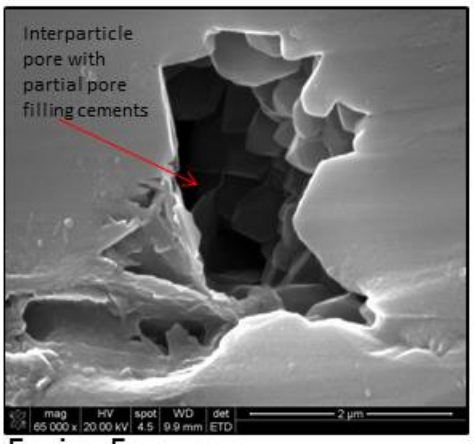

Facies 5

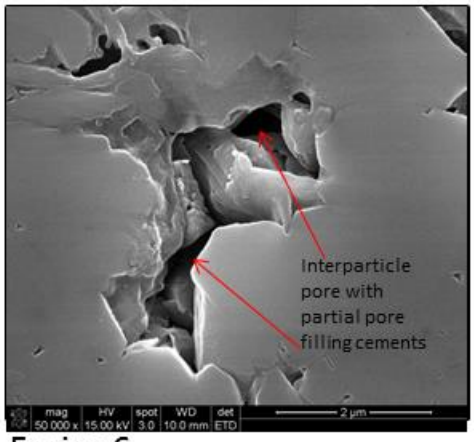

Facies 6

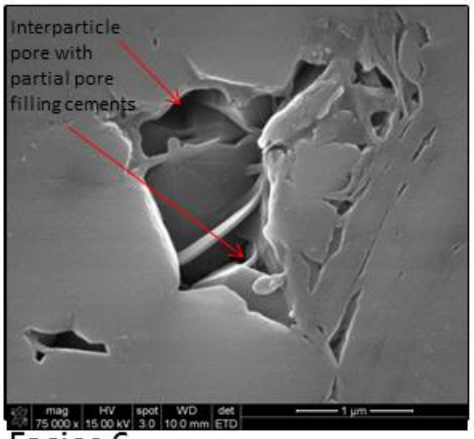

Facies 6

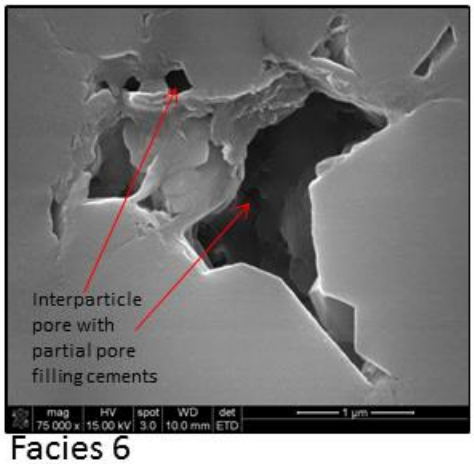

Facies 6

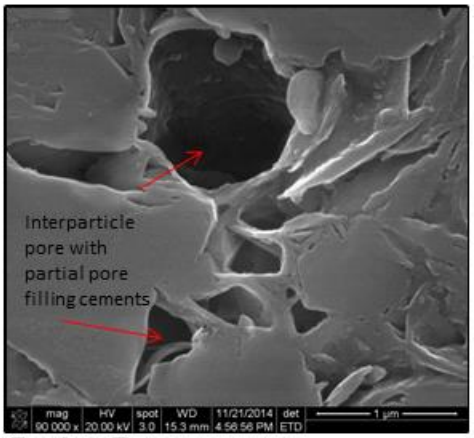

Facies 7

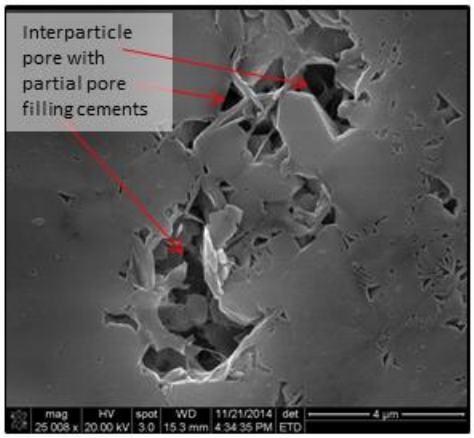

Facies 7

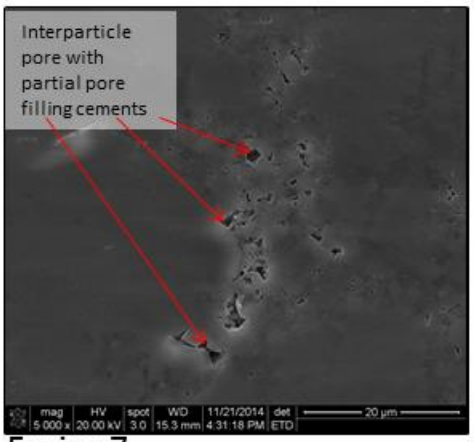

Facies 7

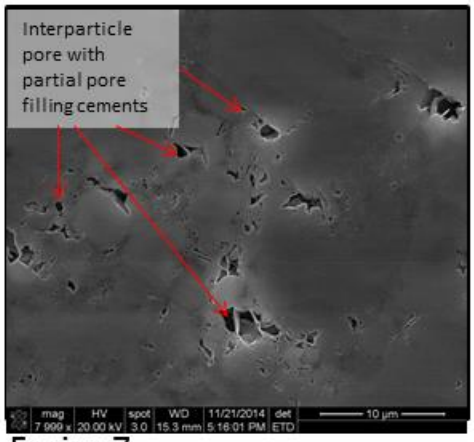

Facies 7

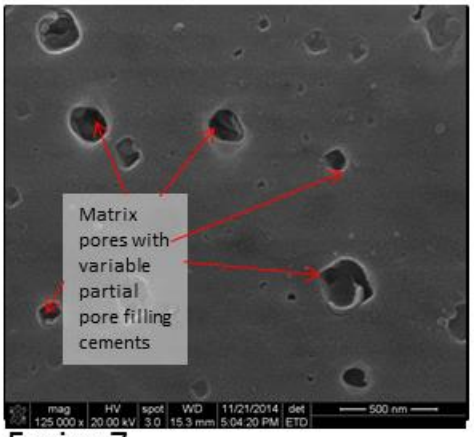

Facies 7

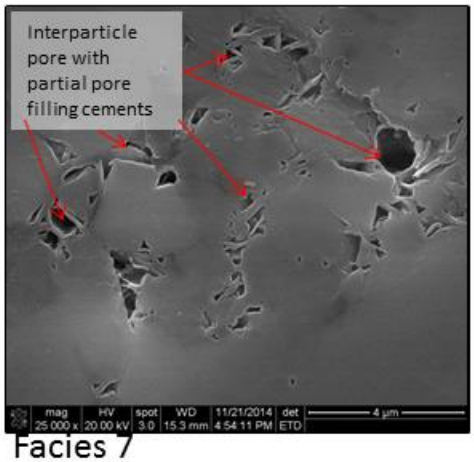

Facies 7

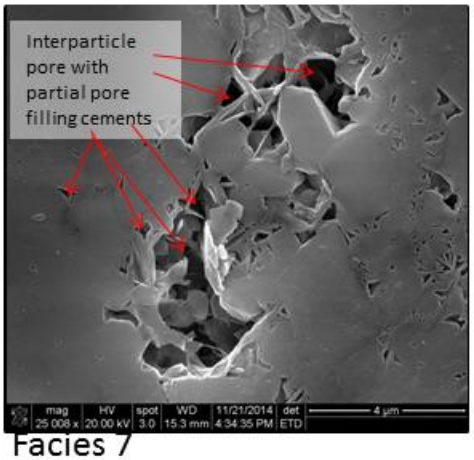

Facies 7

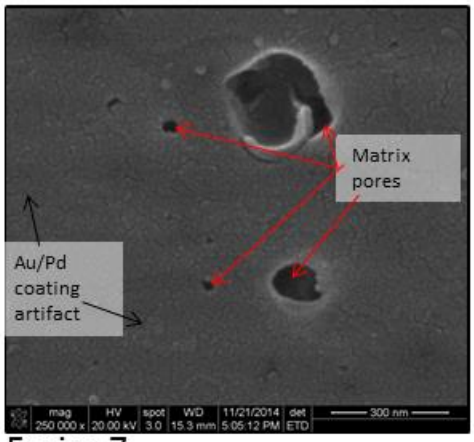

Facies 7

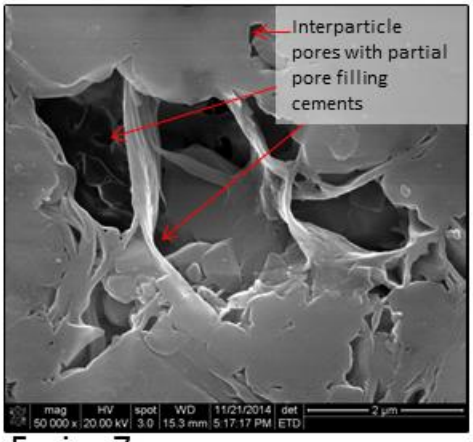

Facies 7

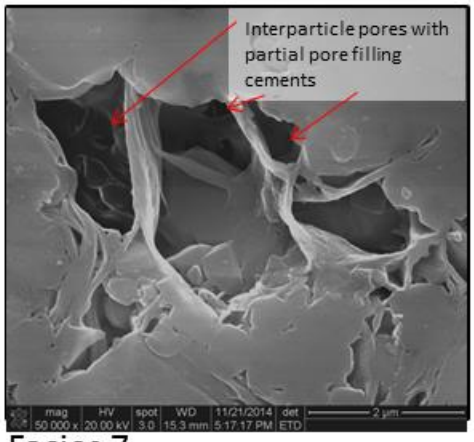

Facies 7